Bond Behaviour of Concrete Beams with Glass Fibre Reinforced Polymer Bars under Fatigue Loading

By

Ayman Sabry Shihata

A thesis

presented to the University of Waterloo

in the fulfillment of the

thesis requirement for the degree of

Doctor of Philosophy

in

Civil Engineering

Waterloo, Ontario, Canada 2019

Examining Committee Membership

The following served on the Examining Committee for this thesis. The decision of the Examining Committee is by majority vote.

External Examiner	**Professor. Mark Green** Civil Engineering, Queen's University
Supervisor	**Professor. Tim Topper** Civil and Environmental Engineering, University of Waterloo
Supervisor	**Professor. Scott Wallbridge** Civil and Environmental Engineering, University of Waterloo
Internal Member	**Professor. Susan Tighe** Civil and Environmental Engineering, University of Waterloo
Internal Member	**Professor. Adil Al-Mayah** Civil and Environmental Engineering, University of Waterloo
Internal-external Member	**Professor. Hamid Jahed** Mechanical and Mechatronics Engineering, University of Waterloo

AUTHOR'S DECLARATION

I hereby declare that I am the sole author of this thesis. This is a true copy of the thesis, including any required final revisions, as accepted by my examiners.

I understand that my thesis may be made electronically available to the public.

Abstract

Since the 1980s and after the aerospace industries faced several periods of economic difficulty, the companies that produced fibre-reinforced polymers (FRPs) started to introduce them as new materials for construction purposes. In one such application, FRPs were proposed for use instead of steel reinforcement in concrete due their mechanical properties including corrosion-resistance, high tensile strength, and light weight. On the other hand, FRPs have a lower modulus of elasticity compared to the steel reinforcement, which can lead to excessive deflection of the reinforced concrete member. Prestressing of the FRP reinforcement was a solution to overcome this serviceability concern. Previous research has been conducted to study the mechanical properties of carbon and aramid fibre reinforced polymers as prestressed reinforcement. Less attention has been given to glass fibre reinforced polymers as prestressing reinforcement because of its high relaxation and creep rupture. Only limited data on the behaviour of the prestressed GFRP under fatigue loading is available. Also, no design guidelines are provided in CAN/CSA-S806-12 or ACI 440.4R-04 for using prestressed GFRP bars in concrete members.

In order to address this knowledge gap, the current study included testing of forty-six GFRP reinforced concrete beams to investigate the bond mechanisms between the GFRP bar and concrete under monotonic and fatigue loading. Each beam was reinforced on the tension side with a single GFRP bar. This study was divided into two phases: a first phase (preliminary study) and a second phase (main study). The main objectives of the preliminary study were to investigate the effect of different variables on the bond mechanism between the GFRP bar and the concrete and choose the most important variables that affect the bond strength between the GFRP bar and the concrete for the main study. Sixteen reinforced concrete beams were cast and tested under monotonic loading. The test variables included in the preliminary study were bar diameter, bar surface type, concrete cover, and prestressing level. The beam geometry was 150 mm wide by 225 or 250 mm high by 2400 mm long with concrete cover equal to 25 mm. For the main study, thirty reinforced concrete beams were cast and tested under monotonic and fatigue loading. The beams dimension was 200 mm in width and 2000 in length. The beams depth and height were varied depends on the clear concrete cover. For the beams with concrete cover of 25 mm the beams height and depth to the flexural reinforcing were 265 mm and 235 mm, respectively. For the beams with concrete cover of 45 mm the beams height and depth were 295 mm and 240 mm, respectively. The test variables

included in the main study were bar surface type, concrete cover, and prestressing level. For the beams tested under fatigue loading, the minimum applied load was 10 % of the static failure load. The peak load was varied to study the effect of load range on fatigue life. The test frequency for all cyclic test was 1.0 Hz.

All of the beams that were tested under monotonic loading failed in bond between the GFRP bar and the concrete. Increasing the concrete cover increased the ultimate beam capacity by almost 20%. For all of the beams tested under monotonic loading, there was no noticeable difference in ultimate load between the beams reinforced with a sand coated GFRP bar and beams reinforced with a ribbed GFRP bar.

For the beams tested under fatigue loading, two failure modes were observed, bond failure between the GFRP bar and the concrete and rupture of the GFRP bar. For the beams that failed in bond, the slope of the load and stress versus fatigue life curves is shallow and consequently a small change in load range will result in a large change in the fatigue life. Increasing the concrete cover thickness increased the fatigue strength. Comparing the load range (kN) versus life curve for the non-prestressed and prestressed beams that failed in bond, shows that the prestressed beams had longer lives than the non-prestressed beams.

A crack growth model based on the one developed by Wahab et al., 2015 was used to calculate fatigue lives and to predict the crack length versus the number of cycles. The calculated number of cycles was in good agreement with the data for the beams with different concrete thicknesses. The model captured the general trends in the test data (e.g. shape of the crack length versus number of cycle curves) and gave good representations of the initial crack length.

Acknowledgements

First of all, all praise to Allah (God) for giving me the patience and the strength to have this work completed.

I will always be grateful to have had the honor of working with my late supervisor, Professor Khaled Soudki, whose support was phenomenal throughout my Master and PhD journey which I worked under his supervision.

I would like to express my special thanks and appreciation to my advisors Professor Tim Topper and Professor Scott Walbridge, you have been an exceptional mentor for me. Your advices on both research as well as on my career have been priceless. Thank you for your help, guidance, patience, and support. Without you, this scientific piece of work would not be done.

I would also like to acknowledge the technical assistance of laboratory technicians Richard Morrison, Douglas Hirst, Peter Volcic. Their technical expertise was invaluable during the experimental phase of this study.

I would like to express my sincere thanks and gratitude to my parents, family, brother and friends who encouraged and support me during the completion of my work. I doubt that I will ever be able to convey my appreciation fully, but I owe them my endless gratitude.

Mum and Dad without your love, guidance, encouragement and influence on my life, I would not have made it that far. I would like to thank my father in-law and my mother in-law who have always encouraged me and given me the love and confidence to reach my goals

Special thanks, from my deeps it heart to my beloved wife, Reham , you have been and always will be my greatest source of joy, whose love, patience and support has carried me through the ups and downs of the past few years and given me perspective of the important things in life. to her, this thesis is dedicated. Sally and Zain, you make my life much more colorful, I love you.

My sister Nahla , I am blessed to have you in my life. a special thanks to my sister Raghd for her support and her special effort during my journey.

I am particularly thankful for my colleagues who assisted me throughout various stages of this study. Special thanks to Noran Abdel-Wahab, Taha Younes, Adham El Menoufy, Rayed Alyousef, Hisham Alabduljabbar, Hesham Elhuni, Amr Ab-del-Havez

I would like to thank the Saudi cultural bureau and King Abdul Aziz University for their support

Table of Contents

List of Figures

List of Tables

Chapter 1: Introduction

1.1 General

The service life of reinforced concrete structures depends on the durability of the reinforced concrete and the severity of environmental exposure. Lack of durability and/or exposure to severe environmental conditions leads to concrete deterioration. Reinforcing bar (rebar) corrosion is the most common deterioration mechanism that decreases the service life of reinforced concrete structures. Many structures in severe environments have experienced an unacceptable loss in serviceability earlier than anticipated due to corrosion of their steel reinforcement.

In order to increase the service life of concrete structures, fibre reinforced polymers (FRP) rebar is being used to replace conventional reinforcing steel, thus resolving the corrosion problem. FRP bars have many advantages over steel bar, namely non-corrosiveness, light weight, high tensile strength, and nonmagnetic and electrical insulation properties (ACI 440.4R-04 2004). Currently, FRP is used as a primary reinforcement in a variety of concrete structures subjected to severe environments such as bridges, sea walls, chemical and wastewater treatment plants, and other marine and underwater structures (Saadatmanesh and Ehsani, 1998; Benmokrane and Rahman, 1998).

The performance of a reinforced concrete member depends mainly on forces transfer between the concrete and the reinforcement bar, which, in turn, depends on the bond between the two materials. The strength of a reinforced concrete member under flexure and shear forces depends on the force developed in the reinforcement rebar. Therefore, the development of an adequate bond is always a critical aspect of structural design, regardless of the type of reinforcement (Benmokrane et al., 1996; Tighiouart et al., 1998). As a result, extensive experimental research has been done to understand the bond behaviour of FRP rebar in concrete structures. In spite of several experimental investigations, the bond behaviour between FRP rebar and concrete is not yet fully understood. This lack of understanding is attributed to the complexity of the parameters affecting the bond behaviour (concrete compressive strength, concrete cover, bar diameter, type of FRP rebar, and type of FRP surface) and the different types and properties of the currently commercially available FRP rebar (Okelo and Yuan, 2005). Equations have been developed for designing FRP reinforced concrete structures based on the available experimental data up to 2007. Since then, considerable

research has been conducted, which has shed new light on the effects of the various parameters on the behaviour of the concrete – FRP rebar bond. For this reason, it has become essential to assess and understand the bond mechanisms between the FRP bar and the surrounding concrete, to update and improve the guidelines that are used to design FRP reinforced concrete structures.

1.2 Research Significance

Comprehensive research studies have been conducted to understand the bond mechanisms between the FRP bar and surrounding concrete for non-prestressed structural members. Since 1990, many researchers have invested their time in conducting extensive research on the use of FRP tendons as a prestressed reinforcement. The focus has been on carbon fibre (CFRP) and aramid fibre (AFRP) reinforcing bar as prestressed reinforcement, because of their mechanical and physical properties. Only a few studies have focused on glass fibre (GFRP) reinforcing bars as prestressed reinforcement. Due to its perceived susceptibility to creep rupture in comparison to CFRP and AFRP, the use of GFRP rebar as prestressed reinforcement has been limited to date.

Improved GFRP bars have been manufactured in the past five years, which are reported to have the ability to be used as a prestressed reinforcement. Given the lack of knowledge and potential improvements in the available products, this research investigates the bond behaviour of non-prestressed and prestressed GFRP bar under monotonic and static loading.

1.3 Research Contributions

The bond behaviour of concrete beams reinforced with non-prestressed and prestressed glass fibre reinforced polymer (GFRP) bars under different type of loading will be investigated in this thesis. The main advantages of GFRP bars are their low cost and high strength/self-weight ratio. On the other hand, the Young's modulus of the GFRP bar is low compared to steel reinforcement, which can lead to excessive deflections. Pre-tension the GFRP bar is very useful to eliminate high deflections and fully utilize the high tensile strength of GFRP bars.

FRP reinforcement is fairly new material and it has the potential to be applied in concrete structures where corrosion resistance materials are needed. Only a few studies can be found in the literature investigating (experimentally or analytically) the static and fatigue behaviour of concrete beams reinforced with prestressed GRFP reinforcing bars.

1.4 Objectives

The specific objectives of the study described in the current thesis are:

- to investigate the bond behaviour of concrete beams reinforced with non-prestressed and prestressed high modulus GFRP bars under monotonic and fatigue loading,
- to investigate the effect of increasing the prestressing level of the GFRP bars beyond the 25% prestressing limit set by CAN/CSA-S6-06 on the bond behaviour between the GFRP bar and concrete,
- to investigate the effect of using different concrete on the bond stress between the GFRP bar and the concrete,
- to study the effect of bar surface type on the bond between the GFRP bar and concrete,
- to assess the feasibility of using high modulus GFRP bars as the main prestressed reinforcement in the concrete structure for building and bridge applications,
- to develop a model that describes the process of failure including the deterioration under cyclic loading and the internal forces at failure in the shear span, and
- to develop a model to predict the rate of splitting crack propagation under fatigue loading.

1.5 Thesis Organization

The current thesis is divided into five chapters, as follows:

Chapter 1: This chapter (the current chapter) briefly introduces the main topic and objectives of the research and lays out the organization of the contents of the thesis that follows.

Chapter 2: This chapter presents a literature review on the bond behaviour between FRP rebar and concrete. Following this, a summary of key findings from the literature is presented.

Chapter 3: This chapter describes the experimental program, including the test matrix, fabrication of the test specimens, the instrumentation, and the test setup.

Chapter 4: This chapter presents the experimental results, including static and fatigue test results, for the tested non-prestressed glass fibre (GFRP) reinforced concrete beams.

Chapter 5: This chapter presents the experimental results, including static and fatigue test results, for the tested prestressed GFRP reinforced concrete beams.

Chapter 6: This chapter presents the description and verification of an empirical model that can be used to describe the bond mechanism between the GFRP bar and concrete.

Chapter 7: This chapter presents the main conclusions and recommendations from this study.

Chapter 2: Background and Literature Review

2.1 Fibre Reinforced Polymers

Fibre reinforced polymers (FRP) are composite materials manufactured of high strength fibres embedded in a resin. The combination of more than one constituent produces a synergistic effect with the composite's properties being superior to those of its components (Badawi, 2003). Most of the applied forces or loads are carried by the fibre. Fibers generally provide stiffness and strength to the composite. The resin matrix transfers the stress between the fibres, provides some ductility to the composite system, and protects the fibres from damage due to impact or scratches.

2.1.1 Resin

Different kind of resin including adhesives, primers, and putty fillers are used in fiber reinforced polymers (FRP) products. Polyesters, epoxies, and vinyl esters are commonly used resin. The main purpose of the resin is to protect, separate the fibres. The currently used resin have been invented to optimize their structural behaviour in different environmental conditions and for easy application by a professional installer. The FRP resin is characterized by the following properties (ACI committee 440):

- low density (high strength to weight ratio),
- resistance to environmental effects (temperature extreme, salt water, moisture, and other chemicals),
- filing ability,
- compatibility and bond strength to the substrate, and
- compatibility and adhesion to the reinforcing fibre.

2.1.2 Fibres

The most common continues fibers that used for civil engineering applications are carbon, glass, and aramid (Soudki, 1997). The fibres can be bi-directional, unidirectional, and pseudo-isotropic, as illustrated in Figure 2.1. The fibres (carbon, glass, and aramid) assumed to have linear stress-strain relation up to failure, as shown in Figure 2.2

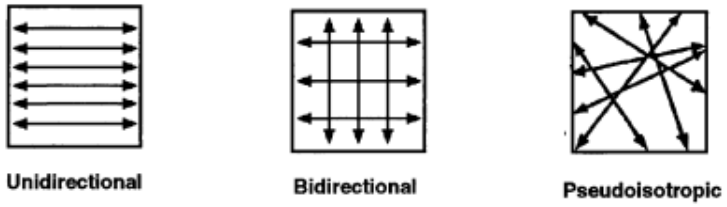

Figure 2.1 Various fibre orientations of FRP laminates (ACI 440, 2002)

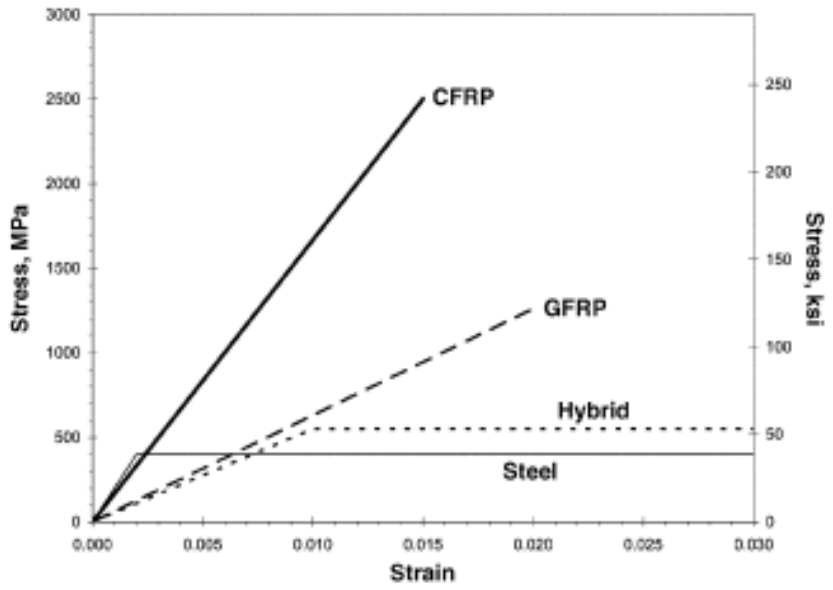

Figure 2.2 Stress-strain behaviour of FRP (ACI 440, 2007)

Glass Fibre Reinforced Polymer (GFRP): There are different types of glass fibre reinforced polymers (GFRP) used in civil engineering applications. E-glass type is commonly used. GFRP has many advantages including high strength, corrosion resistance, low cost, and heat resistance. Due to the low Young's modulus, the stiffness of the GFRP is low which leads to serviceability issue.

Carbon Fibre Reinforced Polymers (CFRP): Carbon fibre reinforced polymers Is the best fiber type used for civil engineering purpose because of its excellent properties including high strength, excellent fatigue behaviour, high stiffness, and light weight. The main disadvantages of the CFRP are low shear strength, low ductility, and expensive to produce

Aramid Fibre Reinforced Polymer (AFRP): Aramid is generic name for aromatic polyamide. In contrast with GFRP and CFRP, which are made from ceramic fibres, aramid is a polymer. Aramid fibres are stiffer than glass fibres and cheaper than carbon fibres. They possess relatively low density, high strength, and high fatigue and corrosion resistance.

2.1.3 FRP in Concrete Structures

In the past decades, composite materials have improved in terms of their suitability for use as a construction material for bridges and buildings. FRP is now used in structural engineering in a number of ways, including several involving reinforced concrete construction and strengthening. In a new concrete structure, FRP can be used as non-pretensioned main reinforcement or pre-tensioned tendons. The surface of the FRP bars are either plain bar (smooth), sand coated, ribbed bar, or spirally wound. Figure 2.3 shows samples of FRP bars/tendons that can be used as main reinforcement (pretensioned or non-pretensioned) in concrete structures.

Figure 2.3 Different types of FRP bar/tendon (Quayyum, 2010)

FRP tendons were used as prestressed reinforcement in Europe in 1980s for the first time to avoid corrosion problems. In the past, the use of FRP prestressing was hindered by the fact that the conventional steel anchor could not be used due to the low transverse strength of the FRP tendon (Erki and Rizkallak, 1993; Nanni *et al.*, 1995; Soudki, 1998). In the past decade, prestressed anchors were successfully invented and produced for FRP prestressing applications (Al-Mayah

and Soudki, 2004). The high cost of the FRP material is the main factor that limits the use of FRP materials in reinforced concrete structure (ACI 440R- 07). CFRP bars/tendons are expensive and the most common FRP type used in prestressed applications because of its high modulus of elasticity and strength. Also, CFRP bars are not susceptible to relaxation or creep rupture. The GFRP bar cost is lower than that of the CFRP bar, but its use in prestressed application is limited because of its high relaxation and susceptibility to creep rupture. The new generation of the GFRP bar has a higher strength and stiffness (40 to 45% comparing with the previous generation). This FRP bar could survive without creep rupture even if it's loaded with sustained load up to 50% of its ultimate capacity in normal conditions (Schoeck, 2009, Zawam, 2015). However, the GFRP bar subjected to a severe environmental condition under sustained loading will have decreased bond between the GFRP bar and the concrete, which will affect total structural performance (Fergani, 2018). The new GFRP bar strength ranges between 1100 MPa and 1450 MPa, with modulus of elasticity higher than 60,000 MPa. The stress-strain behaviour of the new generation of GFRP bar is shown in Figure 2.4

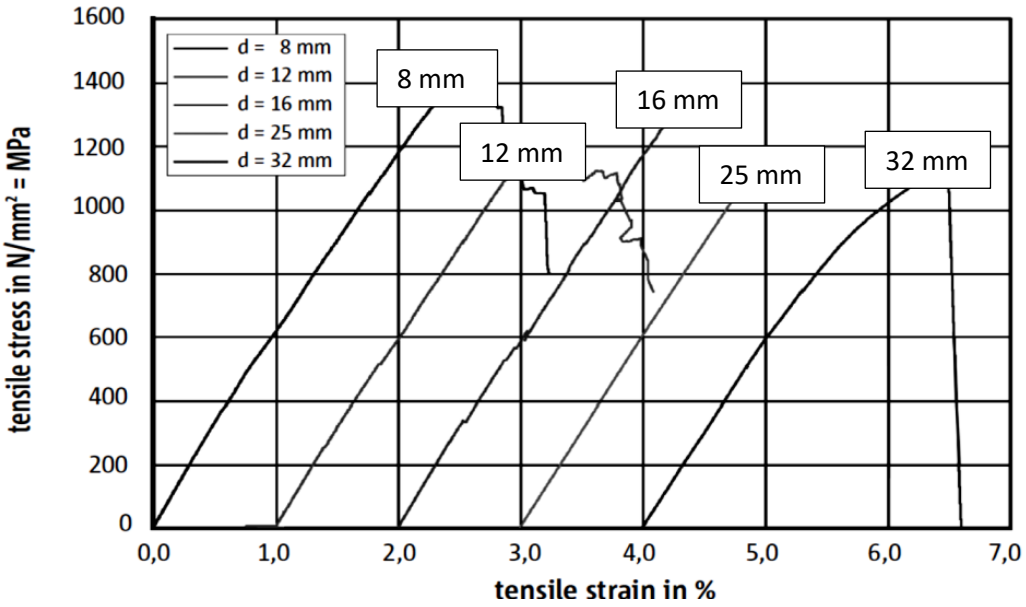

Figure 2.4: Stress-strain relation for new GFRP bar (Schoeck, 2009)

2.1.4 Transfer Length of Prestressed FRP Bars

Transfer length is the length that is required to transfer the prestressing force to the concrete after the release of a prestressing tendon (ACI 440R-07). (ISIS Canada-08) defines the transfer length

in prestressed members as the length starting from the point of zero stress at the end of the prestressed member to the point where the prestress at maximum effective. Measuring the transfer length is important to check the stress limit at the service limit state, calculate the actual bond stress at the end of prestressed member, and check the shear design.

The transfer length of prestressed FRP tendons/bars depends on bar diameter, surface type, concrete cover, prestress level, and concrete compressive strength (Hwan Oh. et al, 2001). The transfer length in pretensioned concrete members decreases with an increase of concrete cover and concrete strength. Furthermore, the transfer length increases with increasing of bar diameter (Hwan Oh. et al, 2001). One of the most important factors that affects the transfer length is the Hoyer effect. Due to the radial expansion of the prestressed bar after release, the normal stresses acting on the surface of the prestressed bar increase (Mahmoud et al. 1999).

2.1.5 Previous Research on Transfer Length

Issa et al. (1993) reported on an experimental study designed to determine the transfer length of FRP bar in normal strength concrete. The ultimate strength of 9.5 mm S-glass wire strand that was used in this study ranged between 1736 and 2212 MPa. The Young's modulus ranged between 38,000 and 50,000 MPa. The concrete strength at 28 days ranged between 38 and 50 MPa. The transfer length for the 45% prestress level ranged between $20 \cdot d_b$ and $28 \cdot d_b$ (254 mm and 279 mm) (d_b = bar diameter). The transfer length increases with time with increasing rate double than the steel tendon.

Soudki et al (1997) designed an experimental study to determine the transfer length for 8.0 mm CFRP rod at three different stress levels (50, 60, and 70 percent of ultimate strength). They cast five large full-scale reinforced concrete T-beams with pre-tensioned CFRP rod. They found that as the prestress level increases, the transfer length increases. For the prestress levels of 50 and 70 percent, the transfer length was 650 mm ($80 \cdot d_b$) and 725 mm ($90 \cdot d_b$), respectively. The beam cross section shape did not affect the transfer length. The instantaneous transfer length measured at the time of release is equal to the long-term transfer length. Strain gauge results obtained by DEMEC gauges or electric strain gauges were found to be similar.

Lu et al. (2000) carried out an experimental study to investigate the transfer length of three types of FRP tendon (Carbon Strawman, Aramid Technora, and Carbon Leadline) in prestressed full-

scale concrete beams. 30 beams were reinforced with pre-tensioned FRP tendon. 12 beams were reinforced with steel strand. The authors conclude that the transfer length of different FRP types were virtually identical. It was found that the transfer length of the FRP tendon should be assumed to be at least 50 times the bar diameter.

Badawi and Wahab (2010) presented an experimental study to estimate the transfer length of prestressed NSM Carbon FRP (CFRP) rod in concrete beams. Two types of CFRP rod (sand coated and spirally wound) were used to strengthen 22 reinforced concrete specimens. Four prestressing levels were used: 60%, 50%, 45%, and 40% of the ultimate tensile strength of the CFRP rod. Electric strain gauges mounted on the CFRP rod were used to measure the CFRP strain at release. The test results showed that the transfer length of CFRP equal $35 \cdot d_b$. The transfer length data curve fitting was found to follow an exponential distribution.

Zawam and Soudki (2015) investigated of the transfer length of HM (high modulus) of GFRP bar in prestressed concrete beams. Eight full-scale prestressed reinforced concrete beams were used in this study. DEMEC points were used to measure the transfer length. The test variables were concrete compressive strength (30 MPa and 70 MPa), nominal bar diameter (12 mm and 16 mm), and prestressing level (25% and 40% of the ultimate strength). For the normal concrete strength (30 MPa), the transfer length of 16M diameter was $17 \cdot d_b$ for the 40% prestressing level and $14 \cdot d_b$ for the 25% prestressing level. The transfer length decreases with decreasing prestressing level and decreased with an increase in the concrete strength.

2.2 Bond Mechanisms

Bond defined as an interaction between two different materials, for an example reinforcement (steel/fibre) and concrete. Bond is an important factor that maintains the integrity in the composite material known as reinforced concrete. The applied load is usually carried by all elements in the reinforced concrete structures including steel reinforcement and concrete. the external load/force transfer from the concrete to the internal reinforcement by shear stress along the internal reinforcement interface. Due to the perfect bond between the internal reinforcement and the concrete, it is assumed that the strains value in the steel/fibre reinforcement and the concrete are equal in the analysis of any reinforced concrete structure (Strain compatibility). The bond stresses transfer by:

1) chemical adhesion between the internal reinforcement and the concrete,
2) friction between the outer surface of the bar and the concrete, and
3) mechanical interlock between the ribs of the reinforcement and the concrete.

Figure 2.5 shows the bond mechanisms for steel reinforcement embedded in concrete. For plain reinforcement, the bond between the bar and the concrete depends mainly on the friction and chemical adhesion. For the deformed reinforcement (rebar), the bond depends on the mechanical interlock between the bar ribs and the concrete. The steel reinforcement must have sufficient embedment length or enough level of confinement (shear reinforcement or clear concrete cover) to avoid bond failure and achieved the ultimate tensile capacity of the bar. If the bar has enough confinement and embedment length, the radial stress that developed along the rebar will be less than the tensile capacity of the surrounding concrete and the beam will fail by different failure mode. Less confinement level and shorter bond length lead to bond failure.

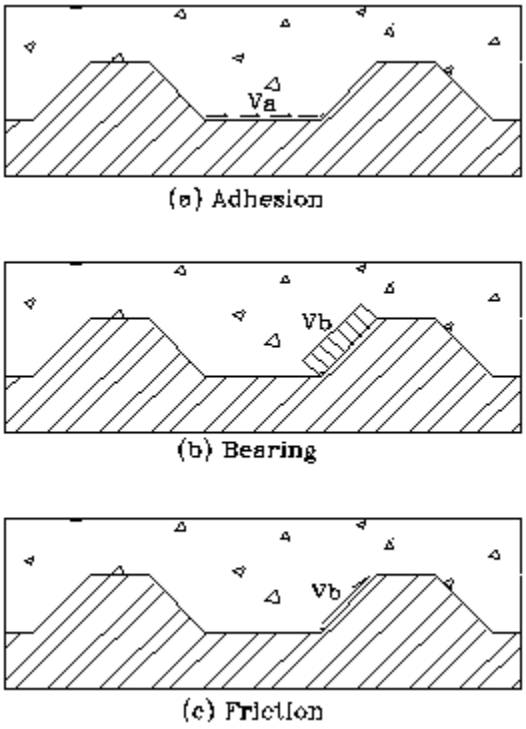

Figure 2.5 Bond mechanisms between steel rebar and concrete

2.2.1 Bond Failure

Bond failure can occur through splitting or pullout failure. A splitting failure occurs when the relative movement between the reinforcing bar and the concrete becomes high enough that the deformations on the bar begin to act as wedges, putting the surrounding concrete in transverse tension and causing the formation of splitting cracks parallel to the bar. Splitting cracks typically radiate outward from the bar and tend to form first where there is the least amount of concrete cover. If the bottom concrete cover is greater than the side concrete cover, a horizontal split develops at the level of the bars and the subsequent failure is termed a "side-splitting failure". With the side clear cover greater than the clear bottom concrete cover, longitudinal cracks develop through the bottom cover followed by splitting along the plan of the rebar. Figure 2.6 shows these splitting type bond failures. With continued loading, splitting cracks grow in width and radiate outward to the face of the specimen or between adjacent bars or splices. As they continue along the development length of the bar, the cracks can cause the delamination of a concrete layer, unless confining transverse reinforcement is provided. Pullout failure occurs when the concrete between the deformations on the bar fails in shear or compression. A pullout failure tends to occur only when the concrete cover is high or when the bar is confined by transverse reinforcement that limits the propagation of splitting cracks

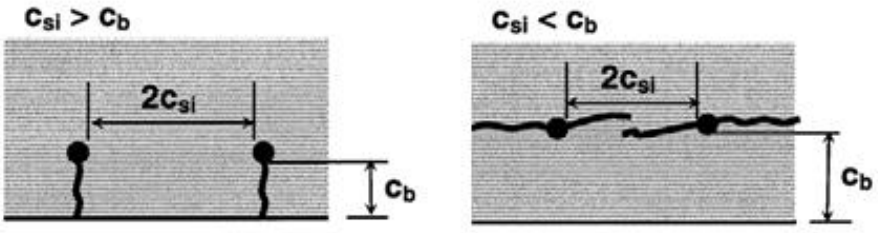

Figure 2.4: Splitting type bond failure (El Maddawy, 2004)

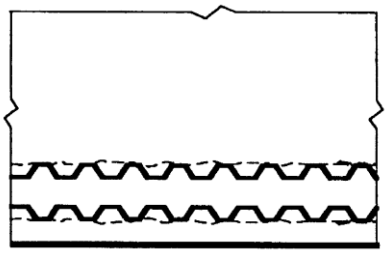

Figure 2.6: Side view of a reinforced concrete member showing shear cracking / local concrete crushing due to bar pullout

2.2.2 Bond Test Specimens

several test specimens have been used to investigate the bond mechanism between the rebars and concrete. The four common specimen configurations are a splice specimen, pullout test specimen, beam anchorage specimen, and beam end specimen (ACI Committee 408, 2003).

Pullout Specimen

Pullout tests are the simplest test specimens to investigate the bond behaviour between the reinforcing bar and the concrete and are outlined in the (ASTM C900-15) standard. The pullout test consists of a single bar embedded at the center of a concrete block or concrete cylinder. A typical pullout test specimen is shown in Figure 2.7a. The reinforcing bar usually subjected to tension forces while the concrete restrained in the opposite direction. Many researchers used the pullout test to investigate the bond between rebar and concrete and they argued about the accuracies of the test results, and the pullout test does not represent a realistic bond situation. Ferguson (1965), conclude that the pullout test places the concrete in compression with no other outside forces acting on the members. The tension crack that occurs around the rebar will not be developed because the concrete is under compression around the specimen. Also, the compression stresses in concrete increase the confinement level around the rebar, resulting in higher bond stresses compared with the one generated in a beam test. In a beam test, the bond region is subjected to stresses due to moment, shear and the confinement by shear reinforcement. Also, in a realistic situation, the concrete in the bond region is under tension stresses. The pullout tests are still used by many researchers because they are simple to set-up, inexpensive, and give a quick estimate of the bond test results.

Beam-End Specimen

The procedure for beam-end tests is specified in the (ASTM A944-15) standard. The beam-end test is a simplification of the RILEM test, essentially only using half of the specimen (Figure 2.7b). The test frame applies a tension force directly to the reinforcing bar to generate bond forces. The advantage of this test over the pullout test is in the way the specimens are mounted in the test frame. Bearing points on the sample are placed in a similar fashion to the reaction forces at the end of a beam, thus inducing tension in the concrete around the bar and moment and shear forces into the member and creating a loading condition that is closer to the real one.

Beam Anchorage Specimen

The simplest method to incorporate the effects of tension in the concrete, shear, and transverse reinforcement into a bond test, is by testing beams. In the case of standard beams, a reinforcing bar may be extended beyond the ends of the beam to monitor free end slip. A modification to the standard beam test is to incorporate pockets (voids with beam) to allow for internal slip measurements on the reinforcing steel. The pockets should be located outside the bond region and are useful for monitoring the loaded end slip and the tensile stresses in the steel bar (Figure 2.7c). The reinforcing bar maybe de-bonded by using plastic sleeves around the bar to control the bond length. The set-up is simple since it uses a standard simply-supported beam test.

Splice Beam Specimen

The splice beam specimen represents a larger-scale beam and is designed to measure the bond in lap-spliced bars (Figure 2.7d). A splice beam specimen is normally fabricated with the lap splice in constant moment region. It is easier to fabricate and produces similar bond strengths to those obtained with beam anchorage specimens. The splice specimens simulate a member with flexural cracks and known bonded length. Both beam anchorage specimen and splice beam specimen provide more realistic measures of the bond strength in actual structures.

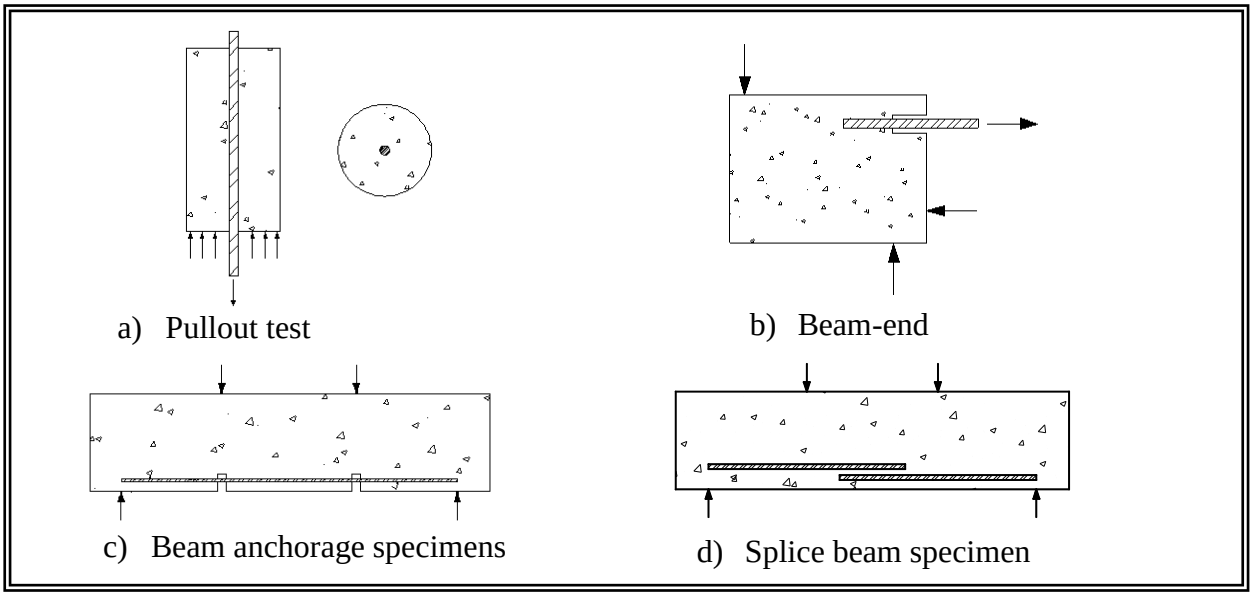

Figure 2.7: Schematic of bond test specimens.

2.3 Bond Behaviour of Steel Reinforcement

The steel rebar is isotropic, homogeneous, and elasto-plastic material. It has been concluded that there are differences in bond mechanisms between the plain steel reinforcement and ribbed steel reinforcement. The bond of the deformed steel bar mainly depends on the mechanical interlock and secondarily on friction and chemical adhesion. The bond of the plain steel bar primarily depends on the friction and chemical adhesion. Due to a small indention on the bar surface, there is some mechanical interlock. The bearing of the rebar ribs against the concrete is the primary bond mechanism restraining the slip between the reinforcement steel bar and the surrounding concrete.

2.4 Bond Behaviour of FRP Reinforcement

There are many differences in the bond behaviour between the fibre reinforcement polymers (FRP) bar and concrete and between the steel bar and concrete. These differences exist because of the differences in failure mechanism between the steel and FRP rebar and in force transfer. The steel bar is an elasto-plastic, homogeneous, and isotropic material while the FRP bar linear elastic, non-homogenous, and anisotropic material. In the FRP bar, the shear and transverse properties are dependent on the type of fibre and the resin. Unlike the steel rebar, the surface roughness type of the FRP bar is different from one manufacturer to another and created by a mix of epoxy and fibre or sand coated which reduces the bond performance. Also, the material properties used to produce the FRP bar is different from one manufacturer to another. The bond mechanism between the FRP bar and the concrete mainly depends on friction and chemical adhesion and secondary on the mechanical interlock

2.5 Factor Affecting Bond Behaviour of FRP Rebar in Concrete

An extensive research has been conducted to investigate the bond mechanisms between the FRP bar and concrete. several test specimens were used to investigate the bond between the FRP bar and concrete including full scale beam, beam end, and pullout specimens (Baena et al., 2009; Aly et al., 2005, 2006, 2007; Rafi et al., 2007; Okelo, 2007; Defreese and Wollmann, 2002; Pecce et al., 2001; Mosley, 2000; Shield et al., 1999; Tighiouart et al., 1998, 1999). It was concluded that bond strength between the FRP bara and concrete is affected by concrete compressive strength,

the clear concrete cover, the bar diameter, development length, type of FRP, surface type, and shear reinforcement.

2.5.1 Concrete Compressive Strength

Splitting and pullout failure modes depend on the tensile concrete strength. It has been observed that the concrete tensile strength is proportional to the square root of the compressive strength of concrete ($\sqrt{f'_c}$) (ACI Committee 408). Statistical analysis on different test results of specimens failed by bond between the FRP bar and concrete has shown a better correlation exists between the bond strength and square root of concrete strength ($\sqrt{f'_c}$) (Mahmoud et al., 2017; Bazil et al.,2017; yoo et al, 2016; yan and lin, 2016; Esfahani et al , 2013; Okelo, 2007; ACI 440.1R-15 ; Okelo and Yuan, 2005; Ehsani et al., 1996; Faza and GangaRao, 1990; Pleimann, 1987, 1991). Ehsani et al. (1995) design a case study to investigate the effect of concrete strength on the bond behaviour of FRP rebar in concrete. The authors conclude that as the concrete strength increased the bond between the FRP bars, and the concrete increased. In addition, as the concrete strength increased, the slip value decreased, and the initial stiffness of the bond stress-slip curve increased. Tighiouart et al. (1998) and Benmokrane et al. (1996) tested a full-scale beam to understand the effect of concrete strength on the bond of FRP bar. The authors observed that the increase of the bond strength is proportional to ($\sqrt{f'_c}$). Yan et al. (2016) who investigated the effect of severe conditions on bond strength between FRP and concrete stated that freeze and thaw cycles decreased concrete strength and the bond between the FRP bar and the concrete. Zemour et al. (2018) studied the effect of different concrete types on the bond between FRP and concrete. They found that using self-compacted concrete will decrease the bond strength between a GFRP bar and concrete compared the bond to a normally vibrated concrete even if the self-compacted concrete compressive strength is higher.

2.5.2 Concrete Cover

Concrete cover has a significant effect on the bond strength between the FRP bars and concrete. The concrete cover increases the level of confinement which results in an increase in the bond strength (Aly and Benmokrane, 2005; Defreese and Wollmann, 2002; Ehsani et al., 1993; Kanakubo et al., 1993). The thickness of the clear concrete cover changes the bond failure mechanism. ACI 440.1R-15 indicated that splitting failure will occur if the concrete beam does

not have enough concrete cover. If the reinforced concrete beam has an adequate concrete cover, pullout failure will occur by shearing along a bar surface at the top of the ribs around the bars. The bond failure mode depends mainly on the concrete cover and the level of confinement. Ehsani et al. (1996) reported on an experimental study to investigate the effect of the concrete cover on the bond strength of GFRP bar. Forty-eight reinforced concrete beams were cast and tested. The authors conclude that splitting failure will occur when the clear concrete cover equal times bar diameter ($c = 1 \cdot db$). When the clear concrete cover is larger than two time the bar diameter ($c > 2 \cdot db$), pullout failure will occur. Aly et al. (2006) designed an experimental study to investigate the effect of concrete cover on bond strength. Six full-scale lap-spliced concrete beams were cast and tested. The concrete cover ranged between one and four times bar diameter. The authors observed that the relationship between the concrete cover and the bond of the bar was not linear. Also, the bond strength increased by 27% if the concrete cover is higher than four times the bar diameter. Veljkovic et al., (2017) investigated the effect of different concrete cover thicknesses on the bond between a GFRP bar and concrete. Three concrete cover thicknesses where used in this study. The authors concluded that increasing the concrete cover from 10 mm to 20 mm increased the bond strength by 20%. Both specimens (with concrete covers equal 10 mm and 20 mm) failed by a splitting mode of failure. Kotynia et al., 2017 studied the effect of increasing the concrete cover thickness on the bond strength between GFRP and concrete. This study was comprised of twelve hinge beams. The authors found that decreasing the concrete cover decreased the shear (bond) stress for all of the bar diameters used in this study.

2.5.3 Bar Diameter

Many researchers investigated the effect of bar diameter on the bond strength of FRP bar embedded in concrete (Baena et al, 2009; Okelo, 2007; Aly et al., 2006; Defreese and Wollmann, 2002; Tighiouart et al., 1998; Benmokrane et al., 1996; Nanni et al., 1995). The authors reported that the effect of bar diameter on the bond strength between of FRP bar and concrete is similar to the effect of bar diameter on the bond strength between of steel bar and concrete. As the bar diameter increases the bond strength decreases. The larger bar diameter loses the adhesive bond mechanism earlier (Achillides and Pilakoutas, 2004). It has been reported that as the bar diameter increases the water bleeding underneath the bar will increases which increases the voids around the bar and reduces the bond strength between the bar and the FRP bar. Benmokrane et al., (2016)

carried out a comprehensive experimental program to evaluate the mechanical and physical properties of a headed GFRP bar and to determine the pullout behaviour of the headed GFRP bar in concrete. A total of 57 pullout specimen were cast and tested. The authors found that the reduction of the bond stress between the 16 mm and 19 mm diameters ranged between 14 and 16%. They suggested that this reduction was due the lower bearing area of the headed 19 mm GFRP bar. Lee et al (2017) investigated the effect of bar diameter on the bond behaviour of a GFRP bar in a high strength concrete. Two bar diameters were used in this study (19 mm and 25 mm) and their behavior was compared with that of steel reinforcement bars. The authors found that bond strength decreased linearly with increasing GFRP bar diameter. For the steel reinforcement, the bond strength decreased linearly as the bar diameter increased up to 19 mm. Then the bond strength remained constant. Also, the author stated that when the concrete compressive strength was increased bond failure occurred between the outer layer and the core of the GFRP bar. Larger bar diameter also led to this mode of failure. Hossain et al studied the bond strength of GFRP bars using RILEM beam tests. One hundred forty-four specimens were cast and tested. The main variables where bar diameter, the young's modulus of the GFRP bar and three different embedment lengths. the authors found that regardless of the concrete compressive strength, the bond strength decreased with an increase of the bar diameter with maximum bond strength reductions of 42% and 12% for HM and LM GFRP bars, respectively. Rolland et al (2018) investigated the effect of FRP bar type and diameter on the bond strength between the bar and concrete. Pull-out tests were performed on aramid, carbon and glass FRP bars and the results were compared with the results of tests on steel reinforcement. The authors found that the bond strength of the small bar diameter FRP bars was slightly higher than that of the steel. Unlike the trend that is usually reported in the literature, the authors found that as bar diameter increased the bond strength increased for a given bonded length.

2.5.4 Type of FRP Bar

Tighiouart et al. (1998) investigated the bond strength of GFRP bar with two different surface types and compared with steel rebar. The authors found that GFRP bar had lower bond strength compared to steel reinforcement. Benmokrane et al. (1996) reported that the bond strength of the GFRP bar was varied from 60-90% of that of the steel bars. (Larralde and Silva-Rodriguez, 1993) Also compared the bond strength of the GFRP bar with the bond strength of the steel bar. The

authors conclude that the bond strengths of GFRP bars were 73-96% of that of the steel bar. Okelo (2007) and Rafi et al. (2007) made a comparison between the bond strength of CFRP bar and steel bar. The authors conclude that the bond strength of CFRP bars was 85% of that of the deformed steel bars. Wambeke and Shield (2006) did an extensive analysis of bond test results data up to 2002. The authors found that the type of FRP bar does not have any effect on the bond strength between the bar and the concrete. CSA S806-02 stated that there is no difference between the bond strength of the GFRP and CFRP bar, but AFRP has lower bond strength than that of CFRP and GFRP bar. Baena et al., 2009 conducted a study to investigate the bond between different types of FRP reinforcement and concrete. Eighty-eight pullout specimens were cast and tested according to ACI 440.3R-04 and CSA S806-02. Two FRP bar types were used (GFRP and CFRP). The authors stated that the amount of slip for the GFRP bar was greater than for the CFRP bar. El-Refai et al., 2014 investigated the bond between two different FRPs (Basalt and Glass) and concrete. Thirty-six-cylindrical specimens were reinforced with BFRP bar and twelve-cylindrical specimens were reinforced with GFRP bar. All BFRP specimens failed by shearing of the outer layer of the bar from the bar core while all the GFRP specimens failed in bond between the bar and the concrete. The average bond strength of the BFRP bars was less than the average bond strength of the GFRP bars bar by 25%. The BFRP bars had higher residual stresses than the GFRP bars. Altalmas et al., 2015 studied the effect of FRP bar type on bond strength under severe conditions. Sixty-two pullout specimens were cast and tested. The authors concluded that the BFRP bars had a better bond strength than the ribbed GFRP bars regardless of the environmental condition. Park et al,.2016 studied the bond performance of various FRP rebar types in different casting positions. A total of sixty-three pullout specimens were cast and tested. The authors found that all specimens of the different FRP bar types failed in bond. Also, the authors found that the FRP bar surface had a more significant effect on bond strength than the FRP bar type. Yang and Xu. 2018 discussed the bond behaviour between concrete and different types of FRP bar. Two FRP bar types were used in this study (GFRP and CFRP). The authors concluded that FRP type has only a small effect on the bond strength.

2.5.5 Type of FRP Rebar Surface

FRP bars are manufactured with different surface type including ribbed bar, spiral wrapped, and sand coated. It has reported that the ribbed FRP bar shows the better bond in comparison with other FRP with surface type. Also, the bond strength of the modified surface FRP bar has a better bond in contrast with the plain FRP bar (Cosenza et al., 1997; Al-Zahrani, 1995; Alunno et al., 1995; Nanni et al., 1995;). Mosley et al. (2008) design an experimental study to investigate the effect of bar surface type of the AFRP and GFRP on the bond strength. The authors conclude that the bar surface did not have any impact on the bond strength. Also, Wambeke and Shield (2006), had the same conclusion as Mosley found after the cast and tested 269 concrete beams. Baena et al. (2009) cast and tested 88 pullout specimens to investigate the effect of the bar surface type on the bond strength between the FRP bar and the concrete. The Authors found that the surface type had a significant effect on the bond strength. Lin and Zhang, (2013) studied the effect of FRP surface on the bond strength between FRP bars and concrete. Full-scale beam test specimens were cast and tested in four-point bending to study bond-slip behaviour. Three types of the FRP reinforcement (Glass, Carbon and Basalt) with different surface conditions (wrapped, grain covered and ribbed) where used. The authors concluded that the bond strength of grain-covered FRP bar was much better than that of the warped and Ribbed FRP bar. Baena et al., (2016) investigated the behaviour of the bond between recycled aggregate concrete and GFRP bar for different surface conditions (spirally wounded and ribbed). Forty-eight pull-out tests specimens were cast and tested. The authors found that the behaviour of the bond failure was same for both concrete types. Also, they found that the bond strength of the ribbed FRP bar was much better than that of the spirally wounded bar. El-Nemr et al., 2016 designed a test to evaluate the bond-dependent coefficient of carbon and glass FRP bar in high and normal concrete strength. Sixteen full-scale beams where cast and tested under static loading. The test variables were FRP bar type, bar diameter, concrete strength and the FRP bar surface type. The authors concluded that the sand coated GFRP bars showed smaller bond-dependent coefficient values than those of the ribbed bars. Veljkovic et al., (2017) assessed the effect of the concrete cover on the bond between GFRP bars and the surrounding concrete. The parameters examined were the GFRP bar external surface, the concrete mechanical properties and the concrete cover. Both spirally wrapped and sand coated GFRP bars demonstrated brittle bond behaviour, but they showed a gradual debonding process. Also, the ribbed GFRP bar showed an excellent bond strength close to that of the steel

reinforcement but a different de-bonding mechanism. Pan and Xu, (2017) reported on an experimental study designed to investigate the effect of the external GFRP bar surface on the bond strength between the bar and the concrete. Two GFRP bar types were used (a plain smooth bar and a ribbed bar). Four full scale beams were cast and tested. The authors found that the bond strength of the smooth GFRP bar was much lower than that of the ribbed GFRP bar. Ruiz Emparanza et al., 2018 studied the effect of different external GFRP bar surfaces on bond strength. Pull-out tests were performed according to ASTM D7913. Three types of bar surfaces were used (helically grooved, sand coated and with surface lugs). The authors concluded that the ribbed rebar had the highest bond strength (22.5 MPa), followed by sand coated bar (18 MPa), and the bar with surface lugs fibre (12.5 MPa). According to the literature, there is no definite answer if the bar surface type has an effect or not on the bond strength of the FRP bar

2.6 Development Length and Bond Strength in Design Codes

The development length of rebar is the embedment length required to transfer the stress to the concrete due to loading without any failure between the bar and the concrete. Design codes usually specify a conservative value of the development length to avoid bond failure, which is a relatively brittle failure mode. Chang et al., (2010) built a case study to model the pullout of FRP bar from the surrounding concrete. The test variables were FRP bar embedment length and bar diameter. The concluded that the debonding started from the loading point and propagated toward the end of the specimen as the load increased. Also, the bond stress decreased gradually (non-linear) from the load point to the end of the specimens. Finally, the ultimate pullout load increased as the embedment length increased. Xue et al., (2014) investigated the bond behaviour of sand coated GFRP bar in concrete. A total of 84 specimens, including 48 pullout specimens, thirty beam specimens, and six RILEM specimens were cast and tested under monotonic loading. Two modes of failure were observed splitting failure and pullout failure. The authors found that splitting failure occurred when the bonded length was bigger than 5 times the bar diameter and pullout failure occurred when bonded length was less than 5 times the bar diameter. Also, the author observed that when the embedment length increased the bond stress decreased similarly to other results reported in the literature (Firas et al., 2011; Vilanova et al., 2015; Yoo and Yoon, 2017; Ashrafi et al., 2017; Li et al., 2018). Tekle et al., (2017) investigated the bond behaviour between the 15 mm sand coated GFRP bar and Geopolymer Cement in beam-end specimen tests. Two embedment

lengths were used (six times the bar diameter and nine times the bar diameter). Strain gauges were installed along the GFRP bar to investigate the strain distributions during a test. The authors found that the bond stress distribution along the bonded length was nonlinear. Also, the authors concluded that the bond stress increases at the free-end for a short embedment length. Available design code equations that can be used to calculate development length are discussed in the following sections.

2.6.1 Canadian Highway Bridge Design Code (CSA S6-14)

Based on the Canadian Highway Bridge Design Code (CSA S6-14), development length can be calculated by Equation 2.1:

$$l_d = 0.45 \frac{k_1 k_4}{\left[d_{cs} + K_{tr} \cdot \frac{E_{FRP}}{E_S}\right]} \left[\frac{f_F}{f_{cr}}\right] A_{f,bar} \qquad \text{Equation 2.1}$$

where:

L_d = development length (mm)

K_1 and K_4 = modification factor

d_{cs} = smallest concrete cover (mm)

K_{tr} = transverse reinforcement index (mm)

F_{frp} = tensile strength of FRP bar (MPa)

E_{frp} = Young's modulus of FRP bar (MPa)

E_s = Young's modulus of steel bar (MPa)

$A_{f.bar}$ = cross sectional area of FRP bar (mm^2)

2.6.2 Design and Construction of Building Structures with Fibre-Reinforced Polymers (CSA S806-12)

Based on the Canadian Building Design Code **(CSA S806-12)** the development length could be calculated by Equation 2.2. This equation does not include the effect of confinement due to transvers reinforcement.

$$l_d = 1.15 \frac{k_1 k_2 k_3 k_4 k_5}{d_{cs}} \frac{f_F}{\sqrt{f'_c}} A_{fbar} \qquad \text{Equation 2.2}$$

where:

l_d = development length (mm)

A_{fbar} = cross sectional area of FRP bar (mm^2)

f'_c = concrete compressive strength (MPa)

$k_1k_2k_3k_4k_5$ = modification factors

f_{Frp} = tensile strength of FRP bar (MPa)

d_{cs} = smallest of the distance from the closest concrete surface to the centre of the bar being developed or two-thirds the c-c spacing of the bars being developed (mm) $d_{cr} < 2.5 \cdot d_b$.

2.6.3 ACI 440.1R-15

American concrete institute published a design guideline in 2015 for FRP reinforced concrete structure (ACI 440.1R-15). They found a new way to calculate the development length of FRP bar in concrete. Their way based on the equilibrium principles for bars embedded in concrete and formula derived for normalized average bond stress.

$$L_d \times d_b \times u = A_{frp} \times f_{frp} \qquad \text{Equation 2.3}$$

$$\frac{u}{0.083\sqrt{f'_c}} = 4.0 + 0.3\frac{c}{d_b} + 100\frac{d_b}{l_d} \qquad \text{Equation 2.4}$$

Based on beams reinforced with GFRP bar tested by Wambeke and Shield (2006), a new formula derived by using Equation 2.3 and Equation 2.4 to calculate the stress in the FRP bar at given development length, Equation 2.5.

$$f_{frp} = \frac{0.083\sqrt{f'_c}}{\alpha}\left(13.6\frac{l_d}{d_b} + \frac{c}{d_b}\frac{l_d}{d_b} + 340\right) \leq f_{frpu} \qquad \text{Equation 2.5}$$

By rearranging Equation 2.5, the development length can be calculated using Equation 2.6.

$$l_d = \frac{d_b\left(\frac{f_{frp}}{0.083\sqrt{f'_c}} \times 340\right)}{13.6 + \frac{c}{d_b}}$$ Equation 2.6

where:

l_d = the embedment length, mm;

d_b = the reinforcement bar diameter, mm;

u = the average bond stress, MPa;

A_{frp} = the cross-sectional area of the FRP reinforcement bar, mm2;

f_{frp} = the tensile stress developed in the FRP bar at the end of the embedment length, MPa;

f'_c = the concrete compressive strength, MPa; and

c = the lesser of the cover to the centre of the bar or one-half of the centre-to-centre spacing of the bars being developed, mm.

f_{frpu} = the rupture tensile stress of the FRP bar

2.7 Fatigue

The fatigue behaviour of concrete structures subjected to cyclic loading is an important limit state that must be considered by designers (Demers 1998). A Class A highway bridge experiences an average daily truck traffic of over 4000 trucks/day over a design life (CSA, 2010). Bridge deck slabs directly carry these repeated loads and are therefore subjected to fatigue damage (El-Ragaby et al., 2007). The fatigue strength and fatigue life of reinforced concrete elements (non-prestressed and prestressed) are influenced by many factors including material properties of the reinforcement and concrete, reinforcement ratio, minimum and maximum values of repeated loading, and the range and rate of loading (El-Ragaby et al., 2007). The response of a structural member subjected to fatigue (cyclic) loading is affected by the interaction between the reinforcement and the concrete and the material strength. The applied load or the induced stress range in each component is the

most important factor influencing fatigue behaviour (ACI 215R-74 1997). Figure 2.8 illustrated by Badawi, 2007 shows a stress versus time chart for any fatigue test with definitions of some important terms used in the fatigue data analysis.

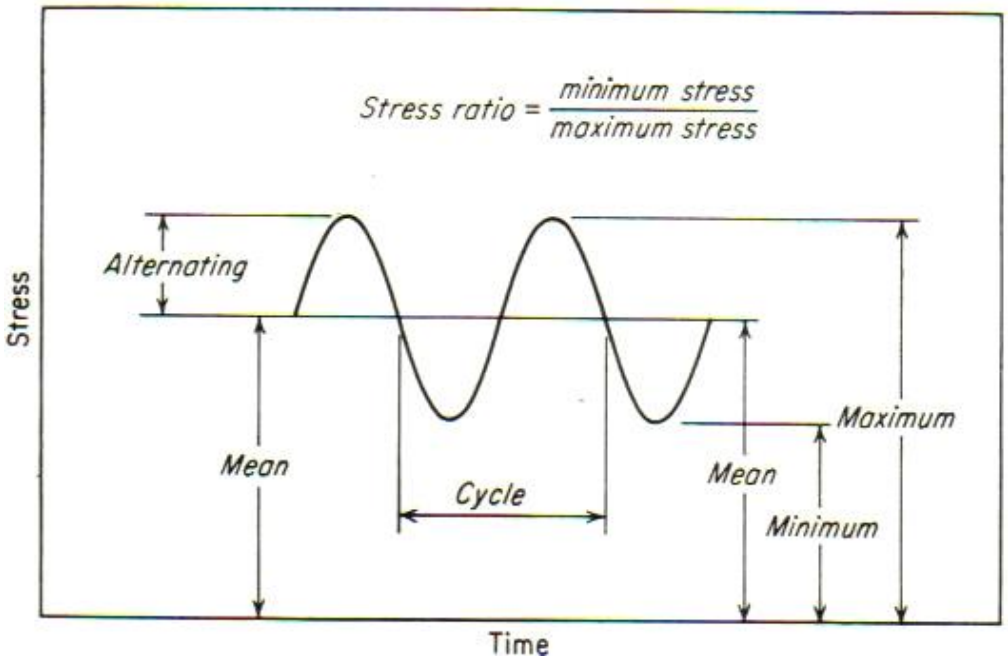

Figure 2.8 Terms used in fatigue analysis (Badawi, 2007)

2.7.1 Fatigue of FRP Materials

The fatigue behaviour of composite materials has been studied for many decades and has focused on aerospace, transportation, and marine applications. A limited number of studies were interested in the fatigue behaviour of the FRP reinforcement in concrete structures.

The fatigue behaviour of FRP reinforcement depends on many parameters including the type of fibre, the resin type, and the configuration of the test specimens (Konur and Mathews, 1989). FRP composites are varied and their fatigue failure mechanisms are different than those observed in steel. The fatigue failure for homogenous metals usually starts in a single crack and then this crack propagates in a single mode, while FRP materials can display a variety of failure modes including fibre-matrix de-bonding, matrix cracking, and FRP rupture (Adimi, 2000; El-Ragaby et al., 2007; Alves et al., 2011; Ju and Oh, 2015; Ahmed et al., 2018; Kim and lee, 2018). Fatigue in metals is generally predictable using fracture mechanics theory and demonstrates a stable crack growth rate until a critical crack length is reached, leading to unstable crack growth and then fracture. For FRP

materials, fatigue failures are usually the result of damage accumulation rather than damage propagation (Reifsnider, 1991). Typical FRP fatigue life curves (S-N curves) plot the peak strain in the first cycle in a constant-amplitude load-controlled test versus number of cycles to failure in a log-log scale. The diagram can be divided into three stages as shown in Figure 2.9 (Talreja, 1981a, Brondsted et al., 1997). In the first region, the S-N curve is almost horizontal in log-log scale diagram and the life to failure depends on the individual fibre strength. At high strain levels, failure occurred by breaking the individual fibres randomly. By breaking the fibres, the amount of fibre will decrease, and the stress will eventually be high enough to break the remaining fibres. The second region represents classical fatigue behaviour where the curve can be described by a power function. The progressive failure in this region begins with matrix breaking and debonding occur between the fibre and resin. In this region, the rate of damage accumulation is strain dependent, while the damage accumulation is cycle dependent. In the third region, the stress is too low to initiate cracks or break the fibres under fatigue loading.

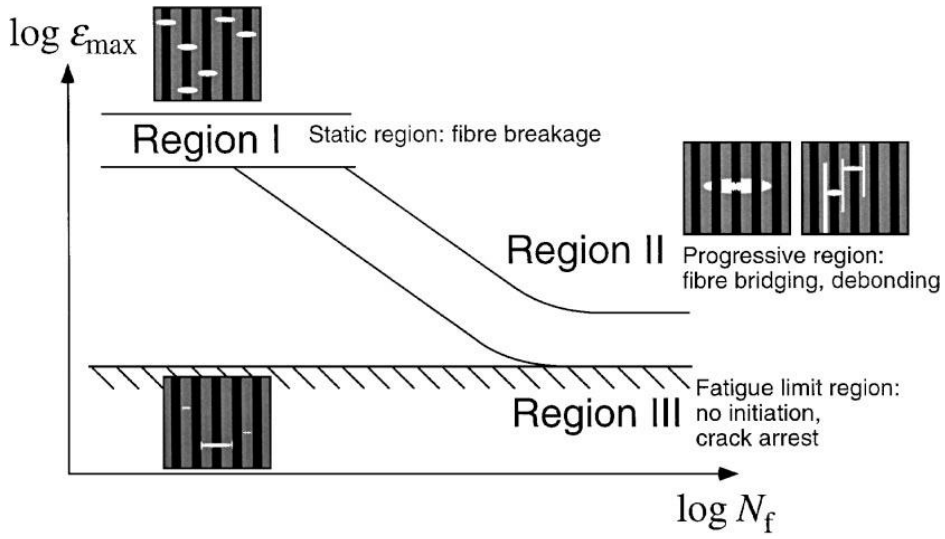

Figure 2.9 Fatigue life diagram for unidirectional composites (Talreja 1981a)

Fatigue of Glass Fibre Reinforced Polymers (GFRP)

GFRP is sensitive to fatigue loading due to its lower stiffness. For the same maximum stress, GFRP shows a lower fatigue life than CFRP (Demers, 1998a). The results of GFRP tests under fatigue loading show a steeper slope than the CFRP when plotted on an S-N curve (Konur & Matthews,

1989). ACI 440 (2015) limits the stress in FRP reinforcement subjected to fatigue loading to 55% and 20% of the ultimate tensile strength for CFRP and GFRP, respectively.

The fatigue behaviour of GFRP is affected by several factors other than the stress limit. the fibre glass itself loses almost 10% of its static strength when embedded into resin to form FRP composite. Also, environmental factors change the fatigue behaviour of GFRP due to its susceptibility to alkaline solutions, acidic solutions, and moisture (ACI 440, 2015). E-glass GFRP reinforcement is most commonly used due to its low cost, good physical properties, and weathering ability. The old generation of E-glass GFRP suffered from a loss of strength with time under loading (Mandell, 1982). However, the new HM E-glass GFRP reinforcements maintain their strength under sustained loading with time (Zawam, 2015). Martin and Soudki, (2014) investigated the behaviour of low modulus GFRP bar in air and embedded in concrete under fatigue loading. The authors found that the GFRP bar tested under fatigue loading in air lasted longer than the same GFRP bar embedded in concrete. Also, GFRP bars embedded in concrete tested under fatigue loading with stress ranges above 300 MPa did not last more than twenty thousand cycles.

2.7.2 Fatigue of Reinforced Concrete Structure

Cyclic loading significantly decreases the ability of reinforced concrete structures to resist applied loads, which eventually lead to excessive deflections and crack opening. Fatigue loading must be considered in the design of concrete structures as it can lead to reduced flexure and shear capacity, bond degradation, and reduced structure life. Concrete failure under fatigue loading is not common. However, the concrete might soften due to repeated load, which can lead to an increase in the tensile stress in the main reinforcement (Heffernan & Erki, 2004). The flexural capacity of a cracked structure under fatigue loading is affected by the type and the ability of the main reinforcement to resist the cyclic loading (Braimah et al., 2006). Testing the FRP bar/rod embedded in the concrete is more realistic comparing to the FRP bar tested in the bare air. The flexure test of the reinforced concrete beam under cyclic loading shows the effect of the interaction between the concrete and the FRP bar. Cyclic loading has a harmful effect on the bond between the reinforcing bar and the surrounding concrete. The crushing of the concrete in front of the reinforcement lugs is the main mechanism governing bond failure in reinforced concrete members (ACI 408.2R-12). Several factors affecting the bond strength between the concrete and the main

reinforcement include: concrete cover, bar size, bar surface condition, reinforcement properties, concrete strength, level of confinement, and stress range (ACI 408.2R-12).

2.7.3 Fatigue Behaviour of FRP Reinforced Concrete Structures

For the past years, many studies reported that the HM CFRP reinforcement shows a better fatigue performance than steel reinforcement in the form of bare bars or bars embedded in concrete as tensile reinforcement (Saadatmanesh and Tannous, 1999; Braimah, 2000; El-Ragaby et al., 2007a). The fatigue behaviour of FRP reinforcement is affected by the concrete surrounding it in two ways: 1) due to the harsh alkaline environment, and 2) due to the friction between the concrete and the FRP bar resulting surface abrasion of the bar (Rahman et al., 1996; El-Ragaby et al., 2007). Failure of the FRP reinforcement begins when the first surface crack occurred due to fritting. Fretting of the FRP reinforcement surface can take place close to the flexural cracks, where the bond stresses are high enough to cause slip between the bar and the concrete (CEB-FIP, 2000).

Balaz (1991) investigated the effect of cyclic loading on bond strength between FRP reinforcement and concrete. Forty-six reinforced concrete pullout specimens were fabricated and cast with a single reinforcement bar placed centrally in the concrete specimens. The test variables were bar diameter, bonded length, and fatigue load level. Balaz concluded that the amplitude of cyclic loading is an important factor in considering the slip development. Higher load cycle amplitude generally leads to higher values of slip. However, amplitudes less than 30% of the ultimate static strength did not show big differences in slip.

Bakis et al. (1998) cast reinforced concrete beams with three different GFRP bars to investigate the effect of the GFRP bar surface on the bond behaviour between the bar and the concrete under cyclic loading. They concluded that the GFRP bar that has grooved surface had better bond strength. Also, there is not much difference in bond strength between are the sand coated and helical GFRP bar.

Katz (1998) reported that the surface treatment of GFRP bars through means such as helical wraps to enhance the bond between the concrete and the bar has a negative impact on the fatigue performance. Local stress concentrations occur due to the surface enhancement such as ribs and wraps, which lead to a decrease in the fatigue life of the structure.

Katz (2000) performed a test study to understand the bond mechanism for five different types of FRP bar embedded in the concrete under fatigue loading. Katz concludes that helical wrapping of the FRP bar reduces the bar resistance by 20–30% of the ultimate strength under cyclic loading. The bond strength between FRP bar and concrete was affected by the physical and mechanical of the bar surface type. The sand coated FRP bars showed better bond performance than the other types. Delamination of the outer GFRP layer that made of resin only and does not have fibre in it reduces the bond strength.

Alves (2010) investigated the durability of the bond between the GFRP and sound concrete under different loading types and environmental conditions. Thirty-six specimens were constructed and tested. The test variables included the bar diameter, the concrete cover, and the environmental condition. Alves concludes that the bond strength increases with increasing concrete cover and decreasing bar diameter.

Abdel Wahab, 2011 cast and tested 40 reinforced concrete beams strengthened with near surface mounted (NSM) CFRP bars to examine bond strength. The beams were 150 mm wide × 250 mm deep × 2200 mm long. Grooves were cut by saw into the beams. Each beam was strengthened with one NSM CFRP bar. The CFRP bar (9 mm) was either sand coated or spirally wound. All of the beams were tested in four-point bending test under static and fatigue loading. All of the strengthened beams failed in bond between the bar and the surrounding epoxy. Abdel Wahab concludes that bond failure started as de-bonding between the CFRP bar and the epoxy at the loading point. As the number of cycles increased, the de-bonding spread toward the supports until the CFRP bar slipped from the epoxy. The mechanics of bond failure were the same for beams tested under static or fatigue loads. Beams strengthened with sand coated bars showed better fatigue performance than those with spirally wound bars. Ju and Oh, 2015 designed a study to investigate the bond between a customized GFRP bar and concrete under repeated loading. The specimens were comprised of two rectangular concrete blocks joined by a steel ball at the top. A single 10 mm GFRP bar was used as main reinforcement. Three different bonded lengths were tested 45 mm, 90 mm and 135 mm. The authors concluded that all specimens failed in bond by crushing the concrete in front of the GFRP bar lugs. The bond strength between the GFRP and the concrete tested under fatigue loading decreased by almost 40 % compared to the value found under monotonic loading.

Mohamed et al. (2017) presented a new test setup to assess the bond performance of FRP bars in concrete under cyclic loading. The test setup was designed to determine the bond between the bar and concrete depending on the actual case and to avoid premature bar failure from direct pullout loading as in the case of a pullout test. Two bars diameters (9 mm and 12 mm) were used as the main reinforcement. The authors found that under monotonic loading, the reduction of the bond stress between a GFRP bar and concrete after reaching the maximum bond stress was about 5% while the reduction of the bond stress for the beams tested under fatigue loading was almost 32%.

Ahmed et al., 2018 designed a case study to examine the effect of cyclic loading on the bond between the basalt FRP bar and concrete. Pullout test specimens reinforced with a single basalt bar were used. The test variables were concrete compressive strength, bar surface type (Sand-coated, wounded, wrapped and smooth). Most of the specimens failed in bond but one specimen failed by bar rupture. The authors concluded that cyclic loading decreased the bond strength between the BFRP and concrete. The amount of reduction depended on the bar surface type, the concrete compressive strength and the cyclic loading characteristics.

2.8 Summary and Conclusions

From the literature presented, it is evident that gaps remain in the current state of knowledge on the bond behaviour of FRP rebar in concrete. Specifically:

- There is a need to re-evaluate the effect of certain parameters (i.e. surface type, bar diameter, and concrete cover) on the bond behaviour FRP rebar in concrete. There are still unresolved questions related to the effects of these parameters and a lack of experimental data for non-prestressed high modulus GFRP rebar.
- Currently, there is no experimental data characterizing the bond behaviour of prestressed high modulus GFRP rebar in concrete. Such data is needed to understand this bond behaviour under both monotonic (static) and fatigue loading.
- A general bond stress-slip law as needed for splitting and pullout modes of failure. This relationship should take into consideration different types of GFRP rebar with different surface type/texture. Moreover, the proposed relationship should consider all the variables that affect the bond performance of FRP bar, i.e.: type of fibre, rebar surface, concrete

strength, bar diameter, concrete cover, and concrete confinement. It should also consider the effects of prestressing and monotonic vs. cyclic loading.

- The use of GFRP in prestressed applications is not allowed by CAN/CSA-S806-12, while CAN/CSA-S6-14 allows prestressing of GFRP bars to not more than 25% of the ultimate tensile strength as an initial prestressing level. Further assessment is needed to determine if these limits are reasonable or overly restrictive.

Chapter 3: Experimental Program

3.1 Introduction

The study aimed to investigate the bond behaviour of concrete beams reinforced with non-prestressed and prestressed GFRP bars under monotonic (static) and fatigue loading. The experimental program included bending tests to failure of forty-eight reinforced concrete beams with glass fibre reinforced polymer (GFRP) reinforcing bars.

This chapter describes the experimental program including test specimen information, beam configuration, the materials used and the fabrication of the beams, the prestressing procedure, and the test setup and loading procedure.

3.2 Test Program

Forty-nine GFRP reinforced concrete beams were cast and tested summarized in Figure 3.1. Sixteen reinforced concrete beams were fabricated as an exploration study and tested under Static (monotonic) loading. These beams where divided into two series based on their concrete cover to bar diameter (c/d) ratios of 1.5 and 3.0. In each series, four beams were reinforced with sand coated GFRP bars while the other four beams were reinforced with ribbed GFRP bars. Two different bar diameters were used in each series; four beams were reinforced with M12 and M16 sand coated GFRP bars, and four beams reinforced with M12 and M16 ribbed GFRP bars. Also, four beams were non-prestressed, and four beams were prestressed to 40% of the ultimate bar strength. After tested the sixteen beams. Three non-prestressed beams were fabricated and tested to see the effect of transverse reinforcement on bond strength. These beams were reinforced with M16 sand coated GFRP with clear concrete cover equal 1.5 times the bar diameter. For the main study, thirty beams were fabricated and cast in six groups.

Group 1: six reinforced concrete beams with non-prestressed M16 Sand Coated GFRP bar with clear concrete cover equal 1.5 times the bar.

Group 2: six reinforced concrete beams with prestressed M16 Sand Coated GFRP bar with clear concrete cover equal 1.5 times the bar.

Group 3: six reinforced concrete beams with prestressed M16 ribbed GFRP bar with clear concrete cover equal 1.5 times the bar.

Group 4: six reinforced concrete beams with non-prestressed M16 sand coated GFRP bar with clear concrete cover equal 3.0 times the bar.

Group 5: six reinforced concrete beams with prestressed M16 sand coated GFRP bar with clear concrete cover equal 3.0 times the bar.

In each group, one beam was tested under static (monotonic) loading and the other beams were tested under different fatigue load levels. The maximum load level was varied from one beam to another as a percentage of the ultimate static loading while the minimum load was kept constant at 10% of the ultimate static test for all beams.

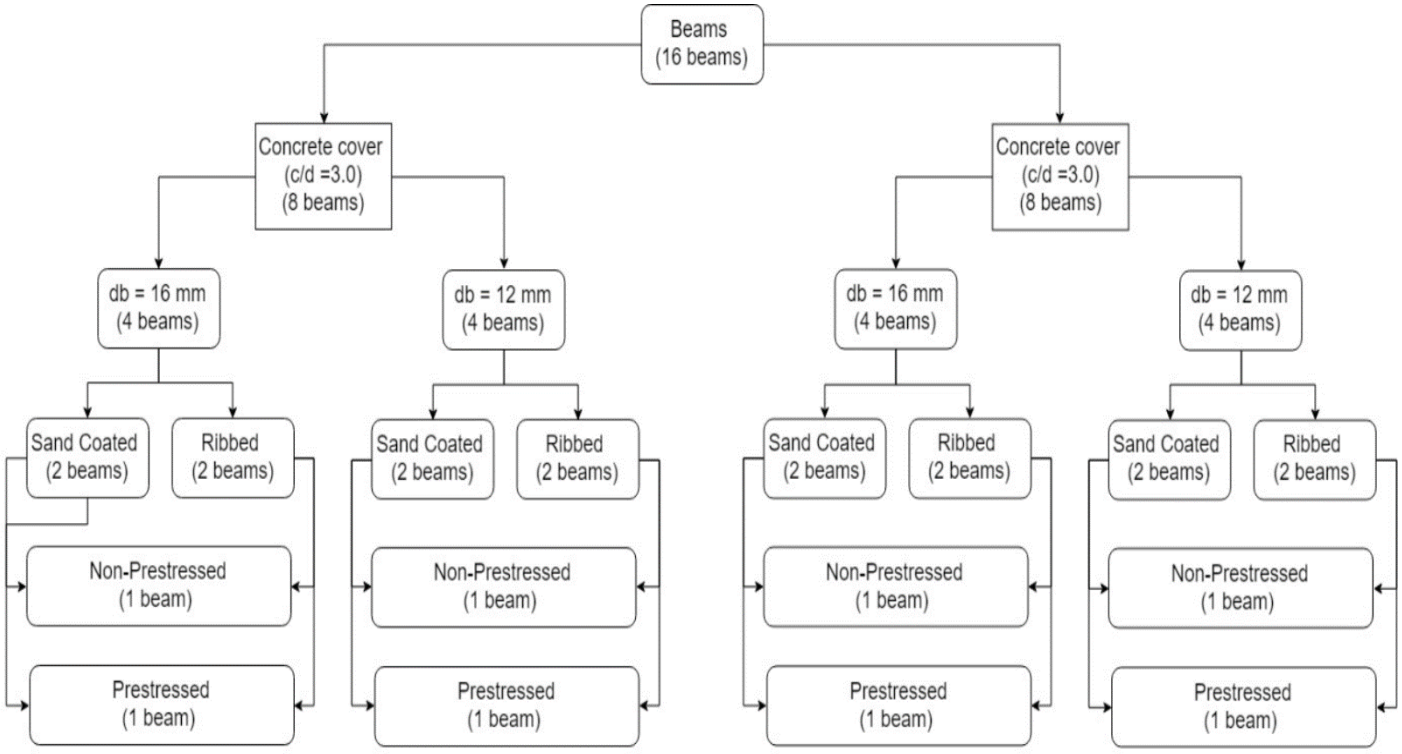

a) Pilot Study

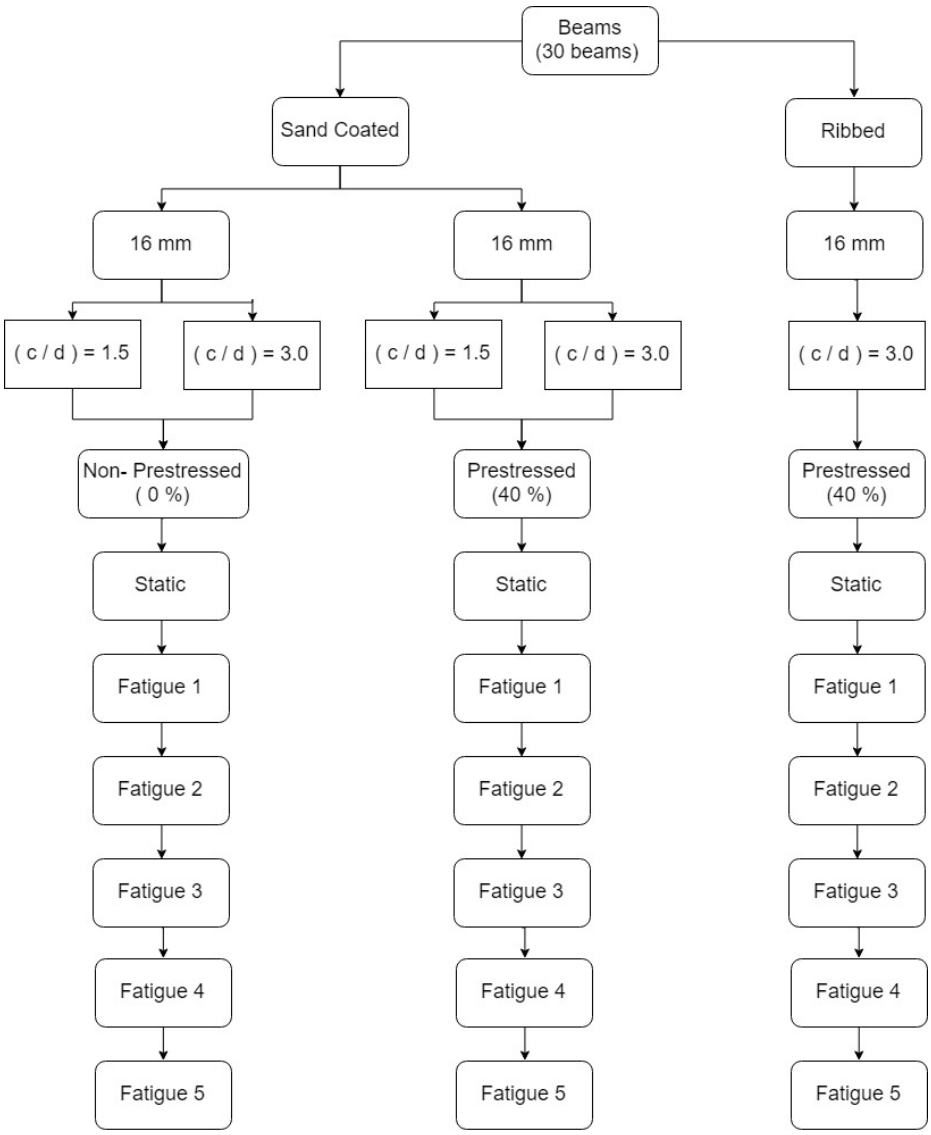

b) Main Study

Figure 3.1 Test matrix

The beam notation used the following five part form: AA-BB-CC-DD-EE. The first part represents the surface type of GFRP bar (SC: Sand Coated, R: ribbed), the second part represents the bar diameter, the third part represents the clear concrete cover to bar diameter ratio (*c*/*d*), the fourth part represents the prestress level (0% and 40%), and the last part represents the static load or fatigue load range (kN) (fatigue load range is the difference between the minimum and the maximum load) as shown in Figure 3.2.

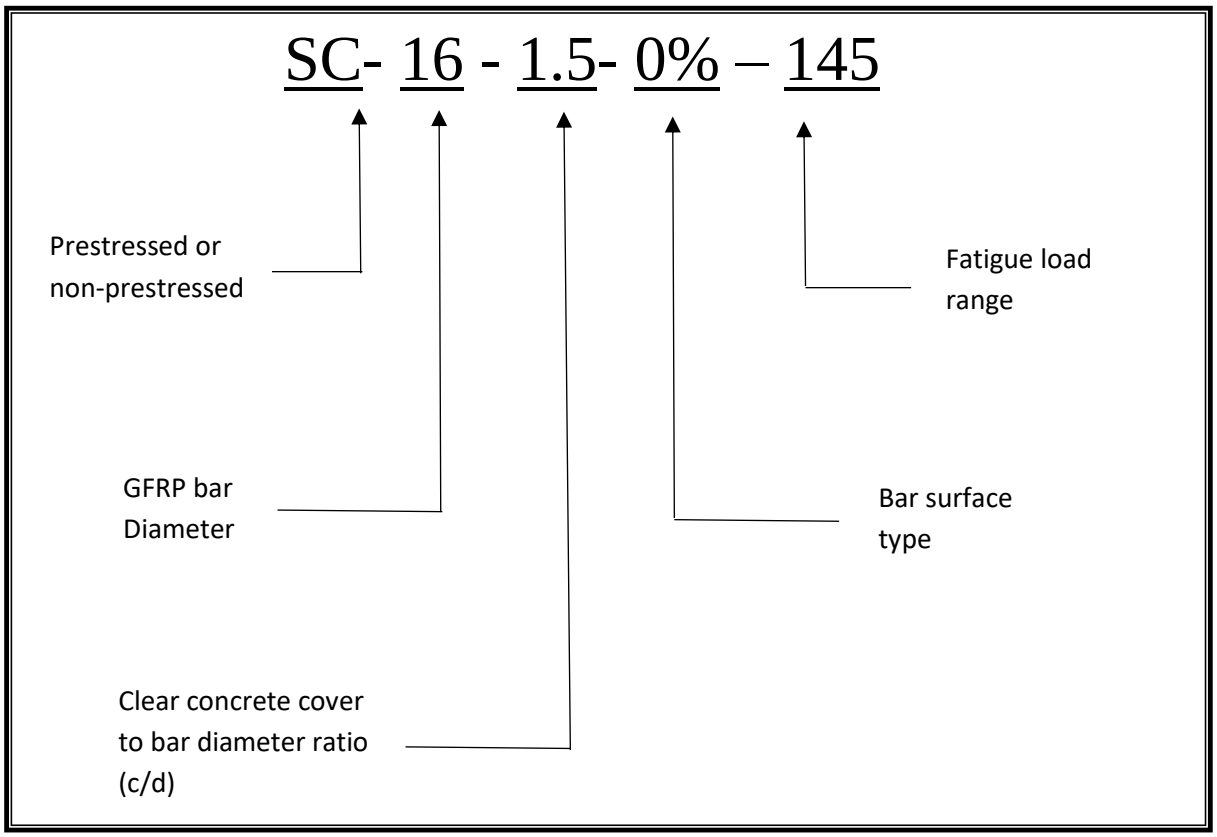

Figure 3.2 Beam notation

3.3 Description of the Test Specimens

3.3.1 Initial Phase

The beam geometry and reinforcement details are shown in Figure 3.3. The overall geometry for all of the beams was the same. The beam cross-section was 150 mm wide × 195 mm deep. The beam depth (from the soffit to centre of reinforcing bar) was kept constant at 195 mm for all of the beams to make sure that the tensile force in the reinforcing bar was the same for a given load. The

total beam height was varied based on the clear concrete cover to bar diameter (c/d) ratio. The total beam length was maintained constant at 2400 mm for all beams, while the shear span length was varied based on the concrete cover to bar diameter (c/d) ratio. For the group of beams that had a clear concrete cover equal to one and half times the bar diameter ($1.5 \cdot d_b$), the shear span length was 500 mm. For the group of beams that had a clear concrete cover equal to three times the bar diameter ($3.0 \cdot d_b$), the shear span length was 350 mm. For the beams with a (c/d) ratio of $1.5 \cdot d_b$, the shear span length was less than the desired bonded length to make sure that the beam would fail in bond and more than 2.5 to ensure slender beam behaviour (no deep beam effect). For the beams with a (c/d) ratio of $3.0 \cdot d_b$, the shear span length was less than the desired bonded length to make sure the beam would fail in bond.

All non-prestressed and prestressed beams were reinforced only with a single GFRP bar in the tension zone. Two bar diameters (M16 and M12) were used as the main tensile reinforcement for both the non-prestressed and prestressed beams. Due to the absence of steel reinforcement in the tension zone, an 8 mm (almost zero resistance) acrylic smooth bar was placed at the mid-height of the concrete beam to help in caging. The acrylic bar was placed at the mid-height of the beam to avoid any structural effect on the bond behaviour between concrete and GFRP bar. All concrete beams (non-prestressed and prestressed) were reinforced with closed steel M10 stirrups (11.3 mm diameter) equally spaced at 80 mm (centreline to centreline) throughout the beam length. The use of uniform shear reinforcement provides a constant confinement along the beam length. Two 10M deformed steel bars were used as a compression steel reinforcement (placed near the top) to increase the compression strength of the beams

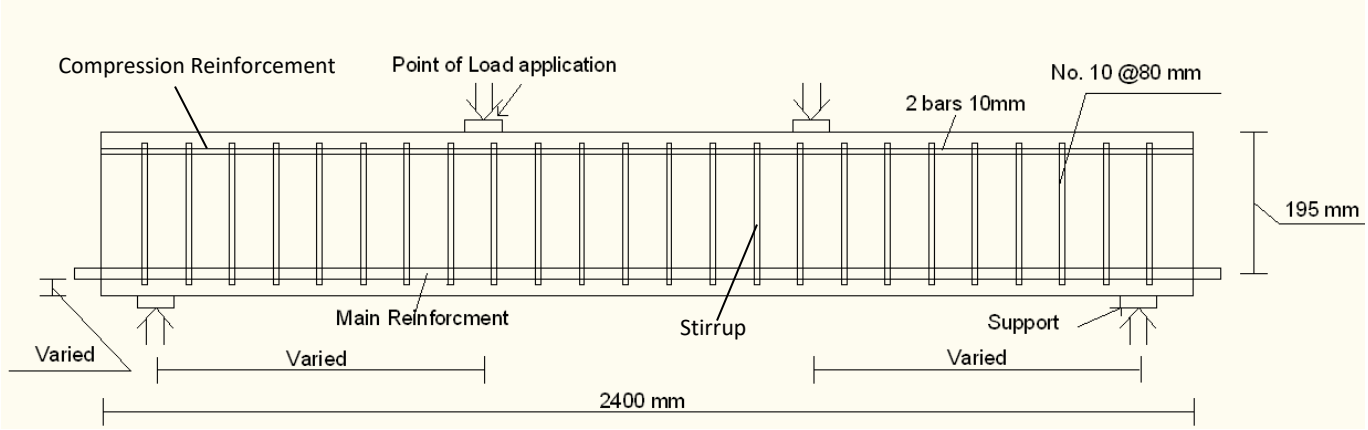

Figure 3.3: Beam configuration and reinforcement details

3.3.2 Main Phase

The beam geometry and reinforcement details are shown in Figure 3.4. The overall geometry for all of the beams was the same. The beam cross-section was 200 mm wide × 235 deep for all beams with concrete cover equal to 25 mm and 200 mm wide × 240 mm for beams with concrete cover equal to 45 mm. The beam depth (from the soffit to centre of reinforcing bar) was kept similar for all the beams to make sure that the tensile force in the reinforcing bar was about equal for a given load . There was a small difference in the beam depth for the beams with 25 mm concrete cover and the beams with 45 mm concrete cover to decrease the difference in bar eccentricity (the distance between the center of the bar to *y'*). The total beam height was varied based on the clear concrete cover to bar diameter (*c*/*d*) ratio. The total beam length was maintained constant at 2000 mm for all beams, while the shear span length was 500 mm for all beams with different concrete cover. The shear span length was less than the desired bonded length to make sure that the beam would fail in bond and more than 2.0 to ensure slender beam behaviour (no deep beam effect). All non-prestressed and prestressed beams were reinforced only with a single GFRP bar in the tension zone. M16 bar diameters was used as the main tensile reinforcement for both the non-prestressed and prestressed beams. Due to the absence of steel reinforcement in the tension zone, a 4 mm (almost zero resistance) acrylic smooth bar was placed at the mid-height of the concrete beam to help in caging. The acrylic bar was placed at the mid-height of the beam to avoid any structural effect on the bond behaviour between concrete and GFRP bar. All concrete beams (non-prestressed and prestressed) were reinforced with closed steel M10 stirrups (11.3 mm diameter) equally spaced at 120 mm (centreline to centreline) throughout the beam length. The spacing between the shear reinforcement was increased to decrease the level of confinement and prompt bond failure between the GFRP bar and the concrete. The use of uniform shear reinforcement provides a constant confinement along the beam length. Two 10M deformed steel bars were used as a compression steel reinforcement (placed near the top) to increase the compression strength of the beams.

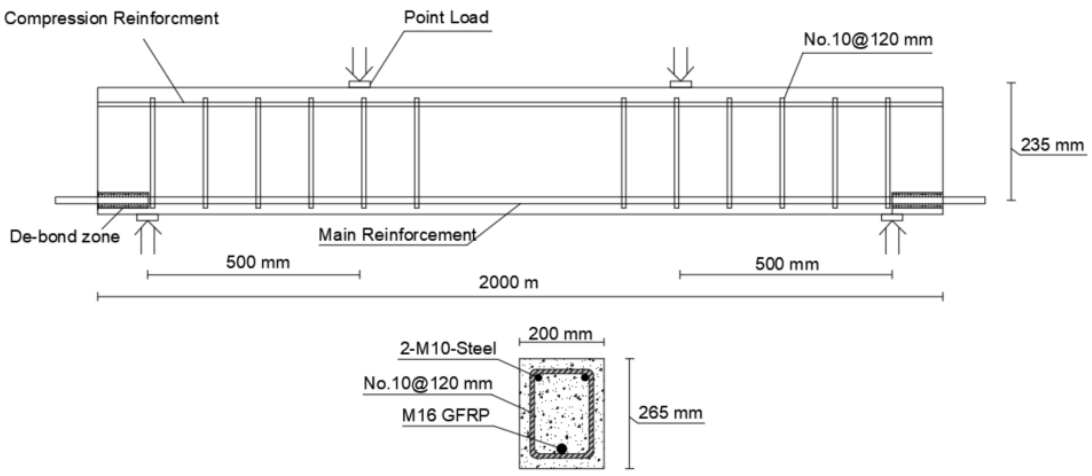

Figure 3.4: Beam configuration and reinforcement details for main Study

3.4 Material Properties

3.4.1 Concrete

The concrete beam specimens were cast in two different concrete pours (batches) for the pilot study and three different concrete pours (batches). The maximum aggregate size for both pours ranged between 10 and 13 mm. In order to measure the ultimate concrete strength, fifteen cylinders, 100 mm diameter × 200 mm long, were cast from each pour. Table 3.1 shows the compressive strength at 28 days for different concrete pours. The third column shows the specimens fabricated from each batch. The concrete strength was decreased in the main study in order to prompt a bond failure between the GFRP bar and the concrete.

Table 3.1 The concrete compressive strength for different pours

Study	Mix #	Compressive Strength (MPa)	Specimens
Pilot Study	1	65.6 ± 4 MPa	All beams reinforced with sand coated GFRP bars.
	2	58.4 ± 2 MPa	All beams reinforced with ribbed GFRP bars.
Main Study	3	46.3 ± 1 MPa	All beams reinforced with sand coated GFRP bars. Concrete cover equal to $1.5 \cdot d_b$.
	4	47.2 ± 1.2 MPa	All beams reinforced with ribbed GFRP bars. Concrete cover equal to $1.5 \cdot d_b$.
	5	47.8 ± 1.6 MPa	All beams reinforced with Sand Coated GFRP bars. Concrete cover equal to $3.0 \cdot d_b$.

3.4.2 GFRP Bars

The mechanical properties for the GFRP bars were provided by the manufacturer. Two types of commercially used GFRP bar were used as primary tensile reinforcement: sand coated, and ribbed bar as shown in Figure 3.5. The sand coated bars were manufactured by Pultrall Inc., Quebec, Canada and the ribbed epoxy coated bar was supplied by Schöck ComBAR, Kitchener, Canada. The nominal mechanical properties for both types of bar are shown in Table 3.

Table 3.2: Properties of GFRP bars

Specifications	Sand Coated		Ribbed	
	#4	#5	#4	#5
Nominal diameter (mm)	12	16	12	16
Tensile strength (MPa)	1434	>1180	1350	>1100
Modulus of elasticity (GPa)	55.3	61.2	55	60
Ultimate strain (%)	2.85	2.60	2.45	2.18
Area (mm^2)	138	196	113	201

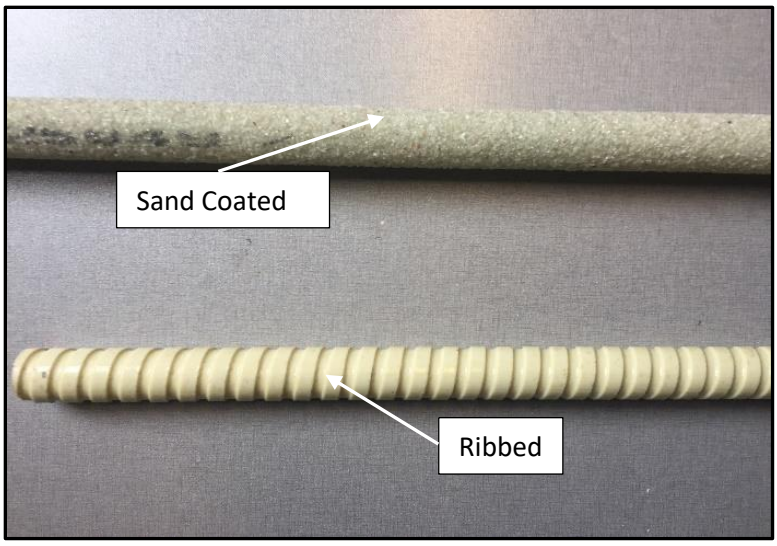

Figure 3.5 GFRP bar used in this study

3.4.3 Steel Reinforcement

Deformed steel bars were used as the compression reinforcement and shear reinforcement for all the concrete beams. Their nominal yield stress was 400 MPa.

3.5 Instrumentation

Instrumentation used for the test specimens included: I) strain gauges mounted on the GFRP reinforcing bar and on the concrete surface, ii) Linear Variable Differential Transformers (LVDT's) and iii) a load cell placed between the actuator and the specimen.

Five mm long strain gauges were mounted on the GFRP bar. Sixty (60) mm long gauges were used for the concrete. Thirteen strain gauges were mounted on the GFRP bar. Six located 50 mm, 200 mm, 350 mm, 500 mm, 650 mm, and 850 mm from the centreline of the support in addition to one gauge at the mid-span, as shown in Figure 3.6. For the sand coated and ribbed epoxy coated bars, the coating was removed over a distance just long enough to glue on the strain gauge. After placing the strain gauge on the GFRP bar, the strain gauge was coated with M-coating to protect the strain gauge. This local protection was used to minimize the disturbance to the bond (between the reinforcement and the concrete) by the strain gauges as much as possible. One strain gauge was mounted on the soffit of concrete beam at mid-span. Two LVDTs were connected to the GFRP

bar at each end of the beam to measure the slip between the bar end and the concrete as shown in Figure 3.6. The vertical deflection of the beam was measured using an external LVDT mounted at mid-span as shown in Figure 3.6.

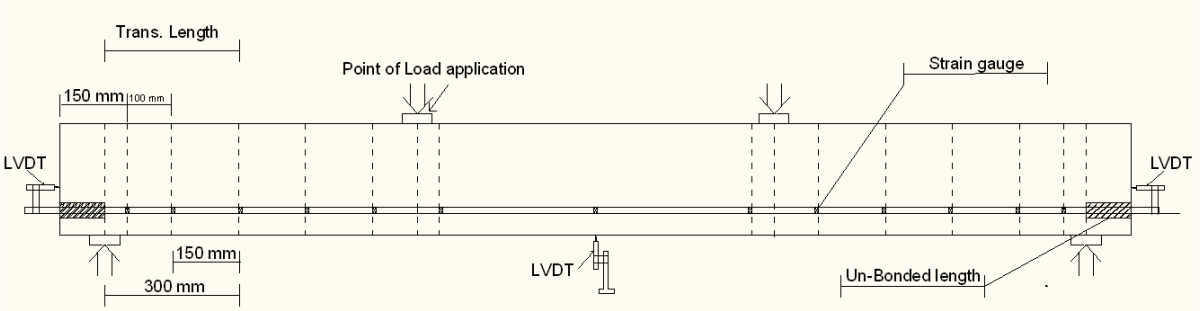

Figure 3.6: Schematic showing strain gauge and LVDT locations

3.6 Specimen Fabrication

3.6.1 Form Work and Steel Caging

Twelve steel and wood forms were assembled to cast twelve reinforced concrete beams (6 non-prestressed reinforced concrete beams and 6 prestressed concrete beams). The six prestressed beams were placed inside the prestressing bed to be ready for prestressed application (will be explained in section 3.7). The formwork made of one steel C channel (250 mm x 65 mm) on the bottom and two re-usable coated ply wood (2200 mm x 350 mm x 20 mm) on both sides. One solid foam (2000 mm x 50 mm) was used to decrease the C channel width to the desire width (200 mm). all plywood sheets were coated oil before casting to ease the beams removal process. Figure 3.7 shows the steel cage inside the form place on the prestressing bed.

Figure 3.7 Steel cage inside the form placed on the prestressing bed

3.6.2 Concrete Placement and Curing

Three cubic meters of ready-mix normal strength concrete was supplied from plant. A conveyer belt was used to cast the concrete inside the forms. Two hand-held concrete vibrators were used to avoid honeycombing problem. After the all forms filled with concrete, a trowel was used to finish the surface and make it ready for flexural test. Figure 3.8 shows the formwork filled with concrete.

Figure 3.8 Formwork filled with concrete

3.7 Prestressing Operation

A special self-reacting steel frame was designed and fabricated to be used as a bed for prestressing operations. Figures 3.10 and 3.11 show prestressing bed photo and the schematic layout of this frame. The serviceability requirement (small deformations under axial prestressing force) was the main factor that governed the design of this frame. The frame consisted of two side beams of W10×39 and double channels (two-C12×20.7) at both ends. The two channels were centred at mid-height of the frame and had a gap of 37.5 mm to allow for free passage of the prestressed FRP bars. All connections were similar and made using eight-1" diameter bolts, so the frame could be easily assembled and disassembled for storage. The frame provided a clear working space 1360 mm wide and 5780 mm long. It has adjustable levelling bolts to allow for precise control of the concrete cover thickness under the prestressed bar. The system allows mechanical locking of the prestressing force, adjustment of the prestress level and gradual release of the load. These advantages make this frame appropriate for a wide range of prestressing applications.

Wedge type anchors were used to grip the prestressing GFRP bars (Figure 3.9a). The patented anchor system was developed previously at the University of Waterloo by Prof. Al-Mayah and Prof. Soudki (2007). The sand coating and the ribbed epoxy coating on the GFRP bars along the length of the anchorage system was removed to allow for uniform gripping (Figure 3.9b). At the live end, each anchorage barrel was fastened to a steel coupler, which has an extended threaded steel bar passing through the steel frame and a 30 Ton single-acting-hydraulic jack (Figure 3.10b). A 240 kN load cell was installed at the dead (restrained) end of each beam. The load from the anchorage barrel at the dead end was transferred to the steel frame. Then the anchorage system at the dead end was seated and placed against the load cell with a spacer plate in between the load cell and the anchorage barrel (Figure 3.10c). The prestressing force was applied gradually using an electrical hydraulic pump. When the target load was achieved, a locking nut on the steel bar was fastened to the steel frame to maintain the load mechanically.

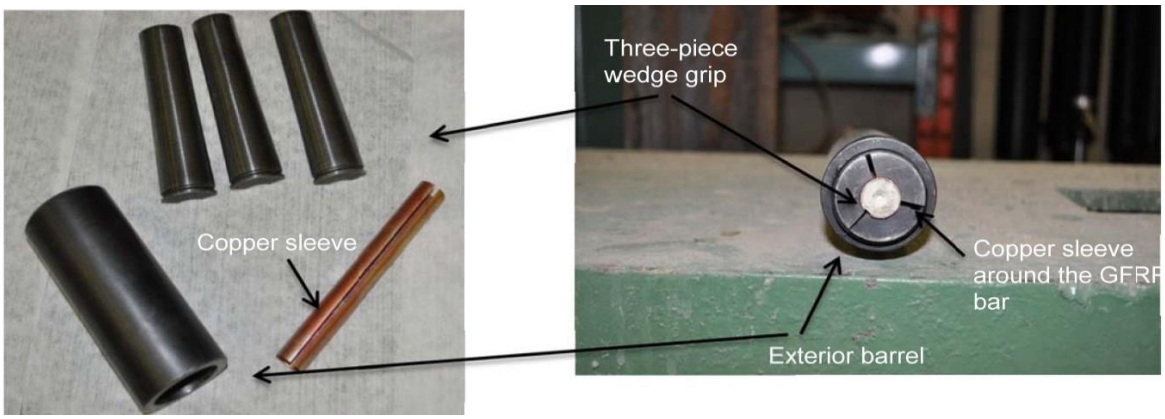

a) Prestressed anchor parts

b) Assembled prestressed anchor

Figure 3.9 Prestressed GFRP bar anchorage device

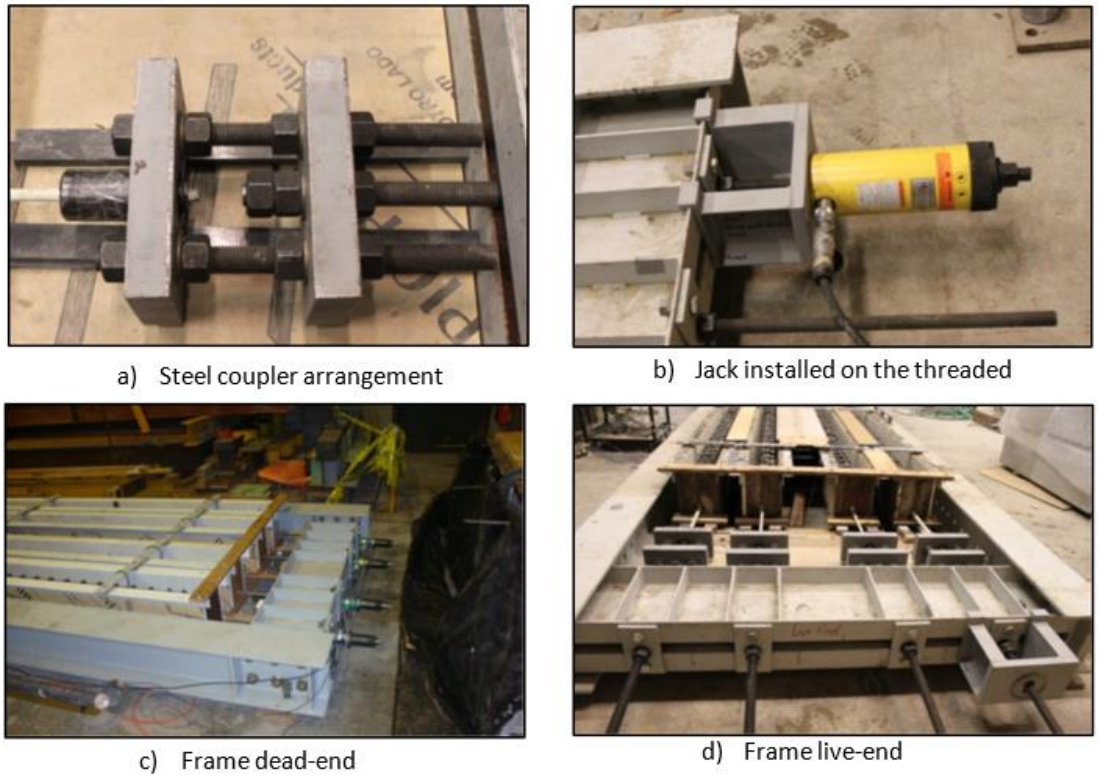

a) Steel coupler arrangement

b) Jack installed on the threaded

c) Frame dead-end

d) Frame live-end

Figure 3.10 Prestressing frame parts

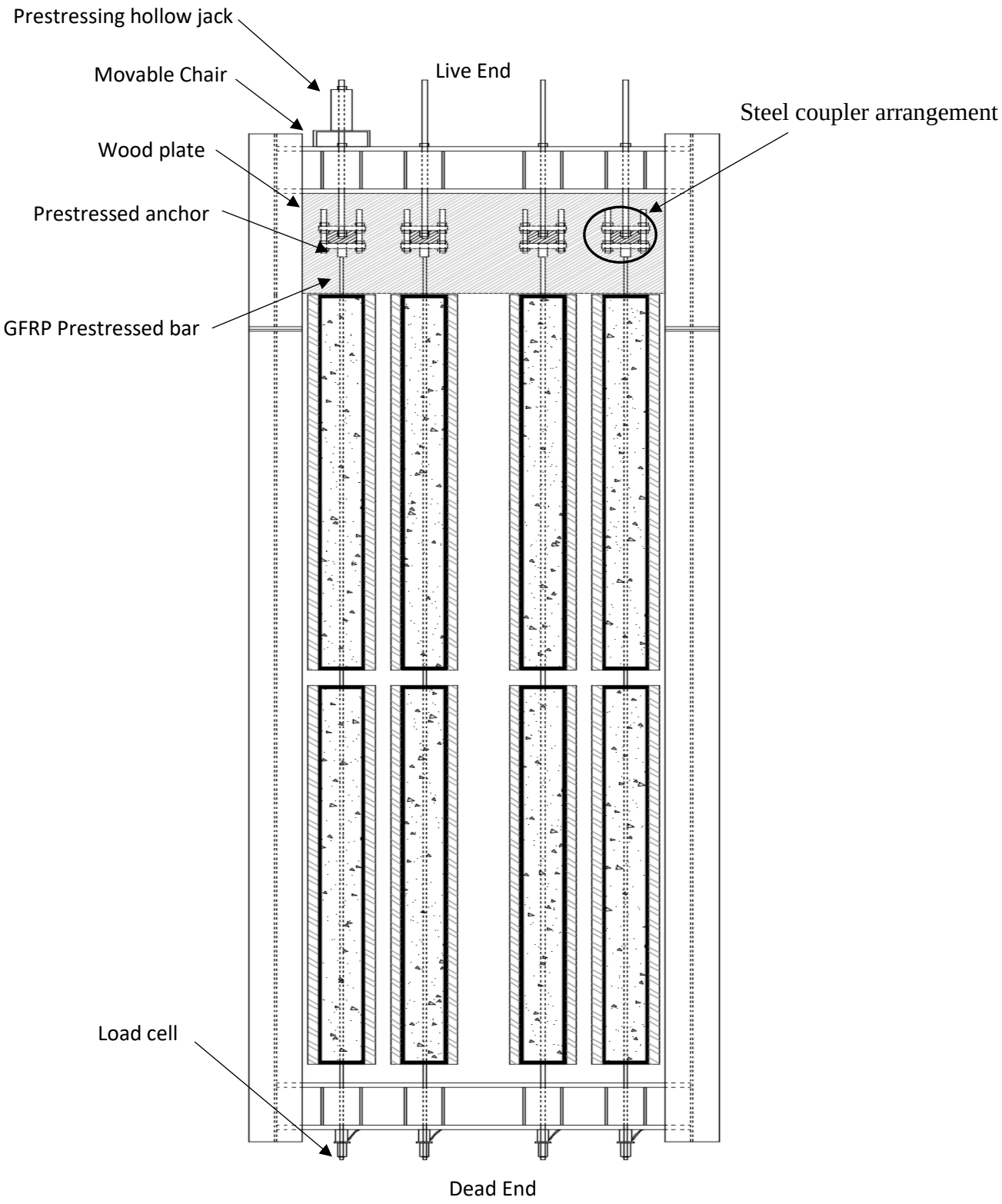

Figure 3.11 A sketch of the prestressing bed (plan view)

3.8 Test Setup and Procedure

Monotonic flexural tests until failure were carried out to determine the failure bond stress for each type of FRP reinforcing bar in this study and to establish the bond stress profile. All prestressed and non-prestressed beams were tested under a four-point static bending regime using a hydraulic 500 kN Uniroyal testing frame. The flexural tests were completed under displacement control at a displacement rate of 1.0 mm/minute. The shear span was 500 mm for all beams. The beam had roller support at one end and a hinge support at the other. Two steel plates (120 mm x 50 mm) were located between the support and the beam. The importance of these plates is to minimize the compression forces produced at the support location at the bottom face of the beam. These compression forces might increase the frictional forces on the GFRP bar, which lead to increase the bond stress between the concrete and the GFRP reinforcement. Figure 3.12 shows the support with extra steel plates. The beam was levelled in the loading frame and centred over the support centrelines. Measurements of load, mid-span deflection (LVDT 1), bar slip at the end of the beam (LVDT 2 and LVDT 3), strain in the GFRP bar, and strain in the concrete at the end of the shear span were collected at a 0.5 second time increments using a National Instruments Data Acquisition System connected to a computer. Figure 3.13 shows the test setup.

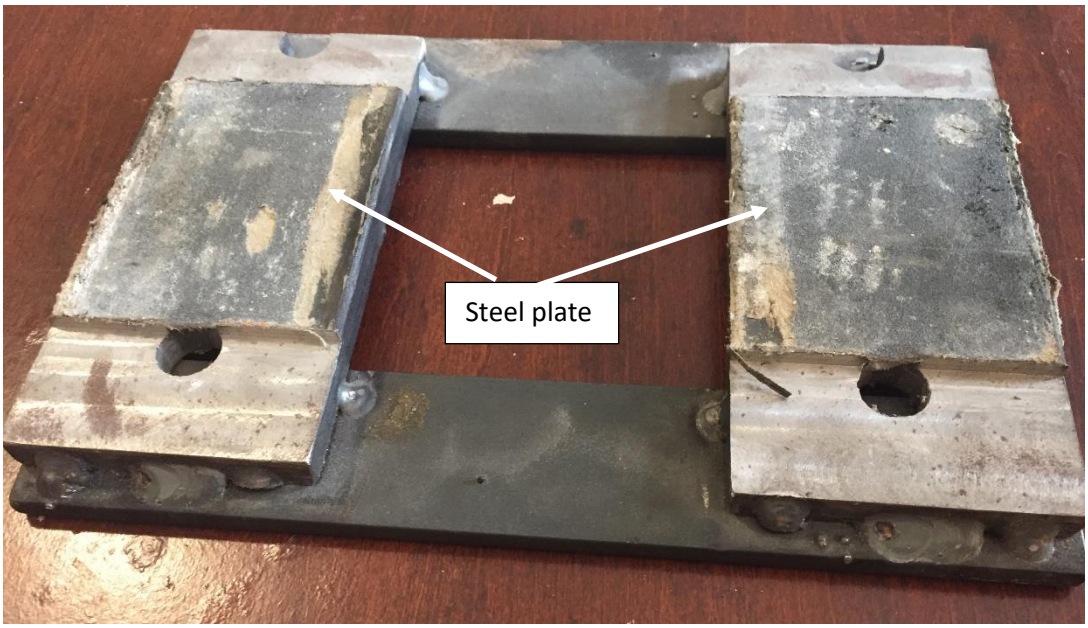

Figure 3.12 Modified support with two steel plates

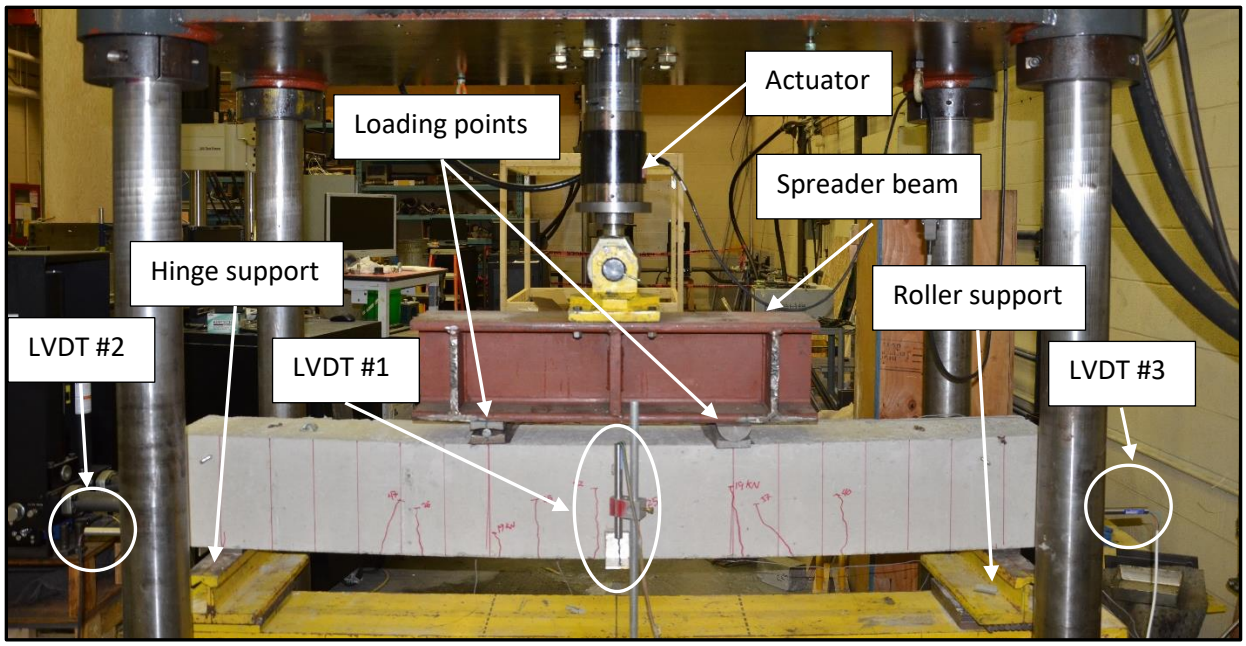

Figure 3.13 Test setup for static and fatigue test

All the fatigue tests were done in load controlled at a frequency of 1 Hz. All beams were loaded manually to the desired ultimate percentage of the static test (peak load) and then the load was dropped to the mean value. Then, the controller was used automatically to apply cyclic loading between the minimum and maximum loading using sine wave curve as shown in Figure 2.8. The minimum loading was kept at 10% of the ultimate monotonic (static) test.

Chapter 4: Experimental Results for Non-Prestressed Beams

4.1 General

This chapter presents and discusses the experimental test results for the beams reinforced with non-prestressed GFRP bar tested under Static and fatigue loading. Twenty-two reinforced concrete beams were cast and tested under monotonic and fatigue loading. These tests were divided into two phases. The first phase was a preliminary study that included ten concrete beams reinforced with GFRP bar. Six concrete beams were reinforced with Sand coated GFRP bars and four beams were reinforced with ribbed GFRP bars. The testing variables were bar diameter (12 mm and 16 mm), GFRP bar surface type (Sand Coated and Ribbed), and concrete cover ($1.5 \cdot d_b$ and $3.0 \cdot d_b$). The second phase was the main study and included twelve reinforced concrete beams. All these beams were reinforced with 16 mm sand coated GFRP bars. The testing variables were concrete cover ($1.5 \cdot d_b$ and $3.0 \cdot d_b$) and type of loading (monotonic and fatigue). For each beam set, one beam was tested under monotonic loading and five beams were tested under fatigue loading.

The objective of this study was to investigate the effect of different loading types (monotonic and fatigue) on the bond strength between the non-prestressed GFRP bar and the surrounding concrete. The first part of this chapter will discuss the test results of phase one (preliminary study). The load deflection curve and the end slip for different beams configuration will be discussed first followed by the typical cracking behaviour and typical strain profile during loading until a beam failed. The second part will present and discuss the phase two (main study) in this study. The same as the first part, the results of the beams that were tested under monotonic (static) loading will be discussed first followed by the beams tested under fatigue loading. Load/life versus mid-span deflection, the cracking behaviour and the strain profile will be presented.

4.2 Test Results for Beams Tested Under Monotonic Loading

4.2.1 Beams Reinforced with Sand Coated GFRP Bar (Preliminary Study)

4.2.1.1 General

Four beams in this phase were tested under monotonic loading until failure. All the beams reinforced with sand coated GFRP bar failed by splitting bond failure between the bar and surrounding concrete. A horizontal splitting debonding cracked started at the loading point and

propagated toward the support. The ultimate capacities are summarized in Table 4.1. Figure 4.1 shows a typical bond failure for the beam reinforced with a sand coated GFRP bar.

Table 4.1: Ultimate capacity and failure mode for sand coated reinforced beams (Pilot)

Specimen notation	Maximum load (kN)	Failure mode
SC-16-1.5-0%	116	splitting bond failure
SC-16-3.0-0%	131	splitting bond failure
SC-12-1.5-0%	96	splitting bond failure
SC-12-3.0-0%	124	splitting bond failure

b- Beam after failure a- GFRP bar after

Figure 4.1: Beam SC-16-1.5-0% after failure

4.2.1.2 Beams Reinforced with 16 mm Sand Coated GFRP Bar

Load vs. mid-span deflection curve

Figure 4.2 shows the Load vs deflection curves for beams reinforced with 16 mm bar diameters and concrete covers equal $1.5 \cdot d_b$ and $3.0 \cdot d_b$. As the load increases, the mid-span deflection increases until the concrete reaches its ultimate tensile strength and cracks appear at mid-span (~18 kN for $1.5 \cdot d_b$ and ~ 25 kN for $3.0 \cdot d_b$). After concrete cracking at mid-span, the load vs. deflection

slope decreases and the mid-span deflection continues to increase with increasing load until the ultimate load is reached.

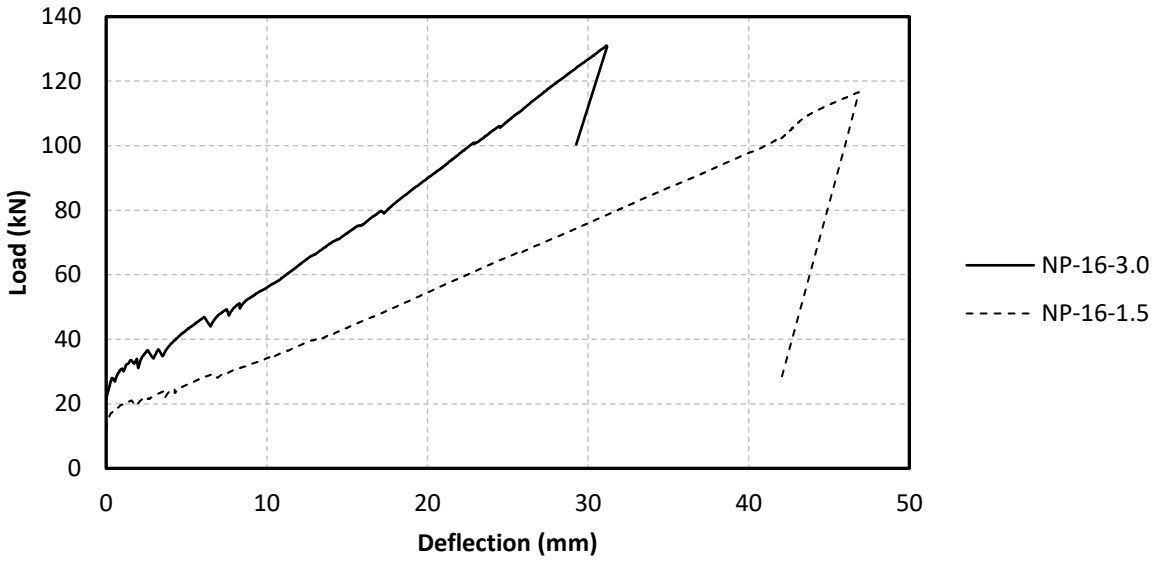

Figure 4.2: Load vs. deflection curve for beams reinforced with 16 mm GFRP bar

The maximum deflection for the beam with a $3.0 \cdot d_b$ concrete cover was almost 32 mm and the maximum deflection for the beam with a $1.5 \cdot d_b$ concrete cover was almost 45 mm. The differences in deflection between the two beams can be attributed to the concrete cover and the shear span length. The shear span for the beam with a concrete cover equal to 3.0 times the bar diameter was 390 mm while the shear span for the beam with the concrete cover equal to 1.5 times the bar diameter was 450 mm.

Cracking behaviour

Figures 4.3a and 4.3b show the load vs. GFRP strain gauge readings and the load versus end slip between the GFRP bar and the surrounding concrete for the beam with a concrete cover equal to 1.5 times the bar diameter, respectively. The GFRP strain readings increase at a low rate with increasing load until the concrete at mid-span cracks at ~20 kN. Then, the readings of the strain gauges located at mid-span increased abruptly as tensile force was suddenly from the concrete transferred to the GFRP bar. As the load increased, cracks appeared in the shear span near the loading point and progressed toward the support. At 80 mm from the loading point, the first crack

appeared when the applied load reached 25 kN. As the test progressed, another crack appeared at 220 mm when the applied load was equal 50 kN. As each crack occurred, the reading of the strain gauge located nearest to the crack increased suddenly as tensile forces were transferred from the concrete to the GFRP bar. The third crack appeared at 390 mm from the loading point at a load level equal 98 kN. As the test proceeded, the crack at 390 mm from the loading point became noticeably wider than any other crack and propagated through the depth of the beam. At the ultimate load, de-bonding occurred between the GFRP bar and the surrounding concrete isolating a prism of concrete. At the same time, a longitudinal crack occurred in the concrete in the shear span starting at 390 mm from the loading point and progressed towards the support. At failure the end slip between the GFRP bar and the beam increased suddenly to 8 mm and coincident with an abrupt drop in load. The cracking behaviour for the reinforced concrete beam with 16 mm sand coated GFRP bar and a concrete cover equal to 3.0 times the bar diameter was similar to that of the beam reinforced with a 16 mm sand coated GFRP bar and a concrete cover equal to 1.5 times the bar diameter. For both beams the crack started at the loading point and moved toward the support as the load increased. Figure 4.4a and 4.4b show the load vs. GFRP strain gauge readings and the load versus end slip between the GFRP bar and the surrounding concrete for the reinforced beam with a concrete cover equal to 3.0 times the bar diameter, respectively

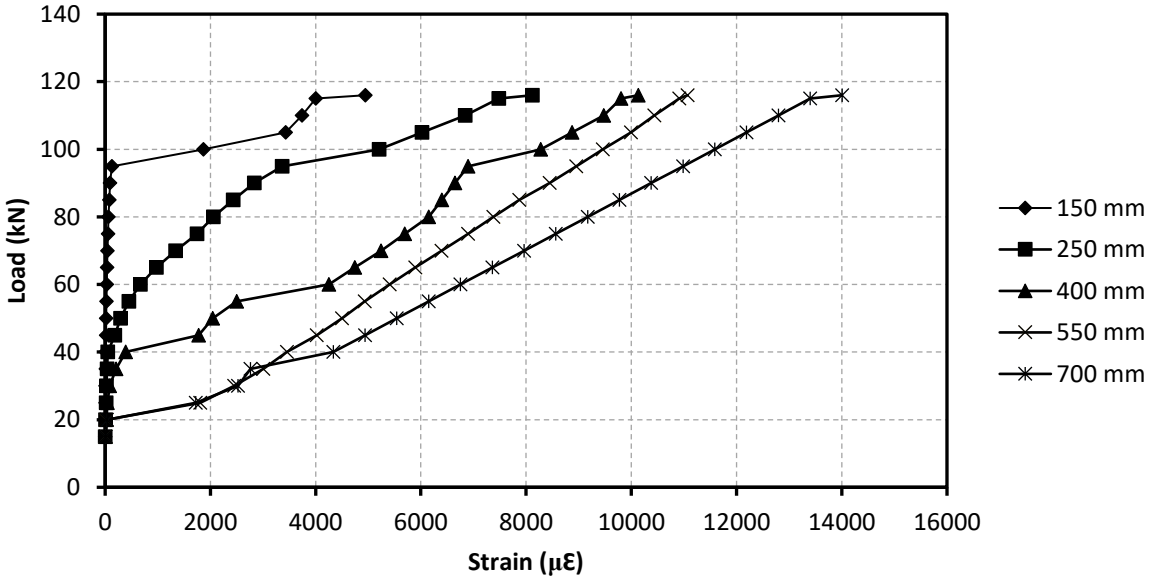

a- Load vs. GFRP bar strain

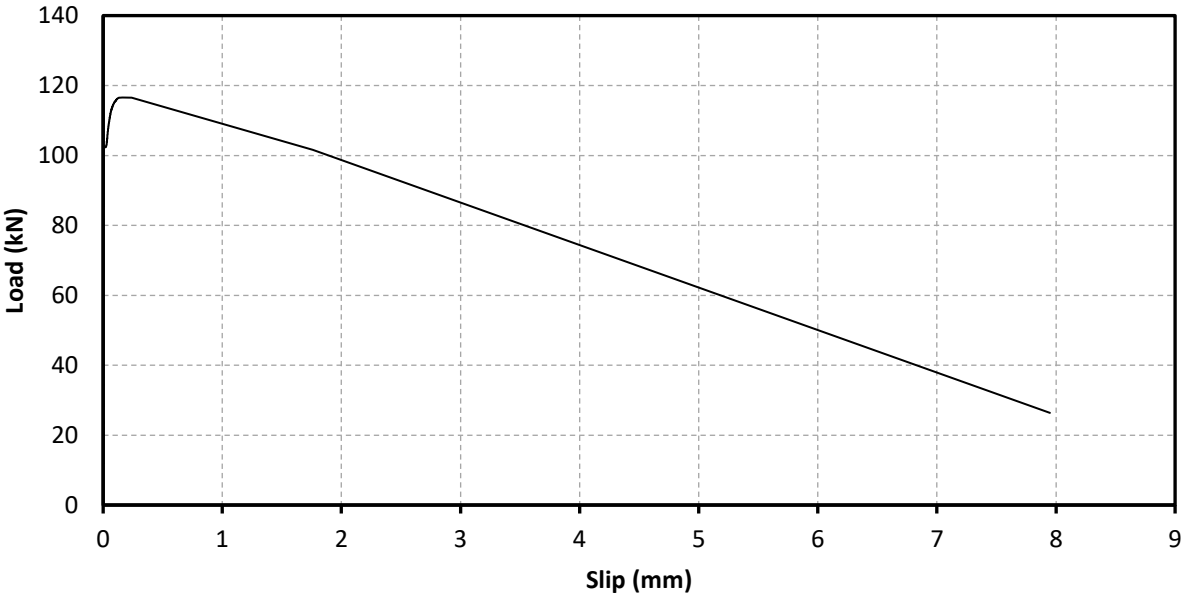

b- Load vs. end slip between the GFRP bar and the concrete

Figure 4.3: Test results for beam SC-16-1.5-0%

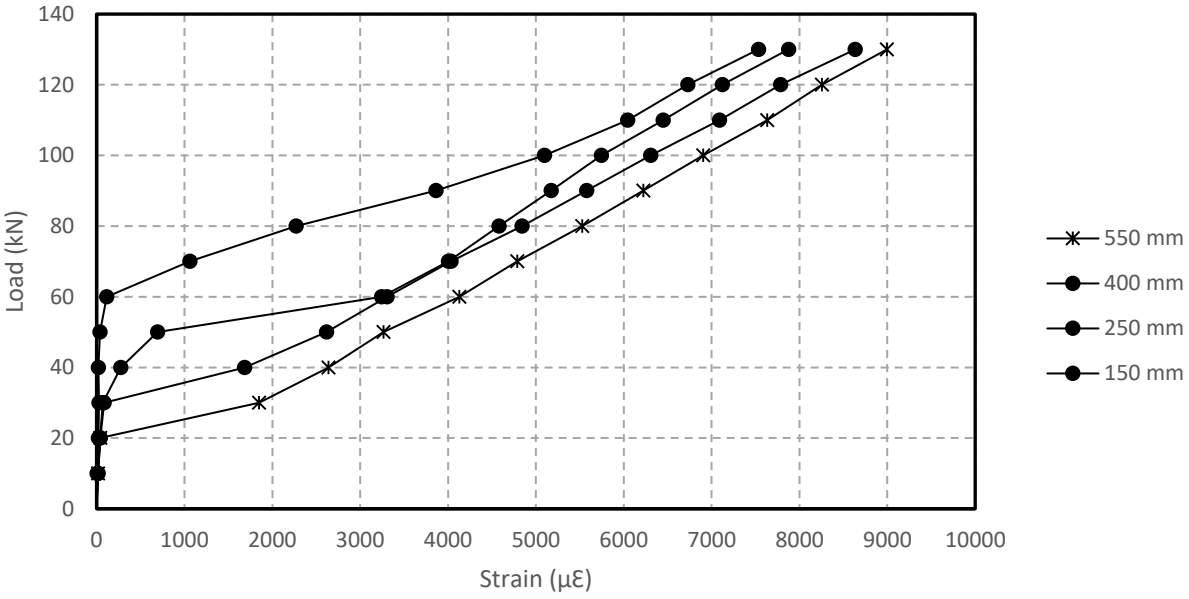

a- Load vs. GFRP bar strain

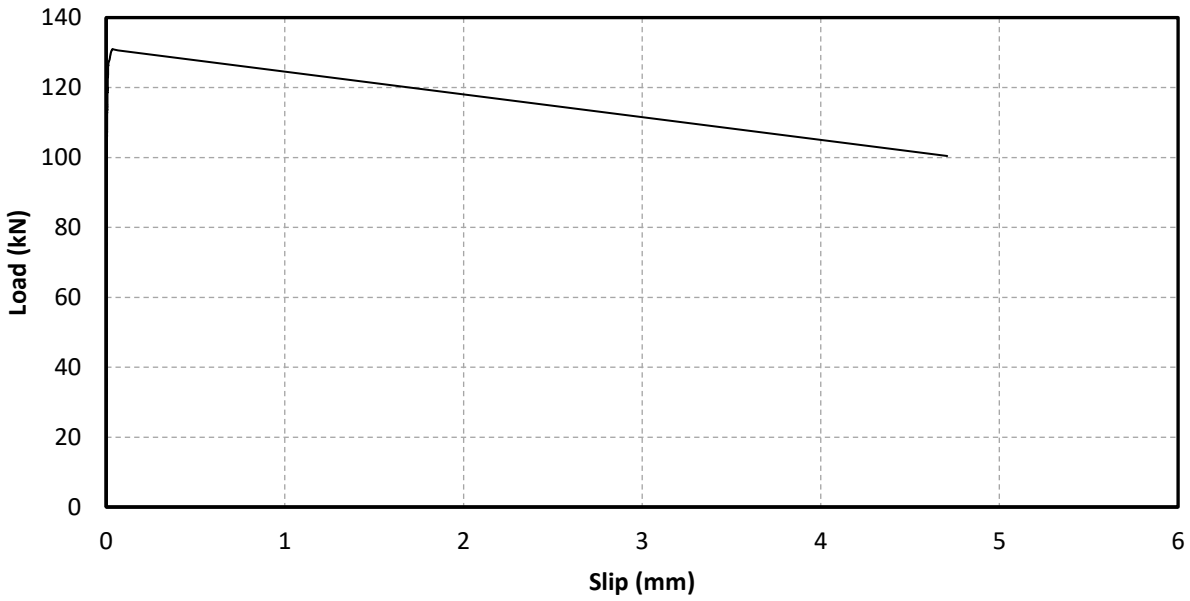

b- Load vs. end slip between the GFRP bar and the concrete

Figure 4.4: Test results for beam SC-16-3.0-0%

Strain profile along the GFRP bar

Typical measured strain distributions along the GFRP bar in the shear span at different load levels are shown in Figure 4.5. At a load level of 15 kN, the strain gauge measurements at all locations was low (between 10 με and 20 με). As the load increased to 20 kN, the first concrete crack appeared at mid-span and the strain gauge reading at mid-span increased. The strain gauge reading at 550 mm increased and was almost equal to the reading at mid-span indicating partial de-bonding between these two locations. At a load of 60 kN, the reading at 400 mm jumped to 4293 με and was almost equal to the strain gauge reading at 550 mm. this change in the strain reading indicates that the GFRP bar is partially de-bonded from the concrete in this region and that the stress raiser along the bar is moving towards the support. As the load increased further, the strain gauge readings at 400 mm, 550 mm, and mid-span increased and remained almost equal and at the same time the readings at 150 mm and 250 mm increased until the peak load of 116 kN was reached. At the peak load, the strain gauge reading at 150 mm was equal to 4942 με.

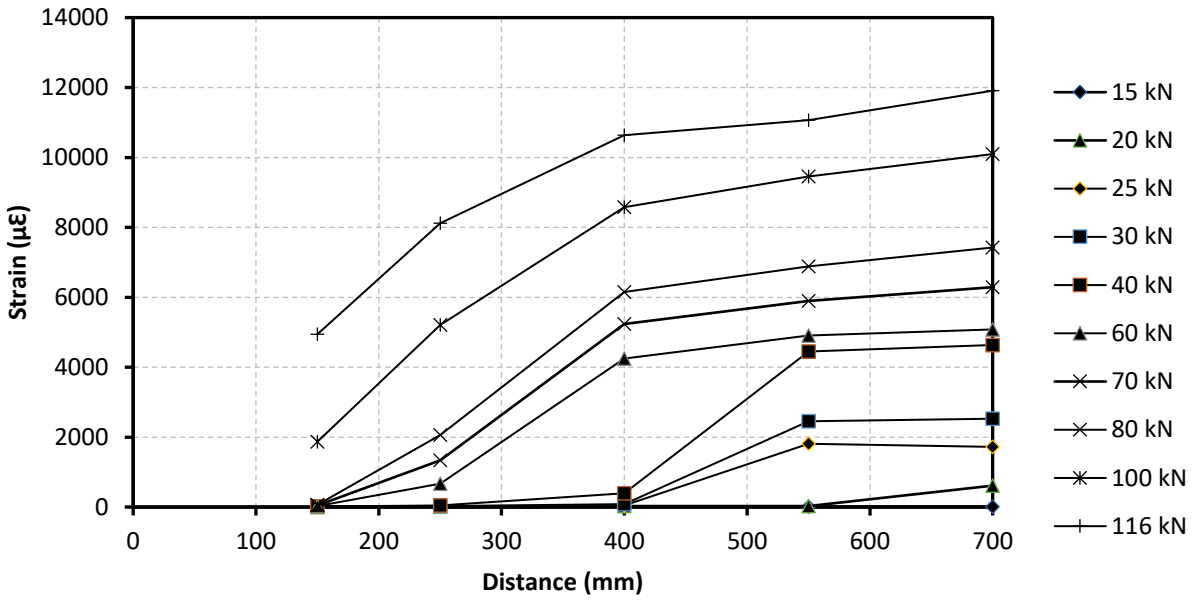

Figure 4.5: Strain distribution along the GFRP bar for beam SC-16-1.5-0%

4.2.1.3 Beams Reinforced with 12.7 mm Sand Coated GFRP Bar

Load vs. mid-span deflection curve

Figure 4.6 shows the load vs deflection curve for beams reinforced with 12 mm bar diameter and a concrete cover equal $1.5 \cdot d_b$ and $3.0 \cdot d_b$. The load vs deflection curve was divided into two segments for both beams. Before the concrete at mid span reached its tensile strength and the first crack appeared, the slope was very steep. As the load increased and the first crack appeared, (~18 kN for $1.5 \cdot d_b$ and ~ 38 kN for $3.0 \cdot d_b$). The load vs. deflection slope decreased and the mid-span deflection continued to increase with the load until the ultimate load was reached. The ultimate mid-span deflection was 48 mm for the beam with a concrete cover equal 1.5 times the bar diameter and 54 mm for the beams with a concrete cover equal 3.0 times the bar diameter.

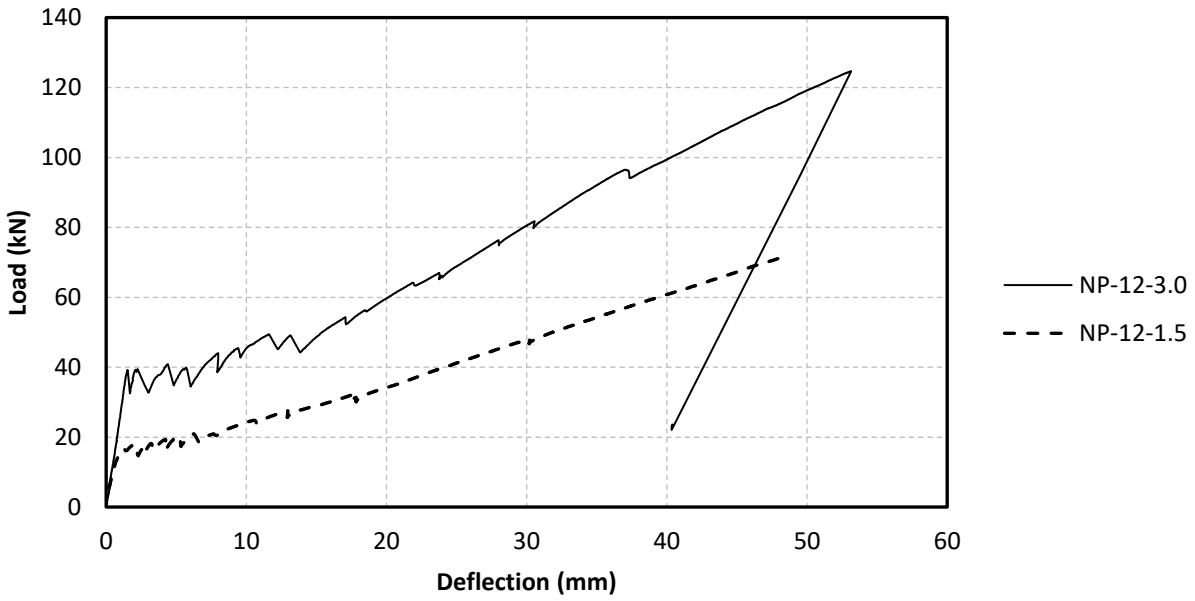

Figure 4.6: Load vs. deflection curve for beams reinforced with 12 mm GFRP bar

Cracking behaviour

Beam SC-12-1.5-0% was reinforced with a 12 mm sand coated GFRP bar. Figure 4.7a shows the load vs. GFRP strain gauge readings and Figure 4.7b shows the load vs. end-slip between the GFRP bar and the concrete. The strain gauge measurements located at mid-span increased as the concrete cracked and the tensile force in the concrete cross section was suddenly transferred to the GFRP bar. Like beam SC-16-1.5-0%, as the load increased, cracks were observed in the shear span starting near the loading point location and progressing towards the support. The first crack that appeared in the shear span was 8 mm from the loading point at a load of 19 kN. As the test proceeded, this crack was at all times noticeably wider than any of the other cracks. When the applied load reached 47 kN, another crack appeared at 190 mm. As each crack occurred, the reading of the strain gauge located nearest to the crack increased suddenly as the tensile forces were transferred from the concrete to the GFRP bar. As the test proceeded, a third crack appeared at 410 mm from the loading point when the applied load was 87 kN. As the load approached its peak value, the crack at 410 mm from the loading point widened and propagated through the depth of the beam. Then, it connected with the large vertical crack at 390 mm from the loading point, isolating a prism of concrete. At the peak load, de-bonding occurred between the GFRP bar and the concrete and an isolated prism of concrete separated from the GFRP bar and the beam. At the

same time, longitudinal cracks occurred closer to the support, but the concrete did not separate from the bar. The cracking behaviour for the reinforced concrete beam with 12 mm sand coated GFRP bar and concrete cover equal to 3.0 times the bar diameter was similar to that of the beam reinforced with 12 mm sand coated GFRP bar and a concrete cover equal 1.5 times the bar diameter. For both beams, the crack started at the loading point and moved toward the support as the load increased. Figure 4.8a and 4.8b show the load vs. GFRP strain gauge readings and the load versus end slip between the GFRP bar and the surrounding concrete for the reinforced beam with a concrete cover equal to 3.0 times the bar diameter, respectively.

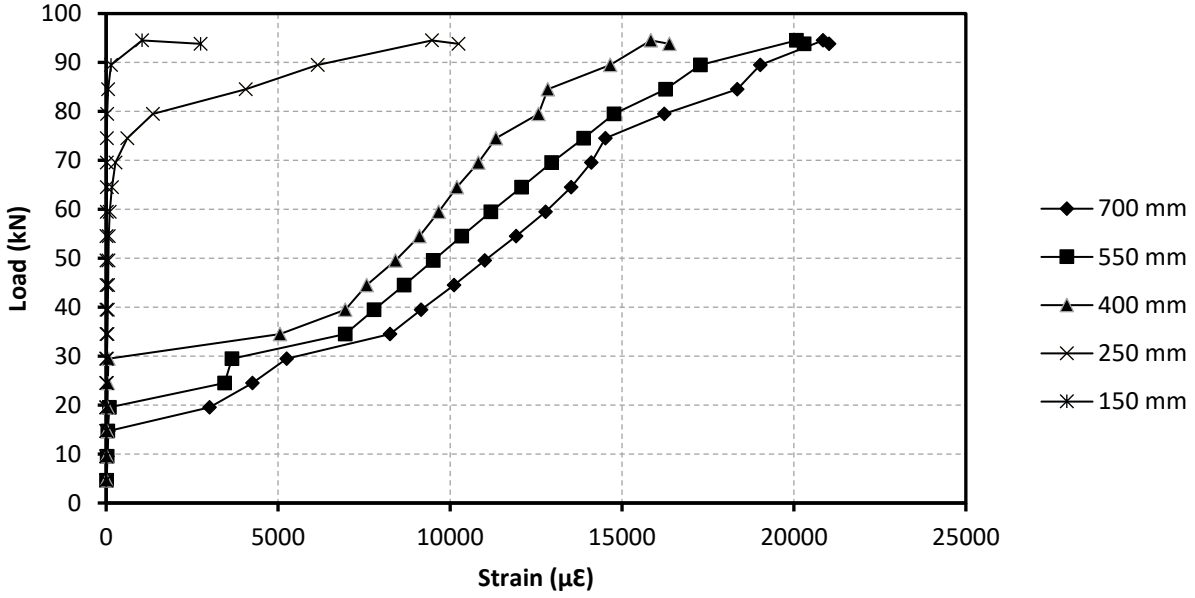

a- Load vs. GFRP bar strain

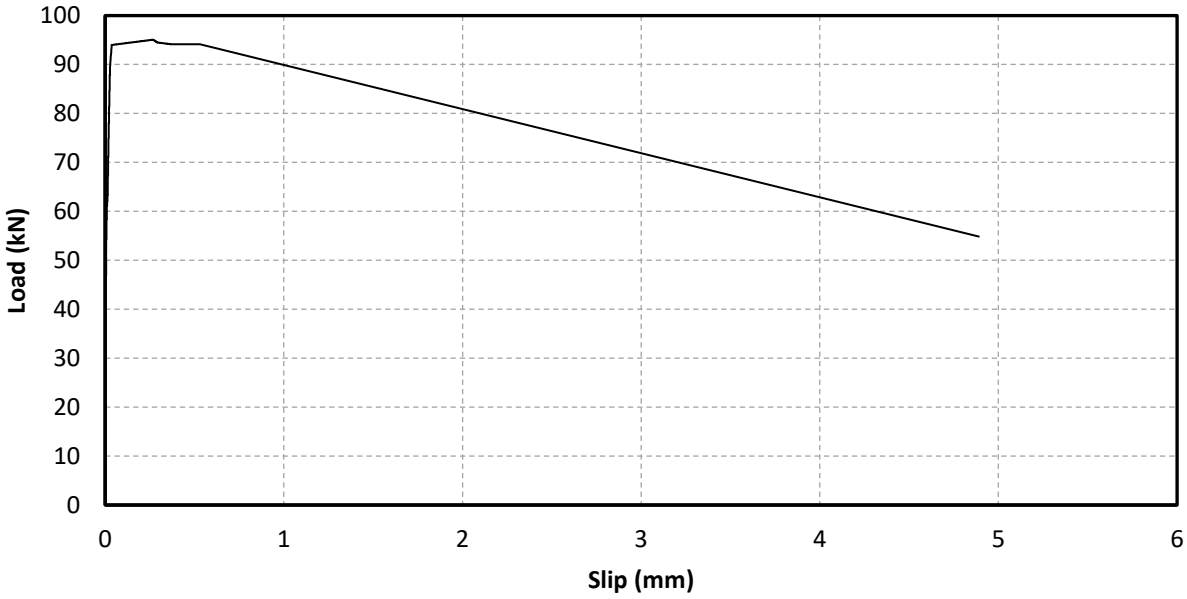

b- Load vs. end slip between the GFRP bar and the concrete

Figure 4.7: Test results for beam SC-12-1.5-0%

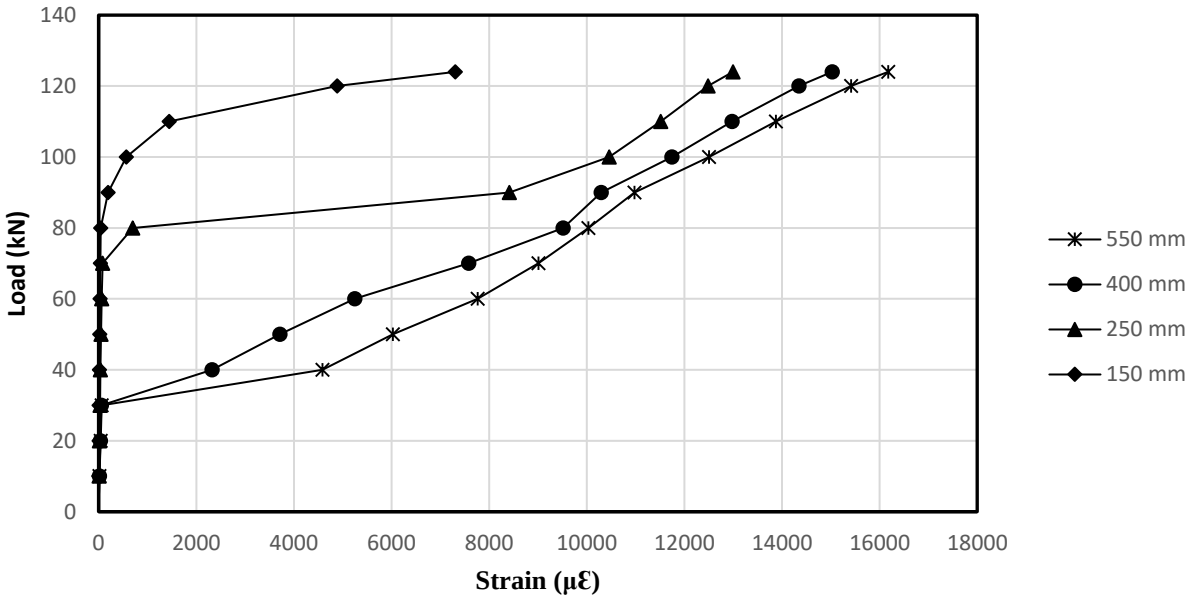

a- Load vs. GFRP bar strain

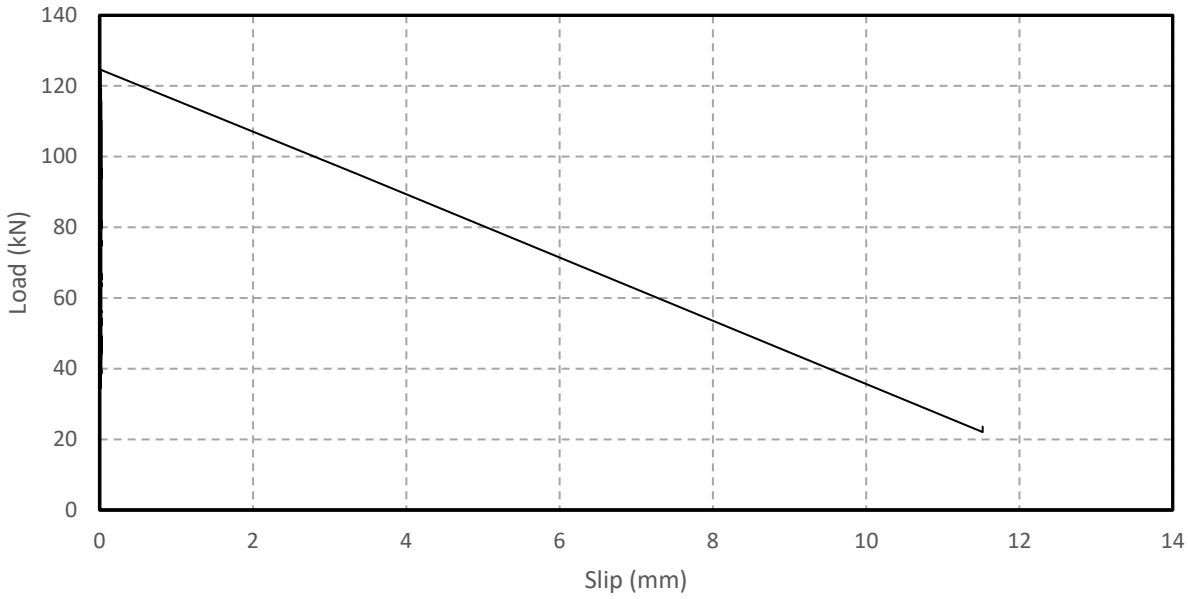

b- Load vs. end slip between the GFRP bar and the concrete

Figure 4.8: Test results for beam SC-12-3.0-0%

Strain profile along the GFRP bar

Figure 4.9 shows the measured strain distribution along the GFRP bar for beam SC-12-1.5-0%. The axial strain distribution along the GFRP bar in the shear span at different load levels is shown on Figure 4.8. At a load level of 12 kN, the strain gauge measurements at all locations were low (between 10 με and 20 με). As the load increased to 19 kN, the first concrete crack appeared at mid-span and the strain gauge reading at mid-span increased to 2346 με. As the test proceeded and the load reached 48 kN, the strain gauge reading at 550 mm increased to 4254 με but it was less than the strain at mid-span indicating only partial de-bonding between 550 mm and mid-span. When the applied load reached 90 kN, the strain gauge reading at 250 mm increased significantly indicating that the partial de-bonding was moving toward the support. At failure (96 kN), the ultimate strain at 150 mm was equal to 2265 με.

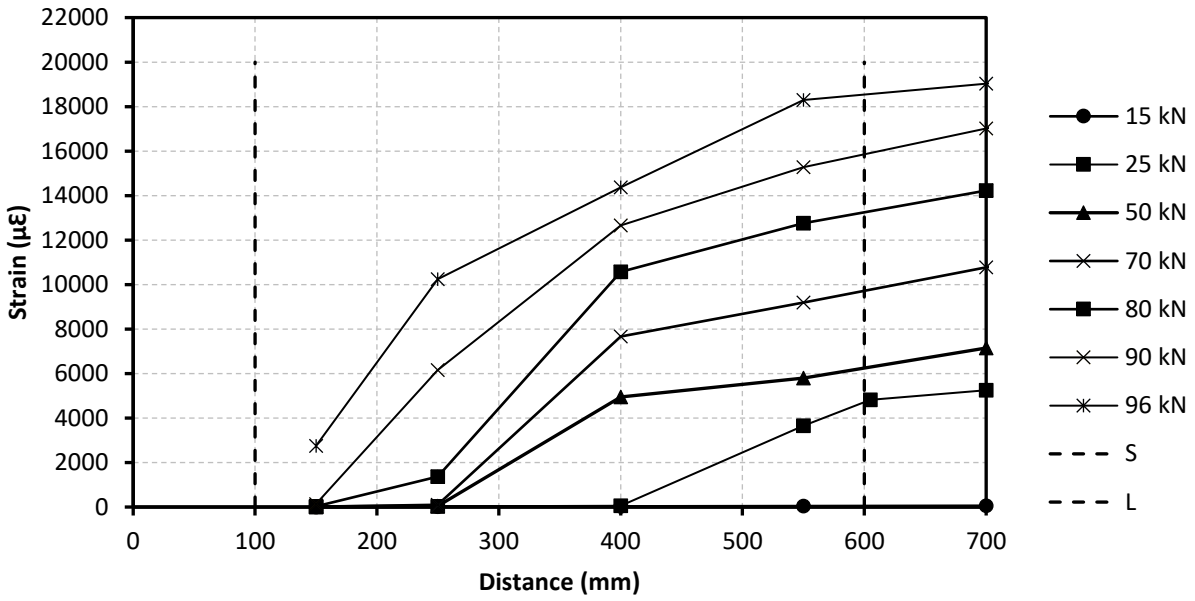

Figure 4.9: Strain distribution along the GFRP bar for beam SC-12-1.5-0%

4.2.2 Beams Reinforced with Ribbed GFRP bar (Preliminary Study)

4.2.2.1 General

Four beams in this phase were tested under monotonic loading until failure. Two failure modes were observed: bond failure between the GFRP bar and the surrounding concrete and the concrete crushing. The ultimate capacity summarises in Table 4.2.

Table 4.2: Ultimate capacity and failure mode for ribbed coated reinforced beams (pilot)

Specimen notation	Max load (kN)	Failure mode
R-16-1.5-0%	123	Concrete crushing/bond
R-16-3.0-0%	115	Splitting bond failure
R-12-1.5-0%	83	Concrete crushing/bond
R-12-3.0-0%	121	Concrete crushing

4.2.2.2 Beams Reinforced with 16 mm Ribbed Bar

Load Vs mid-span deflection curve

Figure 4.10 shows the Load vs deflection curve for beams reinforced with a 16 mm bar diameter and concrete cover equal $1.5 \cdot d_b$ and $3.0 \cdot d_b$. As the load increases, the mid-span deflection increases until the concrete reaches its ultimate tensile strength and cracks appear at mid-span (~18 kN for $1.5 \cdot d_b$ and ~ 35 kN for $3.0 \cdot d_b$). After concrete cracking at mid-span, the load vs. deflection slope decreases and the mid-span deflection continues to increase with the load until the ultimate load is reached.

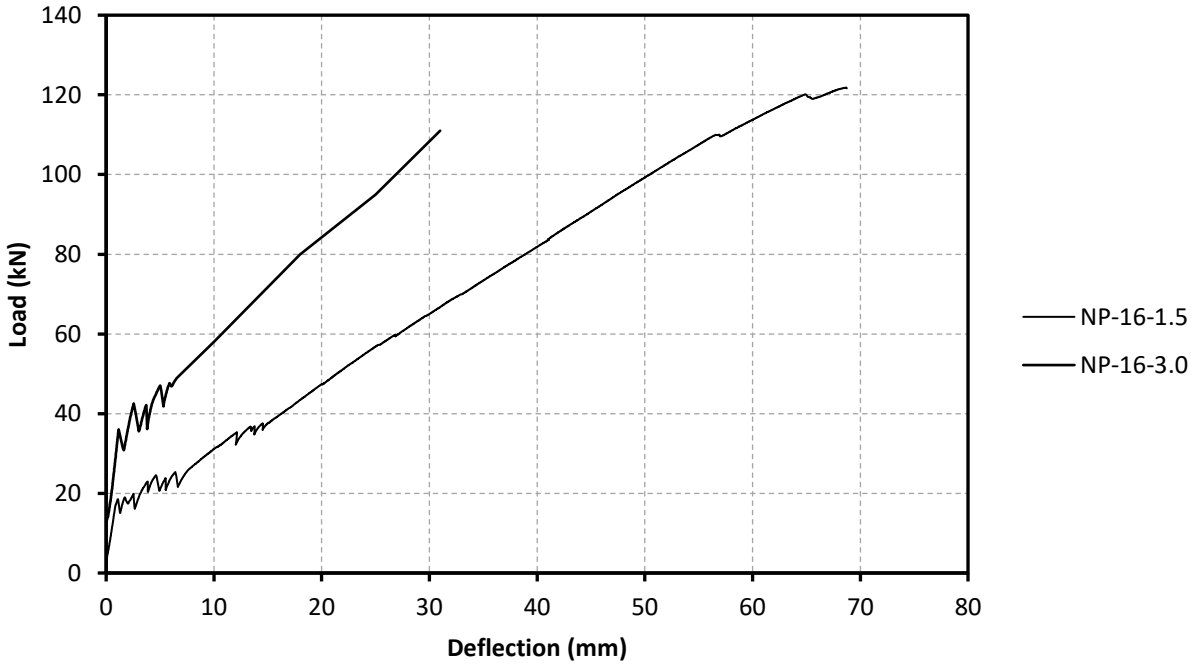

Figure 4.10: Load vs. deflection curve for beams reinforced with 16 mm GFRP bar

Cracking behaviour

Beam R-16-1.5-0% was reinforced with a 16 mm Ribbed GFRP bar. Figure 4.11a shows the load vs. GFRP strain gauge readings and Figure 4.11b shows the load vs. end-slip between the GFRP bar and the concrete. The strain gauge measurements located at mid-span increased as the concrete cracked and the tensile force in the concrete cross section was suddenly transferred to the GFRP bar. As the load increased, cracks were observed in the shear span starting near the loading point

location and progressing towards the support. The first crack that appeared in the shear span was 15 mm from the loading point at a load of 19 kN. As the test proceeded, this crack was at all times noticeably wider than any of the other cracks. When the applied load reached 35 kN, another crack appeared at 100 mm. As each crack occurred, the reading of the strain gauge located nearest to the crack increased suddenly as the tensile forces were transferred from the concrete to the GFRP bar. As the test proceeded, a third crack appeared at 210 mm from the loading point when the applied load was 62 kN. As the load approached its peak value, the crack at 210 mm from the loading point widened and propagated through the depth of the beam. Then, it connected with the large vertical crack at 310 mm from the loading point, isolating a prism of concrete. At the peak load, de-bonding occurred between the GFRP bar and the concrete and an isolated prism of concrete separated from the GFRP bar and the beam. For the beam reinforced with a 16 mm ribbed GFRP bar, the concrete crushed at top of the beam due to the large deflection of the beam at mid span making the area that resisted the compression force too small to carry more force even with the compression reinforcement. Figures 4.11a and 4.11b show the cracking behaviour just before the concrete crushed. The cracking behaviour for the reinforced concrete beam with a 16 mm Ribbed GFRP bar and a concrete cover equal to 3.0 times the bar diameter was similar to the beam with a concrete cover equal to 1.5 times the bar diameter, but the concrete did not crush, and the beam failed by de-bonding between the GFRP bar and the surrounding concrete. Figure 4.12a and 4.12b show the load vs. GFRP strain gauge readings and the load versus end slip between the GFRP bar and the surrounding concrete for reinforced beam with concrete cover equal 3.0 times the bar diameter, respectively.

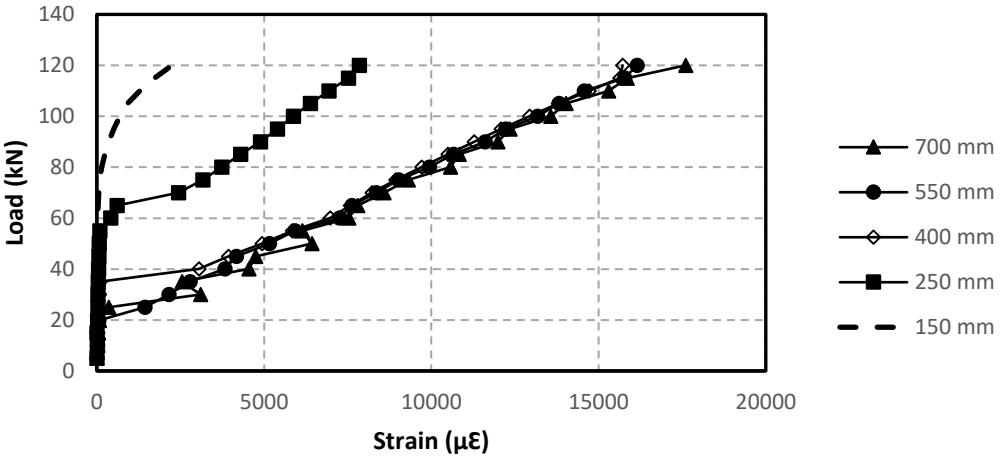

a- Load vs. GFRP bar strain

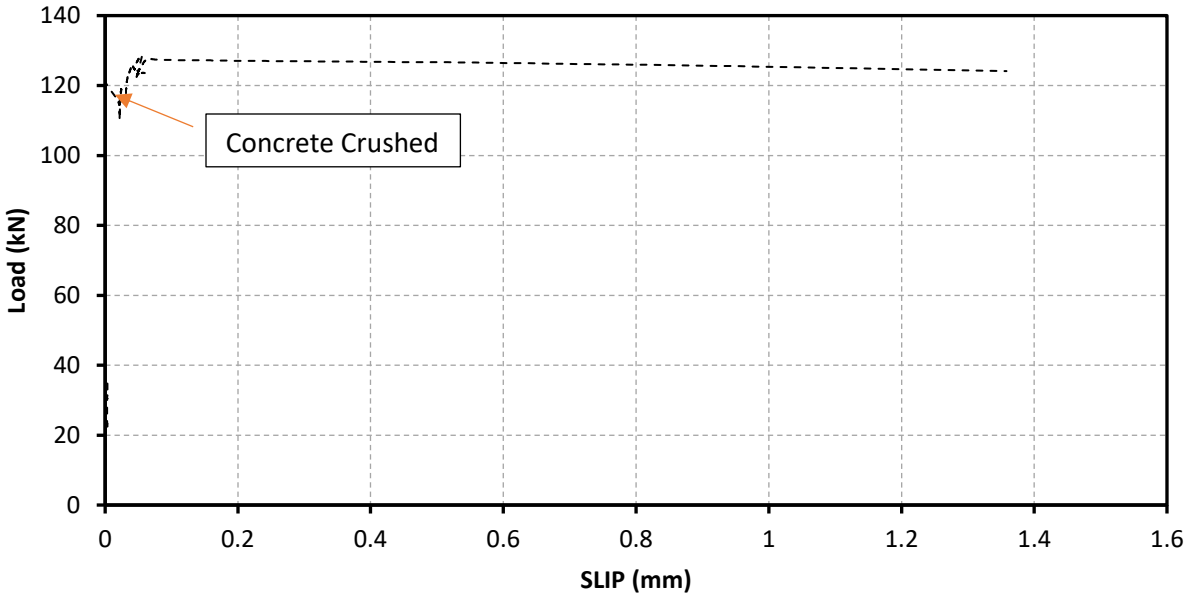

b- Load vs. end slip between the GFRP bar and the concrete

Figure 4.11: Test results for beam R-16-1.5-0%

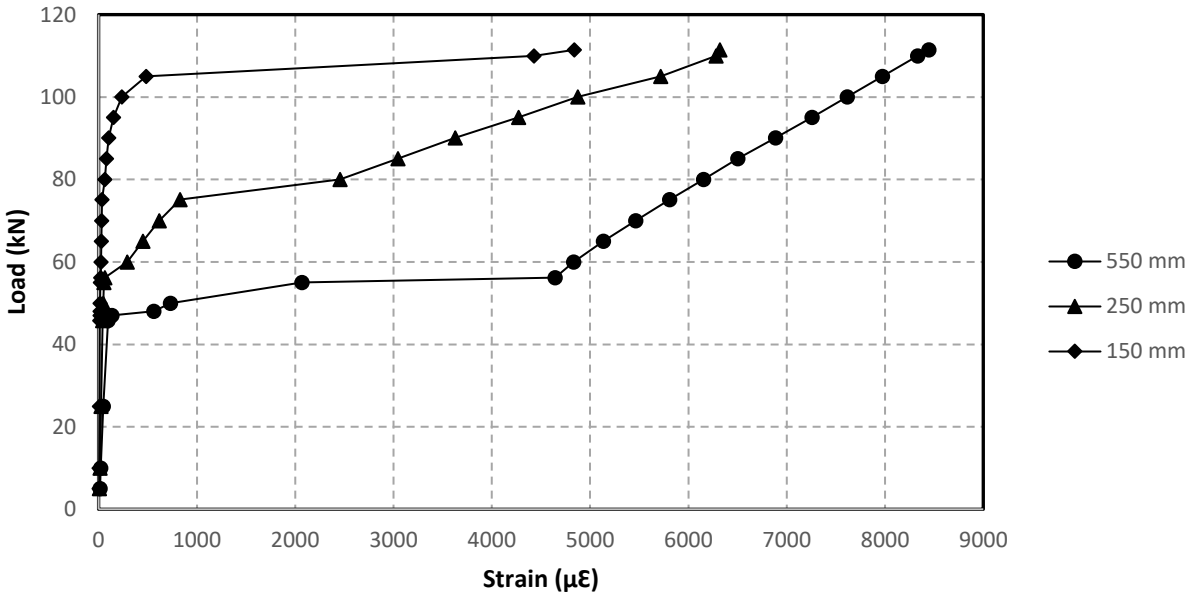

a- Load vs. GFRP bar strain

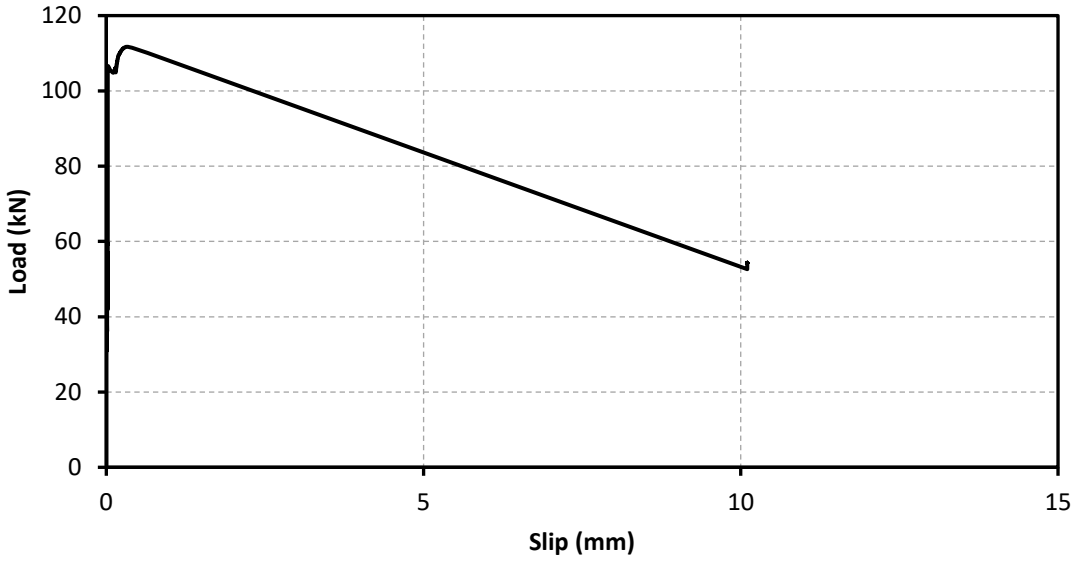

b- Load vs. end slip between the GFRP bar and the concrete

Figure 4.12: Test results for beam R-16-3.0-0%

4.2.2.3 Beams Reinforced with a 12 mm Ribbed Bar

Load Vs mid-span deflection curve

Figure 4.13 shows the Load vs mid-span deflection curves for beams reinforced with a 12 mm bar diameter and a concrete cover equal $1.5 \cdot d_b$ and $3.0 \cdot d_b$. As the load increases, the mid-span deflection increases until the concrete reaches its ultimate tensile strength and cracks appear at mid-span (~18 kN for $1.5 \cdot d_b$ and ~ 38 kN for $3.0 \cdot d_b$). After concrete cracking at mid-span, the load vs. deflection slope decreases and the mid-span deflection continues to increase with the load until the ultimate load is reached.

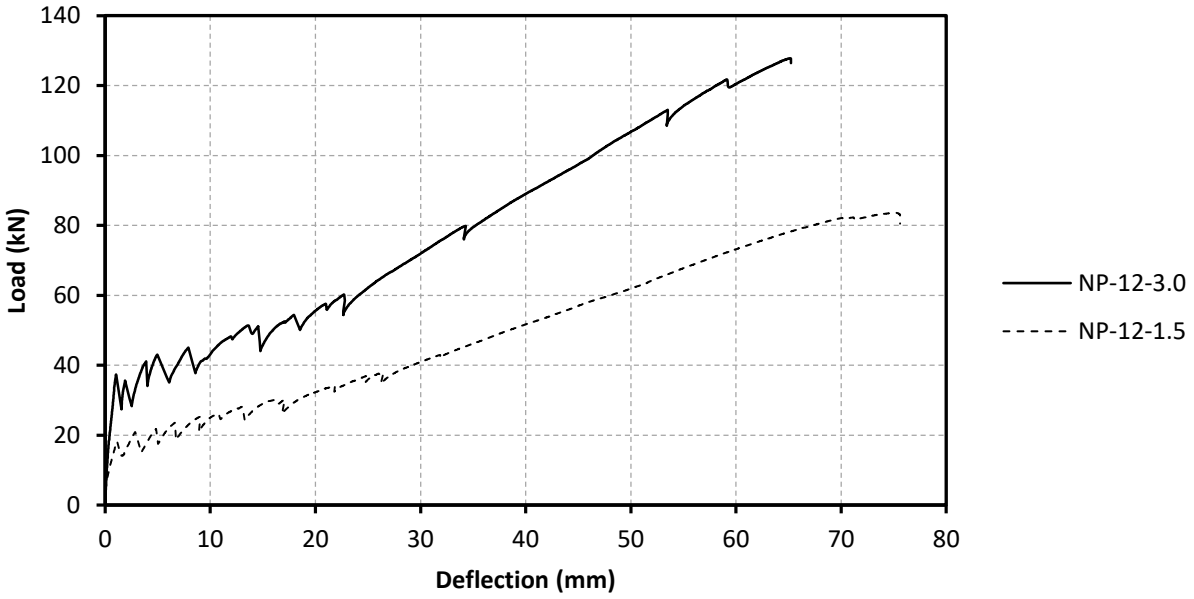

Figure 4.13: Load vs. deflection curve for beams reinforced with 12 mm GFRP bar

Cracking behaviour

Beam R-12-1.5-0% was reinforced with a 12 mm Ribbed GFRP bar. Figure 4.14a shows load vs. GFRP strain gauge readings and Figure 4.14b shows load vs. end-slip between the GFRP bar and the concrete. The strain gauge measurements located at mid-span increased as the concrete cracked and the tensile force in the concrete cross section was suddenly transferred to the GFRP bar. As the load increased, cracks were observed in the shear span starting near the loading point location and progressing towards the support. The first crack that appeared in the shear span was 35 mm from the loading point at a load of 18 kN. As the test proceeded, this crack was at all times noticeably wider than any of the other cracks. When the applied load reached 35 kN, another crack appeared at 60 mm. As each crack occurred, the reading of the strain gauge located nearest to the crack increased suddenly as the tensile forces were transferred from the concrete to the GFRP bar. As the test proceeded, a third crack appeared at 210 mm from the loading point when the applied load was 62 kN. As the load approached its peak value, the crack at 210 mm from the loading point widened and propagated through the depth of the beam. Then, it connected with the large vertical crack at 185 mm from the loading point, isolating a prism of concrete. At the peak load, de-bonding occurred between the GFRP bar and the concrete, and an isolated prism of concrete separated from the GFRP bar and the beam. For the beam reinforced with 12 mm Ribbed GFRP bar, the concrete

crushed at top of the beam due to excessive deflection of the beam at mid span and the area that resisted the compression force was too small to carry any extra force even with compression reinforcement. Figure 4.14a and 4.14b show the cracking behaviour just before the concrete crushed.

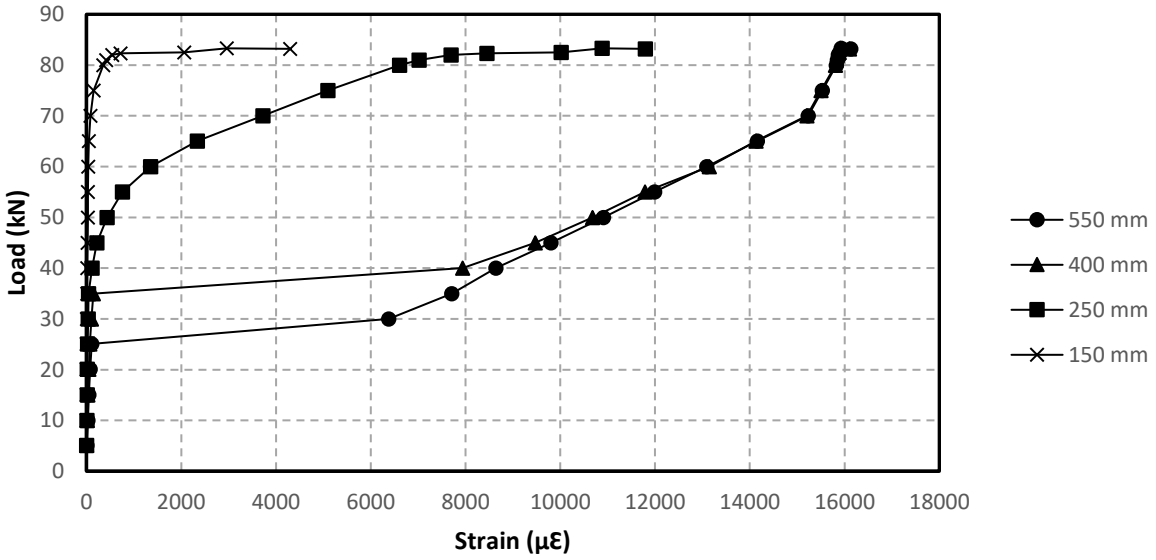

a- Load vs. GFRP bar strain

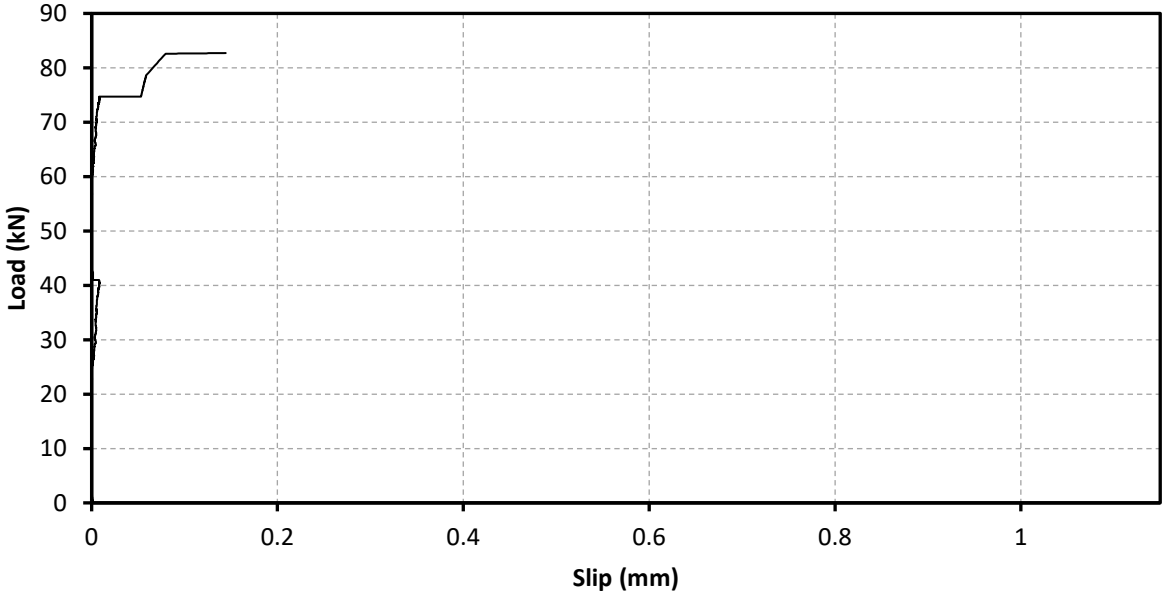

b- Load vs. end slip between the GFRP bar and the concrete

Figure 4.14: Test results for beam R-12-1.5-0%

Strain profile along the GFRP bar

Figure 4.15 shows the strain distribution along the GFRP bar for beam R-12-1.5-0%. The axial strain distribution along the GFRP bar in the shear span at different load levels is shown on Figure 4.15. At a load level of 10 kN, the strain gauge measurements at all locations were low (between 10 με and 20 με). As the load increased to 22 kN, the first concrete crack appeared at mid-span and the strain gauge reading at mid-span increased to 5346 με. As the test proceeded and the load reached 48 kN, the strain gauge reading at 400 mm increased to 8254 με but it was less than the strain at mid-span indicating only partial de-bonding between 550 mm and mid-span. When the applied load reached 70 kN, the strain gauge reading at 250 mm increased significantly indicating that the partial de-bonding was moving toward the support. At failure (83 kN), the ultimate strain at 150 mm was equal to 4265 με

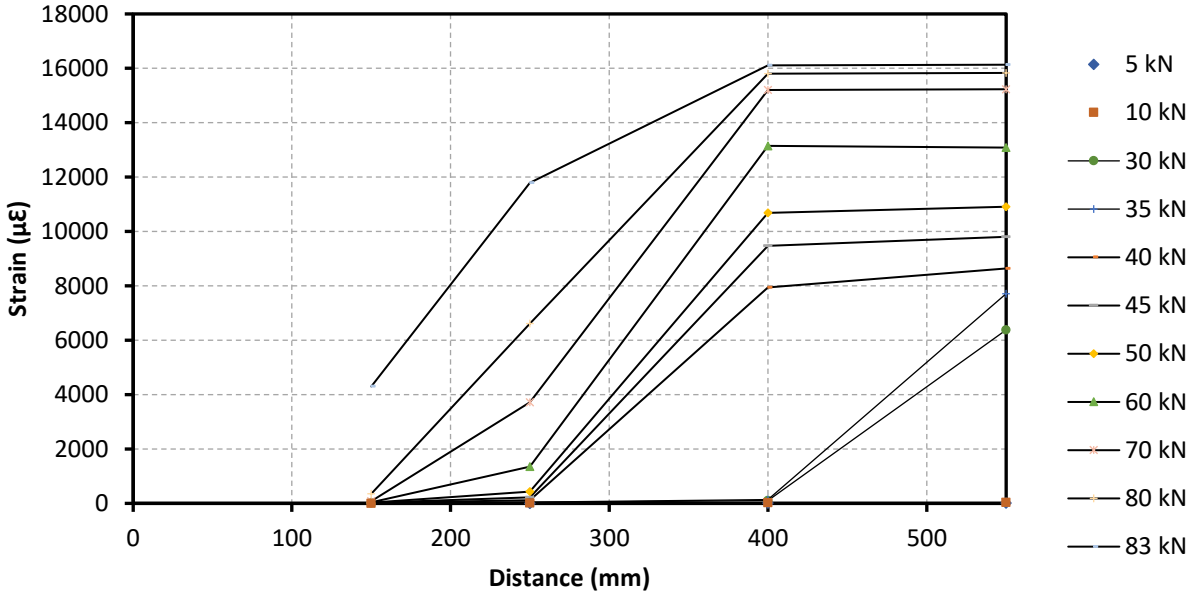

Figure 4.15: Strain distribution along the GFRP bar for beam R-12-1.5-0%

4.2.2.4 Concluding Remarks for the Preliminary Study

The following concluding remarks are made based on the preliminary study findings:

- The objective of this phase was to investigate the importance of studying the bond between the HM GFRP bar and the surrounding concrete.
- All beams were designed to fail in bond by choosing a development length shorter than the desired development length for the beam to fail in concrete crushing or bar rupture.
- The development length was chosen to be 500 mm, which was shorter than any calculated or suggested in any design or building code.
- This phase was built to choose the most important variables affected the bond between the GFRP bar and the concrete.
- The concrete strength for this study was higher than the designed concrete strength. Increasing in the concrete strength added more confinement effect on the bond between the bar and the concrete which prevented the beam from failing in bond with the chosen development length (500 mm), for example beam R-16-1.5-0%.
- Because of the unexpectedly high concrete strength, the development length was even shorter than 500 mm for all tested beams with different concrete covers and bar diameters.
- The ultimate strain in the GFRP at failure for the beam reinforced with a 12 mm bar is higher than the beam reinforced with a 16 mm GFRP bar.
- The ultimate load at failure for the beams reinforced with ribbed GFRP bar was slightly higher than for the beams reinforced with sand coated GFRP bar for all concrete covers and bar diameters. The increases in strength ranged from 6 % (for beam reinforced with 16 mm bar diameter and 25 mm concrete cover) to 11% (for beam reinforced with 12 mm bar diameter 25 mm concrete cover)

4.2.3 Beams Reinforced with Sand Coated GFRP Bar (Main Study)

4.2.3.1 General

For the main study, twelve beams were cast and tested under static and fatigue loading. all beams were reinforced with 16 mm non-prestressed sand coated GFRP bar. Two different concrete covers were used in this study to investigate the effect of the concrete cover on the bond stress between the bar and the concrete. The first group of beams (six beams) had a concrete cover equal 1.5 times the bar diameter (≈ 25 mm) and the second group (six beams) had a concrete cover equal to 3.0 time the bar diameter (≈ 45 mm). The beam geometry was different for beams that had concrete covers equal to 25 mm and 45 mm. The beam geometry was 267 mm high, 200 mm in width and 2000 mm long for the smaller concrete cover and 297 mm high, 200 mm width and 2000 mm long for the beam with the larger concrete cover. For each group, one beam was tested under monotonic loading until failure while the other five beams were tested under fatigue loading until failure. In this section, the test results for beams tested under monotonic loading will be presented and discussed but the test results for beams tested under fatigue loading will be presented in different section. All beams were tested in four-point bending and failed in bond. In the following sections, load vs deflection, cracking behaviour and the strain profile will be presented. Table 4.3 shows the ultimate capacity for both beams. Figure 4.16 shows a typical bond failure.

Table 4.3: Ultimate capacity and failure mode for sand coated reinforced beams (main study)

Specimen notation	Max load (kN)	Failure mode
SC-16-1.5-0%	146	splitting bond failure
SC-16-3.0-0%	174	splitting bond failure

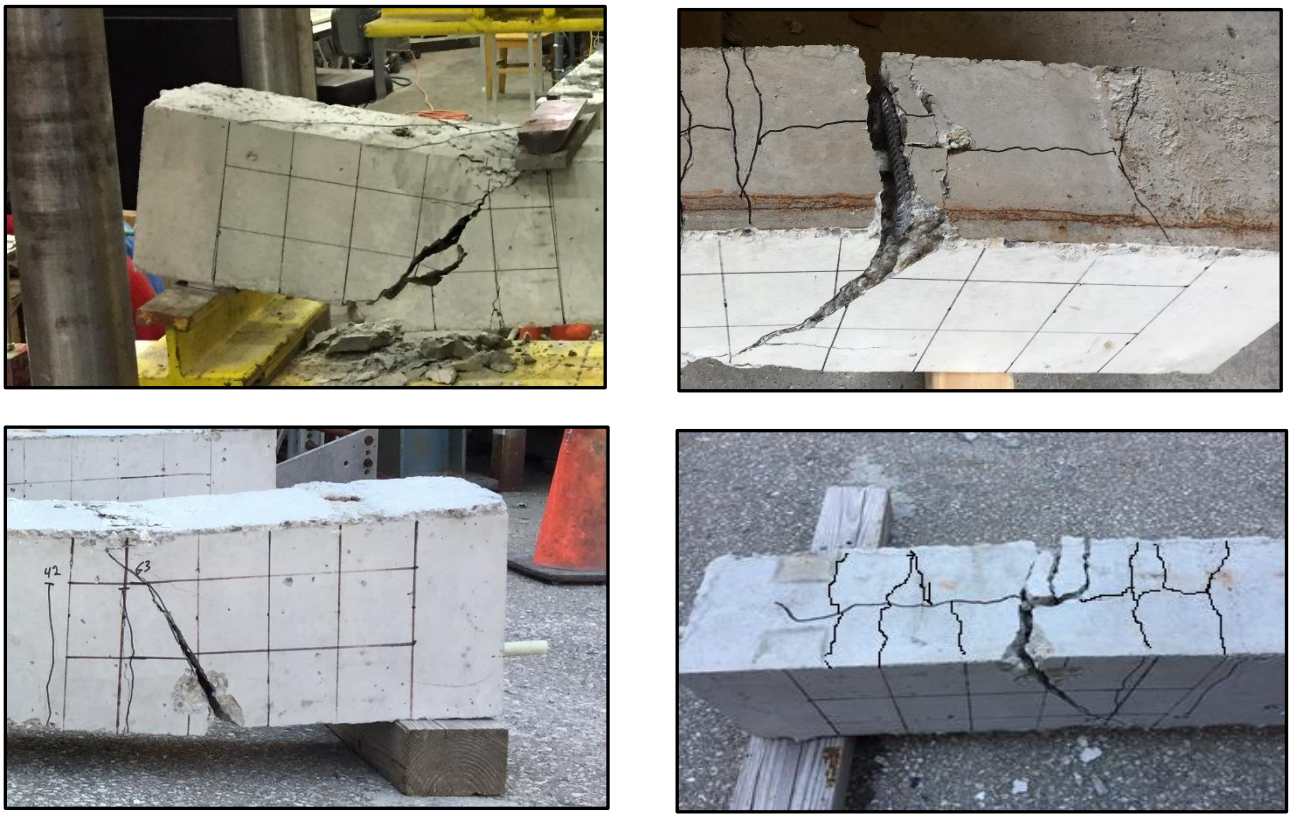

Figure 4.16: Bond failure for beams reinforced with non-prestressed sand coated GFRP bar

Load vs. mid-span deflection curve

Figure 4.17 shows the Load vs deflection curve for beams reinforced with 16 mm bar diameter and a concrete cover equal to $1.5 \cdot d_b$ and $3.0 \cdot d_b$. As the load increases, the mid-span deflection increases until the concrete reaches its ultimate tensile strength and cracks appear at mid-span (~36 kN for $1.5 \cdot d_b$ and ~ 43 kN for $3.0 \cdot d_b$). After concrete cracking at mid-span, the load vs. deflection slope decreases and the mid-span deflection continues to increase with the load until the ultimate load is reached.

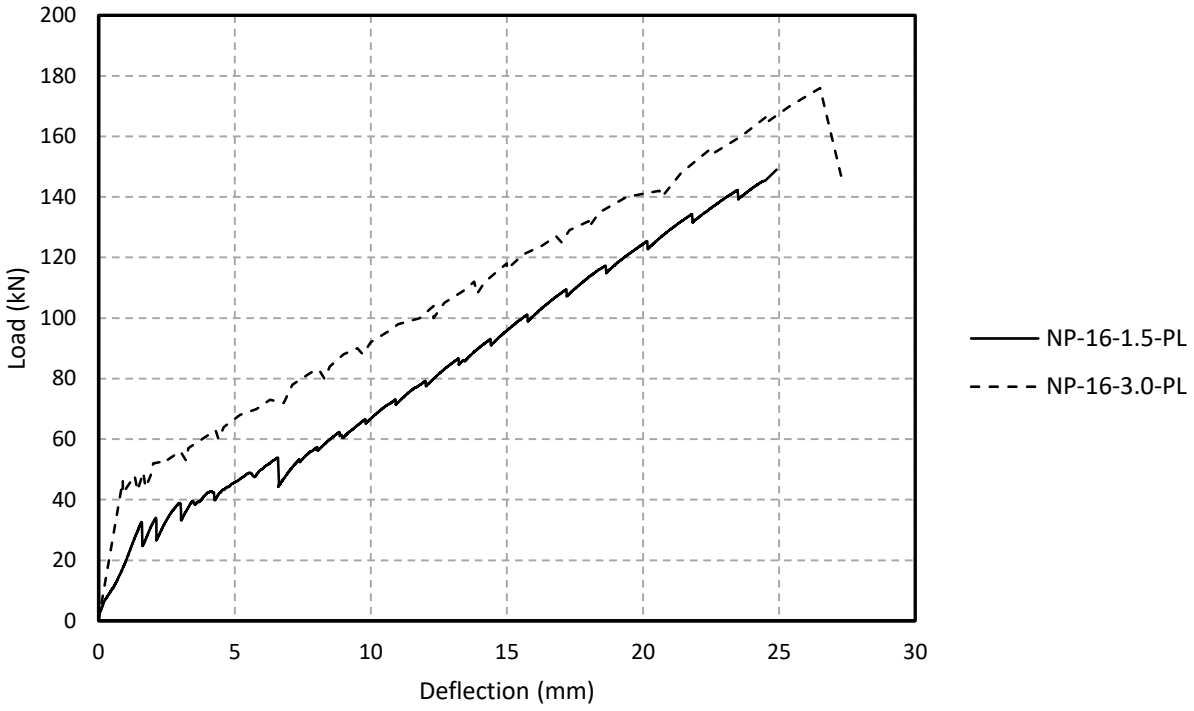

Figure 4.17: The load vs. deflection curve for beam reinforced with 16 mm GFRP and two different concrete cover (25 mm and 45 mm)

Cracking behaviour

Both beams were reinforced with 16 mm sand coated GFRP bars. Beam SC-16-1.5-0% was reinforced with a 16 mm sand coated GFRP bar and the concrete cover was 25 mm. Beam SC-16-3.0-0% was reinforced with a 16 mm sand coated GFRP bar and the concrete cover was 45 mm. Figure 4.18a shows the load vs. GFRP strain gauge readings and Figure 4.18b shows the load vs. end-slip between the GFRP bar and the concrete for the beam with a 25 mm concrete cover. The strain gauges were mounted on the GFRP bar at different locations from the support (50 mm, 200 mm, 350 mm and 500 mm). The strain gauge measurements for the gauges located at mid-span increased as the concrete cracked and the tensile force in the concrete cross section was suddenly transferred to the GFRP bar. As the load increased, cracks were observed in the shear span starting near the loading point location and progressing towards the support. The first crack that appeared in the shear span was 20 mm from the loading point at a load of 36 kN. When the applied load reached 60 kN, another crack appeared at 350 mm from the support. As each crack occurred, the reading of the strain gauge located nearest to the crack increased suddenly as the tensile forces

were transferred from the concrete to the GFRP bar. As the test proceeded, a third crack appeared at 225 mm from the support when the applied load was 87 kN. As the load approached its peak value, the crack at 225 mm from the support widened and propagated through the depth of the beam. At the peak load, de-bonding occurred between the GFRP bar and the concrete, and an isolated prism of concrete separated from the GFRP bar and the beam. The ultimate strain at mid-span for the beam with a concrete cover equal to 25 mm was almost 13000 με. The cracking behaviour for the beam reinforced with a 16 mm Sand coated GFRP bar and a concrete cover equal to 45 mm was almost the same as that for the beam with a concrete cover equal to 25 mm. Both beams had the same cracking behaviour that started from the loading point and moved toward the support. The ultimate strain gauge at mid-span was almost 15400 με. Figure 4.19a shows the load vs. GFRP strain gauge readings and Figure 4.19b shows the load vs. end-slip between the GFRP bar and the concrete for the beam with a 45 mm concrete cover.

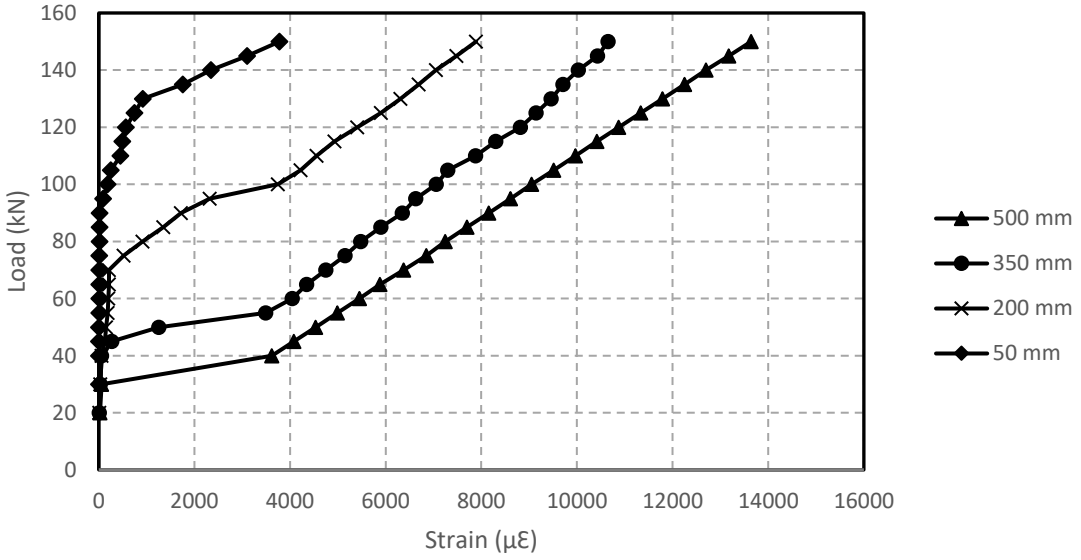

a- Load vs. GFRP bar strain

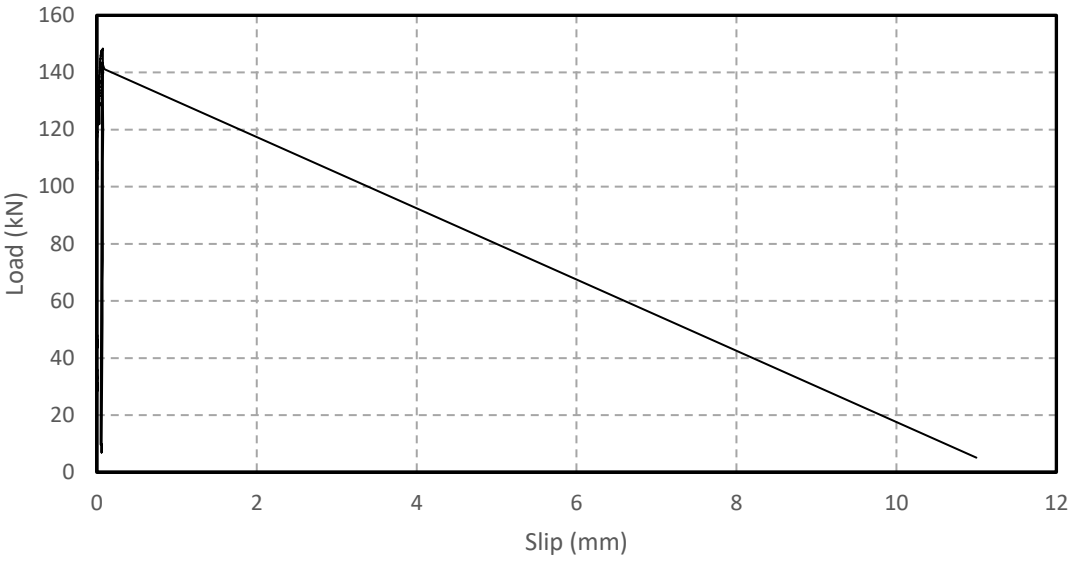

b- Load vs. end slip between the GFRP bar and the concrete

Figure 4.18: Test results for beam SC-16-1.5-0%

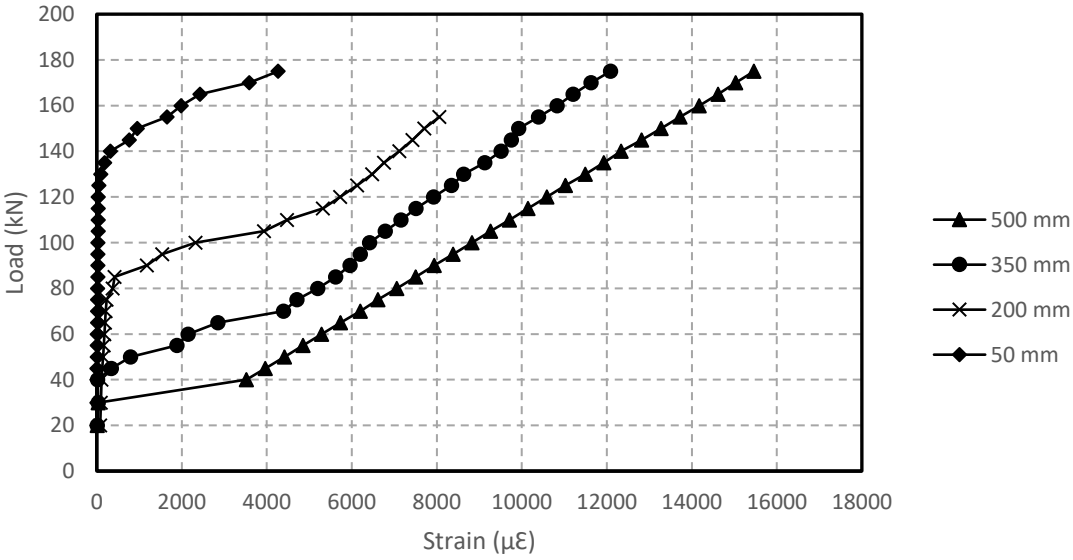

a- Load vs. GFRP bar strain

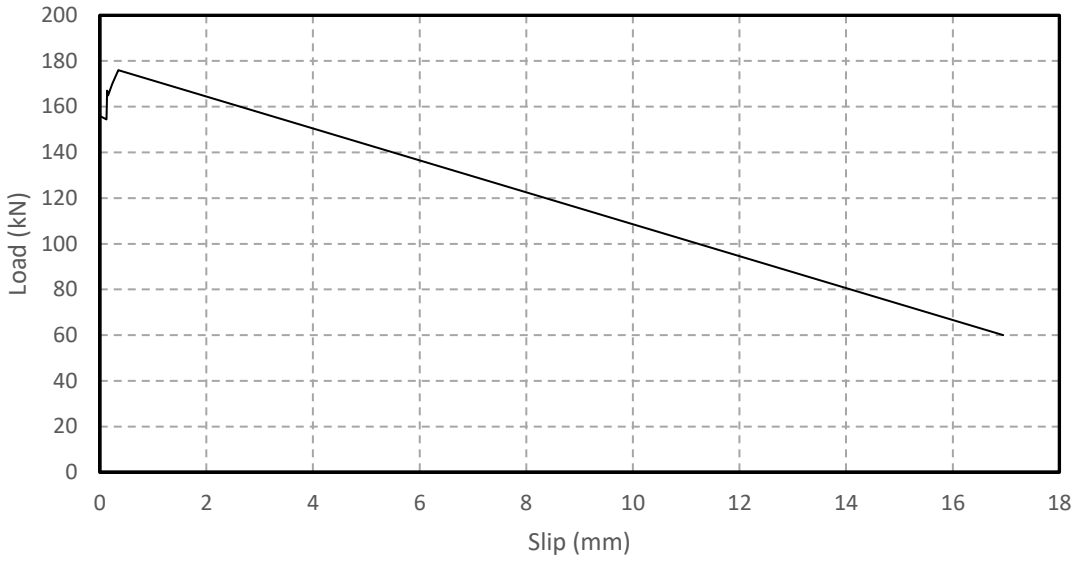

b- Load vs. end slip between the GFRP bar and the concrete

Figure 4.19: Test results for beam SC-16-3.0-0%

Strain profile along the GFRP bar

Figure 4.20 shows the measured strain distributions along the GFRP bar for beam SC-16-1.5-0%. The axial strain distribution along the GFRP bar in the shear span at different load levels is shown on Figure 4.20. At a load level of 20 kN, the strain gauge measurements at all locations were low (between 10 με and 90 με). As the load increased to 36 kN, the first concrete crack appeared at mid-span and the strain gauge reading at mid-span increased to 2682 με. As the test proceeded and the load reached 40 kN, the strain gauge reading at 500 mm increased to 3620 με. When the applied load reached 60 kN, the strain gauge reading at 350 mm increased significantly indicating that the partial de-bonding was moving toward the support. At failure (146 kN), the strain at 200 mm was equal to 7890 με and the strain at 50 mm from the support was almost 3740 με.

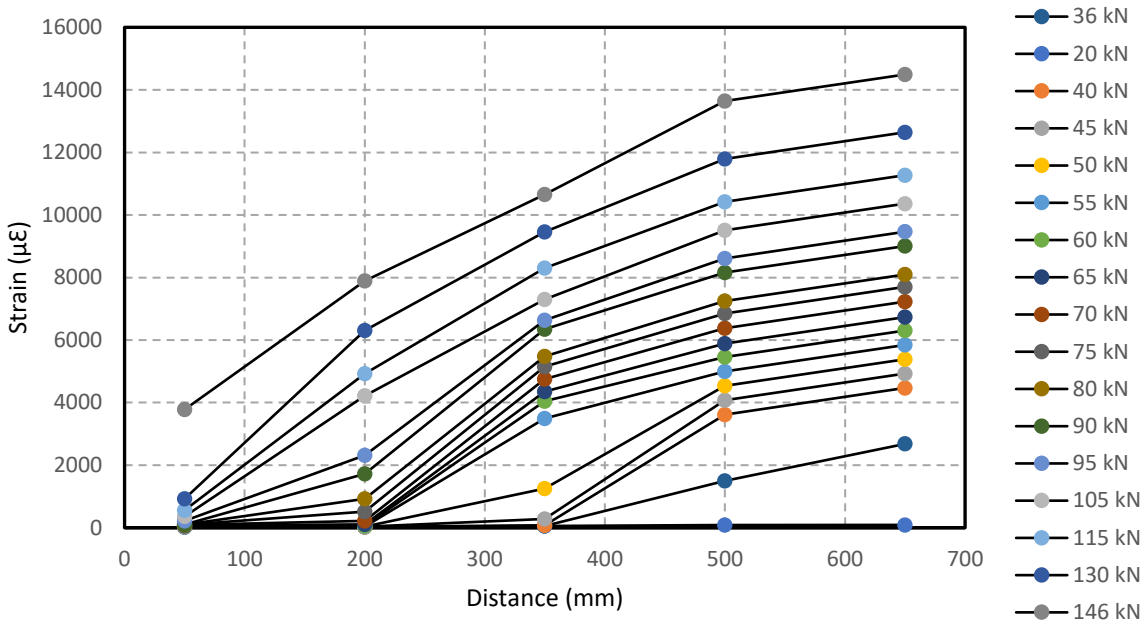

Figure 4.20: Typical strain profile for beam SC-16-1.5-0%

4.4 Discussion of the Monotonic Test Results

All beams were designed to fail in bond between the GFRP bar and the surrounding concrete. The shear span length was chosen to be less than the desired development length to make sure that the beam would fail in bond. Before the concrete cracked at mid-span, the concrete carried most of the tensile stress. When the concrete reached its ultimate tensile strength, the first crack appeared within the constant moment region or under the loading point and the tensile stress was then carried by the main reinforcement. A sudden jump in the strain gauge reading occurred when the concrete cracked, and all the tensile force was taken by the main reinforcement. The readings of a strain gauge are very sensitive to the crack location. If the strain gauge is close to the crack location, the change in the strain gauge reading will be very large. When a strain gauge is far from a crack the change in its strain on cracking will be much smaller. As we move away from a crack, the tensile stress in the concrete will increase rapidly while the stress in the main reinforcement will rapidly decrease to the low value. This difference in the normal stress along the main reinforcement creates a high local shear stress at crack locations. Figure 4.21 and Figure 4.22 show the normal and shear stress distributions after a beam has cracked the and the location of the of strain gauges that measure the normal bar forces.

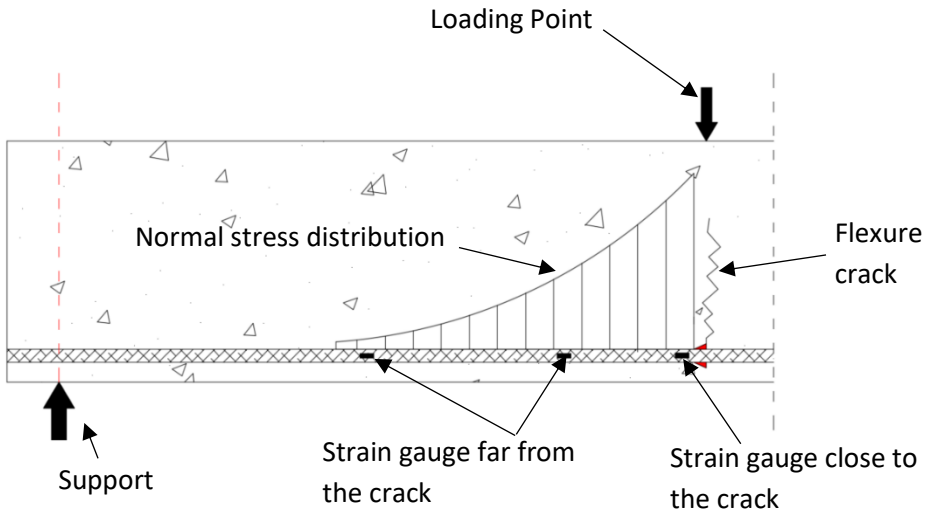

Figure 4.21: Normal stress distribution along the bar

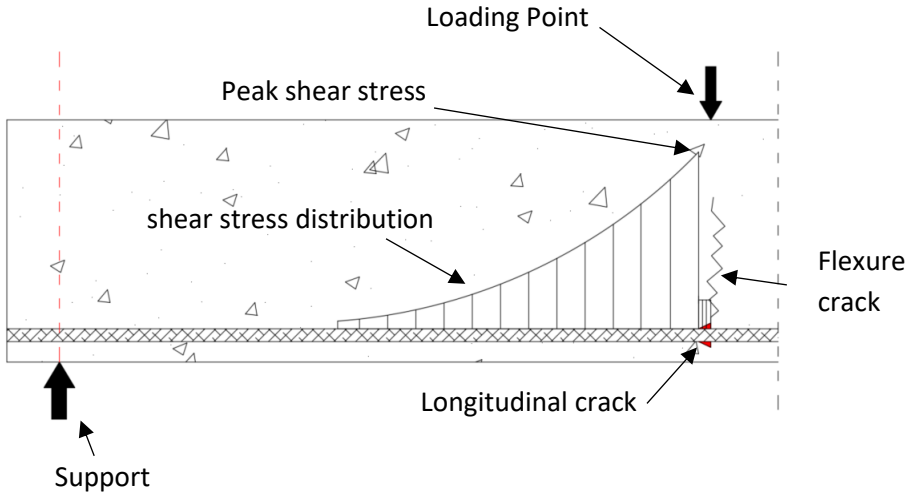

Figure 4.22: Shear stress distribution after beam cracked

When the shear stress at a crack location is high enough, the concrete surrounding a bar will slip and de-bond from the surrounding concrete. After slipping occurs, the peak shear stress in the still bonded region will move toward the support. Within the de-bonded region, the strain reading at the new crack tip location (at the peak shear stress location) and the strain at the loading point will be equal or slightly different. Due to the peak shear stress movement from the loading point toward the support, the normal stress and the shear stress along the main reinforcement will be divided into two regions. The first region (de-bonded) located between the loading point and the peak shear

stress. The second region is between the peak shear stress and the support. Figure 4.23 shows the two regions along the GFRP bar. This will be discussed in detail in Chapter 6.

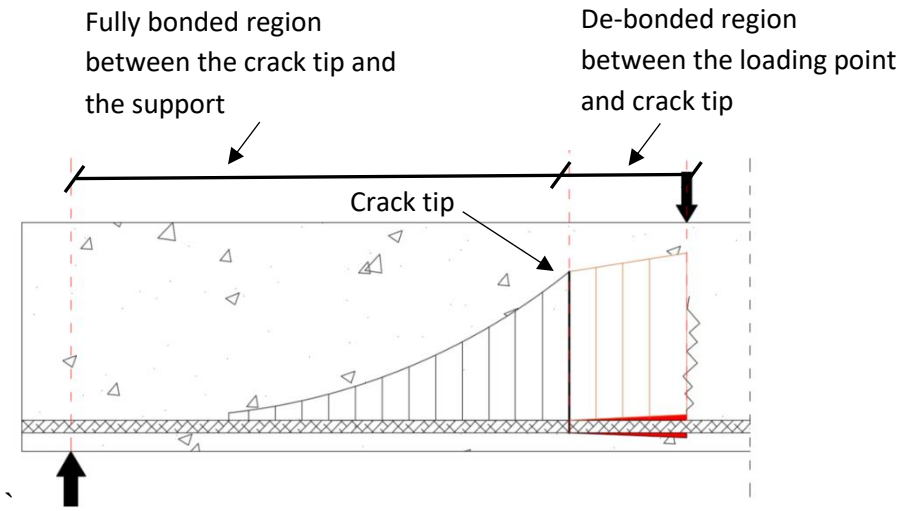

a- Normal stress distribution after the crack propagated

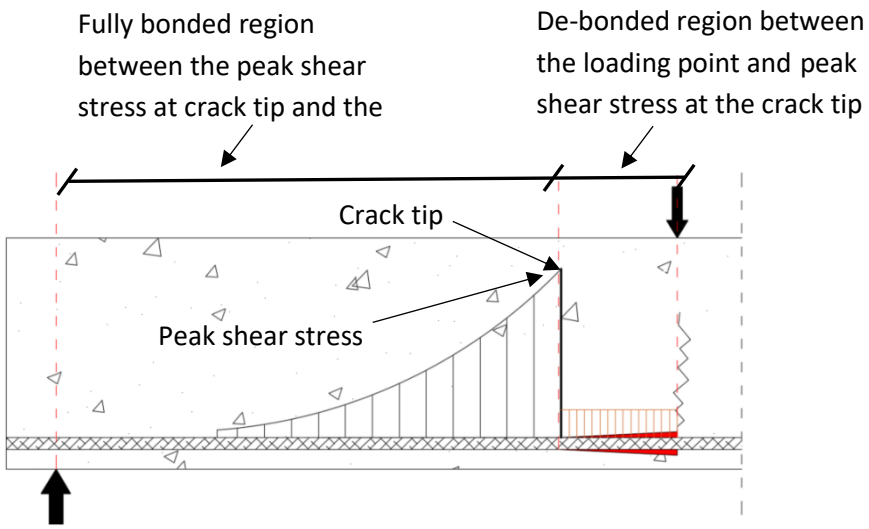

b- Shear stress distribution after the crack propagated

Figure 4.23: Ahead and behind the crack tip region

4.5 Test Results for Beams Tested Under Fatigue Loading

4.5.1 General

This section presents and discusses the test results for the non-prestressed beams tested under a fatigue loading. In total, ten non-prestressed beams were cast and tested under fatigue loading. These beams were divided into two groups based on the concrete cover. The first group (five beams) were reinforced with 16 mm sand coated GFRP bar and the concrete cover was 25 mm. For the second group, five beams were reinforced with 16 mm sand coated GFRP bar and the concrete cover was 45 mm. All beams failed in bond between the GFRP bar and the concrete except one beam that was reinforced with a sand coated 16 mm GFRP bar and had a concrete cover equal 45 mm, which failed by bar rupture. Table 4.5 summarizes the fatigue test results including beam type, minimum, maximum load, load range as a percentage of failure load of the beam tested under monotonic loading, strain range, the number of cycles to failure and the failure mode.

Table 4.4 Summary of the fatigue test results

Group	Beam	Load		Stress (MPa)	Number of cycles	Failure mode
		Min (kN)	Max (kN)			
Group 1 (25 mm concrete cover)	SC-16-1.5-0%-82.5	15	97.5	422	1504	splitting bond
	SC-16-1.5-0%-78	15	93	397	2010	splitting bond
	SC-16-1.5-0%-66	15	81	333	40896	splitting bond
	SC-16-1.5-0%-55.5	15	70.5	287	472562	splitting bond
Group 2 (45 mm concrete cover)	SC-16-3.0-0%-108.5	17.5	126	557	297	splitting bond
	SC-16-3.0-0%-98	17.5	115.5	503	1493	splitting bond
	SC-16-3.0-0%-94.5	17.5	112	485	2639	splitting bond
	SC-16-3.0-0%-89	17.5	106.5	458	11683	splitting bond

4.5.2 Fatigue life

The fatigue test results for all non-prestressed beams reinforced with a 16 mm sand coated GFRP bar are shown in Figures 4.24 and 4.25. Figure 4.24 shows the load range (kN) versus the fatigue life in cycles and Figure 4.25 shows the stress range versus fatigue life in cycles. All beams failed in bond between the GFRP bar and the concrete except one beam reinforced with a sand coated 16

mm GFRP bar that had concrete cover equal to 45 mm that failed by bar rupture. The fatigue life of the non-prestressed beams varied linearly with the load range (kN) on log-log scales. As the load range or stress range increased the fatigue life decreased. The fatigue life curve for beams that failed by de-bonding between the bar and concrete has a shallow slope. Because the slope of the curve is shallow, a small change in the load range will result a major change in beam life under a fatigue loading. The two curves (beams with concrete covers equal to 25 mm and 45 mm) were almost parallel. Due to the weakness of the GFRP bar subjected to fatigue loading, beams with a concrete cover equal 45 mm only failed in bond at lives below eleven thousand cycles (11000 cycles). The stress range and load range were increased higher than the service load maximum stress (approximately 300 MPa) for beams that had a concrete cover equal to 45 mm to avoid bar rupture and to make sure that the beam would fail in bond between the GFRP bar and the concrete. If the best fit curve is extended for the set of beams with a concrete cover equal 45 mm as shown in Figure 4.24, it is clear that the beam with higher concrete cover last longer in life compared to the beams that had a lower concrete cover. Most of the test data fell close to the best fit line.

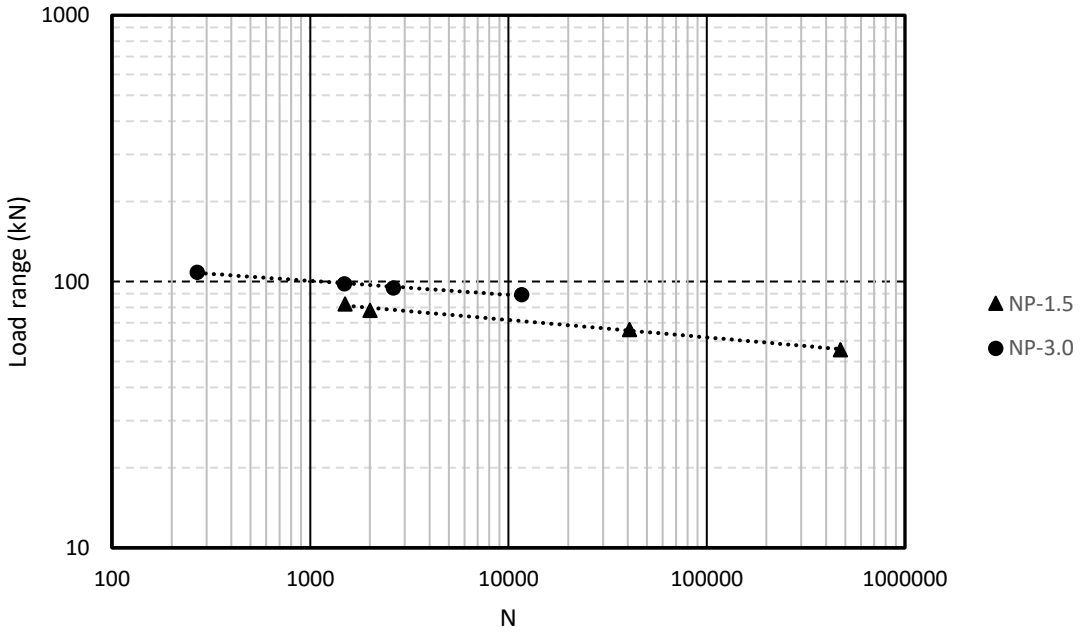

Figure 4.24: Fatigue life versus the load range (kN) for beams with concrete cover equal 25 mm and 45 mm

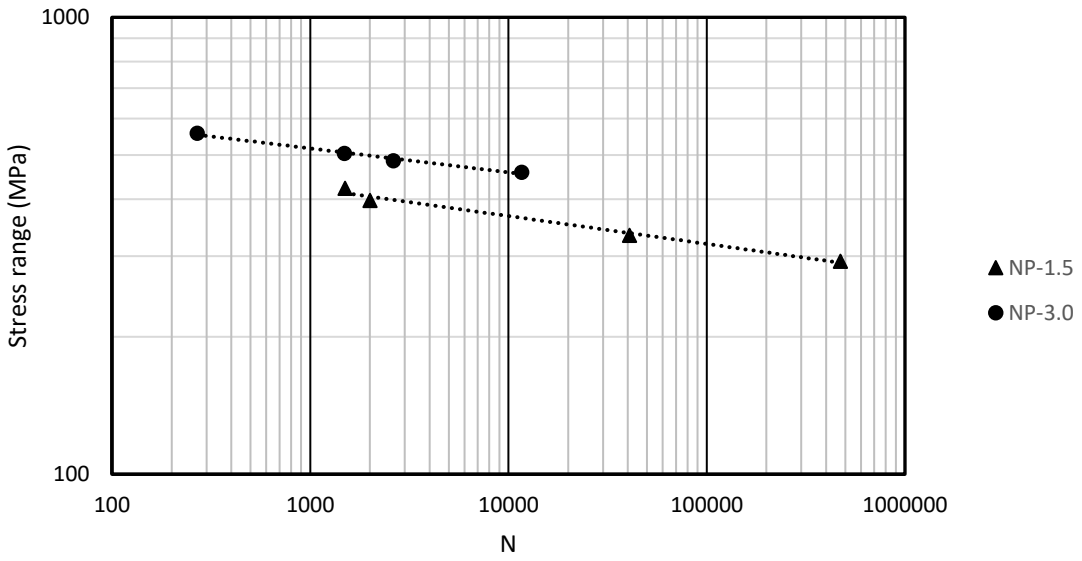

Figure 4.25: Fatigue life vs stress range test results for beam with concrete cover equal 25 mm and 45 m

4.5.3 Failure mode

In this section, the typical bond failure that occurred for non-prestressed beams tested under fatigue loading will be discussed. All beams were loaded manually to the specified maximum load before fatigue loading started. During the first cycle, the first crack appeared at the loading point location or with a few millimeters from the loading point. At the same time, a horizontal crack initiated on the bottom side of the beam started close to the loading point. As the load increased during the first cycle, the debonded crack propagated towards the support. The length of the de-bonded crack varied from one beam to another depending on the maximum specified load. As the maximum specified load increased the de-bonded crack length at the end of initial loading increased. After the fatigue loading started, the de-bonded crack grew towards the support until failure occurred. The rate of crack growth was affected by many factors including the applied load range and the confinement level. As the applied load range increased the crack growth rate increased. Figure 4.26 shows a typical bond failure for beams reinforced with non-prestressed beams with different concrete covers and failed under fatigue loading

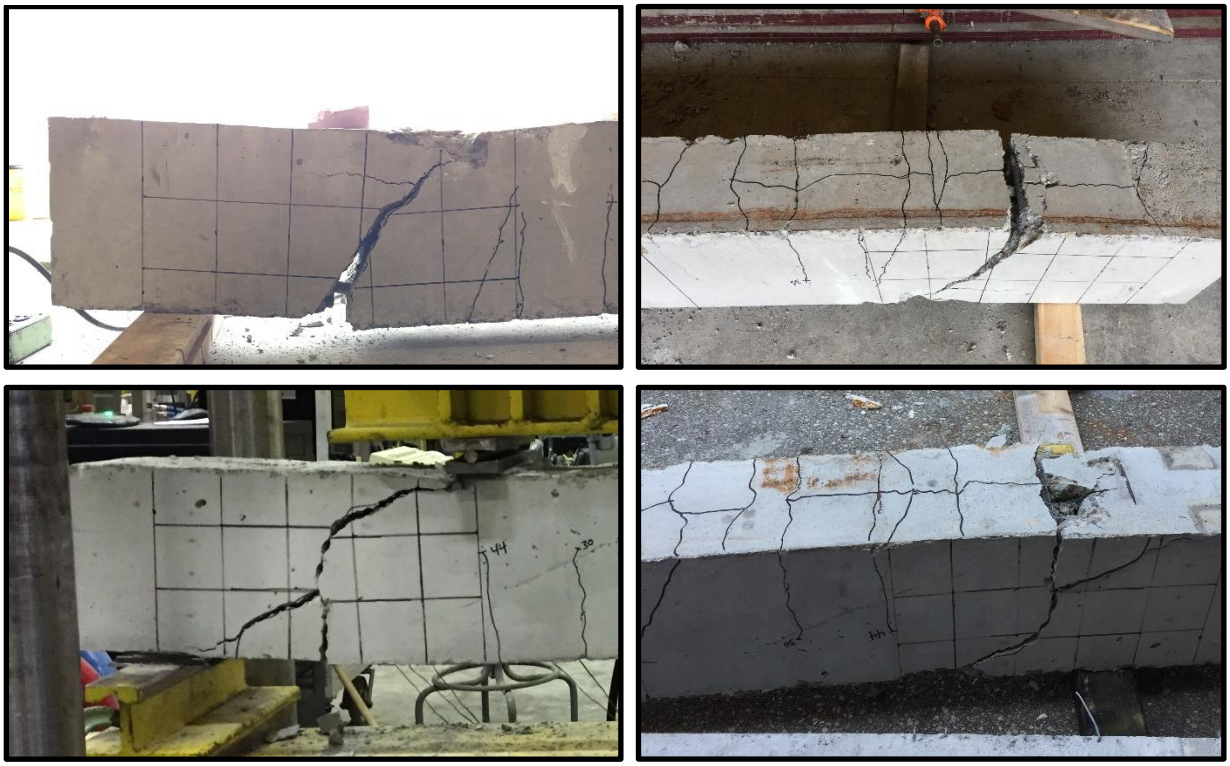

Figure 4.26 Typical bond failure for non-prestressed beams

4.5.4 Load-Deflection Behaviour

Typical deflection versus number of cycles as a percentage of fatigue life are shown in Figures 4.27 Figure 4.28 for beams with concrete covers equal to 25 mm and 45 mm, respectively. The maximum mid-span deflection at the peak load during the tests under fatigue loading was plotted versus the number of cycles as a fraction of fatigue life. For all the non-prestressed beams tested under fatigue loading, three stages were observed in the beam deflection behaviour. In the first stage, the beam deflection suddenly increased as the concrete cracked and the GFRP bar carried all the tensile force. Simultaneously, the de-bonded crack initiated and decreased the bond between the GFRP bar and the concrete. In the second stage, the deflection increased slowly from the first 5% of the fatigue life until about 95% of the fatigue life of the beam. In the final stage and during the last 5% of the fatigue life, as the de-bonded crack approached to the support and there was not enough bonded length to resist the bar force, so the mid-span deflection increased suddenly and

the beam failed. For both beam sets (with concrete cover equal to 25 mm and 45 mm), the mid span deflection increased as the applied load increased.

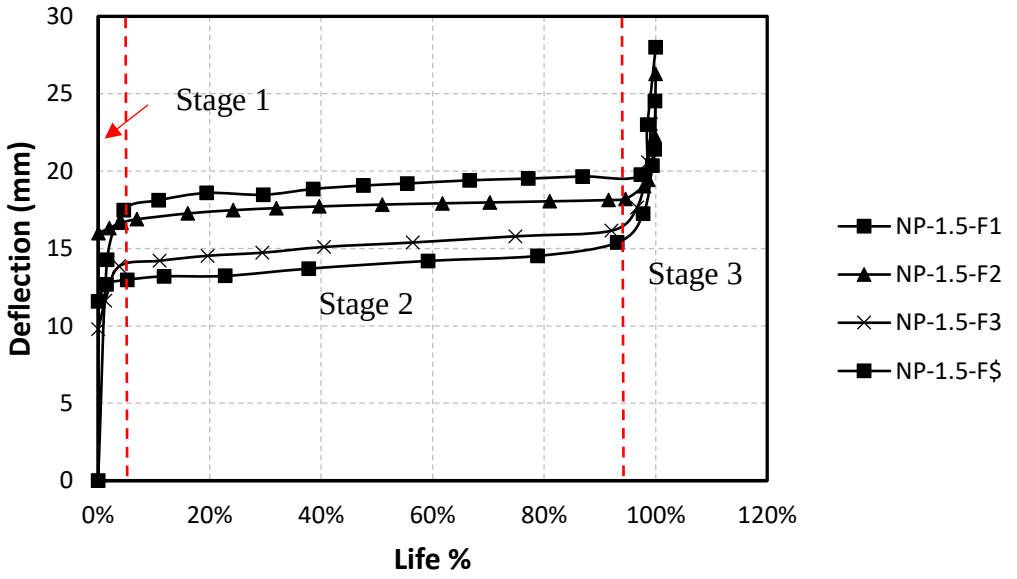

Figure 4.27 Load vs. deflection curves for all beams with 25 mm concrete cover

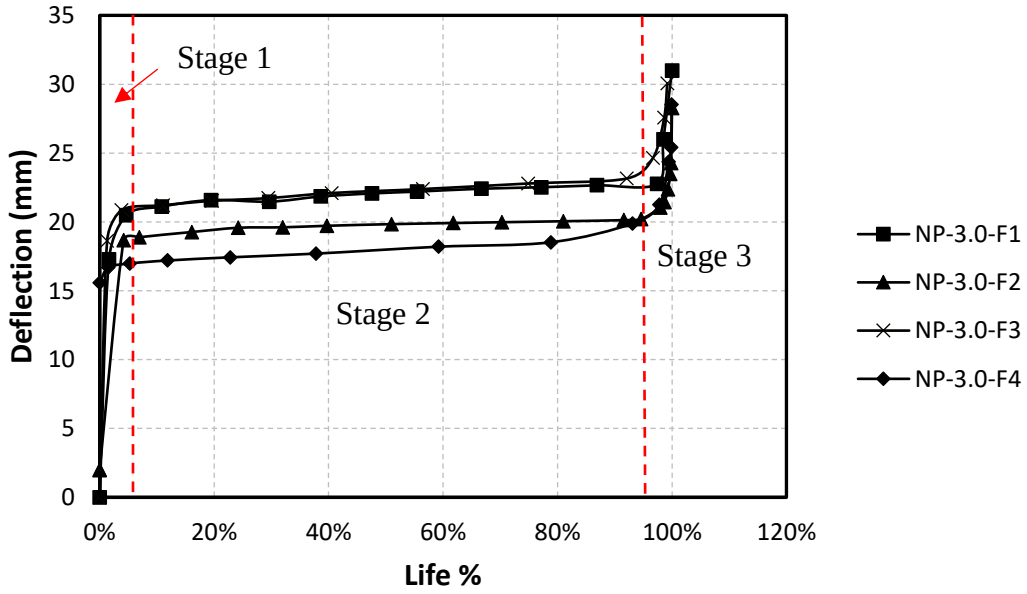

Figure 4.28 Load vs. deflection curves for all beams with 45 mm concrete cover

4.5.5 Strain Distribution Along the GFRP Bar

Figure 4.29 shows a typical strain profile along the GFRP bar under a fatigue test for beam SC-16-1.5-0%-66. During the first cycle, the strain gauges located at 500 mm and 350 mm from the support read a high value of strain and the strain while the strain gauges located at 200 mm and 50 mm from the support read low strain values. The strain readings from the first cycle indicated a partial de-bond between the strain gauges located at 500 mm and 350 mm while the GFRP bar remained bonded to the concrete between strain gauges located at 350 mm and 50 mm from the support. At 10% of the fatigue life, the reading of the strain gauge located at 200 mm from the support suddenly increased to high value but one that is less than the strain reading at 350 mm, which means the de-bonded crack tip was approaching the strain gauge located at 200 mm. As the number of cycles increased the strain gauge readings increased all along the GFRP bar. As the beam reached almost 90 % of the fatigue life, the strain reading of the gauges located at 500 mm, 350 mm and 200 mm from the support were almost equal indicating that and GFRP bar in that region had de-bonded from the concrete. Close to failure the ultimate strain gauge reading at 50 mm was almost 3665 με. Similar behaviour was observed for beams reinforced with non-prestressed GFRP bar and a concrete cover equal to 45 mm. Figure 4.30 shows a typical strain profile along the GFRP bar for beam SC-16-3.0-0%-94. The peak strain reading for the strain gauge located at 50 mm was almost 4652 με.

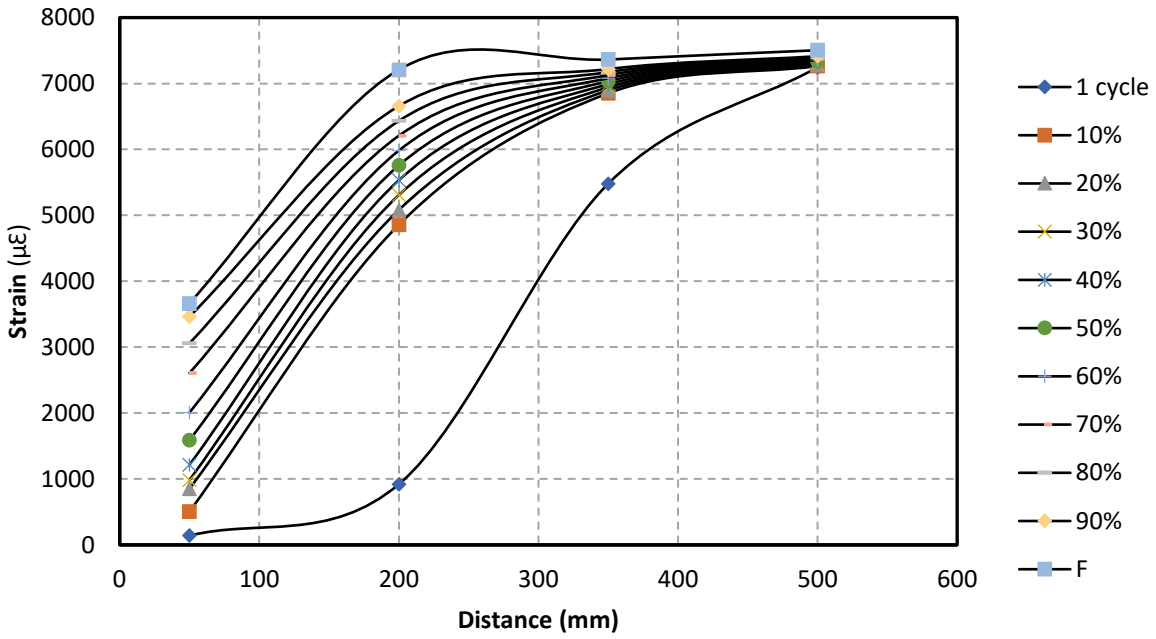

Figure 4.29: Strain distribution along GFRP bar for beam SC-16-1.5-0%-66

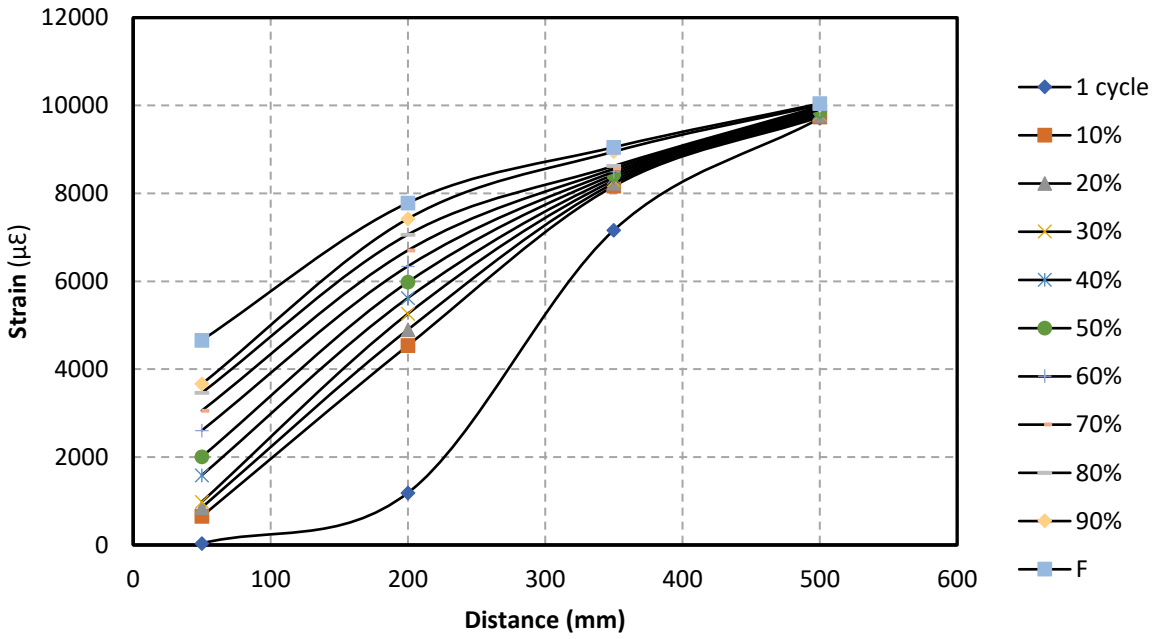

Figure 4.30: Strain distribution along GFRP bar for beam SC-16-3.0-0%-94.5

Chapter 5: Experimental Results for Prestressed Beams

5.1 General

This chapter presents and discusses the experimental test results for the beams reinforced with prestressed GFRP bar tested under Static and fatigue loading. Twenty-four reinforced concrete beams were cast and tested under monotonic and fatigue loading. These beams were divided into two phases. The first phase was a preliminary study and includes eight reinforced concrete beams with prestressed GFRP bar four concrete beams reinforced with Sand coated GFRP bar and four beams reinforced with ribbed GFRP bar. The testing variables were bar diameter (12 mm and 16 mm), GFRP bar surface type (Sand Coated and Ribbed), and concrete cover ($1.5 \cdot d_b$ and $3.0 \cdot d_b$). The second phase was the main study and includes eighteen reinforced concrete beams. Six beams were reinforced with prestressed ribbed GFRP bar and twelve beams were reinforced with 16 mm sand coated GFRP bar. The testing variables were concrete cover ($1.5 \cdot d_b$ and $3.0 \cdot d_b$) and type of loading (monotonic and fatigue). For each beam set, one beam was tested under monotonic loading and five beams were tested under fatigue loading.

The objective of this study was to investigate the effect of different loading types (monotonic and fatigue) on the bond strength between the prestressed GFRP bar and the surrounding concrete. The first part of this chapter will discuss the test results of phase one (preliminary study). The load deflection curve and the end slip for different beam configurations will be discussed first followed by the typical cracking behaviour and the typical strain profile during loading until a beam failed. The second part will present and discuss phase two (main study) of this study. As in the first part, the results for the beams that were tested under monotonic (static) loading will be discussed first followed by the beams that were tested under fatigue loading. Load/life versus mid-span deflection and the cracking behaviour and the strain profile will be presented. Table 5.1 summarizes the prestress force as a percentage of the ultimate strength for each bar configuration.

Table 5.1: Prestress percentage of the ultimate tensile strength for each bar

Phases	Beam	Bar Type	Bar Diameter (mm)	Concrete cover (mm)	Prestress (%)
Phase 1 (Preliminary study)	SC-12-1.5-40%	Sand Coated	12	25	37.40
	SC-16-1.5-40%	Sand Coated	16	25	38.28
	R-12-1.5-40%	Ribbed	12	25	38.5
	R-16-1.5-40%	Ribbed	16	25	38.71
	SC-12-3.0-40%	Sand Coated	12	45	37.25
	SC-16-3.0-40%	Sand Coated	16	45	38.42
	R-12-3.0-40%	Ribbed	12	45	37.55
	R-16-3.0-40%	Ribbed	16	45	37.69
Phase 2 (Main study)	SC-16-1.5-40%	Sand Coated	16	25	37.21
	SC-16-3.0-40%	Sand Coated	16	45	37.32
	R-16-1.5-40%	Ribbed	16	25	37.19

5.2 Strain Distribution

During the testing, the stress in the prestressed GFRP bar is a combination of the stress due to prestressing and the stress due to applied load.

5.2.1 Stress Distribution Due to Prestressing

During the prestressing process, the strain in the GFRP bar was constant along the bar length and was equal to the prestressing strain. When the prestressing force was released, the stress and strain in the bar at the beam free end dropped to zero. The free end is considered be at the support centreline because the GFRP bar was de-bonded from the beam free end to the support centreline as mentioned in Chapter 3. The slip that occurred during release between the GFRP bar and the concrete was measured. The expected normal and bond stress (shear stress) distribution along the shear span are shown schematically in Figure 5.1. The bond stress between the GFRP bar and the

concrete is highest at the centreline of the support (at the end of the de-bonded region) and then decreases until it reaches zero at the end of the transfer length.

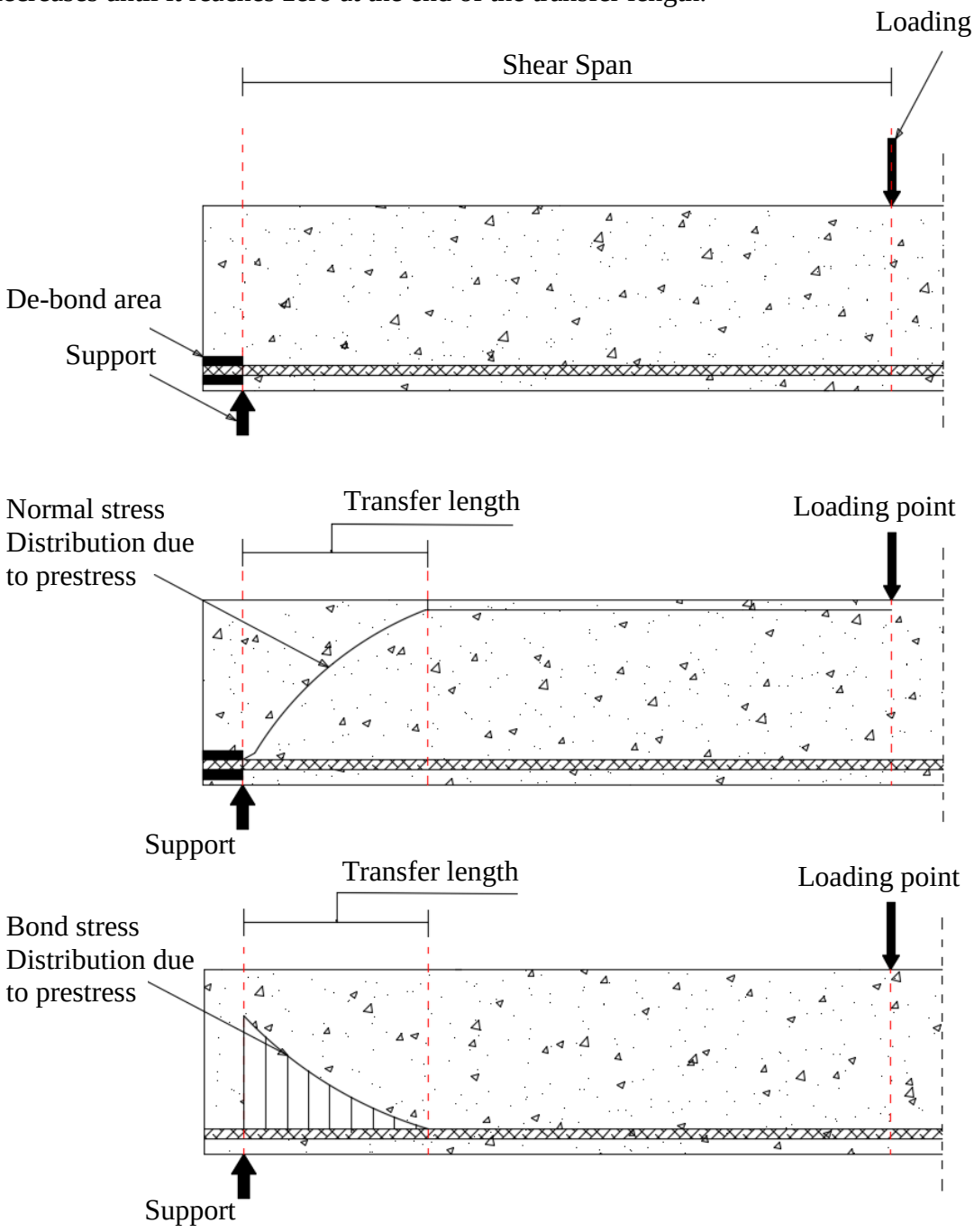

Figure 5.1: Stress distribution in the GFRP due to prestressing

5.2.2 Stress Distribution Due to Applied Load

The total stress in the GFRP bar is the summation of the stress due to prestressing and the stress due to the applied load. The peak bond stress (shear stress) due to prestressing is at the centreline of the support and the peak bond stress due to the applied load is uniform in the shear span (between support and load point). When the two stresses are superimposed, the critical cross-section along the span will be the one where the total stress is the greatest.

5.3 Transfer Length

The transfer length is the length from the end of the bonded portion of the beam (centreline of the support) to the point at which the normal stress in the GFRP bar is equal to the normal stress in the GFRP bar at mid-span of an unloaded beam Figure 5.1. The GFRP bars were prestressed to the chosen stress for both sand coated and ribbed bar. The prestressing force was released after the concrete reached its 27-day strength. During the prestressing force release, the strain gauges recorded the remaining strain in the GFRP bar. All the strain gauges were located within 700 mm of the end of the bonded length. Plots of the strain readings in the GFRP bar after its release versus the distance from the end of the bonded length for all beams are given in Figure 5.2. Figure 5.2 show a typical transfer length for prestressed beams.

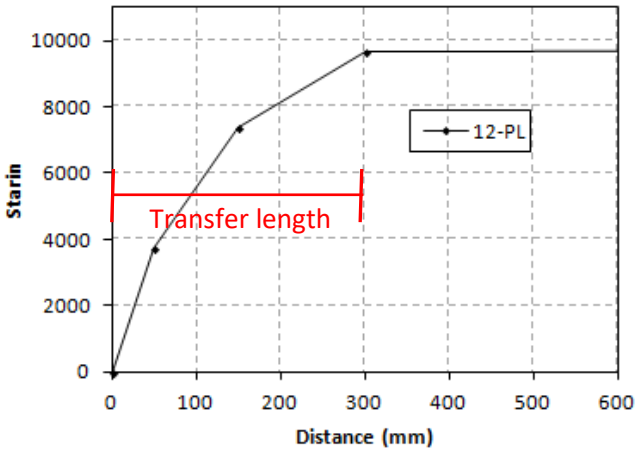

a) Beam SC-12-1.5- 40%

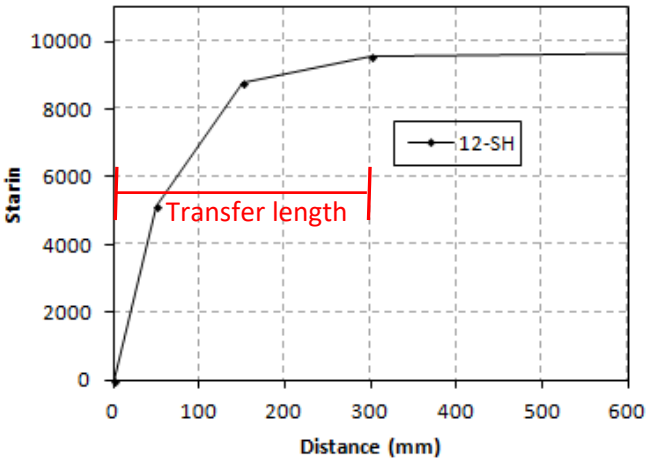

b) Beam R-12-1.5- 40%

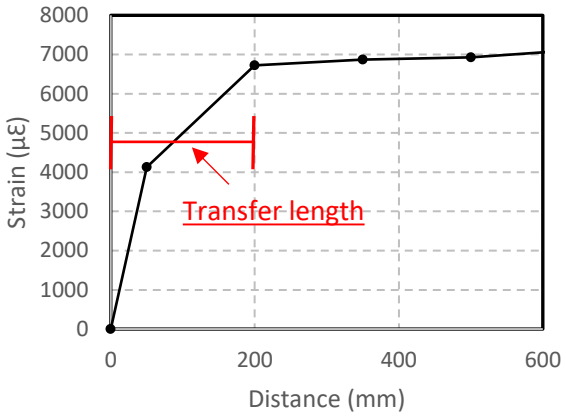

c) Beam SC-16-1.5-40%

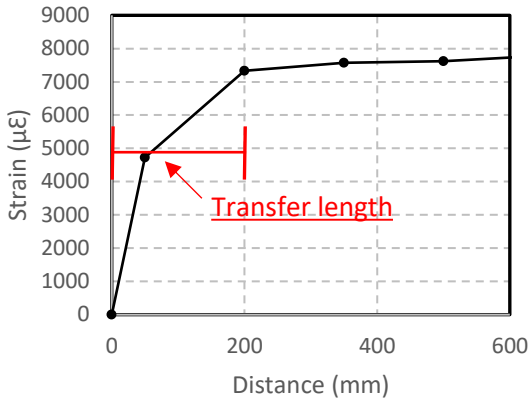

d) Beam SC-16-3.0-40%

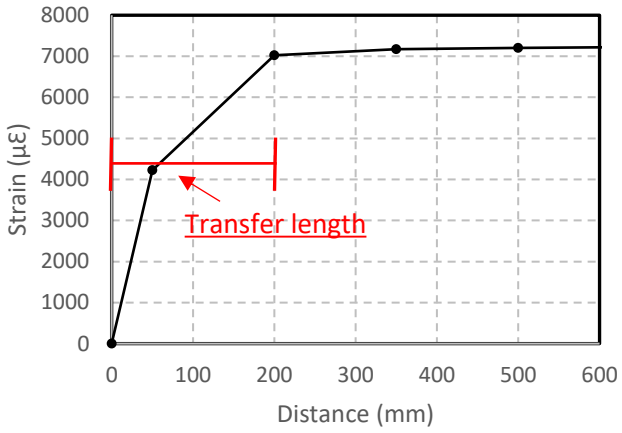

E) Beam R-16-1.5-40%

Figure 5.2 Strain readings for different beams.

5.4 Test Results for Beams Tested Under Static Loading

5.4.1 Beams Reinforced with Sand Coated GFRP Bar (Preliminary Study)

5.4.1.1 General

Four beams in this phase were tested under monotonic loading until failure. All beams reinforced with Sand coated GFRP bar failed by bond failure between the bar and surrounding concrete. The

ultimate capacities are summarized in Table 5.2. Figure 5.3 shows a typical bond failure for the beam reinforced with sand coated GFRP bar. Figure 5.3-b shows that the GFRP bar pulled out of the surrounding concrete during bond failure.

Table 5.2: Ultimate capacity and failure mode for pre-stressed sand coated reinforced beams (pilot)

Specimen notation	Max load (kN)	Failure mode
SC-16-1.5-40%	143	splitting bond failure
SC-16-3.0-40%	186	splitting bond failure
SC-12-1.5-40%	116	splitting bond failure
SC-12-3.0-40%	126	splitting bond failure

b) Prestressed beam after failure

a) Prestressed GFRP bar after failure

Figure 5.3: Typical bond failure for beam SC-16-1.5-40%

5.4.1.2 Beams Reinforced with 16 mm Sand Coated GFRP Bar

Load vs. mid-span deflection curve

Figure 5.4 shows a typical load versus mid-span deflection curve for a reinforced concrete beam with a prestressed 16 mm sand coated GFRP bar. As the load increases, the mid-span deflection increases until the concrete cracks at mid-span and at 700 mm from the centreline of the support

(at a load of about 68 kN). After mid-span cracking, the load vs. deflection slope decreases. The mid-span deflection continues to increase linearly with load as the load increases until complete failure.

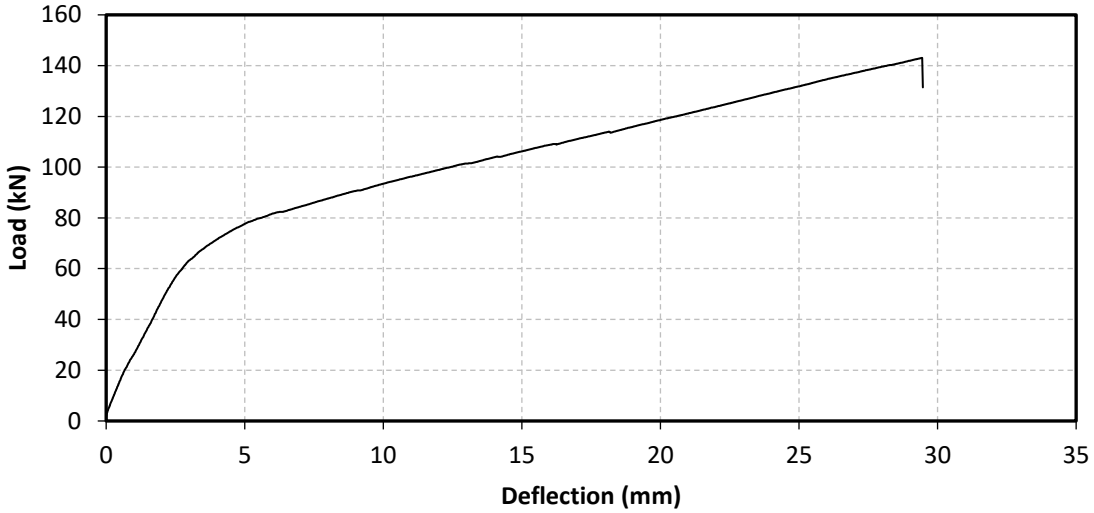

Figure 5.4: Load vs. mid-span deflection for beam SC-16-1.5-40%

Cracking behaviour

Figure 5.5 shows the load vs. GFRP bar strain for beam SC-16-1.5-40%. As the load increases, the GFRP strain readings increase at all locations along the beam length until the load reaches 65 kN at which point the beam cracked at mid-span. Then at the crack location the tensile forces were transferred from the concrete to the GFRP bar and there was a sudden increase in the reading of the strain gauge mounted near the crack on the GFRP bar. When the load reached 91 kN, another crack appeared within the shear span region at 520 mm from the centreline of the support. As the test proceeded, the crack at 520 mm from the centreline of the support was noticeably wider than any other cracks and propagated through the depth of the beam. As the load reached 109 kN, another crack appeared at 415 mm also within the shear span region. As the load approached its maximum value, the crack at 415 mm propagated through the beam depth. Then, it connected with the large vertical crack at 520 mm from the support centreline, isolating a prism of concrete. At failure, de-bonding occurred between the GFRP bar and the concrete with total slip at the free end equal to 8.34 mm as shown in Figure 5.6

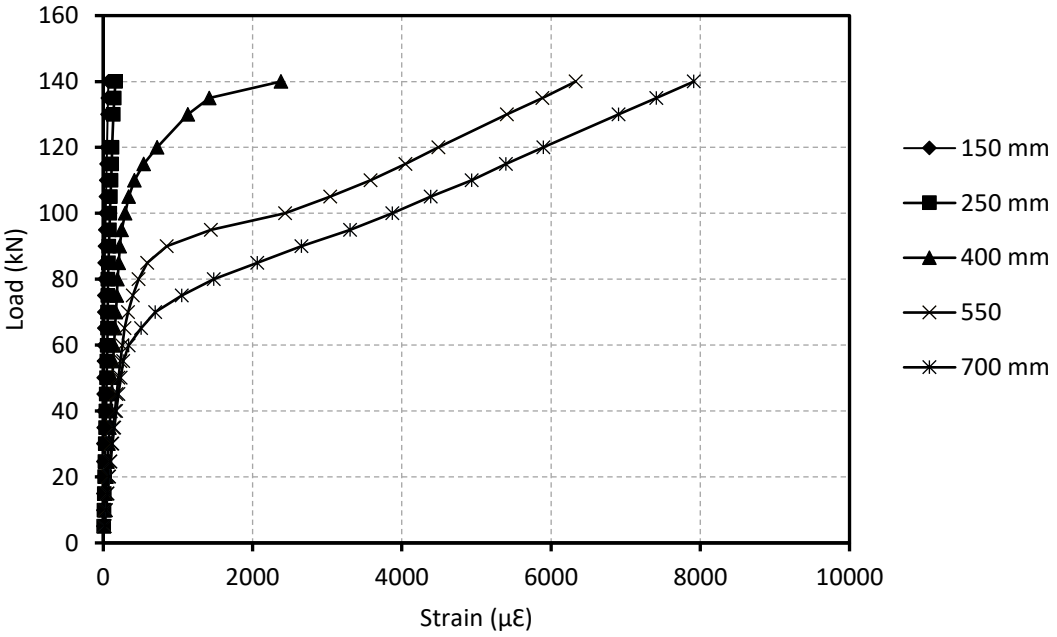

a) GFRP strain due to loading

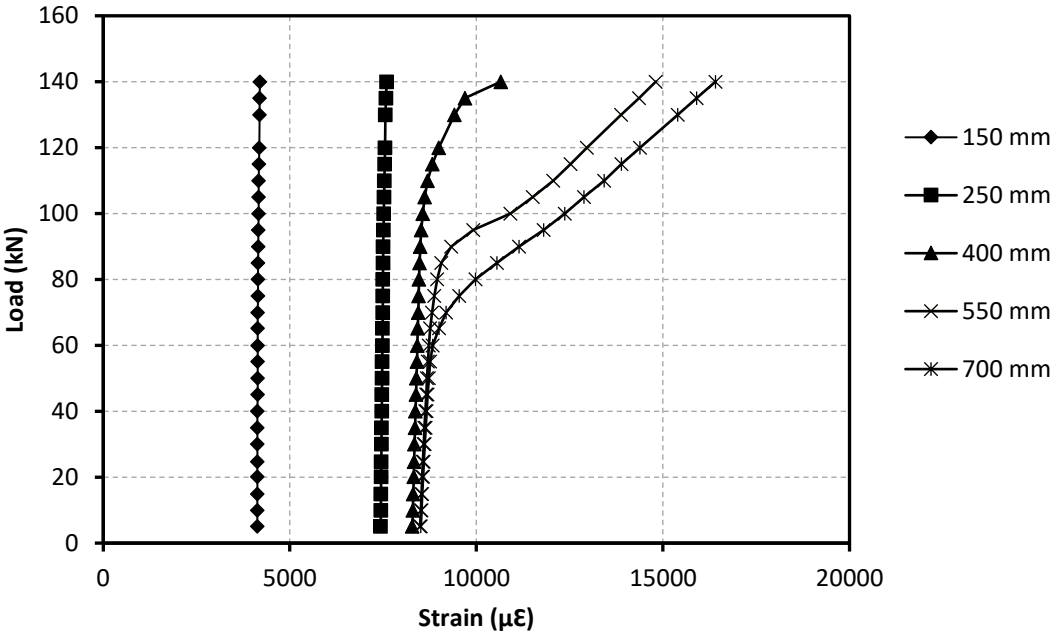

b) Total GFRP strain (GFRP strain due to loading and prestressing)

Figure 5.5: Load vs. GFRP strain for beam SC-16-1.5-40%

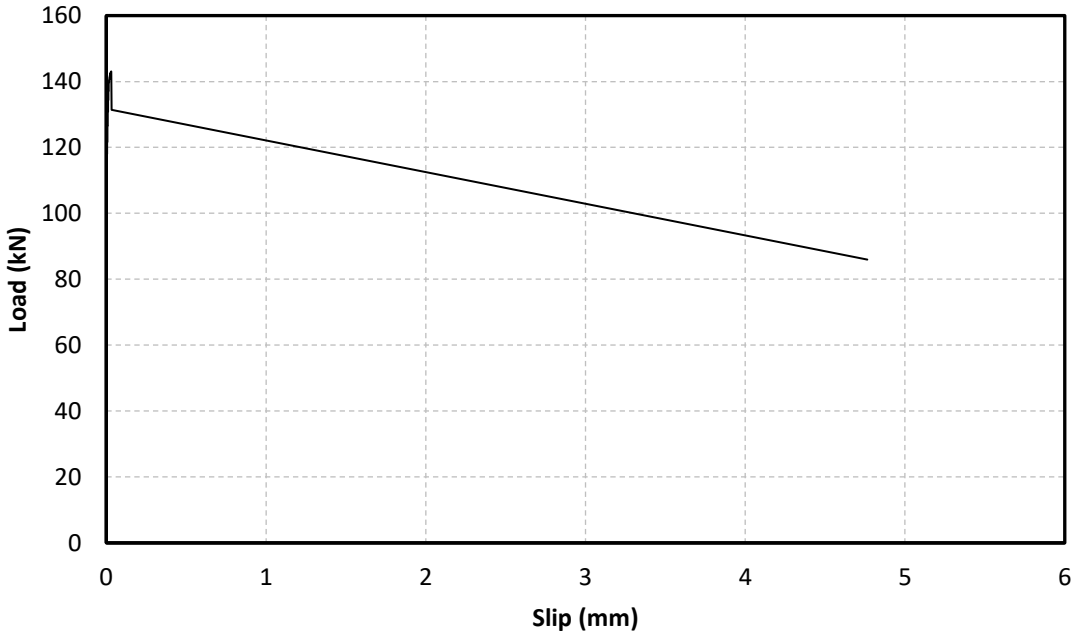

Figure 5.6: Load vs. end slip for beam SC-16-1.5-40%

Strain distribution in the shear span

Figure 5.7 shows the total strain profile (GFRP strain due to prestressing plus strain due to applied load) in the GFRP bar at various load levels for beam SC-16-1.5-40%. As shown in Figure 5.7, there were no significant changes in the strain gauge readings due until the applied load reached the cracking load of 65 kN. As the test proceeded and the load reached 105 kN, the strain gauge readings at 550 mm and 700 mm increased by 2815 με and 3212 με indicating that the concrete cracks at these locations are getting wider and deeper. When the load reached 120 kN, the strain reading at 550 mm increased and was almost equal to the reading at mid-span indicating partial de-bonding between these locations. At failure (140 kN), the strain gauge readings at 550 mm and 700 mm and mid-span increased and remained almost equal. At the same time the readings at 400 mm increased until the beam failed by de-bonding failure.

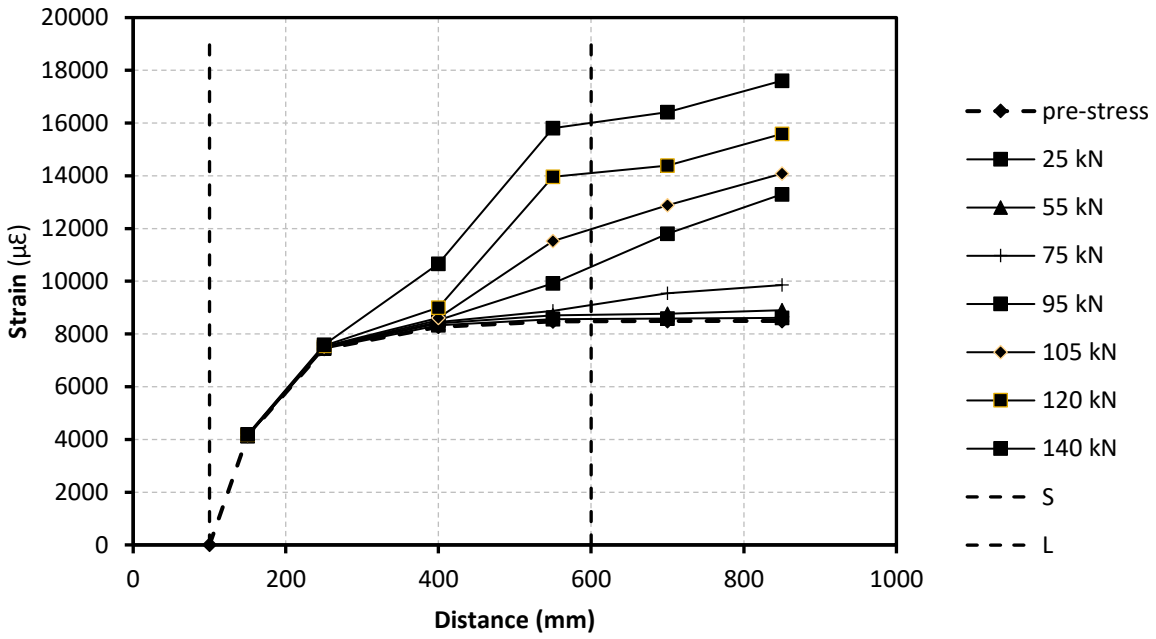

Figure 5.7: Total strain distribution along the GFRP bar at different load levels

5.4.1.3 Beams Reinforced with 12.7 mm Sand Coated GFRP Bar

Load vs. mid-span deflection curve

Figure 5.8 shows the load vs deflection curves for beams reinforced with 12 mm diameter bar and a concrete cover equal to $1.5 \cdot d_b$ and $3.0 \cdot d_b$. The load vs deflection curves were divided into two segments for both beams. Before the concrete at mid span reached its tensile strength and the first crack appeared, the slope is very steep. As the load increases and the first crack appeared, (~42 kN for $1.5 \cdot d_b$ and ~ 68 kN for $3.0 \cdot d_b$). The load vs. deflection slope decreases and the mid-span deflection continues to increase with the load until the failure load is reached. The ultimate mid-span deflection was 43 mm for the beam with concrete cover equal to 1.5 times the bar diameter and 34 mm for the beam with a concrete cover equal to 3.0 times the bar diameter.

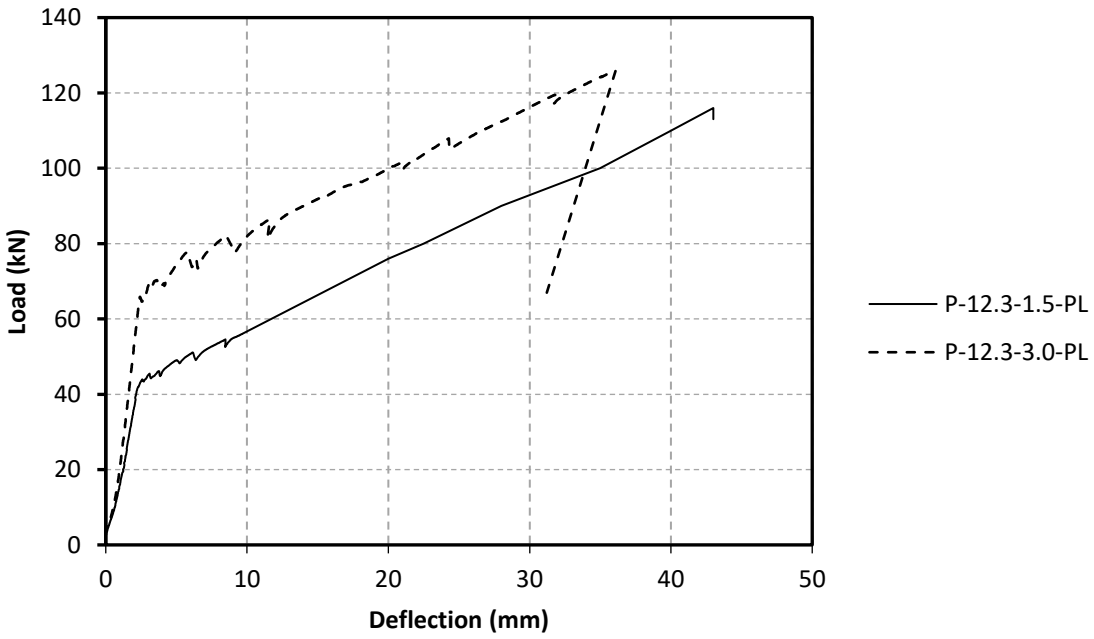

Figure 5.8: load vs. deflection curve for beams reinforced with 12 mm GFRP bar

Cracking behaviour

Figure 5.9 shows the load vs. GFRP bar strain for beam SC-12.3-1.5-40%. As the load increased, the GFRP strain readings increased at all locations along the beam length until the load reached 43 kN at which point the beam cracked at mid-span. Then at the crack location the tensile forces were transferred from the concrete to the GFRP bar and there was a sudden increase in the reading of the strain gauge mounted near the crack on the GFRP bar. When the load reached 56 kN, another crack appeared within the shear span region at 550 mm from the centreline of the support. As the test proceeded, the crack at 550 mm from centreline of the support was noticeably wider than any other cracks and propagated through the depth of the beam. As the load reached 81 kN, another crack appeared at 400 mm also within the shear span region. As the load approached its maximum value, the crack at 400 mm propagated through the beam depth. Then, it was connected with the large vertical crack at 250 mm from the support centreline, isolating a prism of concrete. At failure, de-bonding occurred between the GFRP bar and the concrete with a total slip at the free end equal to 14 mm as shown in Figure 5.10.

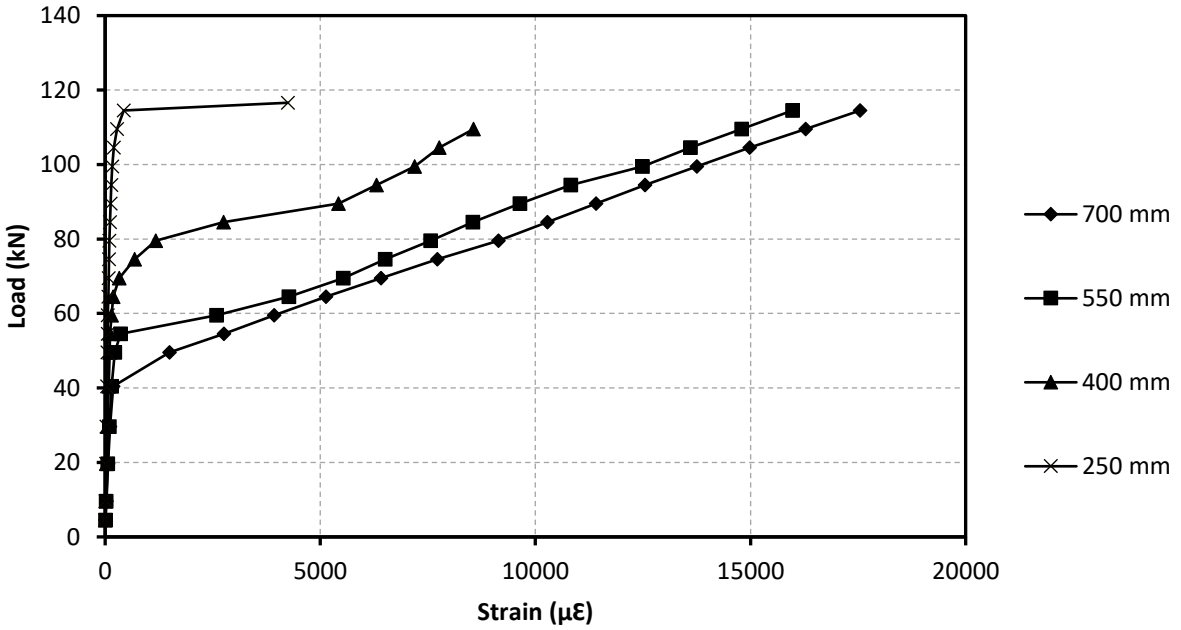

a) GFRP strain due to loading

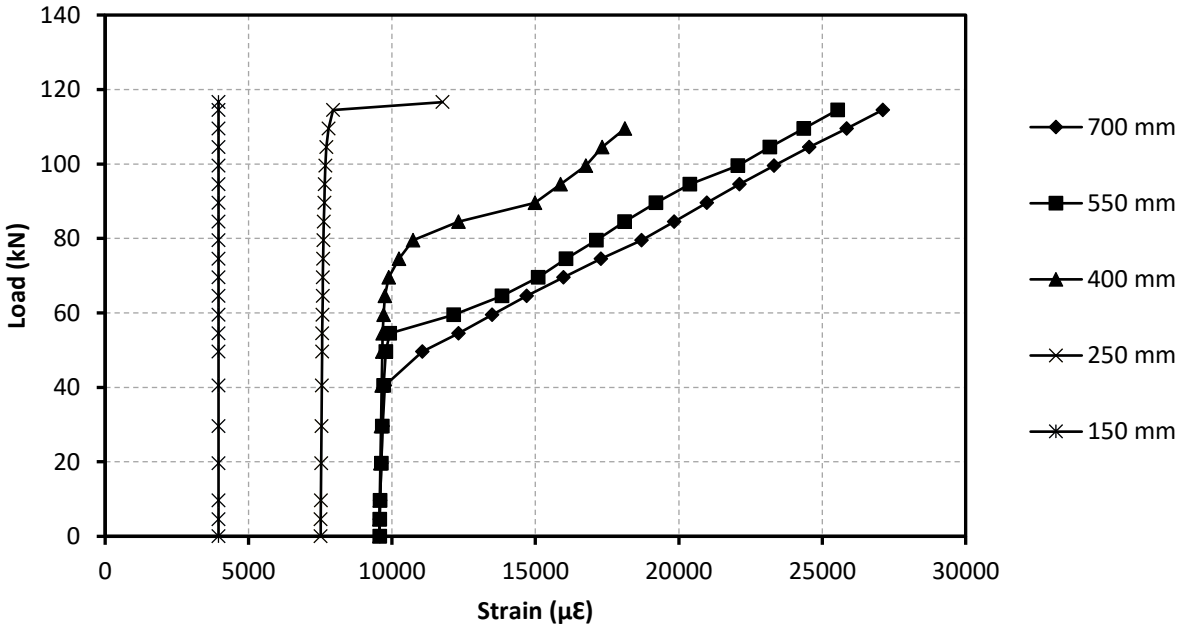

b) Total GFRP strain (GFRP strain due to loading and prestressing)

Figure 5.9: Load vs. GFRP strain for beam SC-12.3-1.5-40%

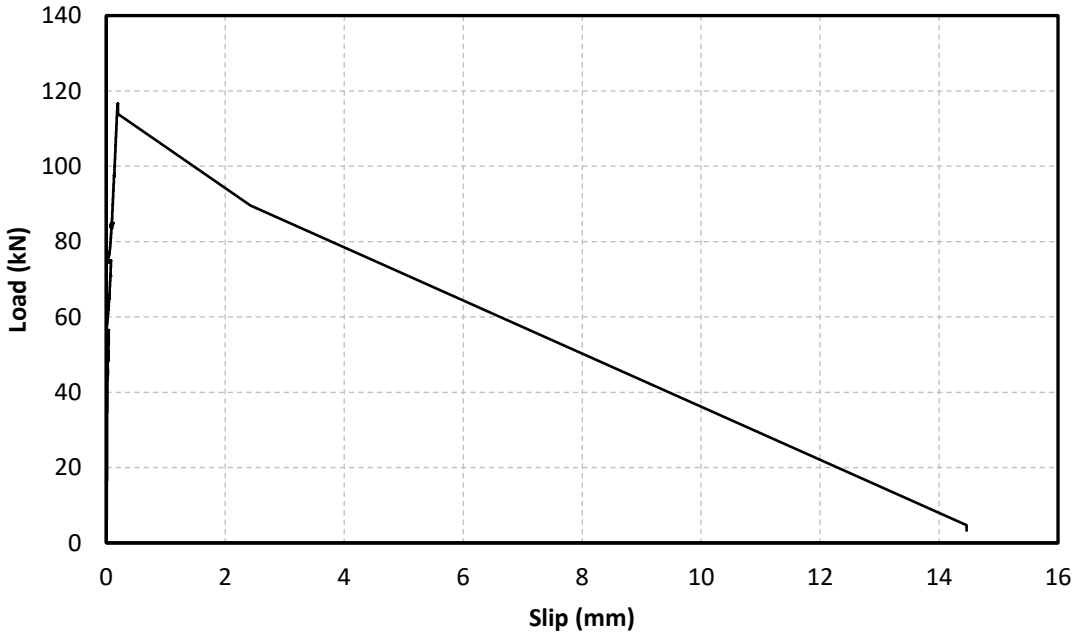

Figure 5.10: Load vs. end slip for beam SC-12.3-1.5-40%

5.4.2 Beams Reinforced with Ribbed GFRP Bar (Preliminary Study)

5.4.2.1 General

Four beams in this phase were tested under monotonic loading until failure. All beams reinforced with Ribbed GFRP bar failed by bond failure between the bar and surrounding concrete. The ultimate capacity summarizes in Table 5.3.

Table 5.3: Ultimate capacity and failure mode for pre-stressed ribbed coated reinforced beams

Specimen notation	Max load (kN)	Failure mode
R-16-1.5-40%	136	splitting bond failure
R-16-3.0-40%	208	splitting bond failure
R-12-1.5-40%	116	splitting bond failure
R-12-3.0-40%	164	splitting bond failure

5.4.2.2 Beams Reinforced with 16 mm Ribbed Bar

Load vs. mid-span deflection curve

Figure 5.11 shows the Load vs deflection curve for beams reinforced with 16 mm bar diameter and concrete covers equal $1.5 \cdot d_b$ and $3.0 \cdot d_b$. As the load increases, the mid-span deflection increases until the concrete reached its ultimate tensile strength and cracks appear at mid-span (~56 kN for $1.5 \cdot d_b$ and ~ 93 kN for $3.0 \cdot d_b$). After concrete cracking at mid-span, the load vs. deflection slope decreases and the mid-span deflection continues to increase with the load until the ultimate load is reached.

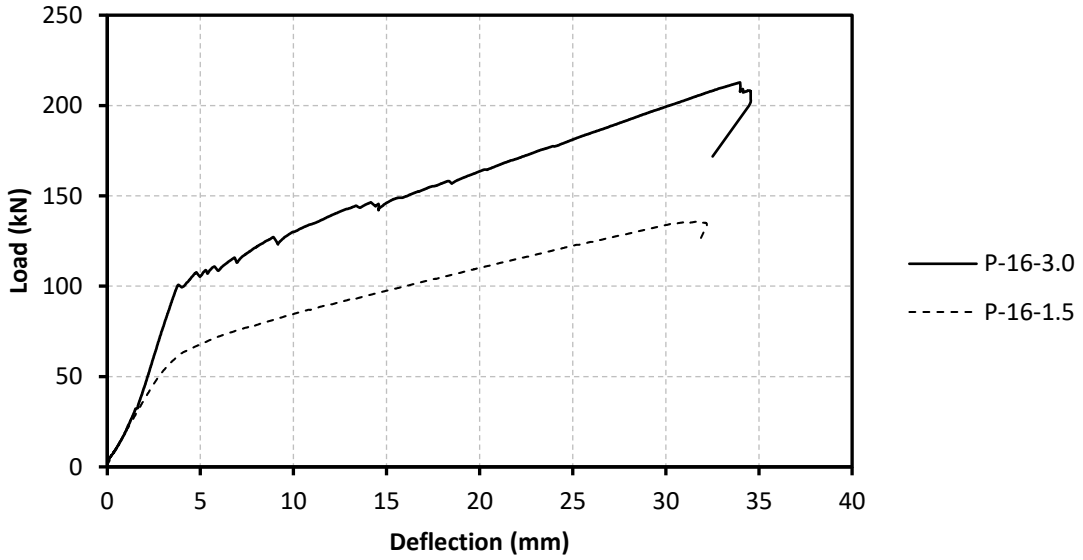

Figure 5.11: Load vs. deflection curve for beams reinforced with 16 mm GFRP bar

Cracking behaviour

Figures 5.12 shows the load vs. GFRP bar strain for beam R-16-1.5-40%. As the load increases, the GFRP strain readings increase at all locations along the beam length until the load reaches 62 kN at which point the beam cracked at mid-span. Then at the crack location the tensile forces were transferred from the concrete to the GFRP bar and there was a sudden increase in the reading of the strain gauge mounted near the crack on the GFRP bar. When the load reached 76 kN, another crack appeared within the shear span region at 550 mm from the centreline of the support. As the load reached 81 kN, another crack appeared at 400 mm also within the shear span region. As

the test proceeded, the crack at 400 mm from the centreline of the support was noticeably wider than any other cracks and propagated through the depth of the beam. As the load approached its maximum value, the crack at 400 mm propagated through the beam depth. Then, it connected with the large vertical crack at 250 mm from the support centreline, isolating a prism of concrete. At failure, de-bonding occurred between the GFRP bar and the concrete with total slip at the free end equal to 14 mm as shown in Figure 5.13

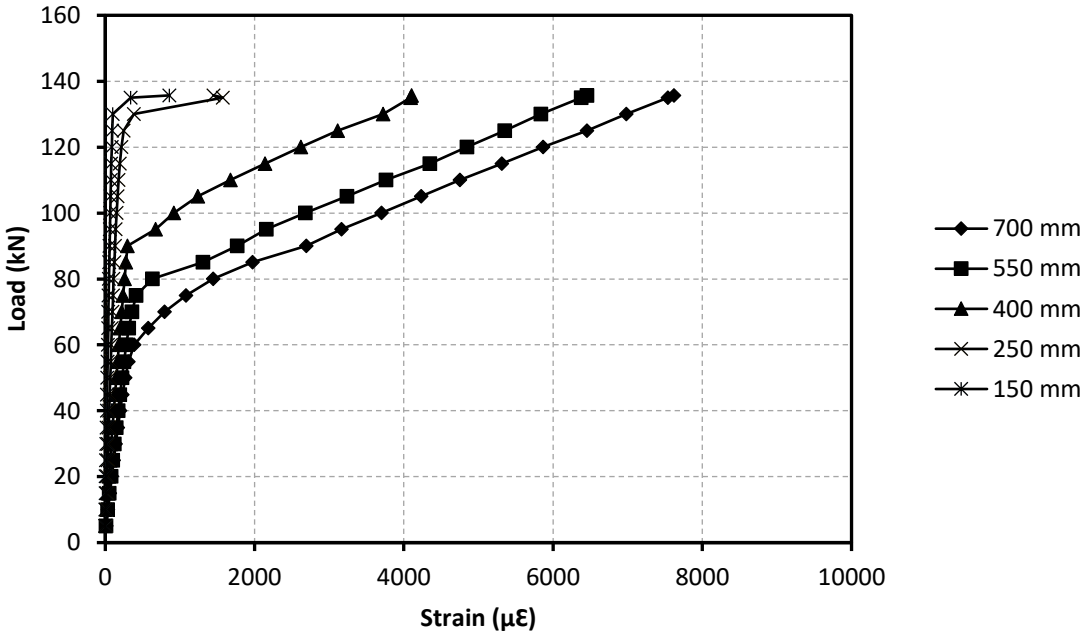

a) GFRP strain due to loading

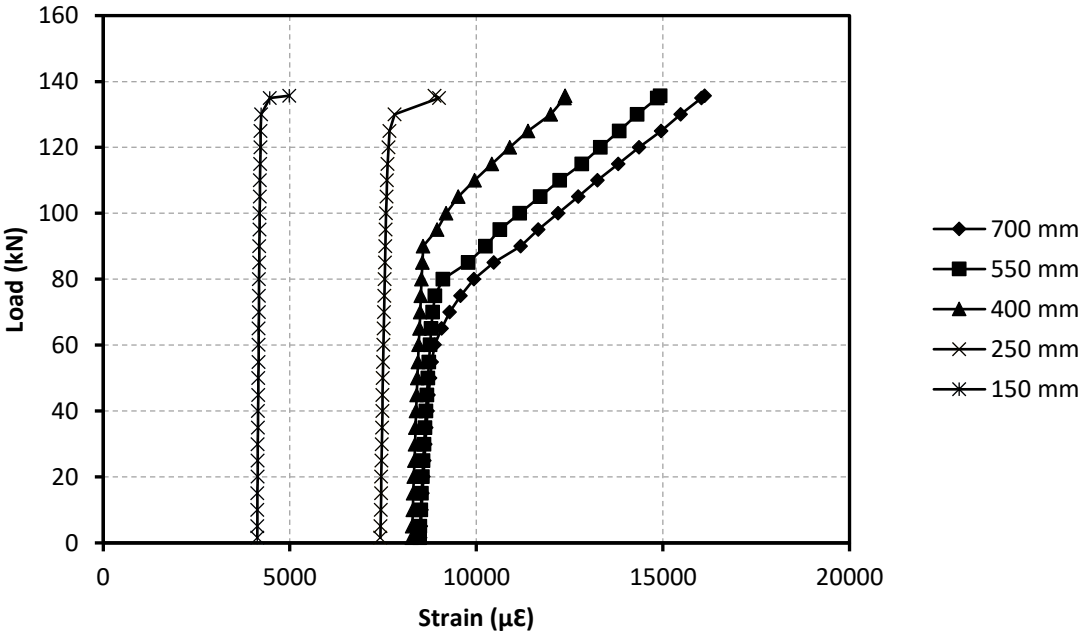

b) Total GFRP strain (GFRP strain due to loading and prestressing)

Figure 5.12: Load vs. GFRP strain for beam R-16-1.5-40%

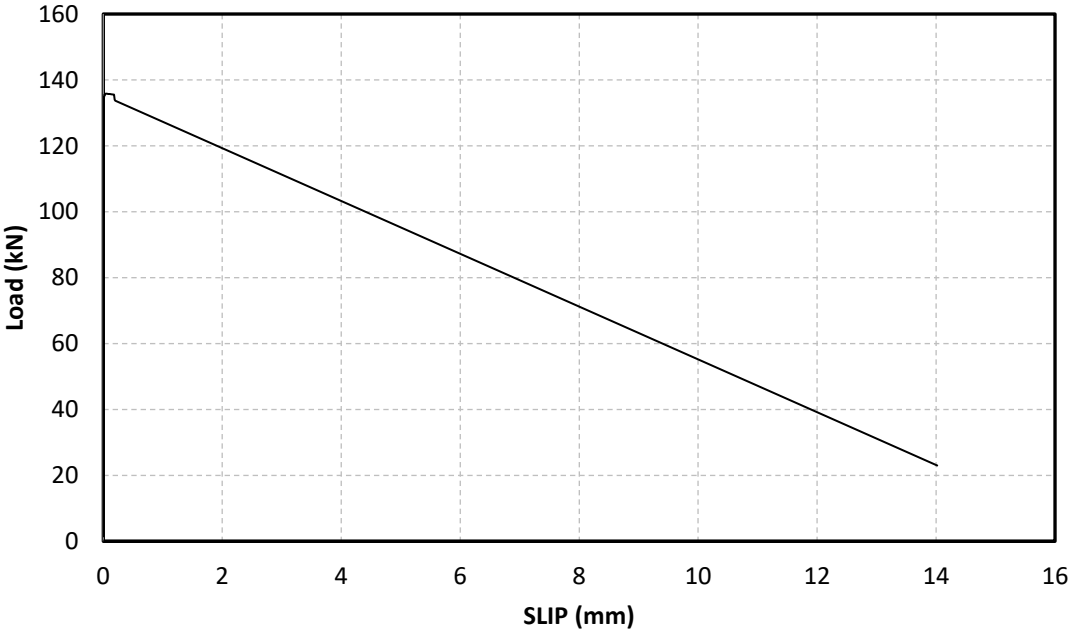

Figure 5.13: Load vs. end slip for beam R-16-1.5-40%

5.4.2.3 Beams Reinforced with a 12.7 mm Ribbed GFRP Bar

Load vs. mid-span deflection curve

Figure 5.14 shows the load vs deflection curve for beams reinforced with 12 mm diameter bar and concrete covers equal to $1.5 \cdot d_b$ and $3.0 \cdot d_b$. The load vs deflection curves were divided into two segments for both beams. Before the concrete at mid span reach its tensile strength and the first crack appeared, the slope is very steep. As the load increased and the first crack appeared, (~ 43 kN for the $1.5 \cdot d_b$ beam and ~ 68 kN for $3.0 \cdot d_b$ beam) the load vs. deflection slope decreased and the mid-span deflection continued to increase with the load until the failure load was reached. The ultimate mid-span deflection was 61 mm for the beam with a concrete cover equal to 1.5 times the bar diameter and 45 mm for the beam with a concrete cover equal to 3.0 times the bar diameter.

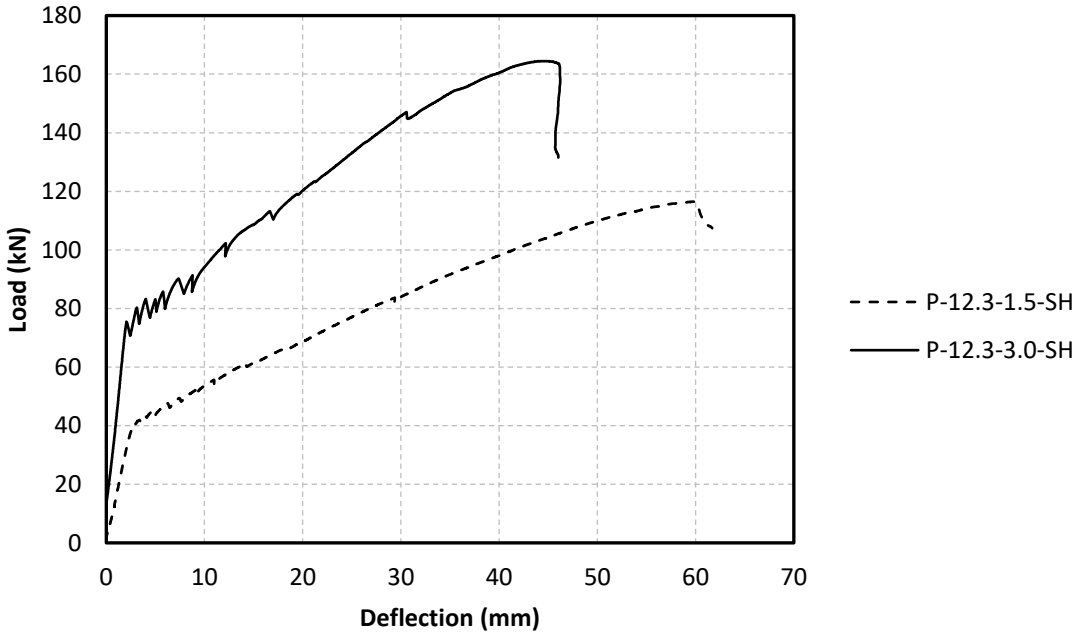

Figure 5.14 Load vs. deflection curve for beams reinforced with 12 mm GFRP bar

Cracking behaviour

Figures 5.15 shows the load vs. GFRP bar strain for beam R-12-1.5-40%. As the load increases, the GFRP strain readings increase at all locations along the beam length until the load reaches 82 kN at which point the beam cracked at mid-span. Then at the crack location the tensile forces were transferred from the concrete to the GFRP bar and there was a sudden increase in the reading of

the strain gauge mounted near the crack on the GFRP bar. When the load reached 91 kN, another crack appeared within the shear span region at 550 mm from the centreline of the support. As the load reached 100 kN, another crack appeared at 400 mm also within the shear span region. As the test proceeded, the crack at 400 mm from centreline of the support was noticeably wider than any other cracks and propagated through the depth of the beam. As the load approached its maximum value, the crack at 400 mm propagated through the beam depth. Then, it connected with the large vertical crack at 250 mm from the support centreline, isolating a prism of concrete. At failure, de-bonding occurred between the GFRP bar and the concrete with a total slip at the free end equal to 9 mm as shown in Figure 5.16.

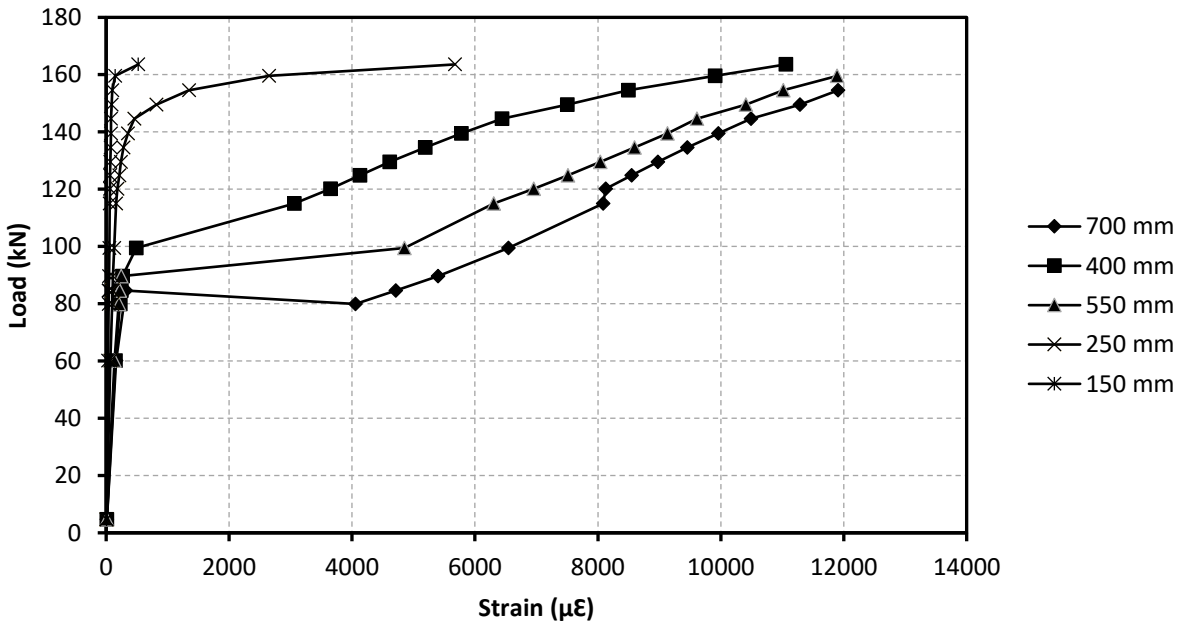

a) GFRP strain due to loading

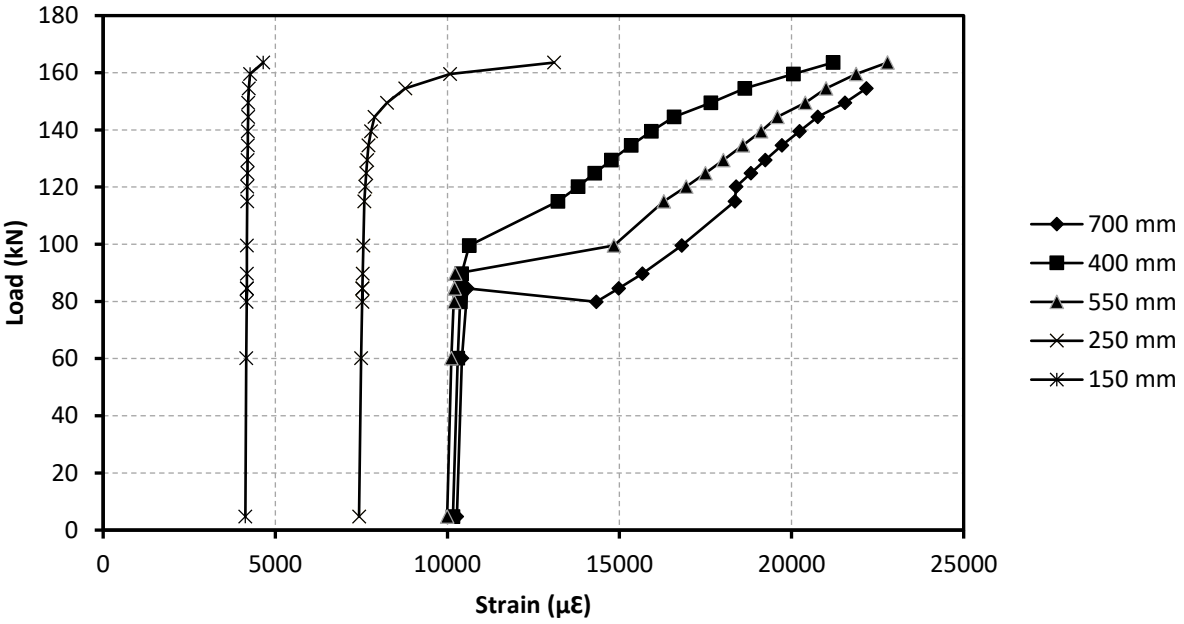

b) Total GFRP strain (GFRP strain due to loading and prestressing)

Figure 5.15: Load vs. GFRP strain for beam R-12-3.0-40%

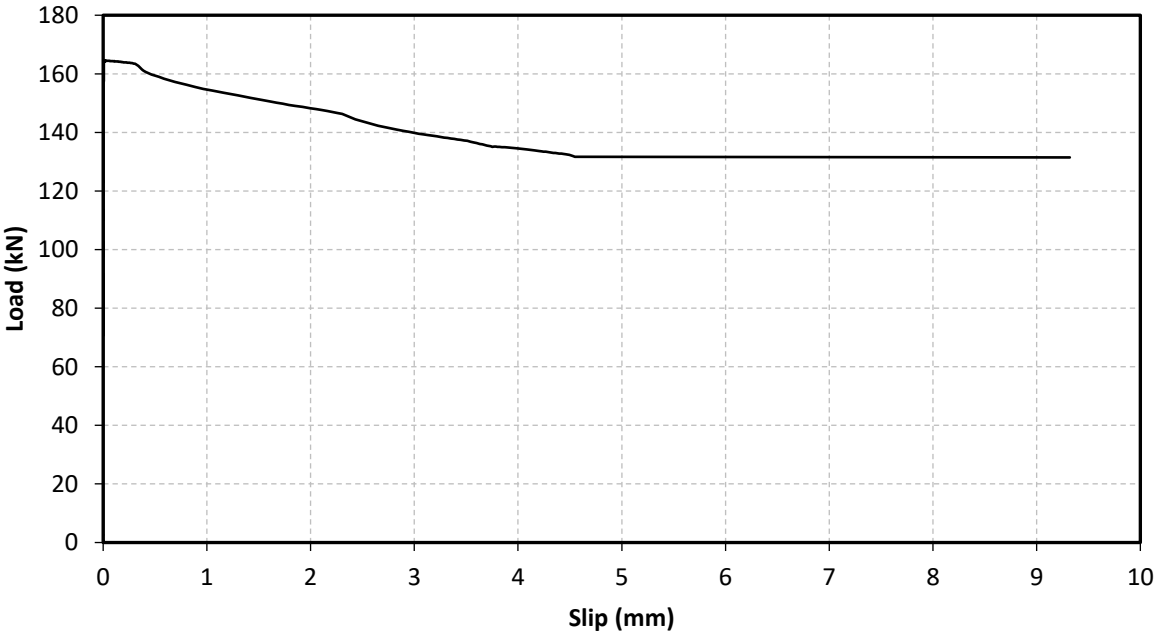

Figure 5.16: Load vs. end slip for beam R-12.3-3.0-40%

5.4.3 Beams Reinforced with Sand Coated GFRP bar (Main Study)

5.4.3.1 General

For the main study, twelve beams were cast and tested under static and fatigue loading. All beams were reinforced with 16 mm prestressed sand coated GFRP bar. Two different concrete covers were used in this study to investigate the effect of the depth of the concrete cover on the strength of the bond between the bar and the concrete. The first group of beams (six beams) had a concrete cover equal to 1.5 times the bar diameter (≈ 25 mm) and the second group (six beams) had a concrete cover equal to 3.0 times the bar diameter (≈ 45 mm). The beam geometries were different for the beams that had concrete covers equal to 25 mm and 45 mm. The beam geometry was (267 mm high, 200 mm wide and 2000 mm long) for the beam with a 25 mm concrete cover and the beam geometry for the beam with a 45 mm concrete cover was (297 mm high, 200 mm wide and 2000 mm long). For each group, one beam was tested under monotonic loading until failure while the other five beams were tested under fatigue loading until failure. In this section, the test results for beams tested under monotonic loading will be presented and discussed followed by and the test results for beams tested under fatigue loading. All beams were tested in four-point bending and failed in bond. In the following sections, the load vs deflection, the cracking behaviour and the strain profile will be presented. Table 5.4 shows the ultimate capacity for both beams. Figure 5.17 shows a typical bond failure.

Figure 5.17 typical bond failure

Table 5.4: Ultimate capacity and failure mode for pre-stressed sand coated reinforced beam (main)

Specimen notation	Max load (kN)	Failure mode
SC-16-1.5-40%	167	Splitting Bond failure
SC-16-3.0-40%	192	Splitting Bond failure

Load Vs mid-span deflection curves

Figure 5.18 shows the load vs deflection curves for beams reinforced with 16 mm diameter bar and concrete covers equal to $1.5 \cdot d_b$ and $3.0 \cdot d_b$. The load vs deflection curves were divided into two segments for both beams. As the load increased, load deflection curve was steep until the concrete reached its tensile strength and the first crack appeared at mid-span (~ 87 kN for the $1.5 \cdot d_b$ beam and ~ 96 kN for the $3.0 \cdot d_b$ beam). After cracking, the slope of the load vs. deflection curve decreases and the mid-span deflection continues to increase for both beams with increasing load until the failure load is reached. The ultimate mid-span deflection was 17.8 mm for the beam with a concrete cover equal 1.5 times the bar diameter and 21 mm for the beam with a concrete cover equal 3.0 times the bar diameter.

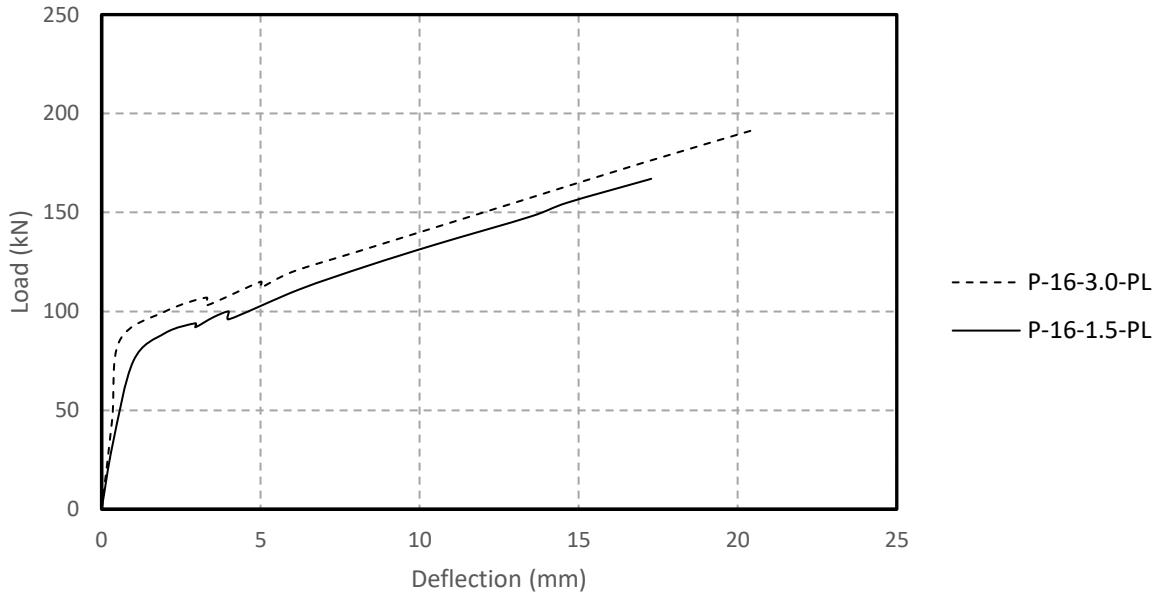

Figure 5.18: The load vs. deflection curves for beams reinforced with 16 mm GFRP bars and two different concrete covers (25 mm and 45 mm)

Cracking behaviour

Figures 5.19 shows load vs strain curves for beams reinforced with 16 mm sand coated GFRP bar and a concrete cover equal to 25 mm. As the load increases, the GFRP strain readings increase at all locations along the beam length until the load reaches 84 kN at which point the beam cracks at mid-span. Then at the crack location the tensile forces were transferred from the concrete to the GFRP bar and there was a sudden increase in the reading of the strain gauge mounted near the crack on the GFRP bar. When the load reached 96 kN, another crack appeared within the shear span region at 350 mm from the centreline of the support. When the load reached at 140 kN, a vertical cracked appeared at 245 mm from the support. The crack at 245 mm from the centreline of the support was noticeably wider and propagated through the depth of the beam as the load increased. As the load approached its maximum value, the crack at 245 mm propagated through the beam depth. Then, it connected with another vertical crack at 200 mm from the support centreline, isolating a prism of concrete. At failure, de-bonding occurred between the GFRP bar and the concrete with total slip at the free end equal to 8.34 mm as shown in figure 5.20.

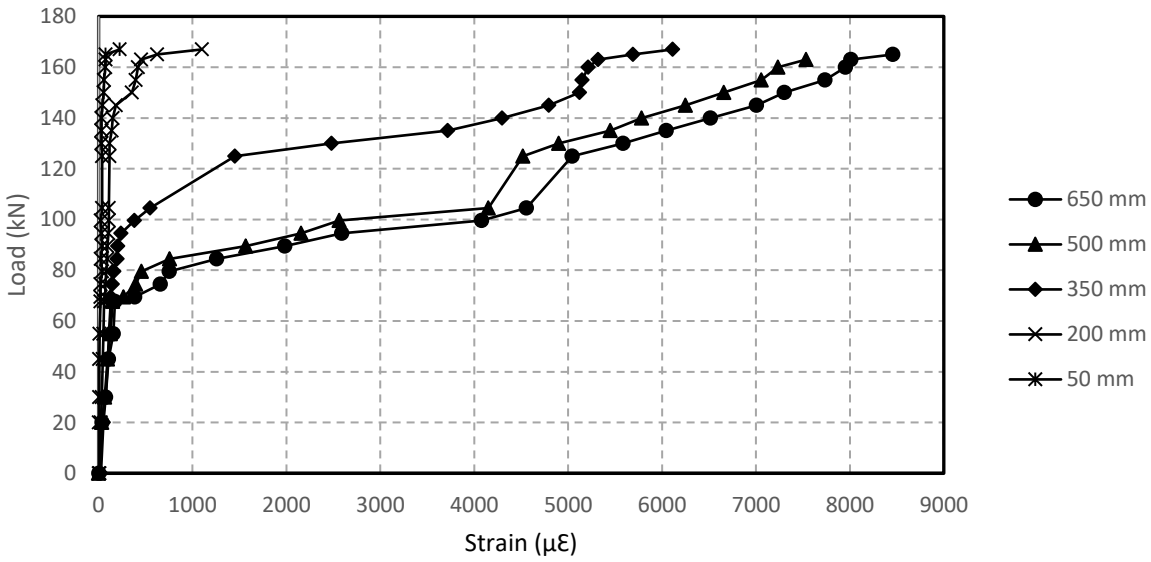

a) GFRP strain due to loading

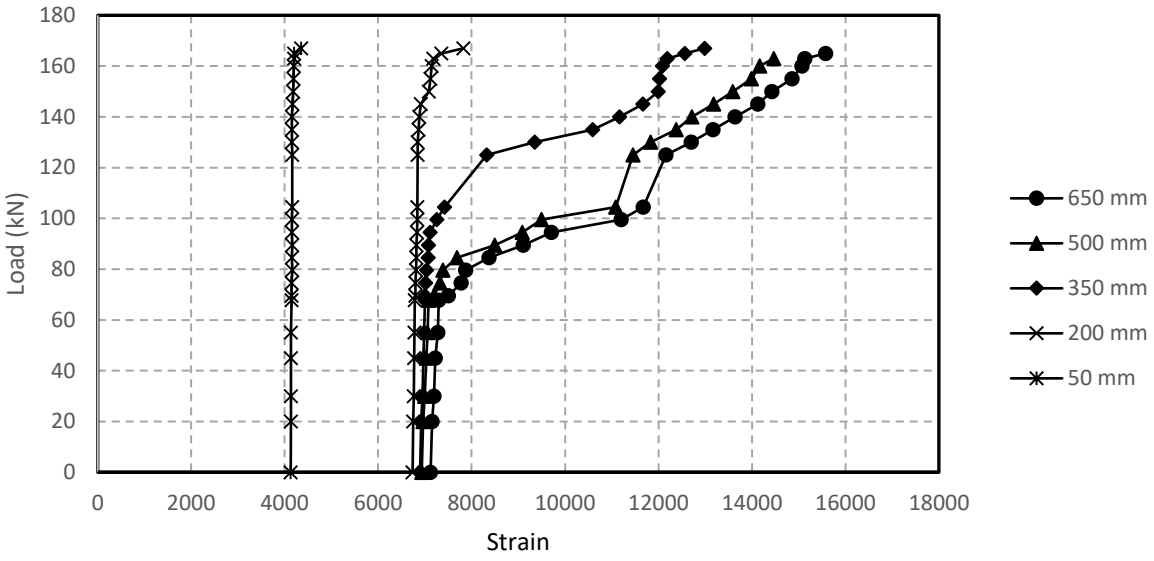

b) Total GFRP strain (GFRP strain due to loading and prestressing)

Figure 5.19: Load vs. GFRP strain for beam SC-16-1.5-40%

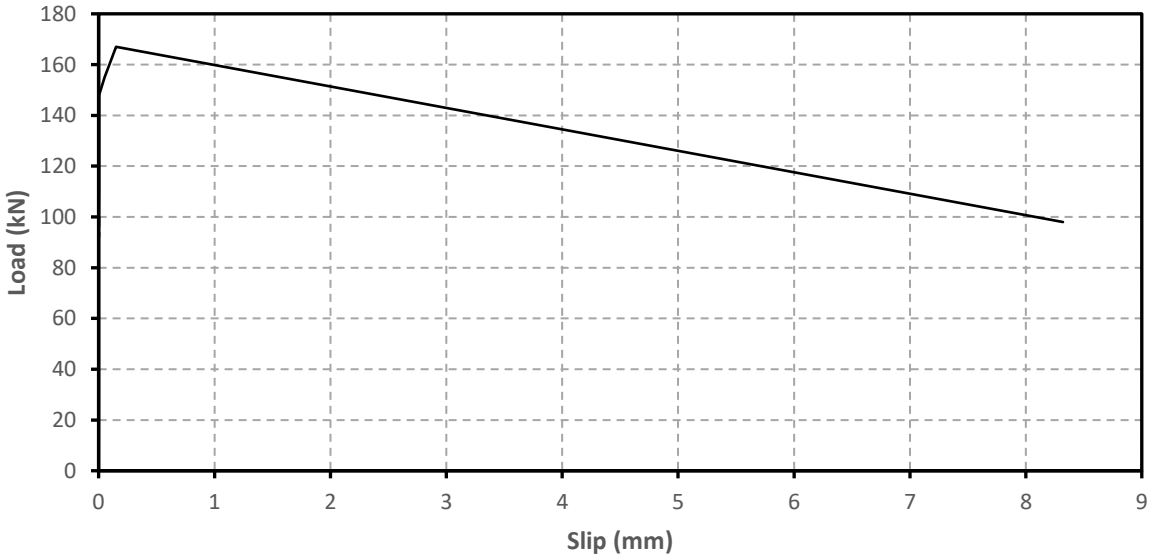

Figure 5.20: Load vs. end slip for beam SC-16-1.5-40%

The cracking behaviour for the beam with a concrete cover equal to 45 mm was similar to the beam with a concrete cover equal 25 mm. The crack initiated at mid span when the concrete reached its ultimate capacity and propagated toward the support. Figures 5.21 and 5.22 show the

load vs strain and load vs slip curves for beams reinforced with 16 mm sand coated GFRP bar having a concrete cover equal to 45 mm.

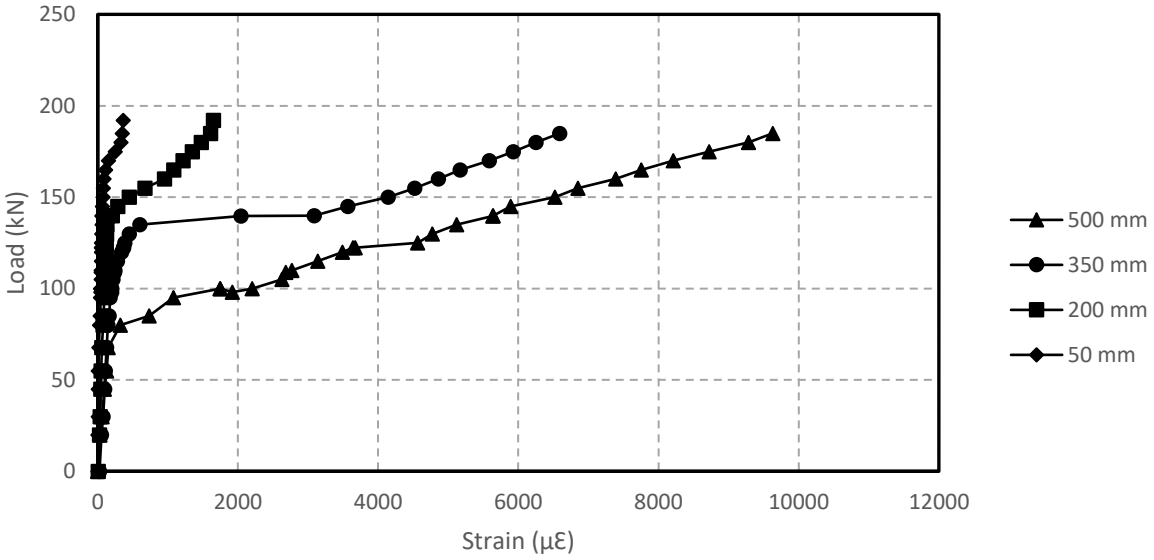

a) GFRP strain due to loading

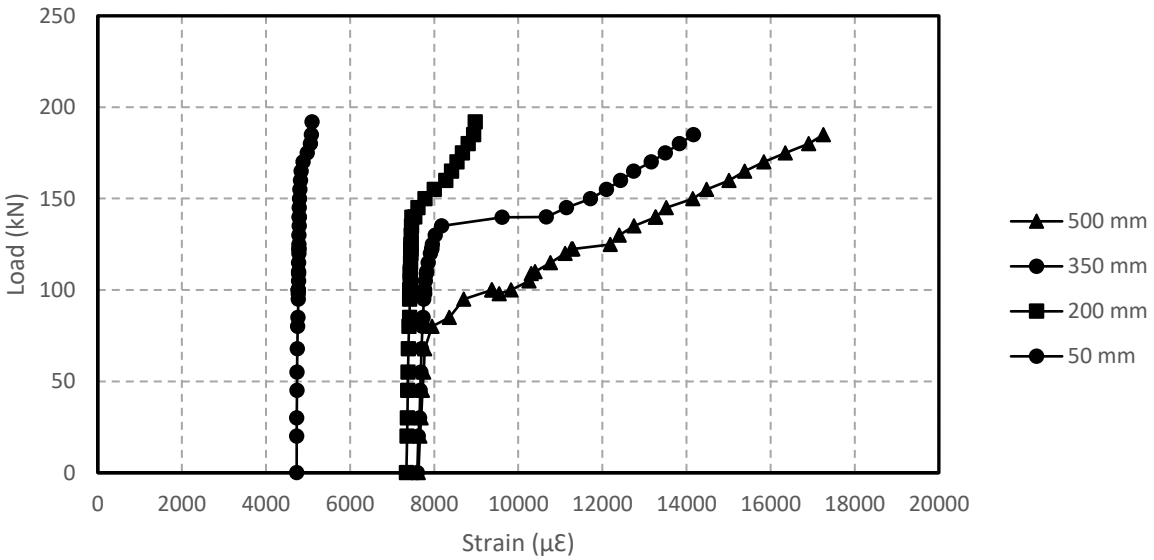

b) Total GFRP strain (GFRP strain due to loading and prestressing)

Figure 5.21: Load vs. GFRP strain for beam SC-16-3.0-40%

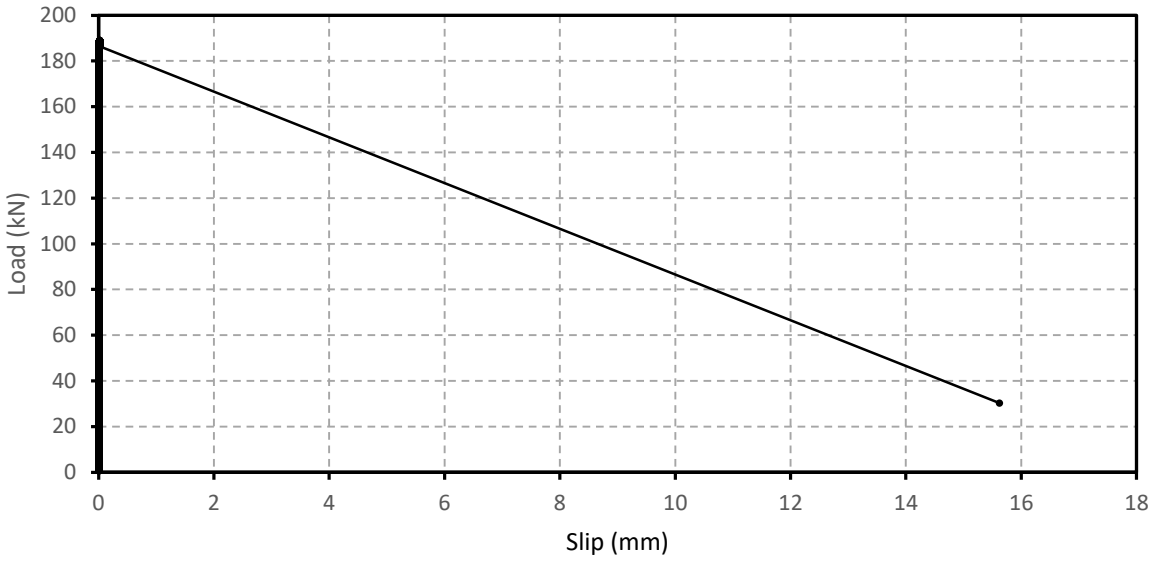

Figure 5.22: Load vs. end slip for beam SC-16-3.0-40%

Strain distribution in the shear span

Figures 5.23 and 5.24 show the total strain profile (GFRP strain due to prestressing plus strain due to the applied load) in the GFRP bar at various load levels for beams SC-16-1.5-40% and SC-16-3.0-40%, respectively. As shown in Figure 5.23, there were no significant changes in the strain gauge readings due to cracking until the applied load reached 95 kN. As the test proceeded and the load reached 105 kN, the strain gauge readings at 500 mm and 650 mm increased by 4305 με and 4865 με indicating that the concrete cracks at these locations were getting wider and deeper. When the load reached 125 kN, the strain reading at 500 mm increased until it was almost equal to the reading at mid-span indicating partial de-bonding between these locations. Also, at the same load level (125 kN) the strain at 350 mm jumped to 2577 με indicating that the de-bond crack had reached this point. At failure (167 kN), the strain gauge readings at 500 mm and 650 mm increased and remained almost equal. At the same time the readings at 350 mm increased until the beam failed by de-bonding failure.

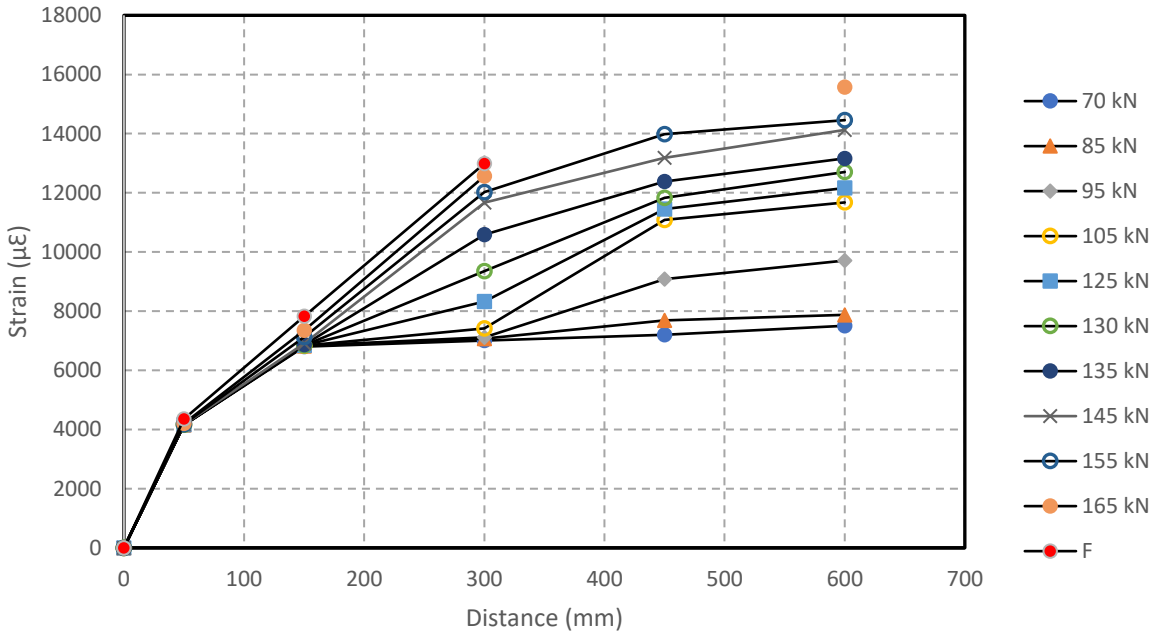

Figure 5.23: Total strain distribution along the GFRP bar at different load levels for beam SC-16-1.5-40%

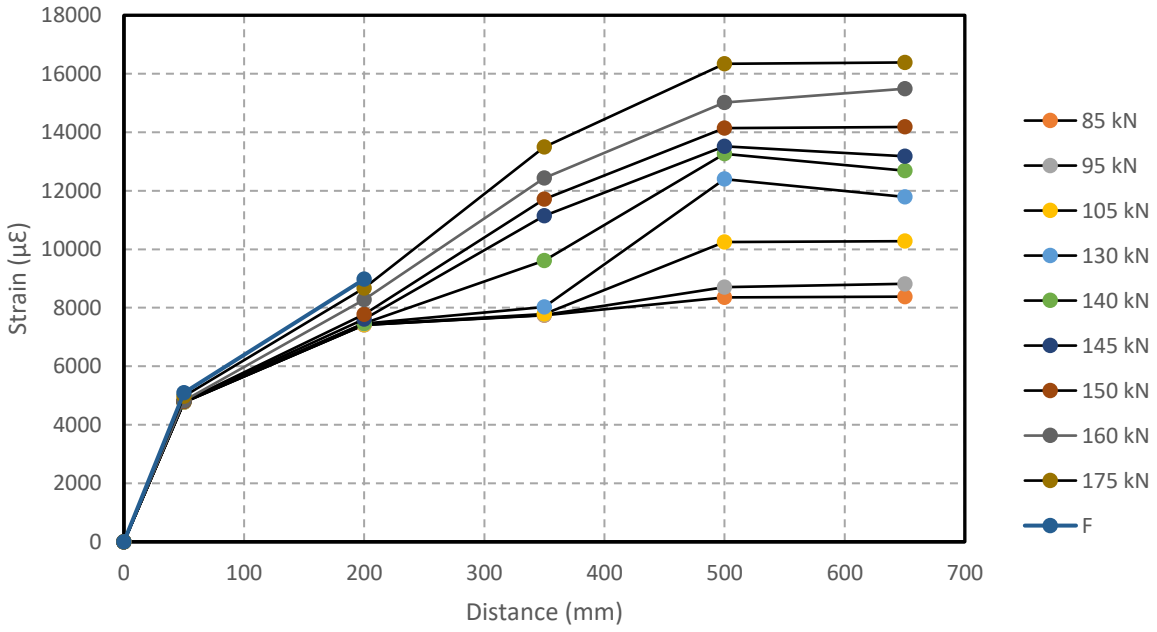

Figure 5.24: Total strain distribution along the GFRP bar at different load levels for beam SC-16-3.0-40%

5.4.4 Beams Reinforced with Ribbed GFRP Bar (Main Study)

5.4.4.1 General

Six beams were cast and tested under static and fatigue loading. All beams were reinforced with a 16 mm prestressed sand coated GFRP bar and had a concrete cover equal to 25 mm. The beam geometry was (267 mm deep, 200 mm in width and 2000 mm long). One beam was tested under monotonic loading until failure while the other five beams were tested under fatigue loading until failure. The test results for beams tested under monotonic loading will be presented and discussed followed by a discussion of the test results for beams tested under fatigue loading. All beams were tested in four-point bending and failed in bond. In the following sections, load vs deflection results, cracking behaviour and the strain profile will be presented. Table 5.5 shows the ultimate capacity for beam R-16-1.5-40%.

Table 5.5: Ultimate capacity and failure mode for pre-stressed ribbed reinforced beams (main)

Specimen notation	Max load (kN)	Failure mode
R-16-1.5-40%	157	splitting bond failure

Load vs. mid-span deflection curve

Figure 5.25 shows the load vs deflection curve for a beam reinforced with 16 mm Ribbed GFRP bar. The load vs deflection curve exhibits two segments. Initially the load deflection curve is steep and then the slope decreases abruptly when the concrete cracks at mid-span (~85 kN). After cracking, the load vs. deflection continues to increase at a nearly constant slope until the failure load is reached. The ultimate mid-span deflection was 14.65 mm.

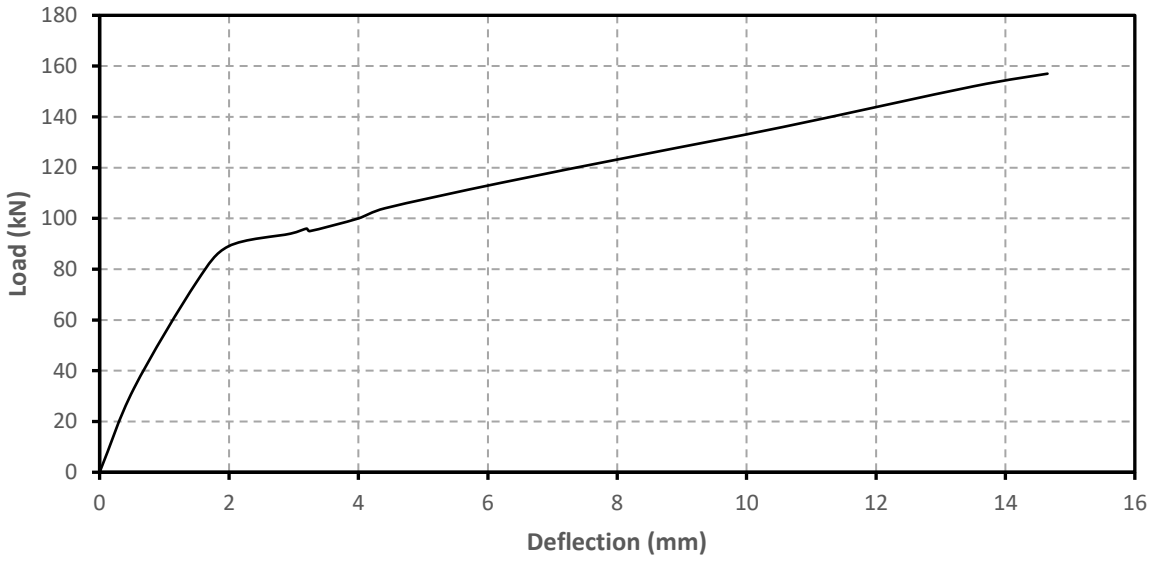

Figure 5.25: The load vs. deflection curve for beam reinforced with 16 mm GFRP

Cracking behaviour

Figures 5.26 shows applied load vs strain plots for locations along the GFRP bar, for beams reinforced with a 16 mm Ribbed GFRP bar having a concrete cover equal to 25 mm. In part A of the figure the strain is given as the strain due to loading while in part B the total strain due to loading plus prestressing is used. As the load increased, the GFRP strain readings increased at all locations along the beam length until the load reached 85 kN at which point the beam cracked at mid-span. Then at the crack location the tensile forces were transferred from the concrete to the GFRP bar and there was a sudden increase in the reading of the strain gauge mounted on the GFRP bar near the crack. When the load reached 105 kN, another crack appeared within the shear span region at 350 mm from the centreline of the support. Furthermore, when the load reached at 135 kN a vertical crack appeared at 240 mm from the support. The crack at 240 mm from the centreline of the support was noticeably wider than the others and propagated through the depth of the beam as the load increased. As the load approached its maximum value, the crack at 245 mm propagated through the beam depth. Then, it connected with another vertical crack at 200 mm from the support centreline, isolating a prism of concrete. At failure, de-bonding occurred between the GFRP bar and the concrete with total slip at the free end equal to 8.34 mm as shown in Figure 5.27.

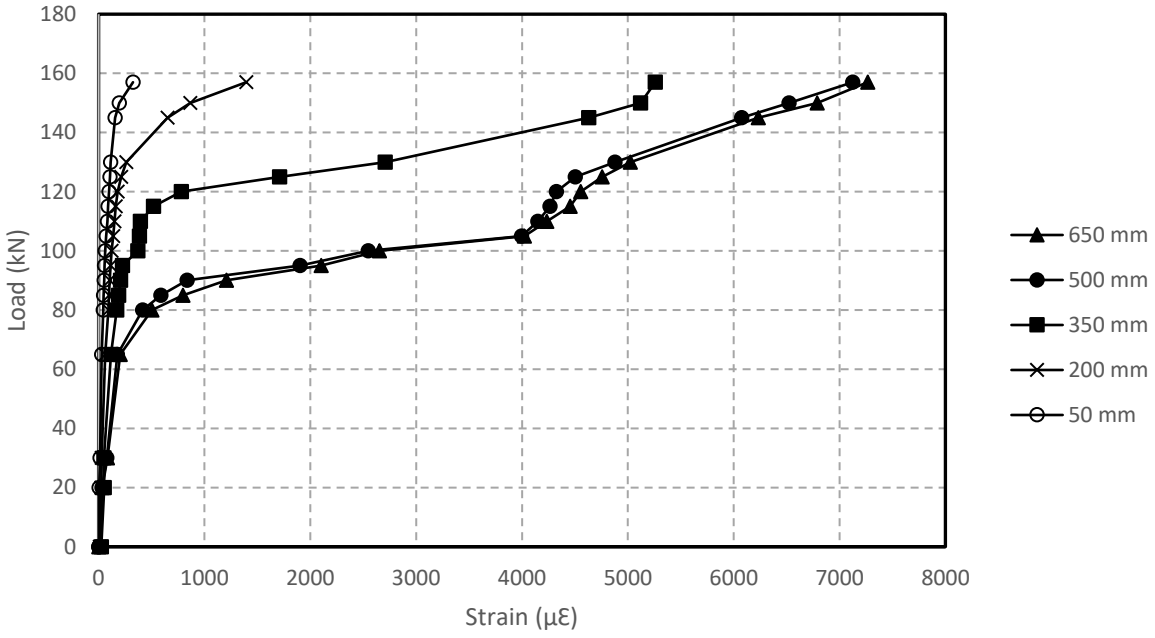

a) GFRP strain due to loading

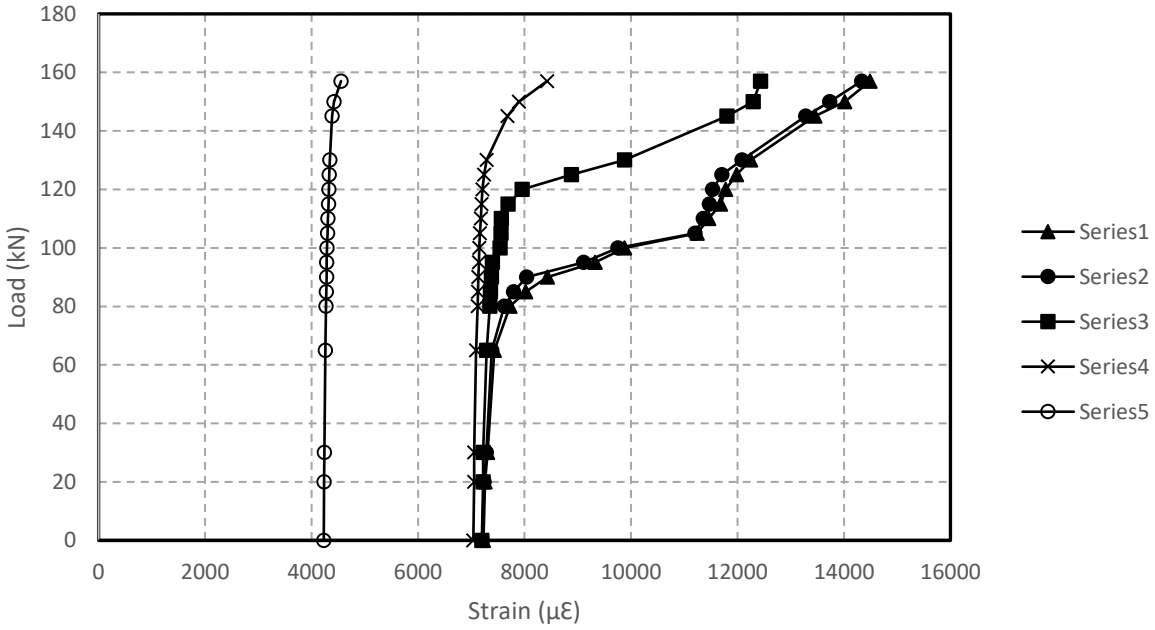

b) Total GFRP strain (GFRP strain due to loading and prestressing)

Figure 5.26: Load vs. GFRP strain for beam R-16-1.5-40%

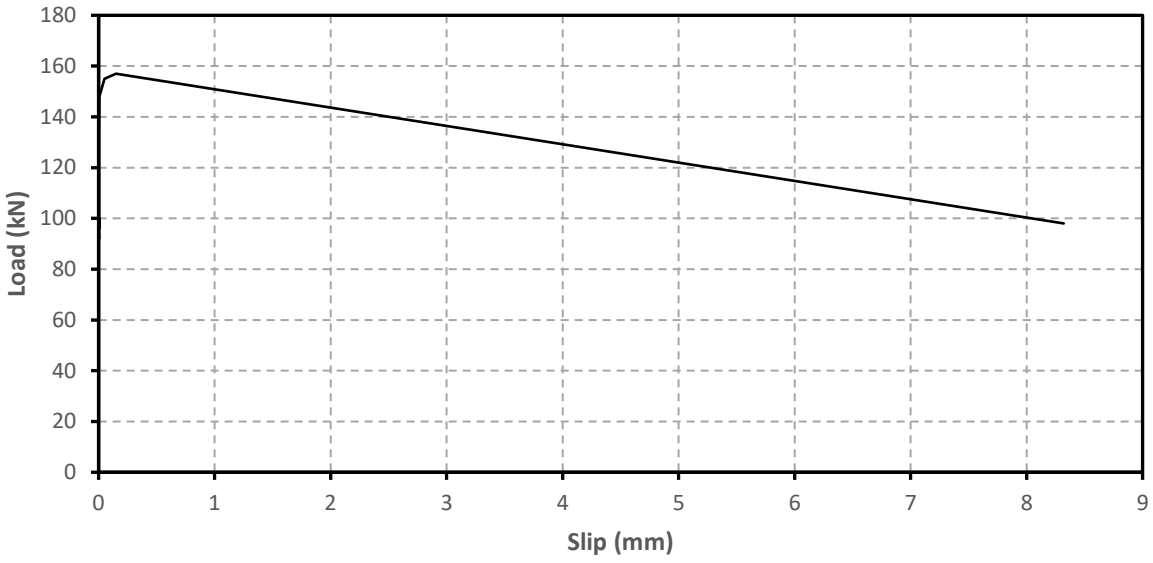

Figure 5.27: Load vs. end slip for beam R-16-1.5-40%

Strain distribution in the shear span

Figure 5.28 shows the total strain profile (GFRP strain due to prestressing plus the strain due to the applied load) in the GFRP bar at various load levels for beam R-16-1.5-40%. As shown in Figure 5.28, at a low load level and before cracking, the concrete was carrying most of the tensile forces due to the applied load while only a small amount was taken by the GFRP bar. When the concrete reached its ultimate tensile strength and a crack occurred at 95 kN, the strain readings near the crack for the GFRP bar increased abruptly. As the test proceeded and the load reached 105 kN, the strain gauge readings at 500 mm and 650 mm had increased by 4305 με and 4865 με from their unloaded values indicating that the concrete cracks at these locations are getting wider and deeper. By the time that the load reached 130 kN, the strain reading at 500 mm had increased until it was almost equal to the reading at mid-span indicating almost complete de-bonding between these locations. Also, at the same load level (139 kN) the strain at 350 mm jumped to 2577 με above its unloaded value indicating that the de-bond crack had reached this point. At failure (167 kN), the strain gauge readings at 500 mm and 650 mm still remained almost equal. By this time the readings at 350 mm had increased enough that the beam failed by de-bonding of the remaining bonded length.

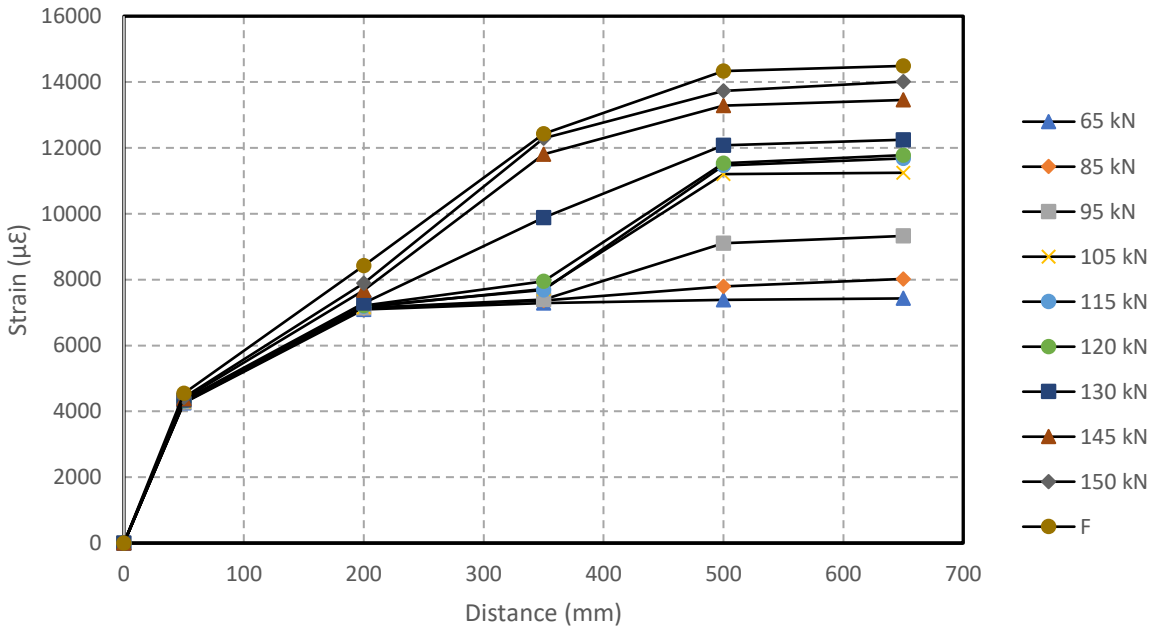

Figure 5.28: Total strain distribution along the GFRP bar at different load levels for beam R-16-1.5-40%

5.5 Test results for beams tested under fatigue loading

5.5.1 Beams reinforced with sand coated GFRP bars

5.5.1.1 General

This section presents and discusses the test results for the prestressed beams tested under a fatigue loading. In total, ten prestressed beams were cast and tested under fatigue loading. These beams were divided into groups based on the depth of their concrete cover. The first group (five beams) were reinforced with a 16 mm sand coated GFRP bar and the concrete cover was 25 mm. For the second group, five beams were reinforced with a 16 mm sand coated GFRP bar and the concrete cover was 45 mm. Two modes of failure were observed, 1) bond failure between the GFRP bar and the concrete and, 2) rupture of the GFRP bar. Table 5.6 summarizes the fatigue test results including (beam type, minimum and maximum load, load range as a percentage of the failure load of the beam tested under monotonic loading, strain range, the number of cycles to failure and the failure mode).

Table 5.6 Summary of the fatigue test results for prestressed sand coated reinforced beams

Group	Beam	Load		Stress range (MPa)	Number of cycles to failure	Failure mode
		Min (kN)	Max (kN)			
Group 1 (Sand Coated GFRP bar with a 25 mm concrete cover)	SC-16-1.5-40%-135.5	16.5	152	491	188	Splitting Bond
	SC-16-1.5-40%-125.5	16.5	145	460	491	Splitting Bond
	SC-16-1.5-40%-115.5	16.5	132	381	3156	Splitting Bond
	SC-16-1.5-40%-112	16.5	128.5	361	14135	Splitting Bond
Group 2 (Sand Coated GFRP bar with a 45 mm concrete cover)	SC-16-3.0-40%-157	19	176	597	87	Splitting Bond
	SC-16-3.0-40%-152	19	171	566	305	Splitting Bond
	SC-16-3.0-40%-136	19	155	478	7652	Splitting Bond
	SC-16-3.0-40%-132	19	151	456	13889	Splitting Bond

5.5.1.2 Fatigue Life

The fatigue test results for all prestressed beams reinforced with a 16 mm sand coated GFRP bar are shown in Figures 5.29 and 5.30. Figure 5.29 shows the load range (kN) versus the fatigue life in cycles and Figure 5.30 shows the stress range versus fatigue life in cycles. Two failure modes were observed, 1) bond failure between the GFRP bar and the concrete, and 2) Rupture of the GFRP bar. The fatigue life of the prestressed beams varied linearly with the load range (kN) on logarithmic scales.

As the load range or stress range increased the fatigue life decreased. The fatigue life curve for beams that failed by de-bonding between the bar and concrete has a shallow slope. Because the

slope of the curve is shallow, a small change in the load range will result a major change in beam life under a fatigue loading. The two curves (beams with concrete covers equal to 25 mm and 45 mm) were almost parallel. Due to the weakness of the prestressed GFRP bar when subjected to a fatigue loading, beams with a concrete cover equal to 25 mm only failed in bond at lives below fourteen thousand cycles and those with a concrete cover equal to 45 mm only failed in bond at lives below fifteen thousand cycles For both beam sets, the stress range and load ranges were increased for all the beams tested under fatigue loading to avoid bar rupture and to make sure that the beams would fail in bond between the GFRP bar and the concrete. It is clear that the beams with thicker concrete cover lasted to longer lives than the beams that had a shallower concrete cover. Most of the test data fell close to the best fit line.

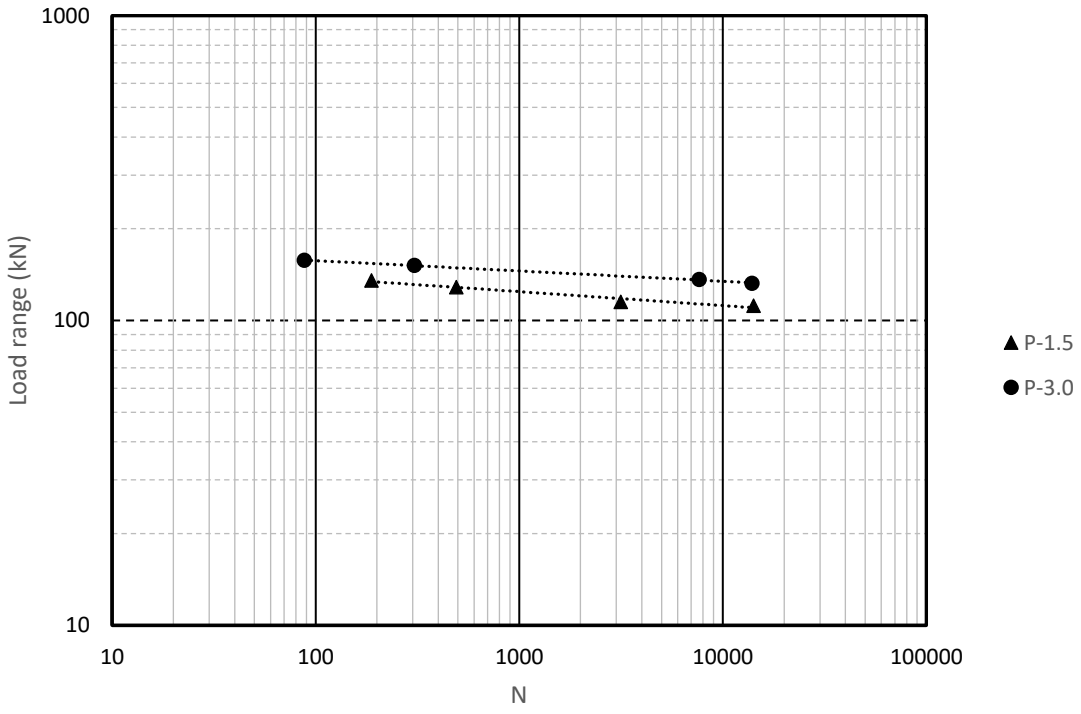

Figure 5.29: Fatigue life versus the load range (kN) for beams with concrete cover equal 25 mm and 45 mm

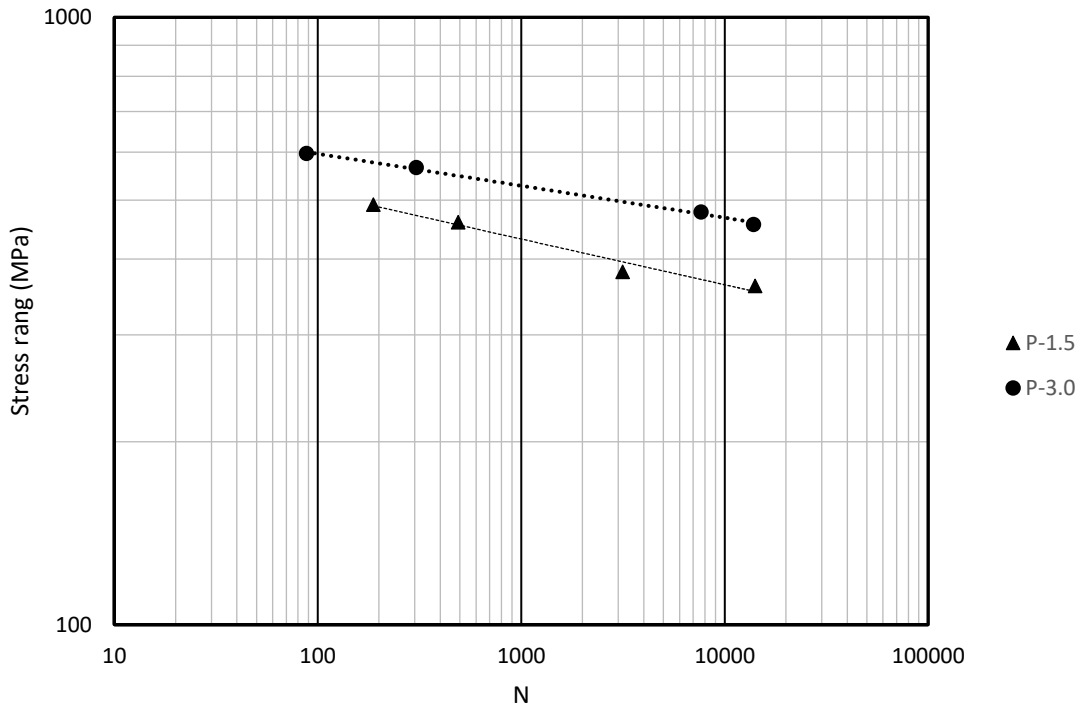

Figure 5.30: Fatigue life vs stress range test results for beam with concrete cover equal 25 mm and 45 m

5.5.1.3 Failure Mode

In this section, the typical bond failure that occurred for prestressed beams tested under fatigue loading will be discussed. The failure mode of the prestressed beams was similar to that of the non-prestressed beams for most of the fatigue life. All beams were loaded manually to the specified maximum load before fatigue loading started. During the first cycle, the first crack appeared at the loading point location or within a few millimeters from the loading point. At the same time, a horizontal crack initiated on the bottom side of the beam started close to the loading point. As the load increased during the first cycle, the de-bonding crack propagated towards the support. The length of the de-bonded crack varied from one beam to another depending on the maximum specified load. As the maximum specified load increased the de-bonded crack length at the end of initial loading increased. After the fatigue loading started, the de-bonded crack grew towards the support. Due to the prestressing of the GFRP bar, the shear (bond) stress is high at the end of the beam and close to the support. After many cycles and close to failure, the horizontal crack that propagated from the loading point toward the support reached the transfer length. As

the number of cycles increased and the horizontal crack propagated further in the transfer length. Another crack initiated at the support and progressed toward the loading point. As both cracks (from the loading point toward the support and from the support to the loading point) approached each other, the shear stress in the region between the cracks reached the ultimate value and the beam failed. The rate of crack growth was affected by many factors including the applied load range and the confinement level. As the applied load range increased, the crack growth rate increased. Figure 5.31 shows a typical bond failure for beams reinforced with prestressed beams with different concrete covers tested under fatigue loading.

Figure 5.31: Typical bond failure for beam reinforced with sand coated GFRP bar

5.5.1.4 Load-Deflection Behaviour

Typical deflection versus number of cycles as a percentage of fatigue life curves are shown in Figures 5.32 and 5.33 for beams with concrete covers equal to 25 mm and 45 mm, respectively. The maximum mid-span deflection at the peak load during the tests under fatigue loading was plotted versus the number of cycles as a fraction of fatigue life. For all the prestressed beams tested under fatigue loading, three stages were observed in the beam deflection behaviour. In the first stage, the beam deflection suddenly increased as the concrete cracked and the GFRP bar carried all the tensile force. Simultaneously, the de-bonded crack initiated and decreased the bond between the GFRP bar and the concrete. In the second stage, the deflection increased slowly from the first 5% of the fatigue life until about 95% of the fatigue life of the beam. In the final stage and during the last 5% of the fatigue life, as the de-bonded crack approached to the support and there was not enough bonded length to resist the bar force, the mid-span deflection increased suddenly, and the

beam failed. For both beam sets (with concrete cover equal to 25 mm and 45 mm), the mid-span deflection increased as the applied load increased.

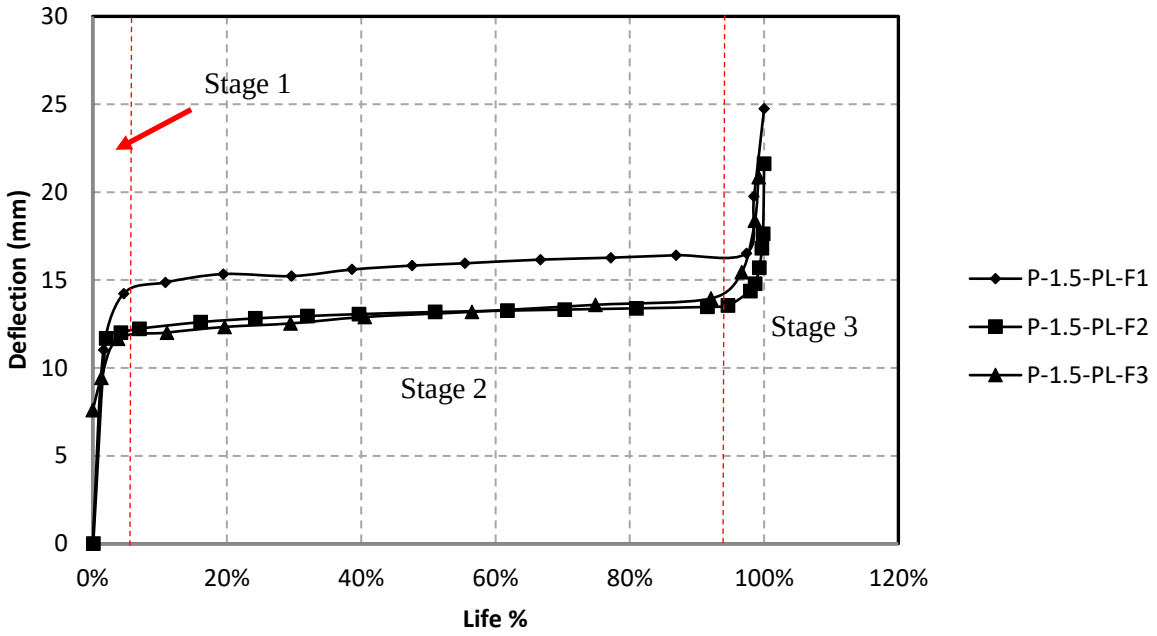

Figure 5.32 The load vs. deflection curves for all beams with 25 mm concrete cover

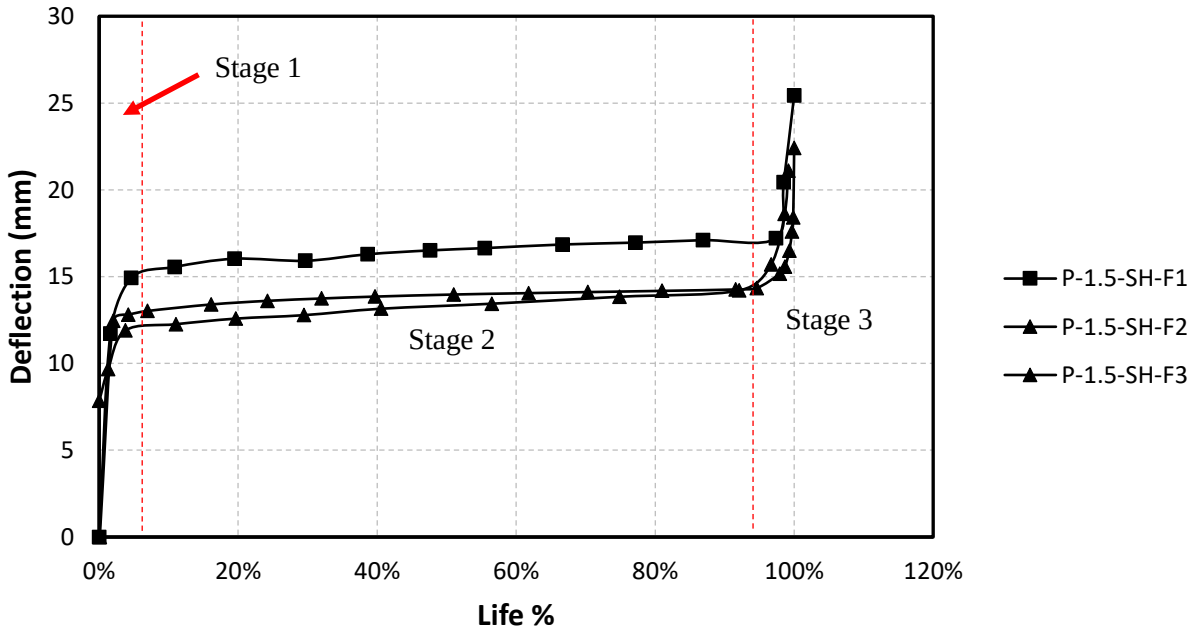

Figure 5.33 The load vs. deflection curves for all beams with 45 mm concrete cover

5.5.1.5 Strain distribution along the GFRP bar

Figure 5.34 shows the total strain profile (GFRP strain due to prestressing plus strain due to applied load) in the GFRP bar at various numbers of cycles for beam SC-16-1.5-40%-115.5. During the first cycle, the strain gauges located at 650 mm, 500 mm and 350 mm from the support read high values of strain while the strain gauges located at 200 mm and 50 mm from the support had lower strain values. The strain readings from the first cycle indicated that there was a partial de-bond between the strain gauges located at 500 mm and 350 mm while the GFRP bar remained bonded to the concrete between strain gauges located at 350 mm and 50 mm from the support. All the strain gauge readings slowly increased from the first cycle until the number of cycles reached almost 80% of the fatigue life. From about 85% of the fatigue life, the strain gauge readings at 350 mm and the strain gauge at 500 mm are almost equal indicating that the GFRP bar had de-bonded from the concrete. As fa as the 350 mm gauge. In the meantime, the strain readings at the 250 mm gauge increased indicating continuing progress of the crack. As cyclic loading continued crack tip moved toward the support and approached crack that initiated from the support and grew toward the loading point. Failure occurred when the remaining uncracked region could not support the applied shear force. Figure 5.35 show the number of cycles as a percentage of the fatigue life versus the end slip.

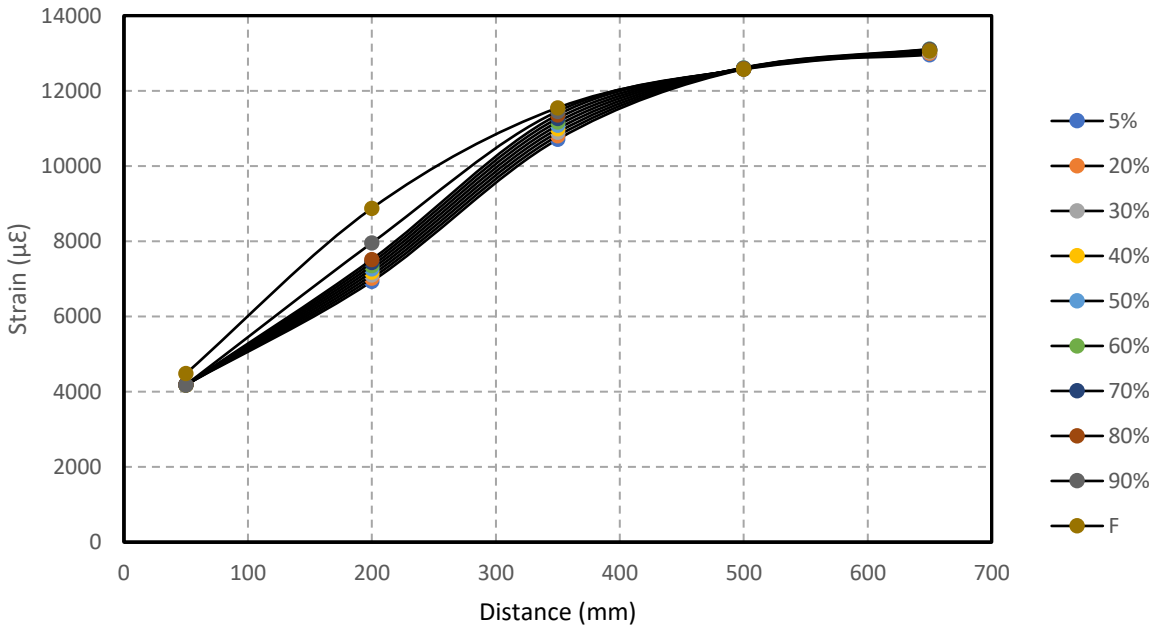

Figure 5.34: Strain distribution along the GFRP bar for beam SC-16-1.5-40%-115.5

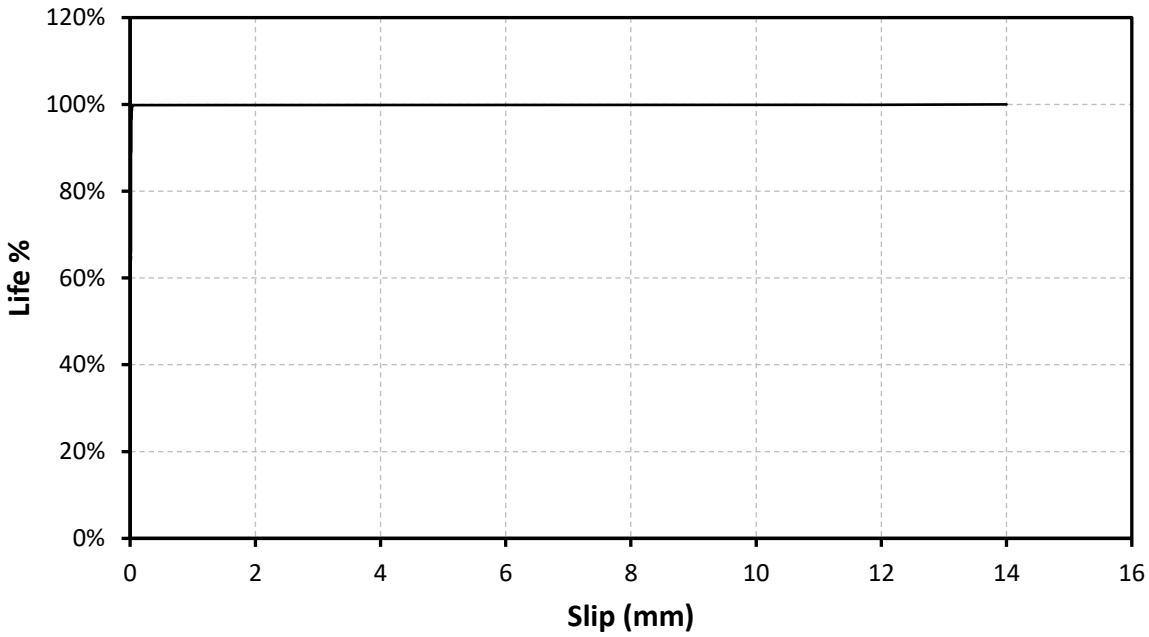

Figure 5.35: Life as percentage vs. GFRP end slip

5.5.2 Beams Reinforced with Ribbed GFRP Bar

5.5.2.1 General

This section presents and discusses the test results for beams reinforced with prestressed ribbed GFRP bar and tested under a fatigue loading. In total, five prestressed beams were cast and tested under fatigue loading. All beams were reinforced with 16 mm ribbed GFRP bar and the concrete cover was 25 mm. Two modes of failure were observed, 1) bond failure between the GFRP bar and the concrete and, 2) rupture of the GFRP bar. Table 5.7 summarizes the fatigue test results including (beam type, minimum, maximum load, load range as a percentage of the failure load of the beam tested under monotonic loading, strain range, the number of cycles to failure and the failure mode).

Table 5.7 Summary of the fatigue test results for prestressed ribbed reinforced beams

Group	Beam	Load		Stress range (MPa)	Number of cycles	Failure mode
		Min (kN)	Max (kN)			
Ribbed GFRP bar and 25 mm concrete cover	R-16-1.5-40%-134	15.8	149.5	483	98	Splitting Bond
	R-16-1.5-40%-129	15.8	145	454	482	Splitting Bond
	R-16-1.5-40%-124	15.8	140	427	2422	Splitting Bond
	R-16-1.5-40%-117.5	15.8	133.5	388	5762	Splitting Bond

5.5.2.2 Fatigue Life

The fatigue test results for all prestressed beams reinforced with a 16 mm Ribbed GFRP bar are shown in Figures 5.36 and Figure 5.37. Figure 5.36 shows the load range (kN) versus the fatigue life in cycles and Figure 5.37 shows the stress range versus fatigue life in cycles. Two failure modes were observed, 1) bond failure between the GFRP bar and the concrete, and 2) Rupture of the GFRP bar. The fatigue life of the prestressed beams varied linearly with the load and stress ranges on logarithmic scales. As the load range or stress range increased the fatigue life decreased. The fatigue life curves for beams that failed by de-bonding between the bar and concrete have shallow slopes. Because the slope of the curves is shallow, a small change in the load range or stress range will result a major change in beam life under a fatigue loading. Due to the weakness of the prestressed GFRP bar when subjected to fatigue loading, beams with concrete cover equal 25 mm only failed in bond at lives below about nine thousand cycles. The stress ranges and load ranges were increased for all the beams tested under fatigue loading to avoid bar rupture and to ensure that the beam would fail in bond between the GFRP bar and the concrete. Most of the test data fell close to the best fit lines.

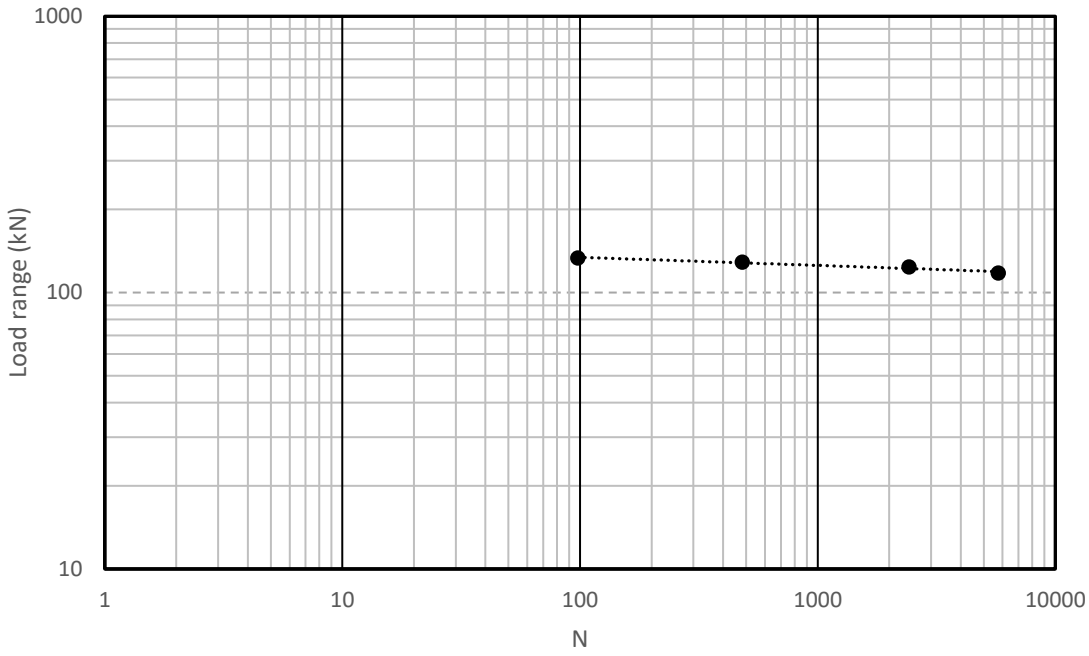

Figure 5.36: Fatigue life versus the load range (kN)

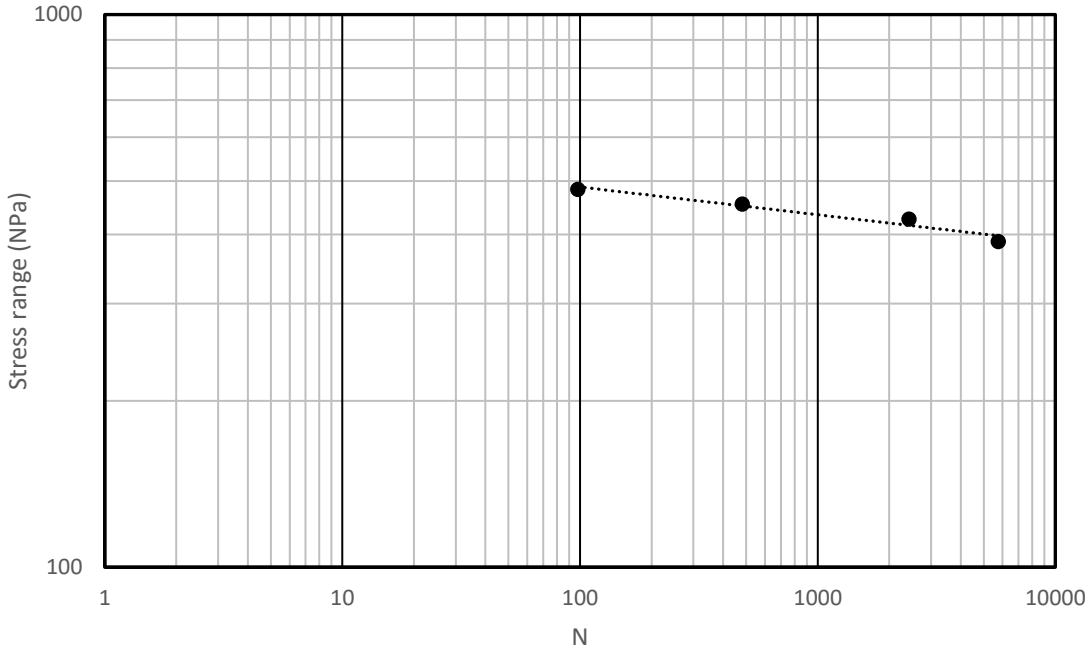

Figure 5.37: Fatigue life vs stress range

5.5.2.3 Failure Mode

In this section, the typical bond failure that occurred for prestressed beams tested under fatigue loading will be discussed. The failure mode of the prestressed beams was similar to that for the non-prestressed beams for most of the fatigue life. All beams were loaded manually to the specified maximum load before the fatigue loading started. During the first cycle, a crack appeared at the loading point location or within a few millimeters of it. At the same time, a horizontal crack initiated on the bottom side of the beam close to the loading point. As the load increased during the first cycle, the de-bonding crack propagated towards the support. The length of the de-bonded crack varied from one beam to another increasing with increasing maximum specified load. After the fatigue loading started, the de-bonded crack grew towards the support. Due to the prestressing of the GFRP bar, the shear (bond) stress is high at the end of the beam and close to the support. After many cycles and close to failure, the horizontal crack that propagated from the loading point toward the support will reached the transfer length. As the number of cycle increased and the horizontal crack penetrated the transfer length, another crack initiated at the support and progressed toward the loading point. When the cracks (one from the loading point toward the support and the other from the support to the loading point) approached each other the shear stress between them reached the failure stress and the beam failed. The rate of crack growth was affected by many factors including the applied load range and the confinement level. As the applied load range increased the crack growth rate increased. Figure 5.38 shows a typical bond failure for beams reinforced with prestressed ribbed GFRP under fatigue loading

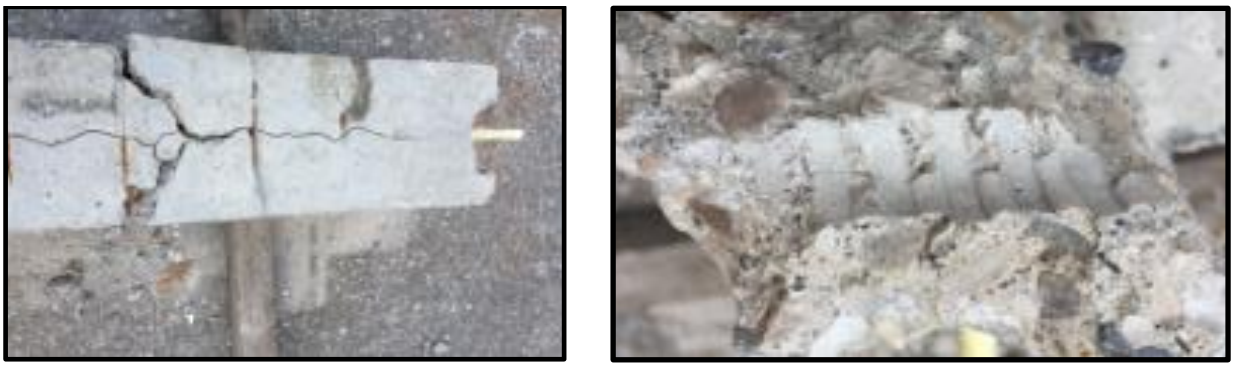

Figure 5.38: A typical bond failure for beams reinforced with prestressed ribbed GFRP bar

5.5.2.4 Load-Deflection Behaviour

Typical deflection versus number of cycles as a percentage of fatigue life curves are shown in Figure 5.39. The maximum mid-span deflection at the peak load during the tests under fatigue loading was plotted versus the number of cycles as a fraction of fatigue life. For all the prestressed beams that tested under fatigue loading, three stages were observed in the beam deflection behaviour. In the first stage, the beam deflection suddenly increased as the concrete cracked and the GFRP bar carried all the tensile force. Simultaneously, the de-bonded crack initiated and decreased the bond between the GFRP bar and the concrete. In the second stage, the deflection increased slowly from the first 5% of the fatigue life until about 95% of the fatigue life of the beam. In the final stage and during the last 5% of the fatigue life, as the de-bonded crack approached to the support and there was not enough bonded length to resist the bar force and the mid-span deflection increased suddenly, and the beam failed. As the applied load increases, the mid-span deflection throughout the test increased.

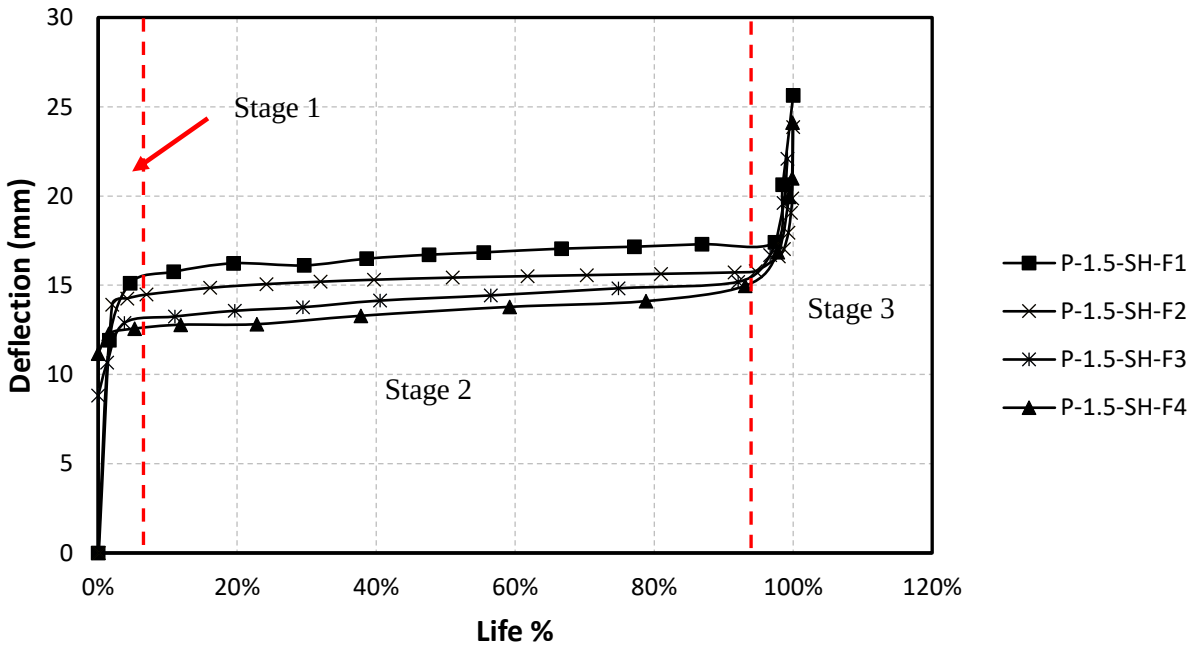

Figure 5.39: The load vs. deflection curves for all beams reinforced with prestressed ribbed bar

5.5.2.5 Strain Distribution Along the GFRP Bar

Figure 5.40 shows the total strain profile (GFRP strain due to prestressing plus strain due to applied load) in the GFRP bar at various numbers of cycles for beam R-16-1.5-40%-117.5. During the first cycle, the strain gauges located at 500 mm and 350 mm from the support read a high value of strain while the strain gauges located at 200 mm and 50 mm from the support read lower strain values. The strain readings from the first cycle indicated a partial de-bond between the strain gauges located at 500 mm and 350 mm while the GFRP bar remained bonded to the concrete between strain gauges located at 350 mm and 50 mm from the support. All the strain gauge readings slowly increased from the first cycle until the fatigue life reached about 80 % of the fatigue life. From 85 % of the fatigue life, the strain gauge readings at 350 mm and the strain gauge at 500 mm are almost equal to each other indicating that the GFRP bar had de-bonded from the concrete in the region between them. In the meantime, the strain reading at 250 mm increased indicating continuing progress of the crack. With continued cycling the de-bonded crack moved toward the support and the crack that initiated from the support toward the loading point. When the remaining uncracked length could not support the shear force failure occurred. Figure 5.41 shows a plot of the number of cycles as a percentage of the fatigue life versus the end slip.

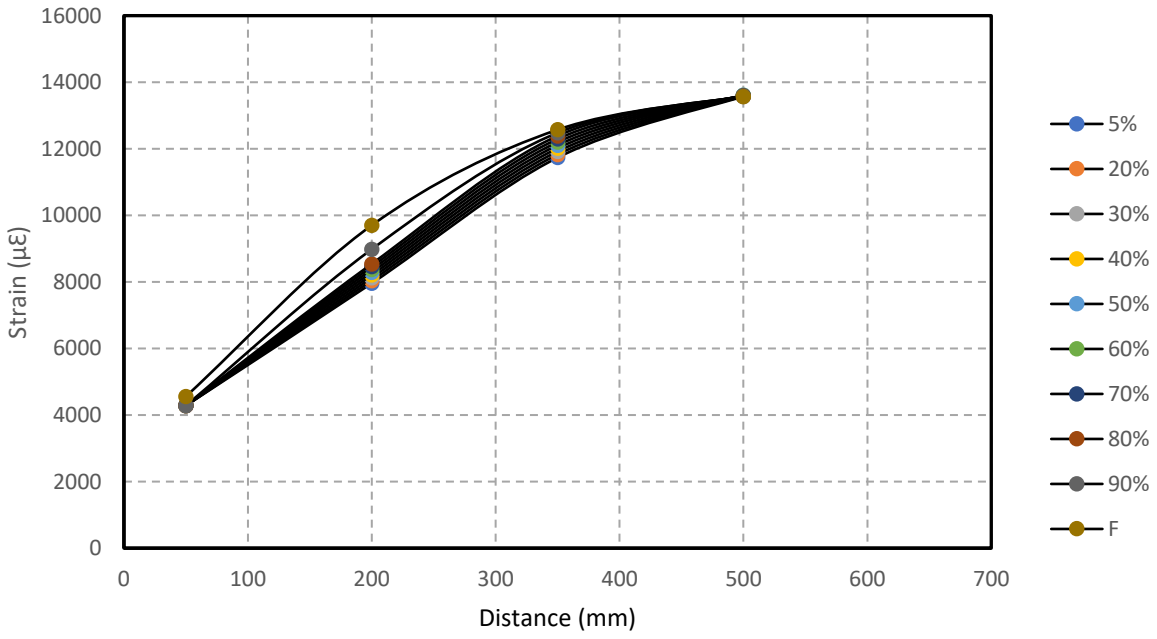

Figure 5.40: Strain distribution along the GFRP bar for beam R-16-1.5-40%-117.5

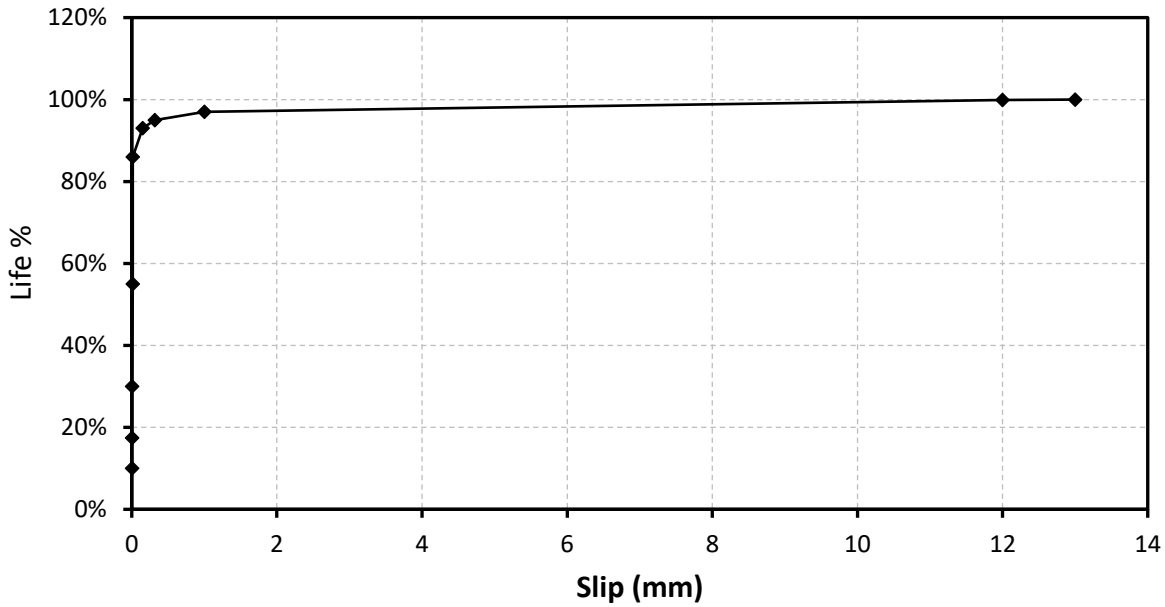

Figure 5.41: Life as percentage vs. GFRP end slip

5.6 Discussion of the fatigue test results

Table 5.8 summarizes the fatigue test results for all beams reinforced with 16 mm GFRP bars (sand coated and ribbed) with different concrete covers (25 mm and 45 mm) including (beam type, minimum, maximum load, load range as a percentage of failure load of the beam tested under monotonic loading, strain range, the number of cycles to failure and the failure mode).

Table 5.8: Fatigue test results for non-prestressed and prestressed beams

Group	Beam	Load		Stress range (MPa)	Beam capacity (kN) or life (cycles)	Failure mode
		Min (kN)	Max (kN)			
Non-prestressed Sand coated GFRP bar and 25 mm concrete cover	SC-16-1.5-0%-S	Monotonic		N/A	149.5 (kN)	S/Bond
	SC-16-1.5-0%-82.5	15	97.5	422	1504	S/Bond
	SC-16-1.5-0%-78	15	93	397	2010	S/Bond
	SC-16-1.5-0%-66	15	81	333	40896	S/Bond
	SC-16-1.5-0%-55.5	15	70.5	287	472562	S/Bond

Table 5.8: Fatigue test results for non-prestressed and prestressed beams-continued

Group	Beam	Load		Stress range (MPa)	Beam capacity (kN) or life (cycles)	Failure mode
		Min (kN)	Max (kN)			
Non-prestressed Sand coated GFRP bar and 45 mm concrete cover	SC-16-3.0-0%-S	Monotonic		N/A	176 (kN)	S/Bond
	SC-16-3.0-0%-108	17.6	126	557	297	S/Bond
	SC-16-3.0-0%-98	17.6	115.5	503	1493	S/Bond
	SC-16-3.0-0%-95	17.6	112	485	2639	S/Bond
	SC-16-3.0-0%-89	17.6	106.5	458	11683	S/Bond
prestressed Sand coated GFRP bar and 25 mm concrete cover	SC-16-1.5-40%-S	Monotonic		N/A	167 (kN)	S/Bond
	SC-16-1.5-40%-135.5	16.5	152	491	188	S/Bond
	SC-16-1.5-40%-125.5	16.5	145	460	491	S/Bond
	SC-16-1.5-40%-115.5	16.5	132	381	3156	S/Bond
	SC-16-1.5-40%-112	16.5	128.5	361	14135	S/Bond
prestressed Sand coated GFRP bar and 45 mm concrete cover	SC-16-3.0-40%-S	Monotonic		N/A	192 (kN)	S/Bond
	SC-16-3.0-40%-157	19	176	597	89	S/Bond
	SC-16-3.0-40%-152	19	171	566	305	S/Bond
	SC-16-3.0-40%-136	19	155	478	7652	S/Bond
	SC-16-3.0-40%-132	19	151	456	13886	S/Bond
prestressed Ribbed GFRP bar and 25 mm concrete cover	R-16-1.5-40%-S	Monotonic		N/A	159 (kN)	S/Bond
	R-16-1.5-40%-134	16	149.46	483	98	S/Bond
	R-16-1.5-40%-129	16	144.69	454	482	S/Bond
	R-16-1.5-40%-124	16	139.92	426	2422	S/Bond
	R-16-1.5-40%-117.5	16	133.56	388	5762	S/Bond

As a reinforced concrete beam is loaded monotonically, the strains resulting from the applied load increase. When the concrete tensile stress at the bottom of a beam due to the imposed load reaches the concrete cracking stress, the concrete cracks and the load-strain curve of the reinforcing bar shows an abrupt increase in strain as the strain increases until the reinforcement has taken up the

tensile force shed by the cracked concrete as shown in Figure 5.42. Afterwards, the load -strain curve continues at a lower slope since the applied tensile force in the beam is carried only by the rebar. However, during unloading following cracking the load strain curve will follow the dashed line of Figure 5.42 since the cracked concrete will no longer contribute to the tensile force. On subsequent load cycles the load strain curve will continue to follow the dashed line. A similar behaviour is seen for a prestressed beam in Figure 5.43. Again, there is an abrupt increase in the strain in the load-strain curve of the reinforcing bar as the concrete at the bottom of the beam cracks followed by a decrease in slope as further tensile forces are taken by the reinforcement. On unloading, the load-strain follows the dashed curve until the crack closes due to the prestressing force. Then it follows the original loading curve as force changes are shared by the reinforcement and the concrete.

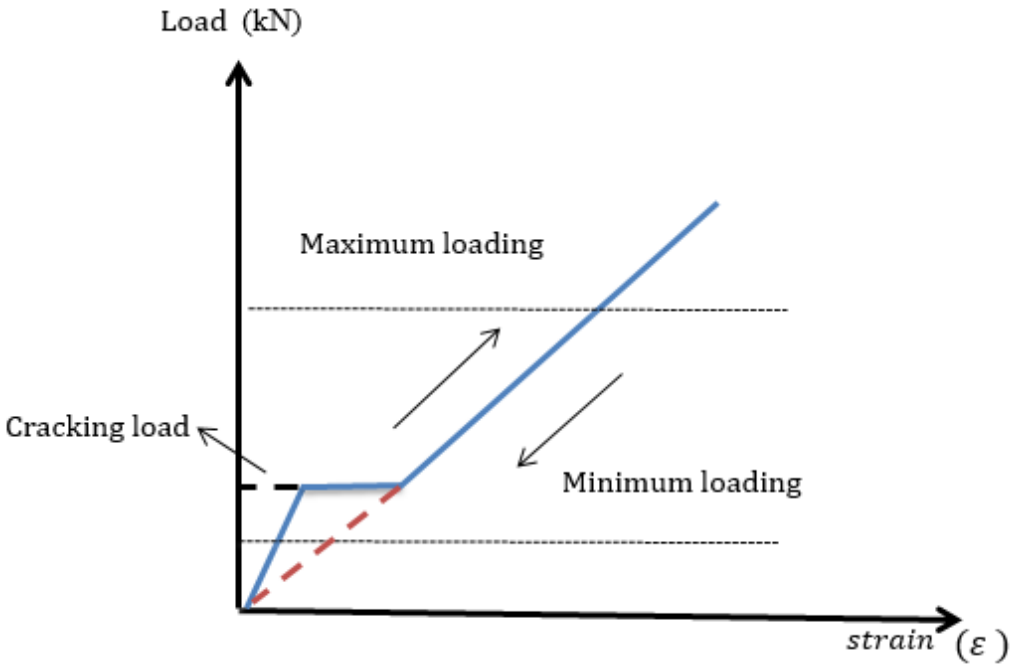

Figure 5.42: Load-strain relationship of non-prestressed concrete under fatigue

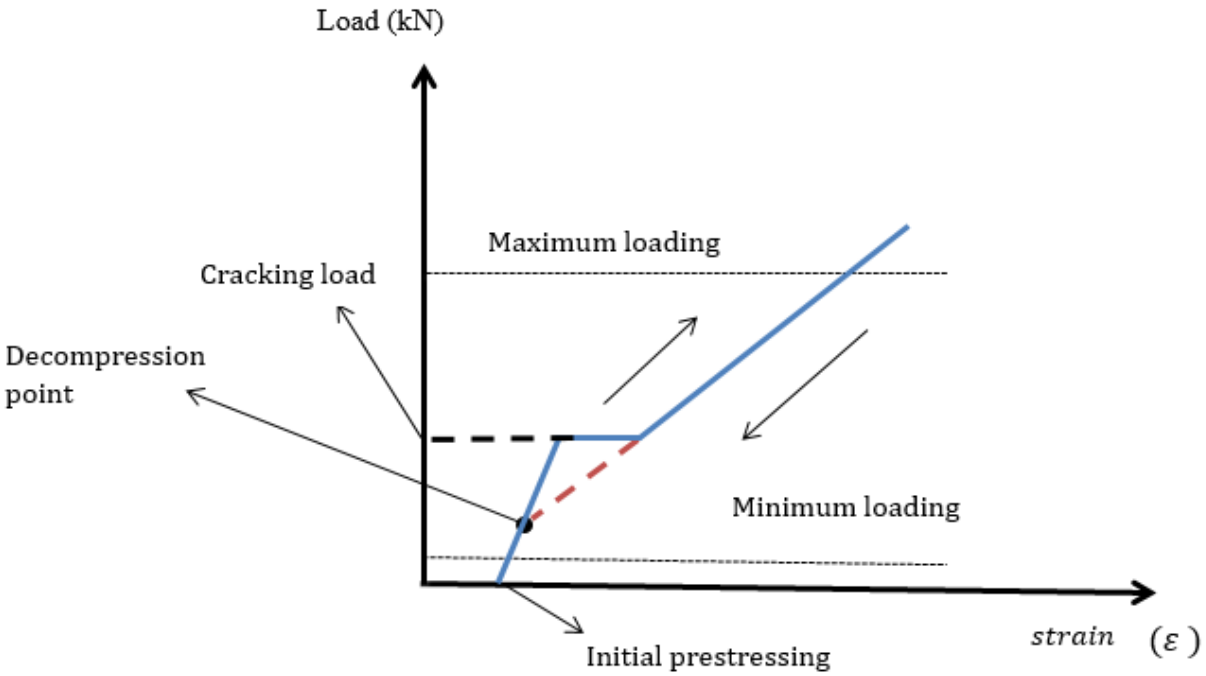

Figure 5.43: Load- strain relationship of prestressed concrete under fatigue

All non-prestressed and prestressed beams reported failed in bond. All beams were loaded manually to the specified maximum load before fatigue loading started. During the first cycle, the first crack appeared at the loading point location or within a few millimeters of it. At the same time, a horizontal crack initiated on the bottom side of the beam started close to the loading point. As the load increased during the first cycle, the de-bonded crack propagated towards the support. The length of the de-bonded crack varied from one beam to another depending on the maximum specified load. As the maximum specified load increased the de-bonded crack length at the end of the initial loading increased. After the fatigue loading started, the de-bonded crack grew towards the support. For non-prestressed beams, the de-bonded horizontal crack moved toward the support until the remaining uncracked length could not resist the shear force imposed by the GFRP bar and failure occurred. As discussed earlier, for the prestressed beams, the same de-bonded horizontal crack moved toward the support and approached a crack that initiated from the support and grew toward the loading point until failure occurred when the remaining uncracked length could no longer support the shear force. Figure 5.44 shows the stress range vs. number of cycles to failure for all of the beams. The fatigue data for prestressed and non-prestressed beams fall into single curves for each concrete cover. For both non-prestressed and prestressed beams, fatigue life increased by the same amount with the change in thickness of the concrete cover. This indicates

that fatigue life is primarily governed by stress range and mean stress has little effect. The effect of prestress on load vs. fatigue life behaviour is due to its change in the stress range for a given load range. It is thought that a thicker cover requires more bar force to overcome the extra confinement and crack the concrete allowing the GFRP bar to de-bond. Due to the weakness of the GFRP bar when subjected to fatigue loading, beams with a concrete cover equal to 45 mm only failed in bond at fatigue lives below eleven thousand cycles (11000 cycles). The stress ranges and load ranges in the tests were increased for beams that had a concrete cover equal to 45 mm to avoid bar rupture and to ensure that the beams would fail in bond between the GFRP bar and the concrete.

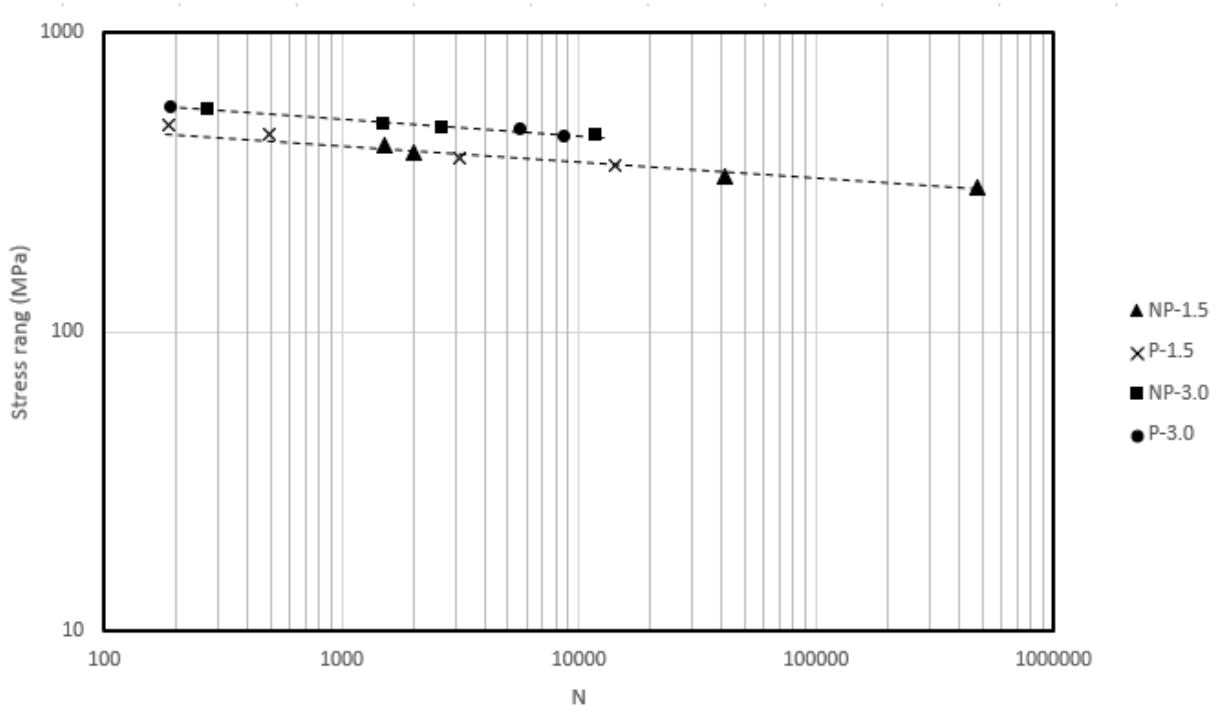

Figure 5.44: Measured stress range for non-prestressed and prestressed beams with different concrete covers

Figure 5.45 shows the fatigue life for beams reinforced with prestressed sand coated and ribbed GFRP bar. The vertical axis (y-axis) represents the stress range and the horizontal axis represents the fatigue life in cycle. Due to the weakness of the prestressed GFRP bar when subjected to a fatigue loading, beams reinforced with prestressed sand coated GFRP bar failed in bond at lives below 14,000 cycles and those reinforced with prestressed ribbed GFRP bar failed in bond at lives

below 9,000 cycles. At longer fatigue lives, they failed by bar rupture. For both beam sets, test stress ranges and load ranges were kept high, so that the beams tested under fatigue loading would avoid bar rupture and fail in bond between the GFRP bar and the concrete. As shown in the figure, the beams reinforced with Sand coated GFRP bar except longer life.

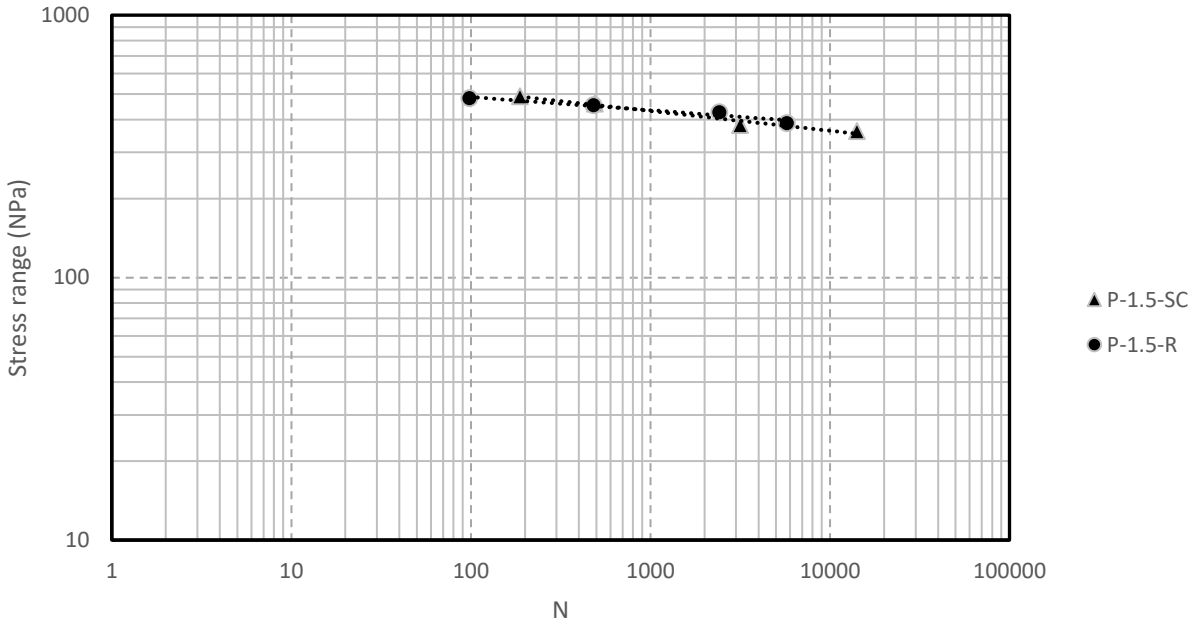

Figure 5.45: Stress range for prestressed beams with different GFRP bar surface type

Chapter 6: Modelling of the Experimental Results

6.1 Introduction

This chapter presents the model that was used to describe the crack growth mechanism that has given rise to the experimental test results. Specifically, the shear (bond) stress distribution and the crack growth model proposed by Abdel Wahab and Topper (2015), which is applied to GRFP in the current study, will be presented. The parameters of the model will then be derived for the GFRP reinforced beams using the fatigue life vs. load range curve. Finally, a comparison will be made between the observed and predicted crack length vs. number of cycles curves.

6.2 Debonding Behaviour

The beam tests of interest are those in which the non-prestressed and prestressed beams failed by de-bonding between the GFRP bar and the surrounding concrete. Two different modes of failure were observed in this study. The mode of failure observed for all non-prestressed beams was de-bonding between the GFRP bar and the surrounding concrete, which started at the loading point and moved toward the support. For the prestressed beams, this behaviour was followed near failure by de-bonding between the bar and the concrete starting from the support and moving towards the loading point.

For the non-prestressed beams, de-bonding between the GFRP bar and the concrete started at the loading point (L) after a flexure crack appeared at a low load level during the first cycle or at a low percentage of the fatigue life. As the load in the first cycle increased or (if cracking did not occur during the first cycle) when the number of cycles increased, a longitudinal (de-bonding) crack appeared and propagated toward the support (S), resulting in de-bonding between the GFRP bar and the concrete. When the longitudinal crack tip reached the location of one of the strain gauges installed along the shear span, the reading of the strain gauge at the crack tip suddenly jumped to a value that was slightly less than the mid-span strain gauge reading. Typical GFRP strain distributions along the shear span at different load levels are shown in Figure 6.1

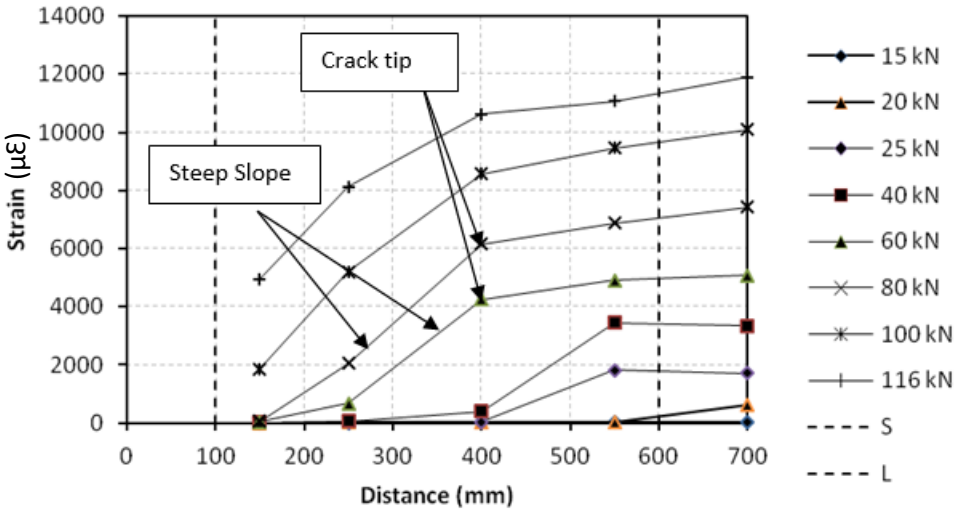

Figure 6.1: Typical strain distribution along the GFRP bar

Ahead of the crack tip, the bar force and shear stress distributions decay in a manner typical of stress raisers as shown in Figure 6.2. As the load in a monotonic test or the number of cycles in a fatigue test increases, the longitudinal crack grows toward the support. The monotonic or cyclic shear stress between the concrete and the GFRP bar at the crack tip is the force driving the crack to grow toward the support. The shear stress distribution along the bar can be divided into two regions. The first region (de-bonded) is characterized by the force and shear stress distributions behind the crack tip shown in Figure 6.2. In the second region (fully bonded) ahead of the crack tip in Figure 6.2 the force and shear stress decay to the value for an uncracked beam as the distance from the crack tip increases.

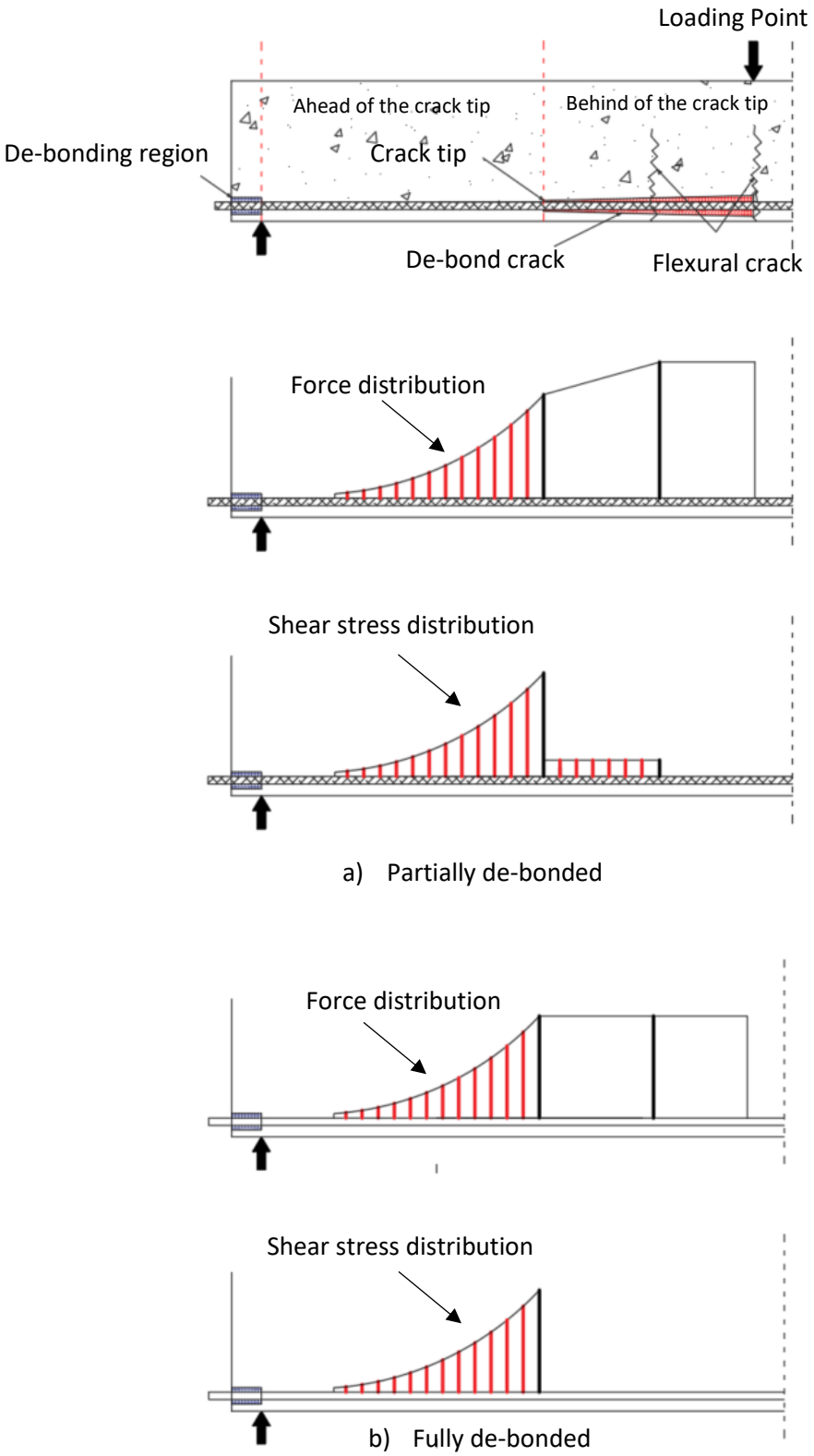

Figure 6.2: Crack at the interface between the GFRP bar and the concrete

Behind the crack tip

The region behind the crack tip can be either partially or fully de-bonded. If this region is fully de-bonded, the GFRP bar is separated from the concrete behind the crack tip. If it is partially de-bonded, there is a de-bonded shear stress (residual shear stress) in part or all of this region between the loading point and the crack tip. If the strain reading at the loading point is equal to the strain reading at the crack tip, the region is fully de-bonded, and the bond shear stress in the region is zero. If the strain reading at the crack tip is less than the strain reading at the loading point, then there is a force transfer between the concrete and the bar and the shear stress is not zero.

Ahead of the crack tip

The region ahead of the crack tip extends from the crack tip to the support centreline. In this region, it is assumed that the GFRP bar is fully bonded to the surrounding concrete. The bond stress (shear stress) ahead of the crack tip decreases until it reaches the shear stress for an uncracked beam. The main parameters that should be accounted for in a crack growth model are:

a) the bond (shear) stress vs. slip behaviour of the GFRP bar to concrete bond,

b) the crack tip shear stress that drives the crack, and

c) the rate of crack propagation.

a) The shear stress versus slip model for the GFRP bar-concrete interface

Two models that have been used to describe the bond stress vs. slip behaviour are shown in Figure 6.3. The horizontal axis represents the slip (mm) and the vertical axis represents the bond stress (shear stress). The bond stress (MPa) increases until it reached its peak value. Past the ultimate bond stress, the bond stress drops suddenly to a lower value or the bond stress drops abruptly to zero.

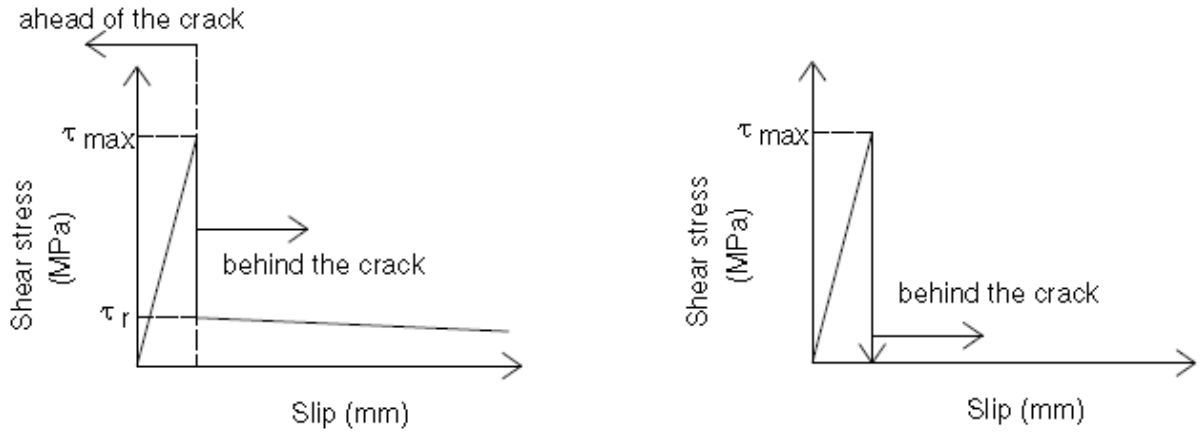

Figure 6.3: Different shear stress versus slip models

- If the GFRP normal stress distribution behind the crack tip (de-bonded region) has a mild slope, then the bond stress in this region drops to an almost constant value from the ultimate shear stress.

- If the GFRP normal stress distribution behind the crack tip is equal to the normal stress at mid-span, then the bond stress drops to zero from the ultimate bond stress.

Figure 6.4 shows the bond stress verses slip between the GFRP bar and concrete. The bond stress increases linearly until it reaches the maximum bond stress. Then, it drops to a residual bond stress (partially de-bonded shear stress). After the drop, there is a descending branch in which the bond stress decreases as the slip increases. Since the GFRP bar is fully bonded to the concrete ahead of the crack tip, the total slip between the crack tip and the loading point is equal to the change in the length of the GFRP bar due to the change in the GFRP normal stress due to de-bonding.

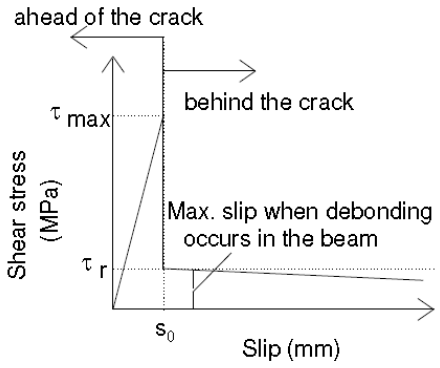

Figure 6.4: Bond stress vs. slip model

Behind the crack tip

Once a flexural crack appears, the bond stress distribution is as shown in Figure 6.5, with the maximum bond stress at the crack location. When the applied load is increased, and the maximum bond stress is exceeded, a de-bonding crack forms between the GFRP bar and the concrete. This de-bonding crack gets longer and moves toward the support, and the partially de-bonded region increases. Under fatigue loading, longitudinal cracking (de-bonding) can occur at shear stress less than the maximum static shear stress. In the partially de-bonded region, the difference in normal force between the force at mid-span and the force at the crack tip in the GFRP bar is equal to the force applied to the bar by the de-bonded bond stress over the partly de-bonded region.

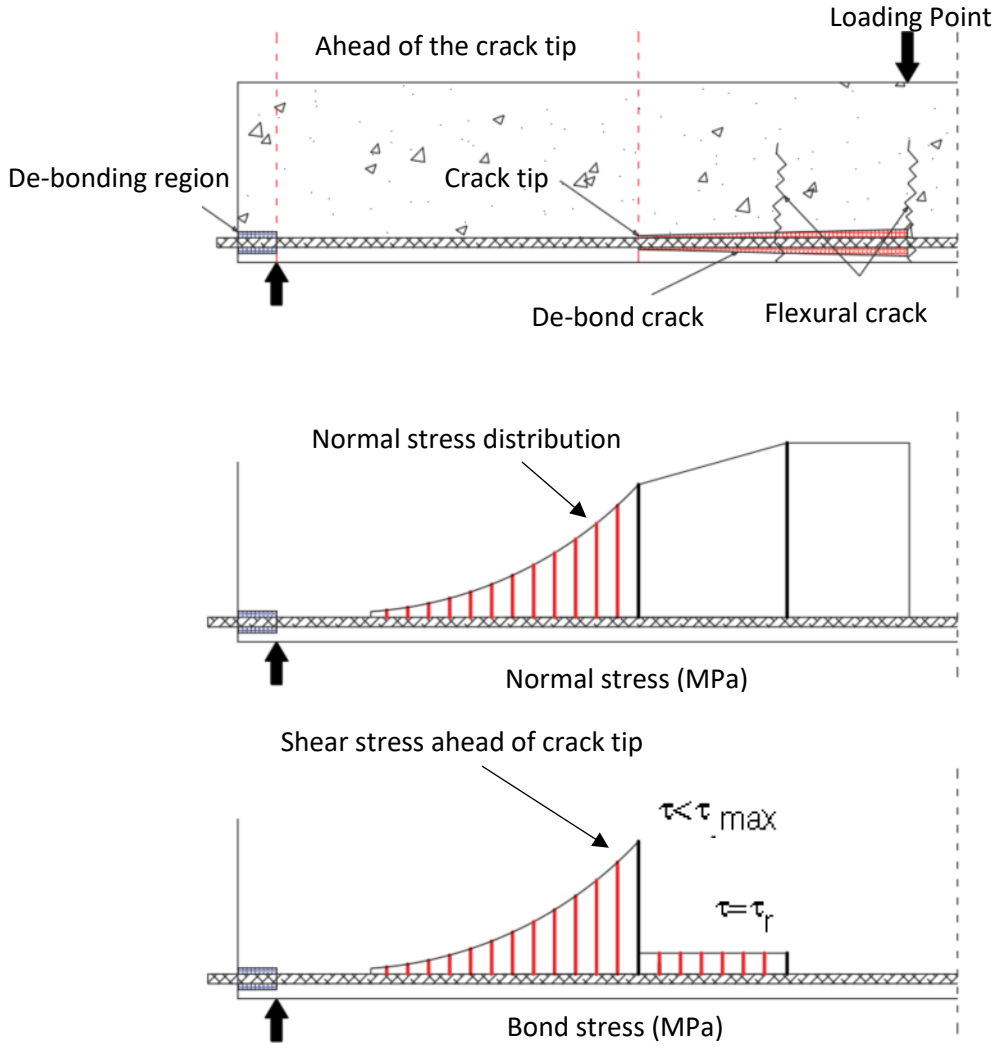

Figure 6.5: Variation of shear stress along the GFRP bar

The value of the bond stress for the de-bonded region was determined from the experimental results as follows: The GFRP strain distribution due to the applied load in the shear span at different load levels and different fatigue life percentages is plotted for a beam in Figure 6.5, which shows normal and shear stress distributions in the GFRP bar similar to those derived from strain gauge readings. The slope of the normal strain along the de-bonded region (between the loading point and the crack tip) is shallow, which means the bond between the GFRP bar and the concrete has been broken, and the rate of force transfer due to friction forces is low. Knowing the difference in measured strain between two points and the distance between them, the change in normal stress in the bar can be obtained and the shear stress can then be calculated by Equation 6.1. This procedure was repeated at different load levels for each beam. The average bond stress for the partially de-bonded region for each beam is shown in Table 6.1.

$$A_f \times \Delta f_s = U \times \pi \times \Delta L$$

$$f_f = \varepsilon \times E \qquad \text{Eq. (6.1)}$$

$$U = \frac{A_f \times \Delta f_f}{\pi \times d \times \Delta L}$$

where:

A_f: is the cross-sectional area of the GFRP bar (mm^2)

Δ: is the in normal stress or length

f_f: is the normal stress in the GFRP bar (MPa)

ε: is the strain in the GFRP bar

E: is the young modulus of the GFRP bar (MPa)

U: is the bond stress (MPa)

L: is the incremental length along the GFRP bar (mm)

Table 6.1 Average bond stress for the de-bonded region behind the crack tip

	GFRP Bar Type	Beams	U (MPa)	Number of Values	Range (MPa)
Preliminary Study	Sand Coated	SC-16-1.5	1.67	2	1.10 to 1.85
		SC-12-1.5	2.89	2	1.6 to 4.17
		SC-16-3.0	2.05	2	1.55 to2.54
	Ribbed	R-16-1.5	0.64	2	0.37 to 0.93
		R-12-1.5	0.82	2	0.36 to 1.28
		R-16-3.0	1.25	2	0.9 to 1.65
Main Study	Sand Coated	SC-16-1.5	1.26	5	1.0 to 1.68
		SC-16-3.0	1.55	5	1.46 to 2.85
	Ribbed	R-16-1.5	1.33	5	1.26 to 2.21

Ahead of the crack tip

In the region ahead of the crack tip, the GFRP bar is assumed to be fully bonded to the concrete. Before flexural cracking at the mid-span, the normal strain distribution increases linearly with distance from the support and the bond stress is uniform along the GFRP bar. As the load increases and the first flexural crack occurs at the mid-span, the normal strain in the GFRP bar suddenly increases at the crack location as tensile force is transferred from the concrete to the bar. Within the fully bonded region, the normal stress is assumed to follow an exponential decay curve. Figures 6.6a and 6.6b show normal and bond stress distributions along the GFRP bar before and after cracking.

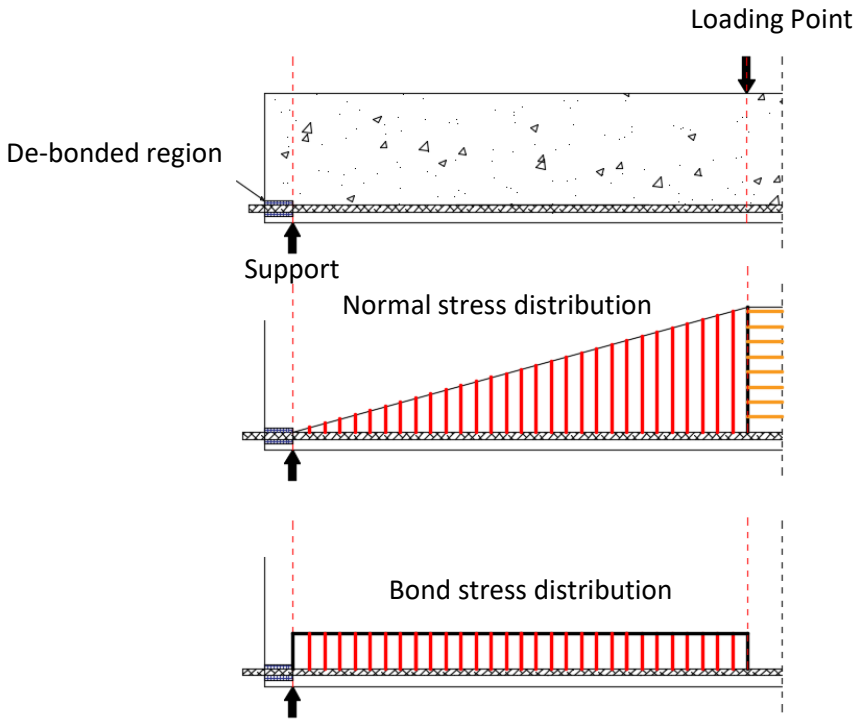

a) Un-cracked beam

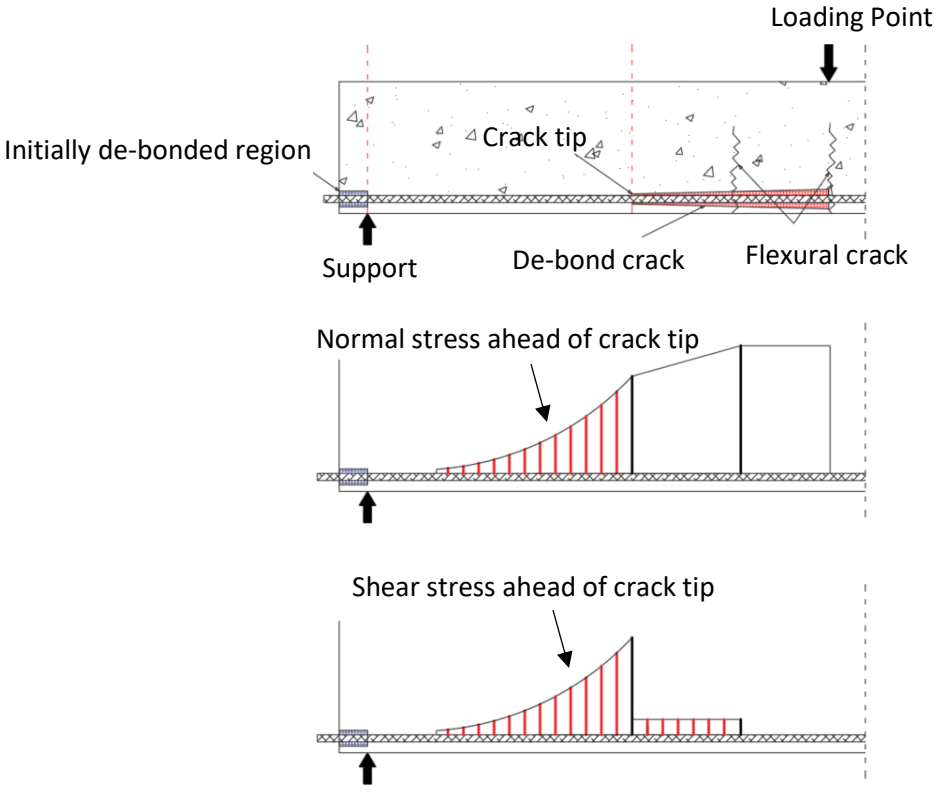

b) Cracked section

Figure 6.6: Normal and shear stress distributions along the GFRP bar before and after cracking

The stresses decrease rapidly ahead of the crack tip in the bonded region. The normal stress and bond stress distributions ahead of the crack tip (fully bonded region) can be approximated by the following exponential equation:

$$f_f(L) = f_f e^{(-C \times L)}$$
$$U(L) = U_0 e^{(-C \times L)} \qquad \text{Eq. (6.2)}$$

where:

$f_f(L)$: is the normal stress in the GFRP bar at any given distance, L (MPa)

f_f: is the normal stress at the crack tip (MPa)

C: is a constant that depends on the GFRP bar texture and beam configuration

L: is the distance from the crack tip (mm)

$U(L)$: is the bond stress along the GFRP bar at any distance, L (MPa)

U_0: is the peak bond stress at the crack tip (MPa)

This exponential distribution ahead of the crack tip was described in previous studies that investigated the bond between the FRP bar/rod and the surrounding concrete (Mazzotti et al., 2005, Huang and Lyons, 2007, Achintha and Burgoyne, 2008, Harries et al. 2010). The constant C in Eq. 6.2 was obtained by fitting an exponential curve to the experimental results for each beam set tested under static and fatigue loading. For each beam, the normal strain distribution of the GFRP bar in the fully bonded region was obtained from the measured strain. The normal strain distribution was superimposed at each load level for each beam as shown in the following figures. Most of the curves show that all of the beams in each beam set have approximately the same exponent C. For each beam, the normal stresses for each curve were normalized by dividing each stress on the curve by the normal stress intercept with the Y-axis. The normalized curve will be presented in Figures 6.7-6.15, starting with the first the group of beams from the preliminary study and then followed by the results for the beams from the main study.

Preliminary Study

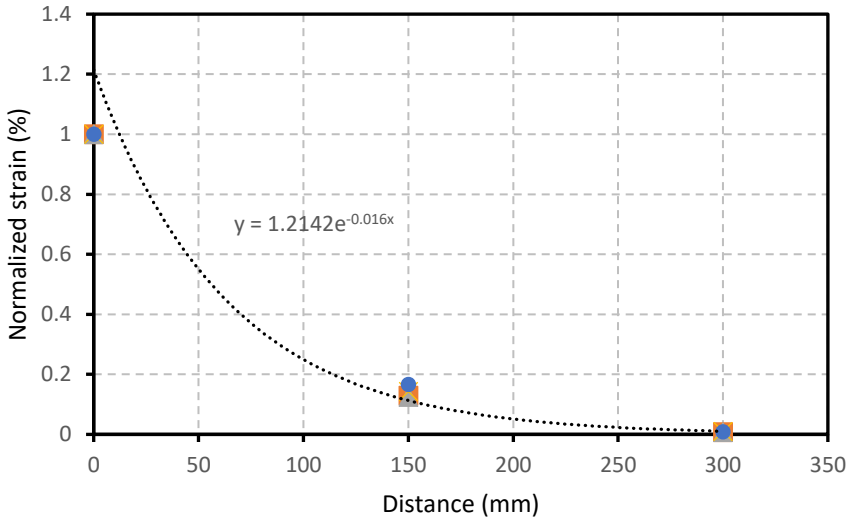

Figure 6.7: Normal strain distribution for beam SC-16-1.5-0%

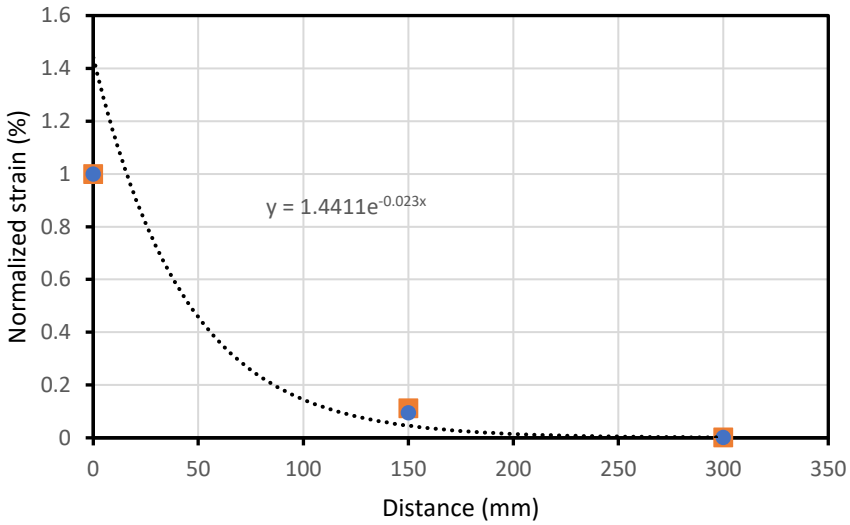

Figure 6.8: Normal strain distribution for beam SC-12-1.5-0%

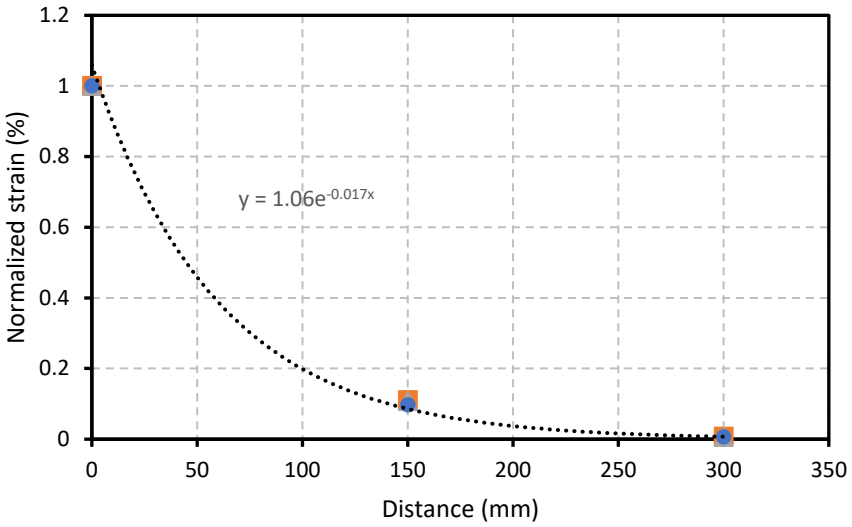

Figure 6.9: Normal strain distribution for beam R-16-1.5-0%

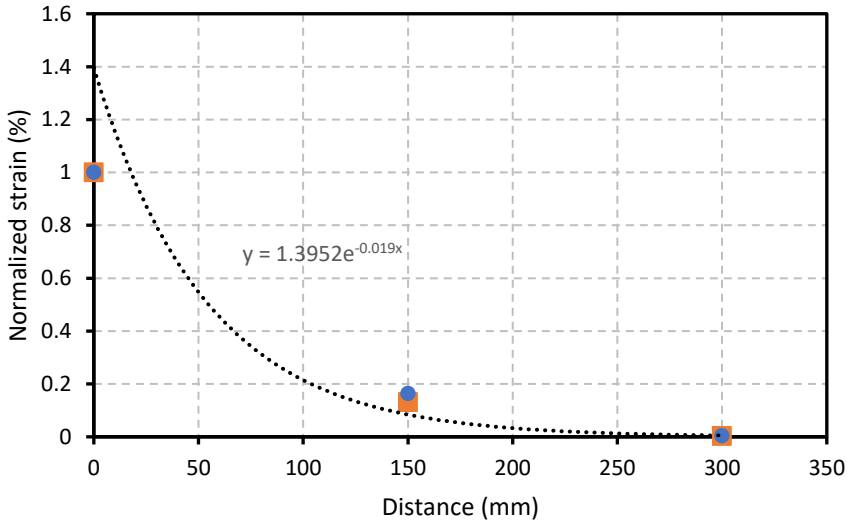

Figure 6.10: Normal strain distribution for beam R-12-1.5-0%

Main Study

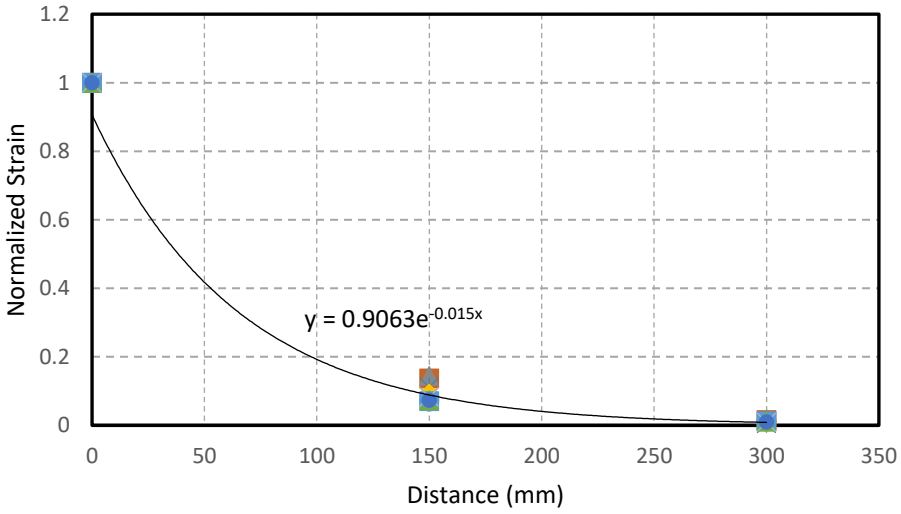

Figure 6.11: Normalized strain distribution for beam SC-16-1.5-S

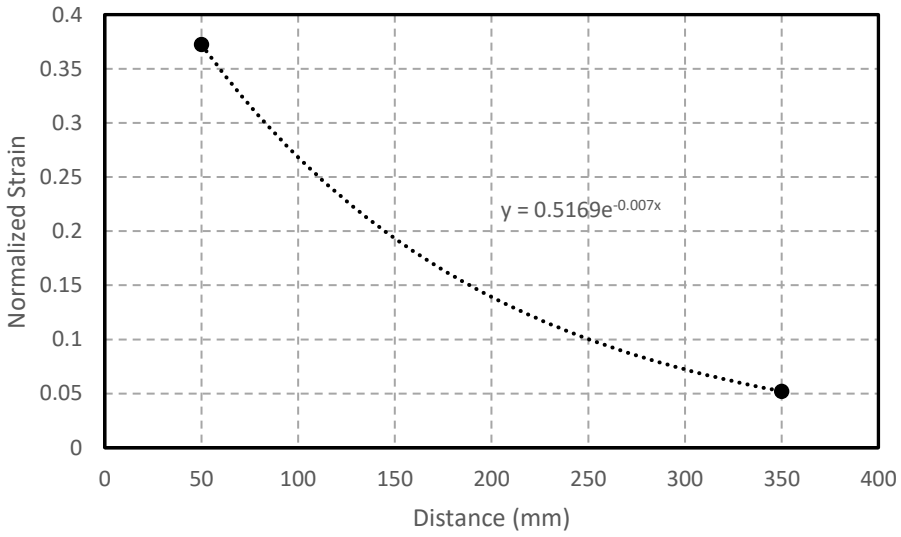

Figure 6.12: Normalized strain distribution for beam SC-16-1.5-F

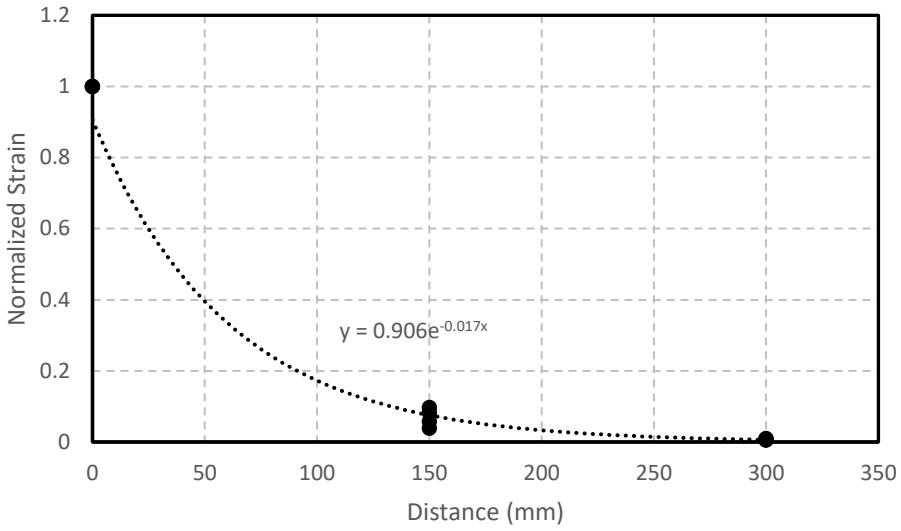

Figure 6.13: Normalized strain distribution for beam SC-16-3.0 -S

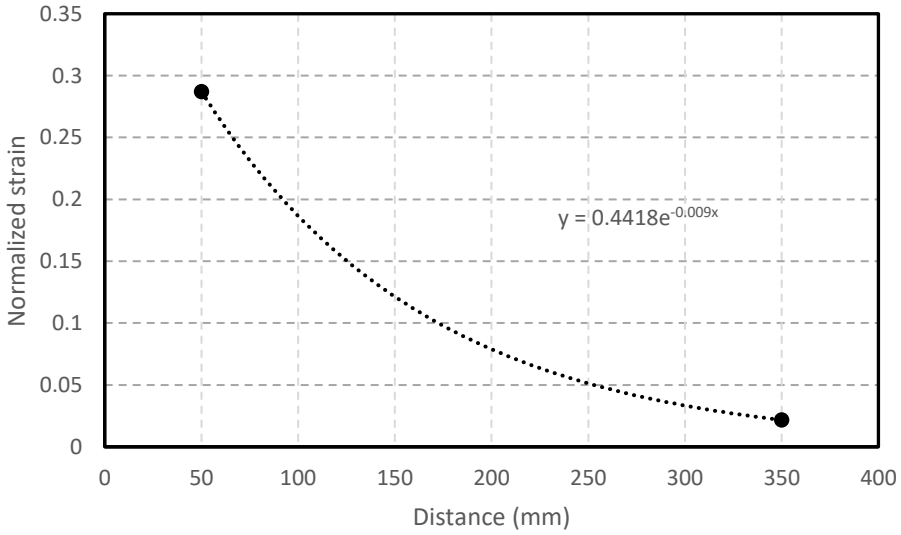

Figure 6.14: Normalized strain distribution for beam SC-16-3.0-F

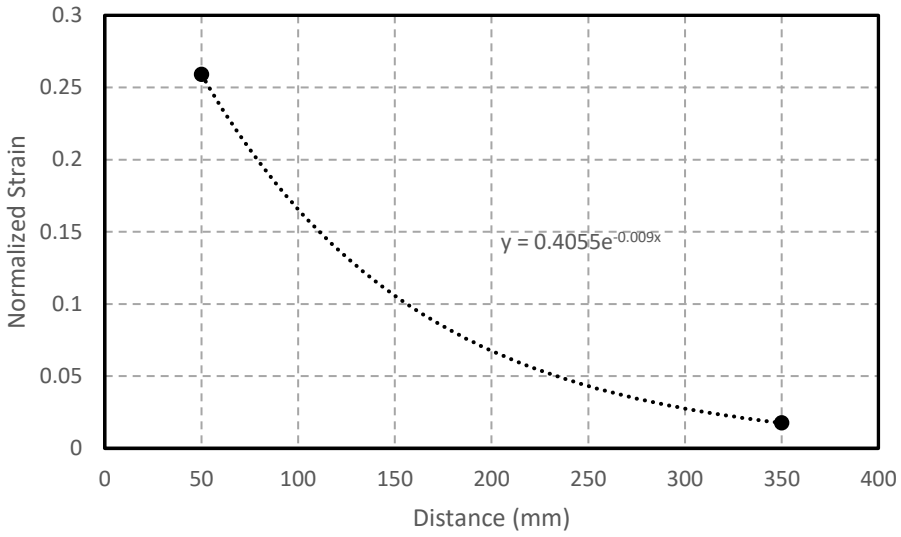

Figure 6.15: Normalized strain distribution for beam R-16-1.5 -F

Table 6.2 summarizes the *C*-values for all of the beam sets. The *C*-value depends on many factors including, bar surface type, concrete cover, and bar diameter dependent slip behaviour. For beams reinforced with sand coated GFRP bar, the normal strain distribution for the beam tested under monotonic loading is slightly different than the normal stress distribution for the beam tested under fatigue loading as shown in Figure 6.11 to 6.15. Because the value of local shear (bond) stress is sensitive to the *C*-value, both values will be taken into consideration in modelling.

Table 6.2 Values of exponent *C*

Phase	GFRP bar type	Beam	C
Preliminary Study	Sand Coated	SC-16-1.5	-0.016
		SC-12-1.5	-0.023
	Ribbed	R-16-1.5	-0.017
		R-12-1.5	-0.020
Main Study	Sand Coated	SC-16-1.5-Static	-0.015
		SC-16-1.5 -Fatigue	-0.007

Table 6.2 Values of exponent *C* (continued)

Phase	GFRP bar type	Beam	C
Main Study	Sand Coated	SC-16-3.0 -Static	-0.017
		SC-16-3.0 -Fatigue	-0.009
	Ribbed	R-16-1.5- Static	-0.016
		R-16-1.5 -Fatigue	-0.009

The integral of the bond stress multiplied by the circumference of the GFRP bar between the centreline of the support and the crack tip is equal to the normal stress multiplied by the cross-sectional area (normal force in the GFRP bar) as shown in Figure 6.16. Substituting Equation 6.2 into Equation 6.1 gives Equation 6.3. Knowing the force at the crack tip, the distance ahead of the crack tip (*L*), and the constant *C*, the shear stress at the crack tip can be calculated by using Equation 6.3.

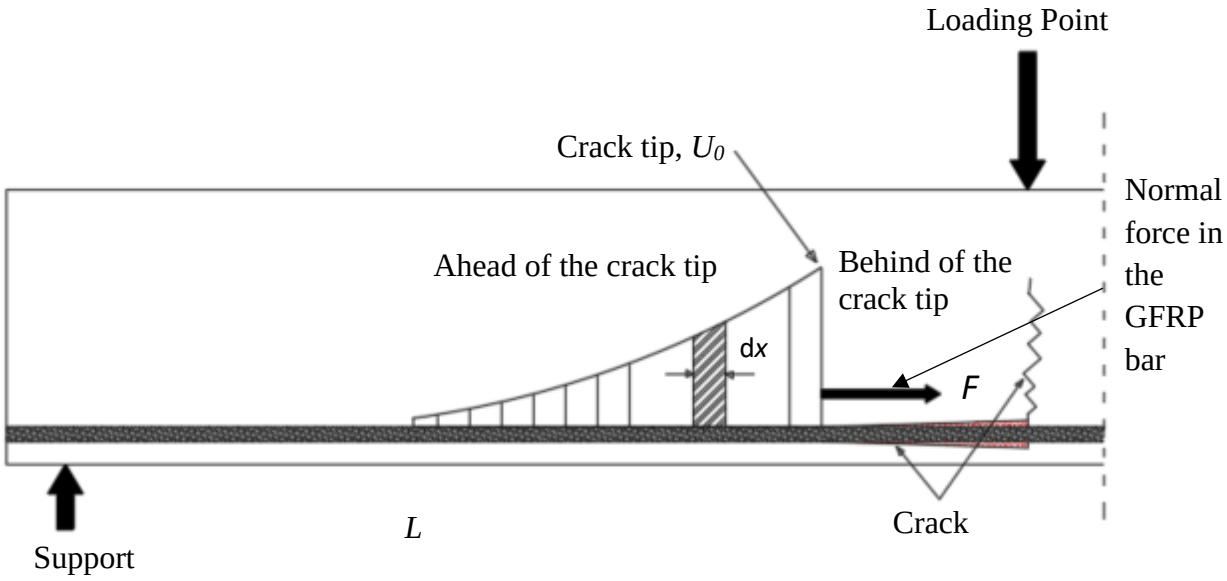

Figure 6.16: typical shear stress distribution at the crack tip

$$A_f \times f_f = \pi d \int U \Delta L$$

$$A_f \times f_f = \pi d \int U_0 e^{(-C \times L)}$$

$$A_f \times f_f = -\frac{\pi d}{C} U_0 e^{(-C \times L)} \Big|_0^L$$

$$A_f \times f_f = -\frac{\pi d}{C} U_0 (e^{(-C \times L)} - 1)$$

$$A_f \times f_f = \frac{\pi d}{C} U_0 (1 - e^{(-C \times L)})$$

$$U_0 = \frac{A_f \times f_f \times C}{\pi d (1 - e^{(-C \times L)})} \qquad \text{Eq. (6.3)}$$

For each beam set, the maximum shear (bond) stress and the constant *C* were obtained from the monotonic test results. By using Equation 6.3, the bond strength can be calculated. Table 6.3 shows the maximum bond stress for each beam of the preliminary study and for each beam set of the main study.

Table 6.3: Ultimate bond stress for different GFRP bar

Phase	GFRP bar type	Beam	Ultimate Bond stress (MPa)
Preliminary Study	Sand Coated	SC-16-1.5	22.95
		SC-12-1.5	40.57
	Ribbed	R-16-1.5	25.25
		R-12-1.5	42.78
Main Study	Sand Coated	SC-16-1.5	19.0
		SC-16-3.0	22.5
	Ribbed	R-16-1.5	20.0

b) <u>The shear stress (U_0) that drives the crack</u>

The differences in the normal stress along the GFRP bar generate the bond stress between the GFRP bar and the concrete. The longitudinal (de-bonding) crack is driven by the shear (bond) stress at the crack tip, which can be calculated using Equation 6.3.

After the first flexural crack appears near the loading point, a longitudinal (de-bonding) crack will start at the point where the flexural crack appears and propagate towards the support. At first, the de-bonding crack will be driven by the peak shear stress in the bar due to the sudden change in bar force that accompanies the mid-span flexural crack. Figure 6.17-a shows a typical shear stress distribution and the peak shear stress that drives the initial bond crack.

As a monotonic load advances a crack or it is advanced by fatigue cycling the shear (bond) stress peak that drives the longitudinal (de-bonded) crack will decrease due to the presence of a residual shear stress (blue color) behind the crack tip as shown in Figure 6.17-b.

The shear stress at a distance (a) along a crack can be calculated by finding the force at distance (a), F(a), and substituting the value of F(a) in Equation 6.3. The force at distance (a) can be calculated by subtracting the change in force at a distance (a) from the bar force at mid span. Equation 6.4 is used to calculate the bar force at any distance from the loading point:

$$F(a) = F - U_r \times \pi \times d_b \times a \qquad \text{Eq. (6.4)}$$

where:

$F(a)$: is the bar force at distance (a), at the crack tip (kN)

F: is the bar force at loading point (kN)

U_r: is the residual stress along the de-bonded region (MPa)

d_b: is the bar diameter (mm)

a: is the distance between the loading point and the crack tip (mm)

when the crack approaches the support with continued cycling, the length of the bonded region ahead of the crack tip (fully bonded) will decrease until the value of the shear stress at the crack

tip begins to increase due to the lack of a sufficient uncracked length to accommodate the shear force produced by the change in bar force even though the bar force continues to decrease due to the presence of the residual shear stress behind the crack tip. Figure 6.17-c shows the distribution of the shear stress from the beginning of a test until failure, including the locus of the peaks shear stress that drives the crack and the residual shear stress.

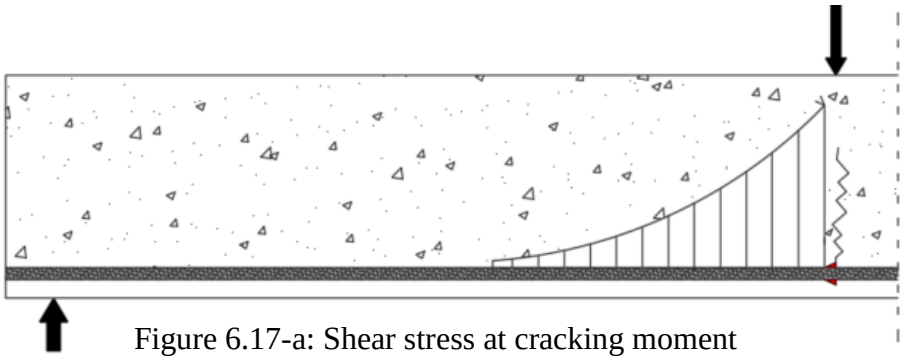

Figure 6.17-a: Shear stress at cracking moment

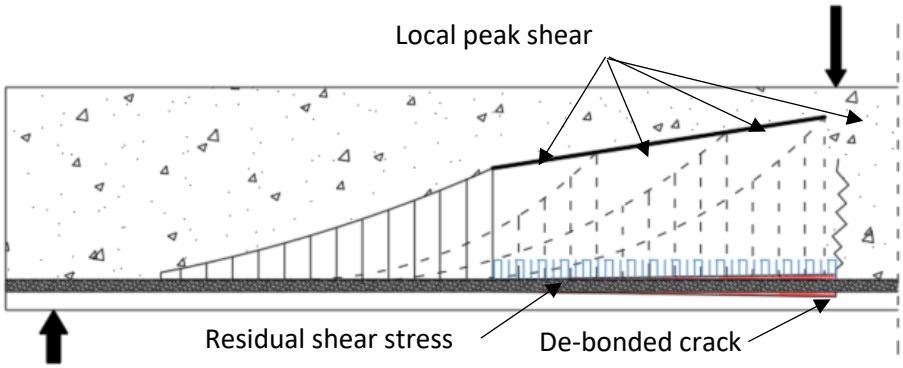

Figure 6.17-b: Shear stress after debonding cracking

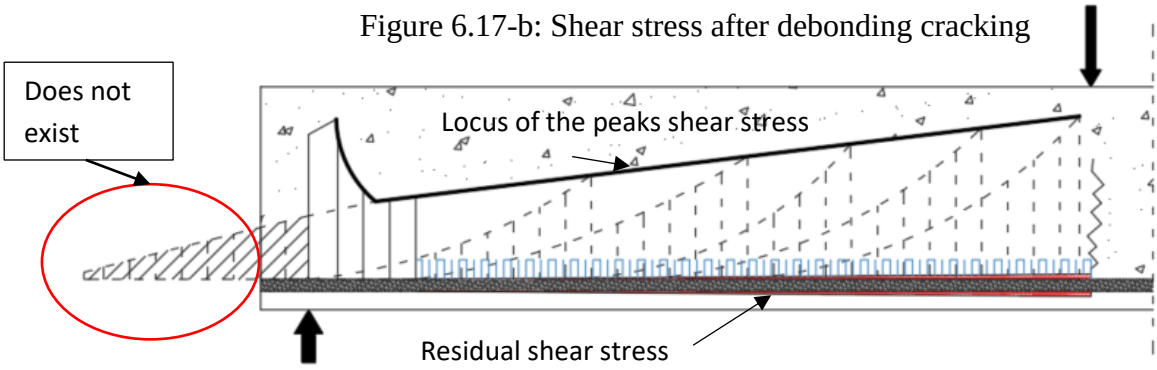

Figure 6.17-c: Shear stress at failure of specimen

Figure 6.17: Shear stress distributions at different crack lengths

c) <u>The rate of crack propagation</u>

The fatigue crack growth rate (d*a*/d*N*) is defined as the increase of the crack length (d*a*) due to the application of a fatigue load cycle. In these bond tests, the crack growth rate depends on the local shear (bond) stress at the tip of the crack between the GFRP bar and the concrete.

The relationship between the shear stress at the tip of a de-bonded crack (U_0) and the crack growth rate (d*a*/d*N*), shown in Figure 6.18-b, can be integrated to find the number of cycles to failure at given load ranges to produce the load vs. number of cycles to failure curves as shown in Figure 6.18-a. Equation 6.5 is used to describe the relationship between the shear stress at the crack tip (U_0) and the crack growth rate (d*a*/d*N*).

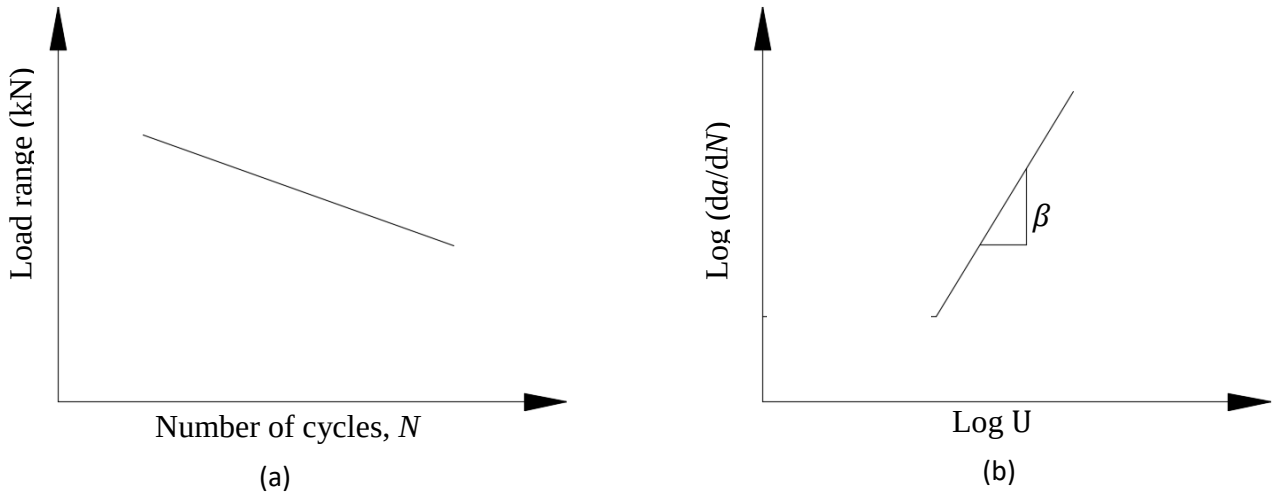

Figure 6.18: Load range vs. *N* and (d*a*/d*N*) vs. Log U

$$\frac{da}{dN} = \alpha \, \mathrm{U}^{\beta} \qquad \text{Eq. (6.5)}$$

where:

d*a*: is the incremental crack length (mm)

d*N*: is the incremental number of cycles (cycles)

U: is the shear stress at the crack tip that is driving the crack (MPa)

β: is the slope of the crack growth versus shear stress curve on a log-log scale (Figure 6.18(b))

α: is the intercept of the best fit shear stress versus da/dN

Determination of α and β

The procedure followed in the current study to determine the intercept (α) and the slope (β) in the crack growth model is the same procedure used by Wahab et al. (2015) and Al-Yousef (2016). The load range versus fatigue life curves were used to calibrate the constants (α) and (β).

In this model, the fatigue life curves are used to derive a crack growth curve for each set of beams. The derivation is treated as an inverse problem. The assumed power function (Equation 6.4) that describes the crack growth curve was used to find the constants (α) and (β) that satisfy a short and a long-life point on the load versus fatigue life curve. First, the value of the constants (α) and (β) were assumed to have values close to those found by Wahab et al. (2015) and Al-Yousef (2016). The fatigue life was calculated for a fatigue short life in each beam set. If the calculated fatigue life was less than the experimental fatigue life, the value of constant (β) was too high and needed to be decreased. If the calculated fatigue life was higher than the experimental fatigue life, the value of constant (β) was too high and needed to be increased. This step was repeated until a value of the constant (β) was found which matched the calculated fatigue life with the experimental fatigue life. Then the procedure was repeated for a chosen long fatigue life but this time varying the constant (α). By repeated iterations the values of (β) and (α) were adjusted for each set of beams to match calculated to the measured fatigue lives. Table 6.4 shows the resulting values of (α) and (β) for each set of beams. The constant β, which is the slope of the crack growth rate vs. shear stress curve, is governed by the slope of the shear stress vs. fatigue life curve. Since, as shown in Figure 5.44, this slope is nearly equal for all the test series, the constant β is roughly the same for all our tests. The constant α, which represents the intercept of the best fit shear stress vs. da/dN curve, is dependent on the height of the stress vs. fatigue life curve, which varies with concrete cover as shown in Figure 5.44. The intercept of the best fit line is different from one set of beams to another based on the concrete cover.

Table 6.4: Values of constants "α" and "β"

Rod Type	Beam Type	β	α
Sand Coated	Reinforced with non-prestressed GFRP bar with concrete cover equal 1.5 times bar diameter	11.15	6.43×10^{-14}
	Reinforced with prestressed GFRP bar with concrete cover equal 1.5 times bar diameter	11.05	9.42×10^{-14}
	Reinforced with non-prestressed GFRP bar with concrete cover equal 3.0 times bar diameter	12.13	7.63×10^{-17}
	Reinforced with non-prestressed GFRP bar with concrete cover equal 3.0 times bar diameter	12.76	2.21×10^{-17}
Ribbed	Reinforced with prestressed GFRP bar with concrete cover equal 1.5 times the bar diameter	11.57	7.51×10^{-15}

6.3 The Crack Growth Calculation Procedure for Non-Prestressed Beams

The crack length versus number of fatigue cycles for a beam can be calculated as follows

1- The bar force at mid-span is calculated using a cracked section analysis.

2- The shear (bond stress) at the crack tip is calculated by using Equation 6.6:

$$U_o = \frac{Force \times C}{\pi d\ (1 - e^{-c \times L})} \qquad \text{Eq. (6.6)}$$

3- Using the Equation 6.5 for the rate of crack growth, the incremental number of cycles (d*N*) is calculated:

$$\frac{da}{dN} = \alpha \, \mathrm{U}^{\beta} \quad ========> \quad da = dN \times \alpha \, U^{\beta}$$

where α and β have already been determined for a given beam configuration.

4- The crack length is obtained by summing successive increments of crack growth $\boldsymbol{\delta a}(\mathrm{N}i)$ until one of the following failure criteria are met:

   a) When the total crack length a > 500 mm (the shear span length) the beam has failed
   Note: if the total crack length a < 500 mm, check the next condition.

When the calculated shear (bond) stress at the crack tip reaches the monotonic failure shear stress, the beam is assumed to have failed.

6.3.1 Comparison Between the Experimental Results and Prediction Model for Non-Prestressed Beams

Fatigue life

The actual fatigue life and the best fit curve calculated using the proposed model are shown in Figure 6.19 for the beams reinforced with sand coated GFRP that have concrete covers equal to 1.5·d_b and 3.0·d_b. The calculated number of cycles was in good agreement with the actual fatigue data for both beams sets indicating that the model was properly calibrated.

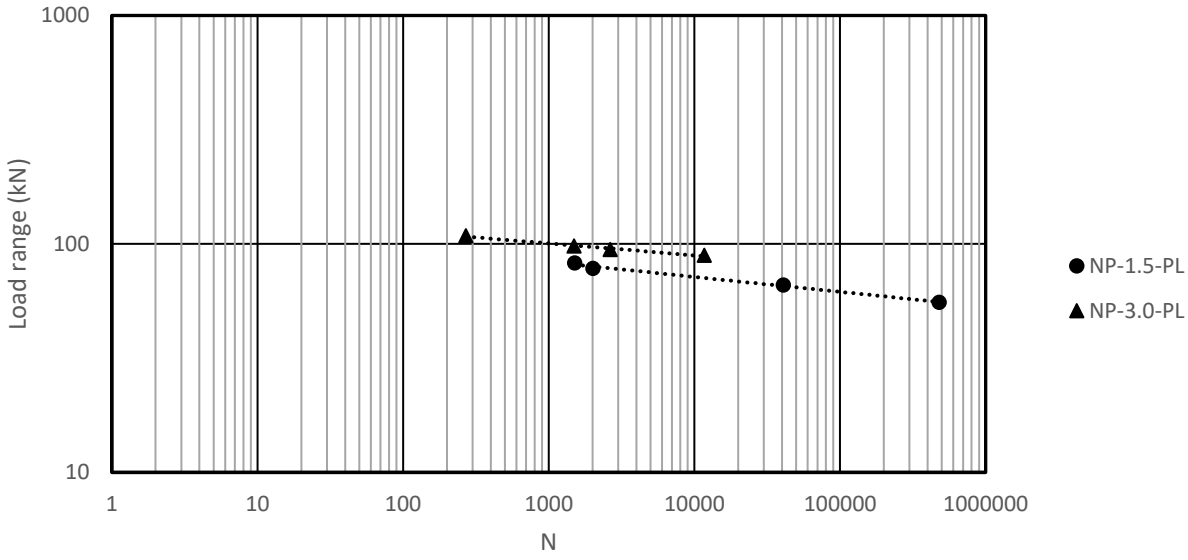

Figure 6.19: The actual fatigue life Vs the calculated curve for two beams reinforced with non-prestressed GFRP

6.3.2 Crack Length vs. Number of Cycles

After calibrating the model, the constants (α) and (β) were found based on the fatigue life for each set. The proposed model was then validated by calculating crack length vs. number of cycles curves. For each set of beams, the observed de-bonding crack length with cycles is compared with the predicted one. Figures 6.20 to 6.23 show the calculated crack length vs. the observed crack length values for different load levels beams with a concrete cover equal to 1.5 times the bar diameter. Figures 6.24 to Figure 6.27 show the calculated crack length versus the actual crack length data for beams with different load levels with a concrete cover equal to 3.0 times the bar diameter. For all beams that were tested under fatigue loading, three stages were observed in the crack length vs. number of cycles curve. In the first stage, the de-bonding crack length suddenly increased as the concrete cracked and the GFRP bar carried all the tensile force. Simultaneously, the de-bonded crack initiated and decreased the bond between the GFRP bar and the concrete. In the second stage, the crack length increased slowly until about 95% of the fatigue life of the beam. In the final stage, as the de-bonded crack approached to the support and there was not enough bonded length to resist the bar force, the debonding crack increased suddenly and the beam failed. The predicted curves give good estimates of initial cracking and the shape of the crack length versus cycles curves. Due to the scatter in the data points for each beam set, the data points falling close to the best fit line show a good agreement between the calculated and observed crack length at failure, and the points that fall far from the best fit line show a poorer agreement. In all cases the crack length versus life predictions describe correctly the trend of crack length versus cycles behaviour.

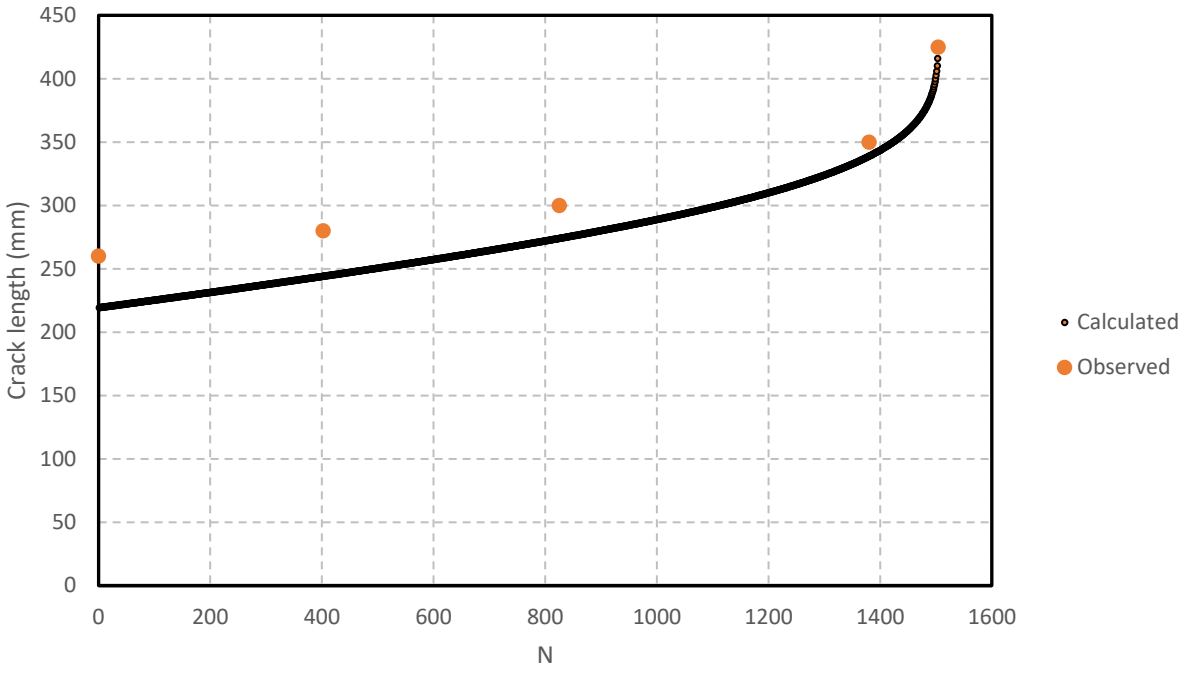

Figure 6.20: Experimental versus calculated crack length for SC-16-1.5-0%-82.5

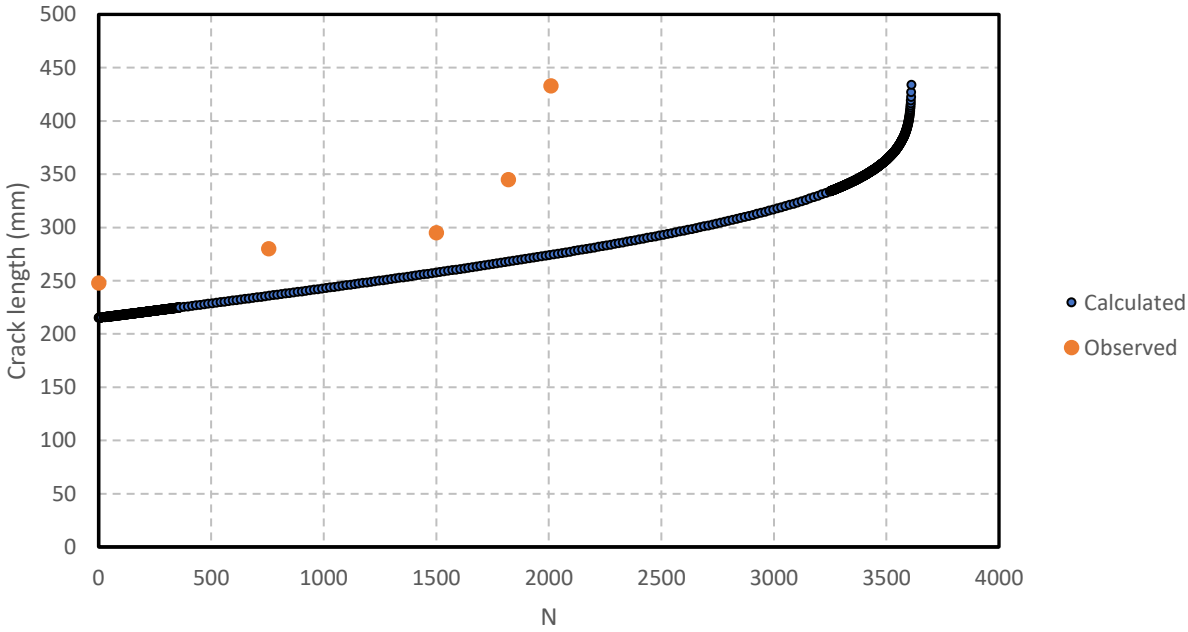

Figure 6.21: Experimental versus calculated crack length for SC-16-1.5-0%-78

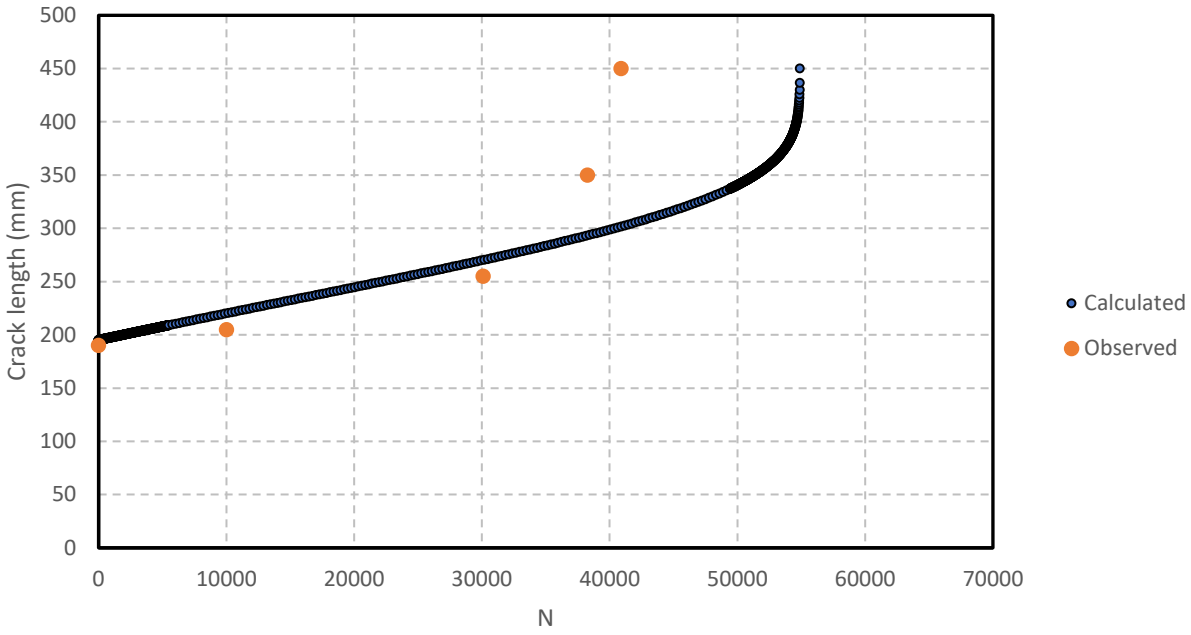

Figure 6.22: Experimental versus calculated crack length for SC-16-1.5-0%-66

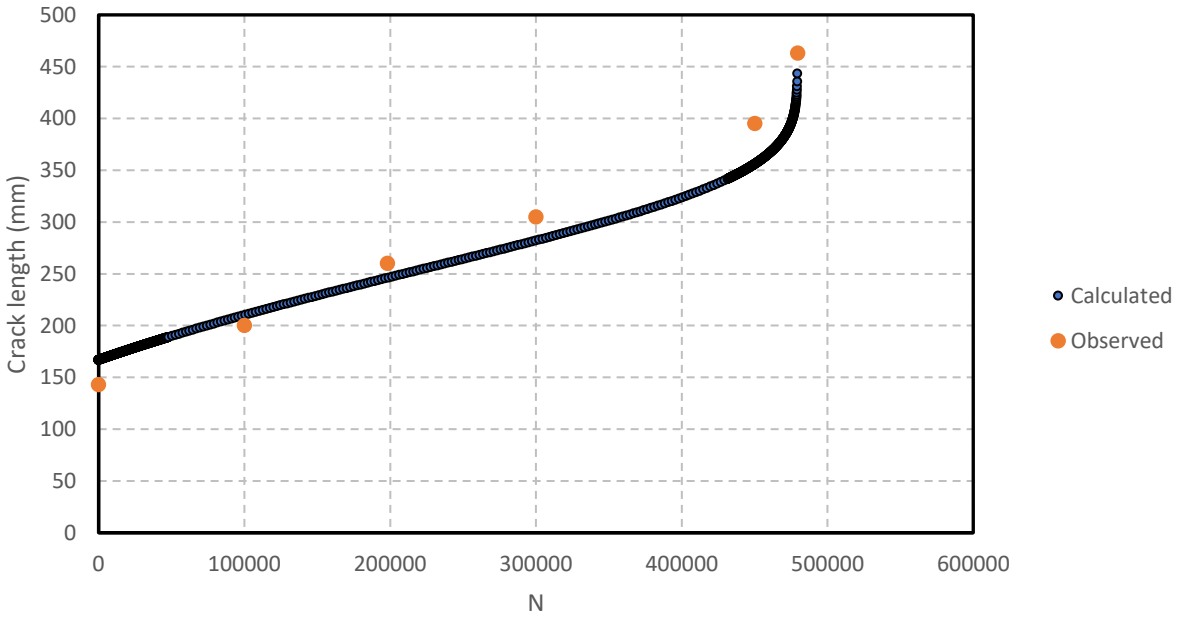

Figure 6.23: Experimental versus calculated crack length for SC-16-1.5-0%-55.5

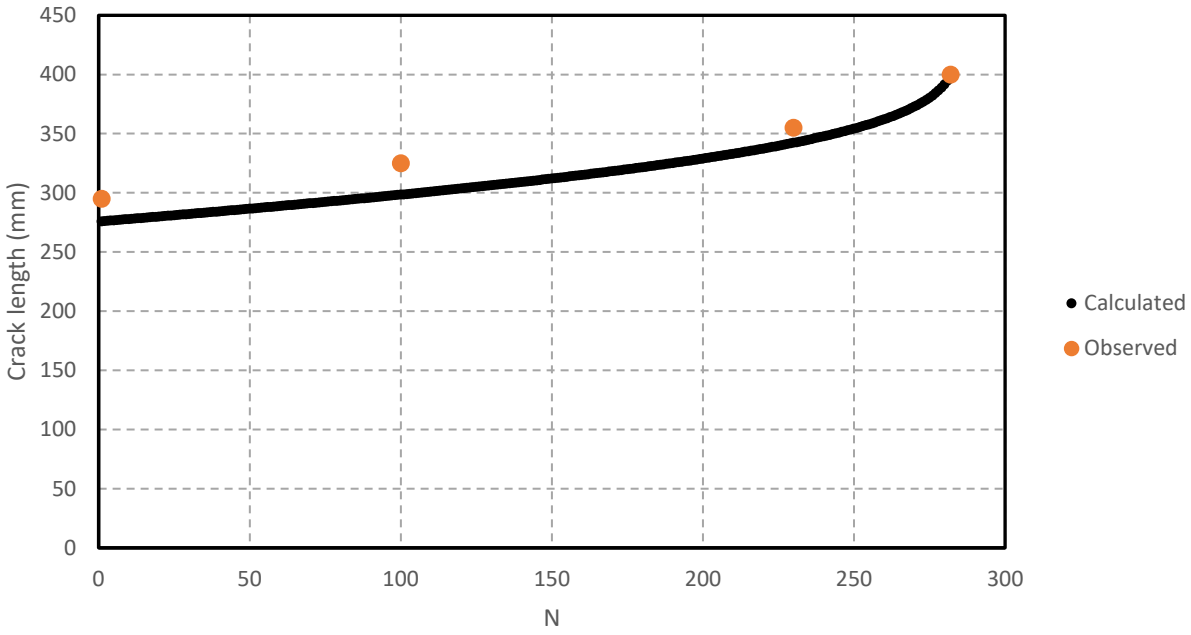

Figure 6.24: Experimental versus calculated crack length for SC-16-3.0-0%-108

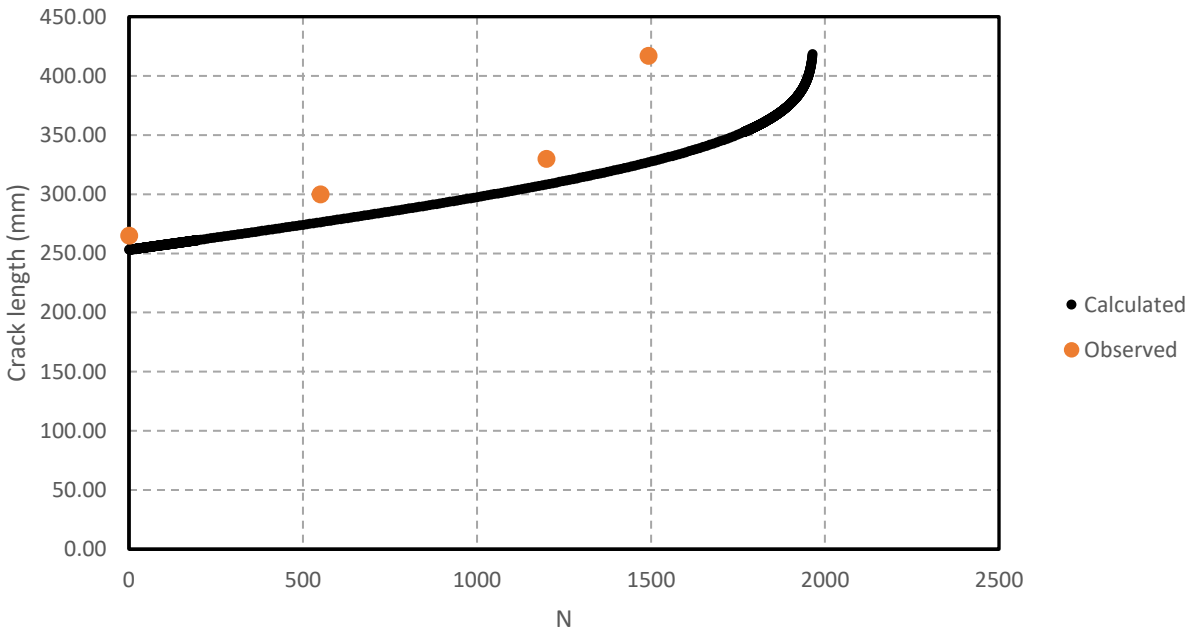

Figure 6.25: Experimental versus calculated crack length for SC-16-3.0-0%-98

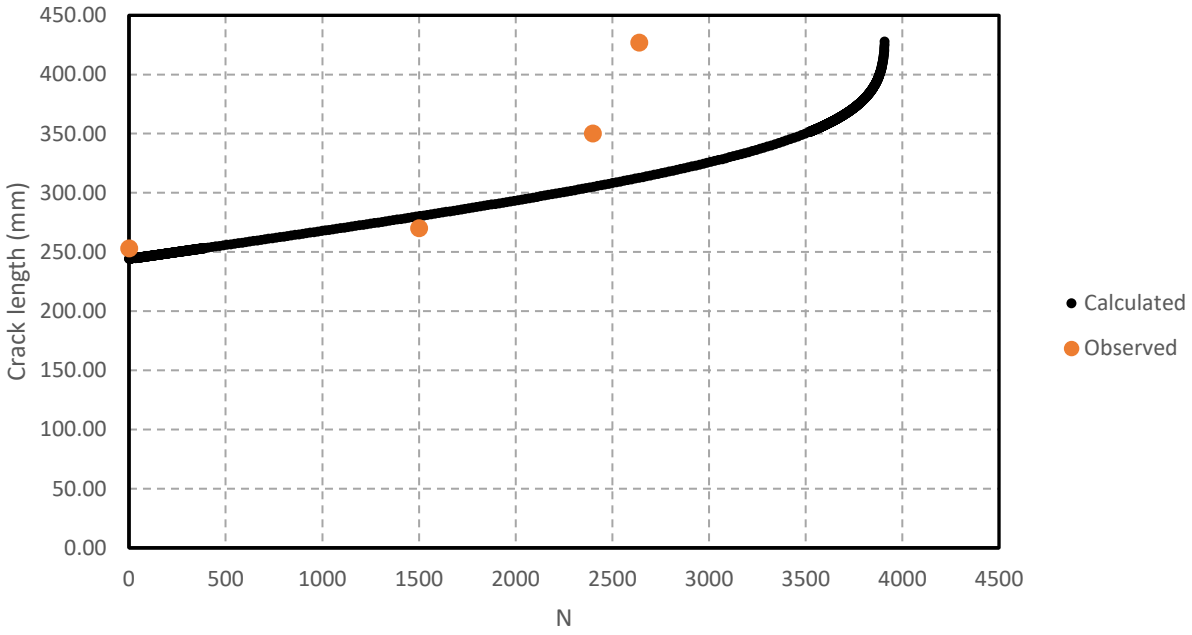

Figure 6.26: Experimental versus calculated crack length for SC-16-3.0-0%-95

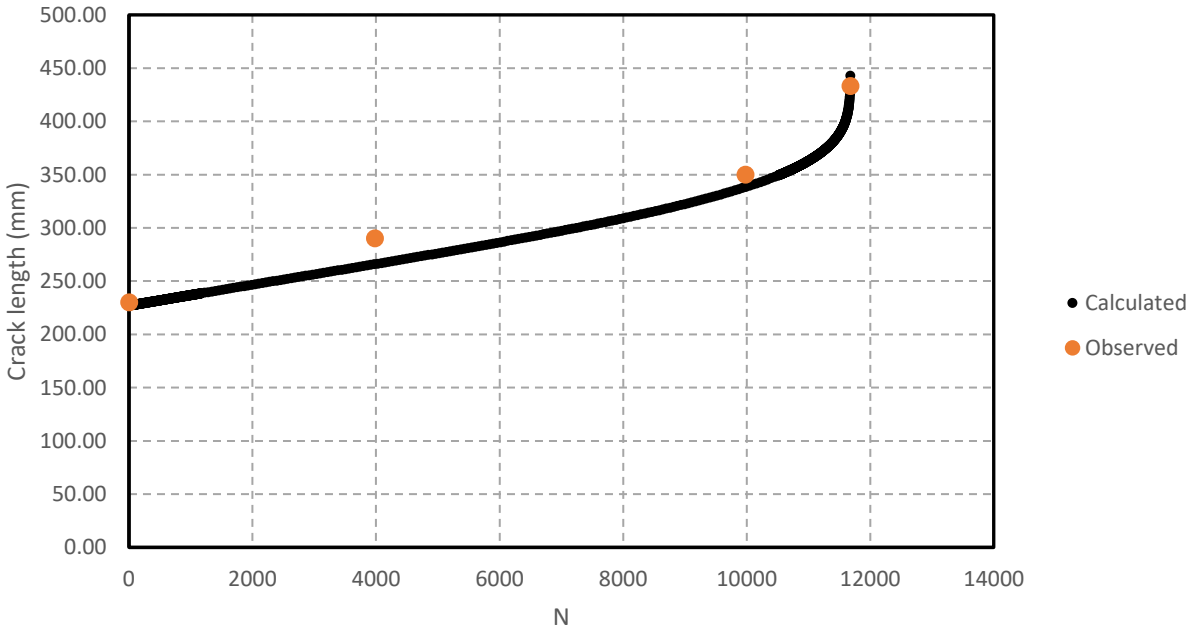

Figure 6.27: Experimental versus calculated crack length for SC-16-3.0-0%-89

6.4 Final Failure by Debonding between the GFRP Bar and the Concrete

This mode of failure occurred for beams reinforced with prestressed GFRP bars when a critical section near the support had a high shear stress. After the prestressing process, the force in the GFRP bar is transferred to the concrete over a certain distance called the "transfer length". The initial bar prestressing force increases from zero at the end of the bonded length to its maximum value at the end of the transfer length. The variation in the bar force along the transfer length creates a shear (bond) stress between the GFRP bar and concrete. The shear stress within the transfer length is assumed to follow an exponential curve. Similarly, to the beam reinforced with a non-prestressed GFRP bar, a debonding crack forms after a flexural crack occurs at the loading point. The de-bonding crack travels toward the support as the load is increased in the monotonic load or number of cycles for a fatigue loading is increased. The overlapping of the cyclic shear stress (the shear stress due to loading only without the prestressing force) and the shear stress due to prestressing will increase the shear stress at the end of the beam and shift the peak shear stress toward the loading point. As the load in a monotonic test or the number of cycles in a fatigue test increases, the crack tip and the peak shear stress will move toward the loading point until failure occurs when the remaining bonded length can no longer support the shear force between the bar and the concrete. Figure 6.28-a shows the shear stress due to the prestressing force along the transfer length. As the monotonic load advances a crack or it is advanced by fatigue cycling the shear (bond) the stress peak that drives the longitudinal (de-bonded) crack will decrease due to the presence of a residual shear stress (blue colour) behind the crack tip as shown in Figure 6.28-b. Figure 6.28-c shows the distribution of the shear stress from the beginning of a test until failure including the locus of the peak shear stresses that drives the crack and the residual shear stress.

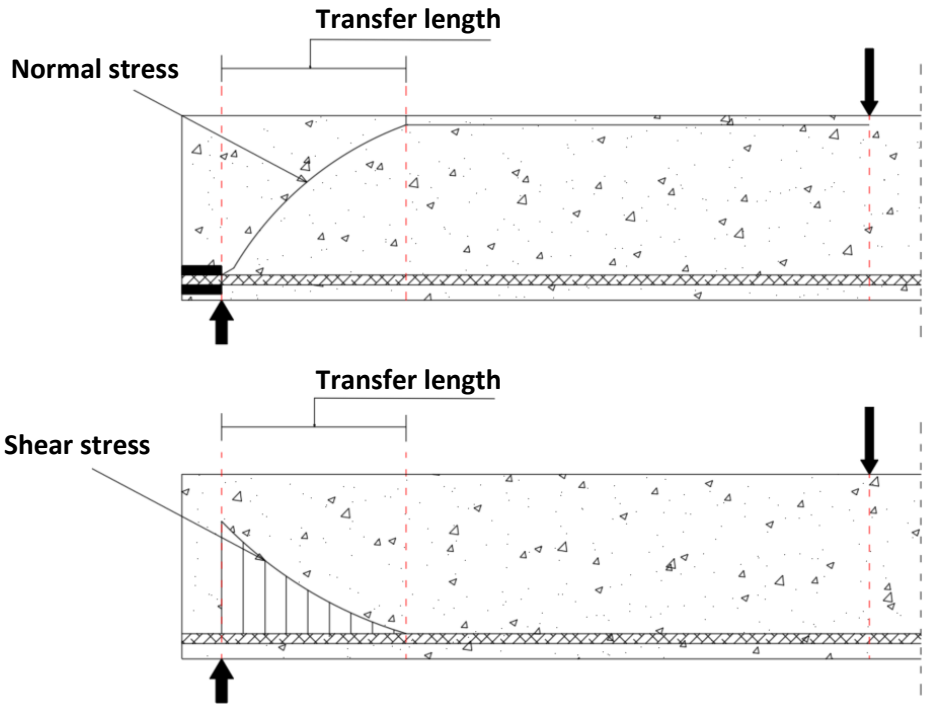

a- Shear stress due to prestressing

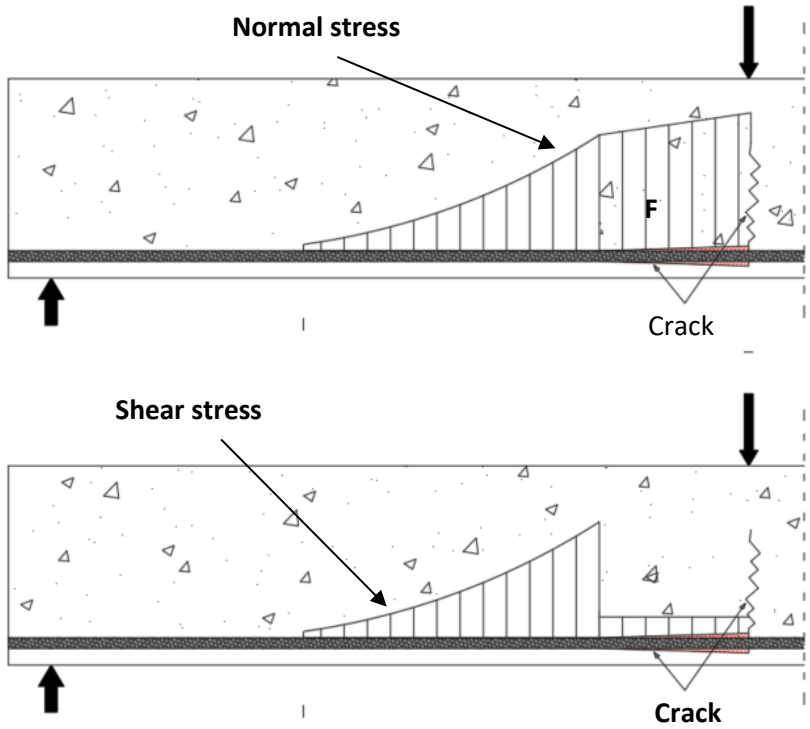

b- Normal and shear stress due to loading

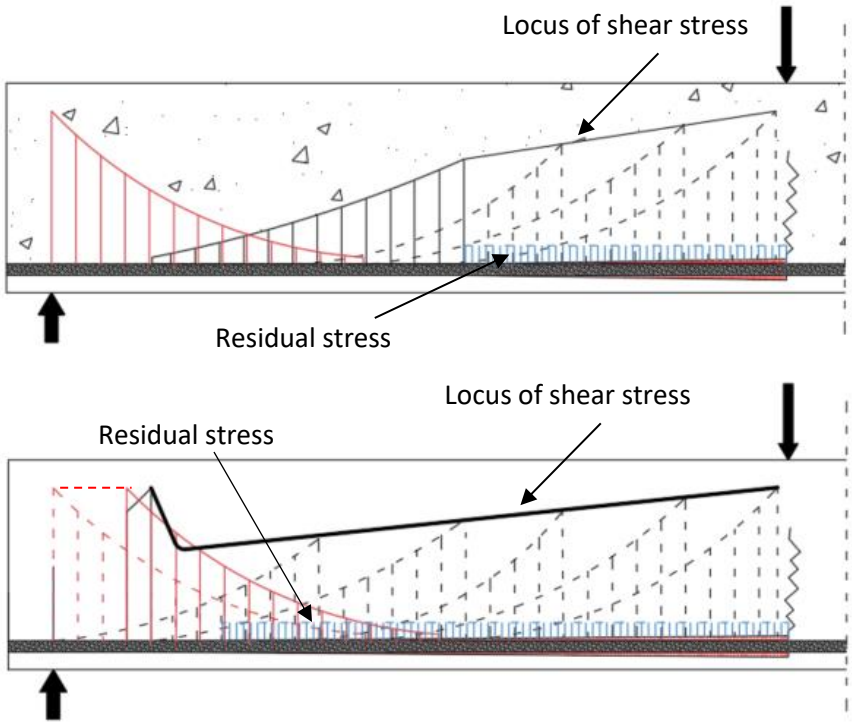

c- Shear Stress at the end of specimen

Figure 6.28: Shear stress and force distributions in prestressed beams

6.4.1 The Crack Growth Calculation Procedure for Prestressed Beams

The crack growth for a given beam and its fatigue life can be calculated as follows:

1- The total bar force at mid span is calculated and the prestressing force subtracted from it.

2- The shear (bond stress) at the crack tip is calculated using Equation 6.7:

$$U_0 = \frac{Force \times C}{\pi d\ (1 - e^{-c \times L})} \qquad \text{Eq. (6.7)}$$

3- Using Equation 6.5 for the rate of crack growth, the incremental number of cycles (d*N*) was calculated:

$$\frac{da}{dN} = \alpha\, U^{\beta} \quad ========> \quad da = dN \times \alpha\, U^{\beta}$$

where *a* and *b* are already known for a given beam configuration.

4- The crack length is obtained by summing successive increments of crack growth $\boldsymbol{\delta a}(N_i)$ until one of the following failure criteria are met:

a) When the total crack length a > 500 mm (the shear span length) the beam has failed.

Note: if the total crack length a < 500 mm, check the next condition.

b) When the calculated shear (bond) stress at the crack tip reaches the monotonic failure shear stress, the beam is assumed to have failed.

6.4.2 Comparison Between the Experimental Results and Prediction Model Results for Prestressed Beams

Fatigue life

The actual fatigue life and the best fit curve calculated using the proposed model are shown on Figure 6.30 for the beams reinforced prestressed GFRP and having a concrete covers equal to $1.5 \cdot d_b$ and $3.0 \cdot d_b$. The calculated number of cycles was in good agreement with the actual fatigue data for all beams sets indicating that the model was properly calibrated.

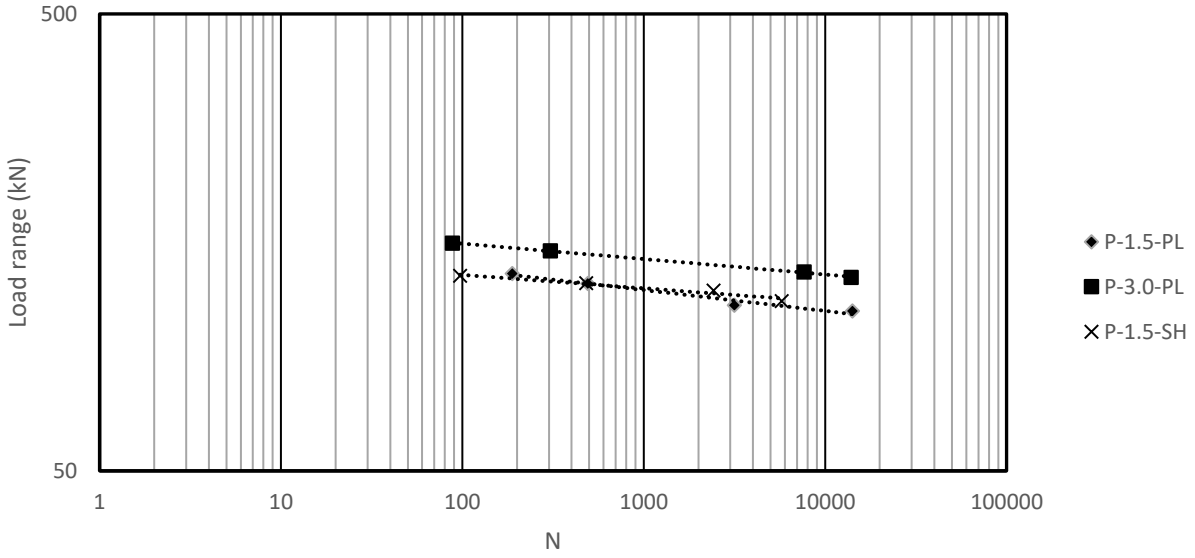

Figure 6.29: Actual vs. calculated fatigue life curve for the beams reinforced with pre-stressed GFRP

6.4.3 Crack Growth vs. Number of Cycles

After calibrating the mode, the constants (α) and (β) were found based on the fatigue life data for each se. The proposed model was then validated by calculating the crack length vs. number of cycles curves and comparing the calculated curves with the measured data. For each set of beams, the observed de-bonding crack length vs. number of cycles curve was compared with the predicted one. Figures 6.30 to Figure 6.32 show the calculated crack length vs. the actual crack length data for beams reinforced with sand coated GFRP bar and concrete cover equal to 1.5 times the bar diameter. Figures 6.33 to 6.35 show the calculated crack lengths together with the actual crack length data for beams reinforced with prestressed sand coated GFRP bar and a concrete cover equal 3.0 times the bar diameter. Figures 6.36 to 6.38 show the calculated crack lengths together with the actual crack length data for beams reinforced with a ribbed GFRP bar and a concrete cover equal 1.5 times the bar diameter. For all beams that were tested under fatigue loading, three stages were observed in the crack length vs. number of cycle curve. In the first stage, the de-bonding crack length suddenly increased as the concrete cracked and the GFRP bar carried all the tensile force. Simultaneously, the de-bonded crack initiated and decreased the bond between the GFRP bar and the concrete. In the second stage, the crack length increased slowly until about 95% of the fatigue life of the beam. In the final stage, as the de-bonded crack approached to the support, there was not enough bonded length to resist the bar force and the debonding crack increased suddenly, causing the beam to fail. Again, the predictions give good estimates of initial crack length and of the shape of the crack length versus cycles curves. Variation in predicted fatigue lives is consistent with the variation in the experimental data. Due to a little scatter in the data points in each beam set, the data points fall close to the best fit line show a good agreement between the calculated and observed crack length at failure and points that fall far from the best fit line was shown a poorer agreement. In all cases the crack length versus life predictions describe correctly the trend of crack length versus cycles behaviour

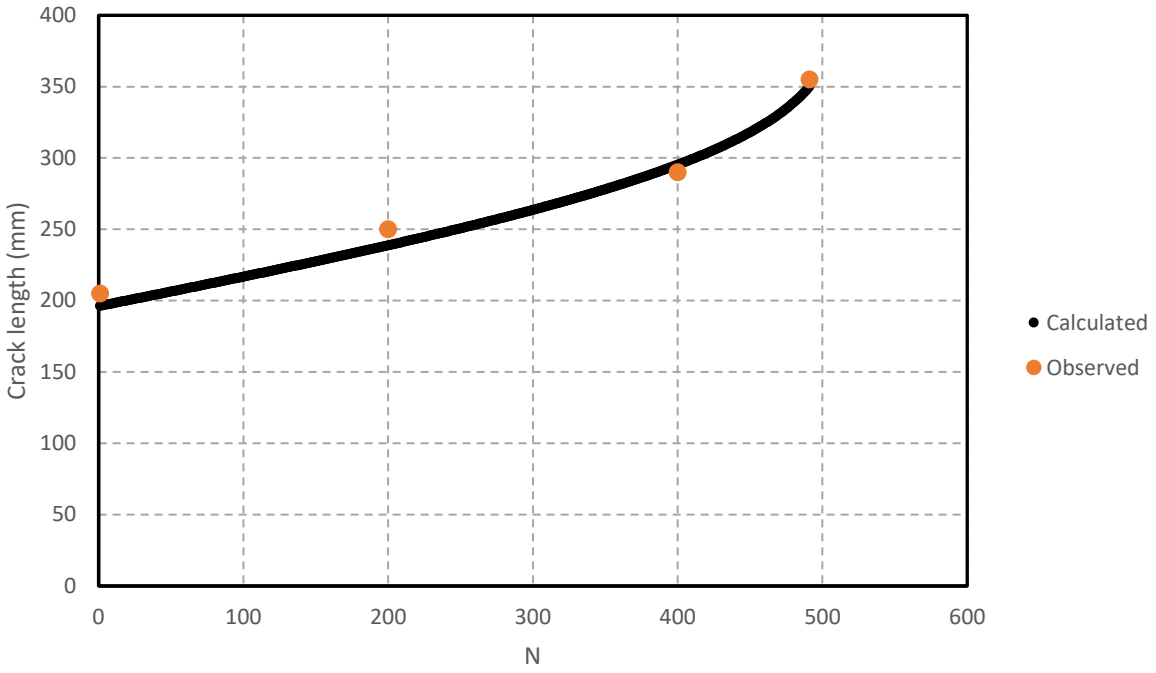

Figure 6.30: Experimental vs. calculated crack length for SC-16-1.5-40%-125.5

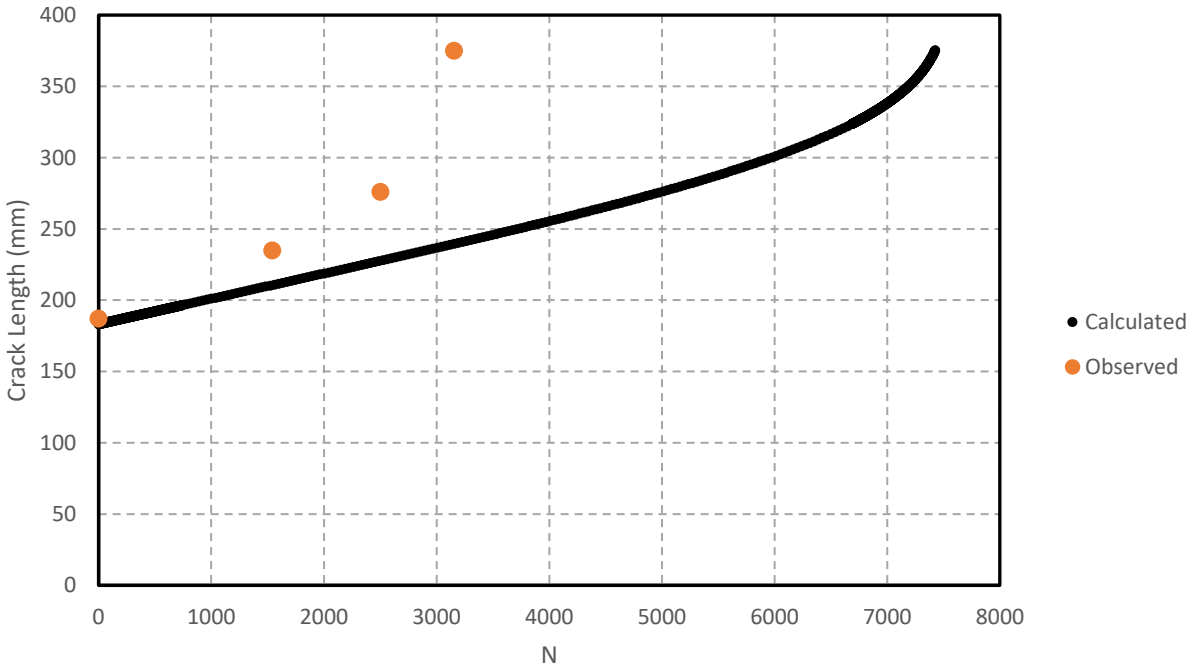

Figure 6.31: Experimental vs. calculated crack length for SC-16-1.5-40%-115.5

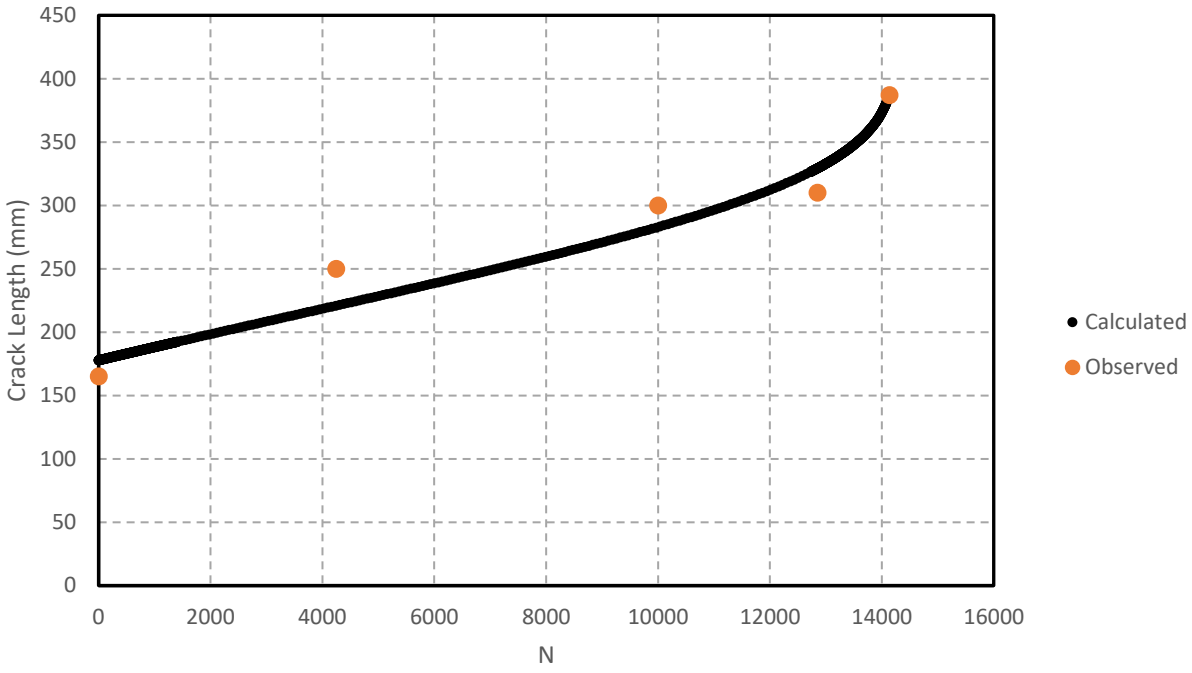

Figure 6.32: Experimental vs. calculated crack length for SC-16-1.5-40%-112

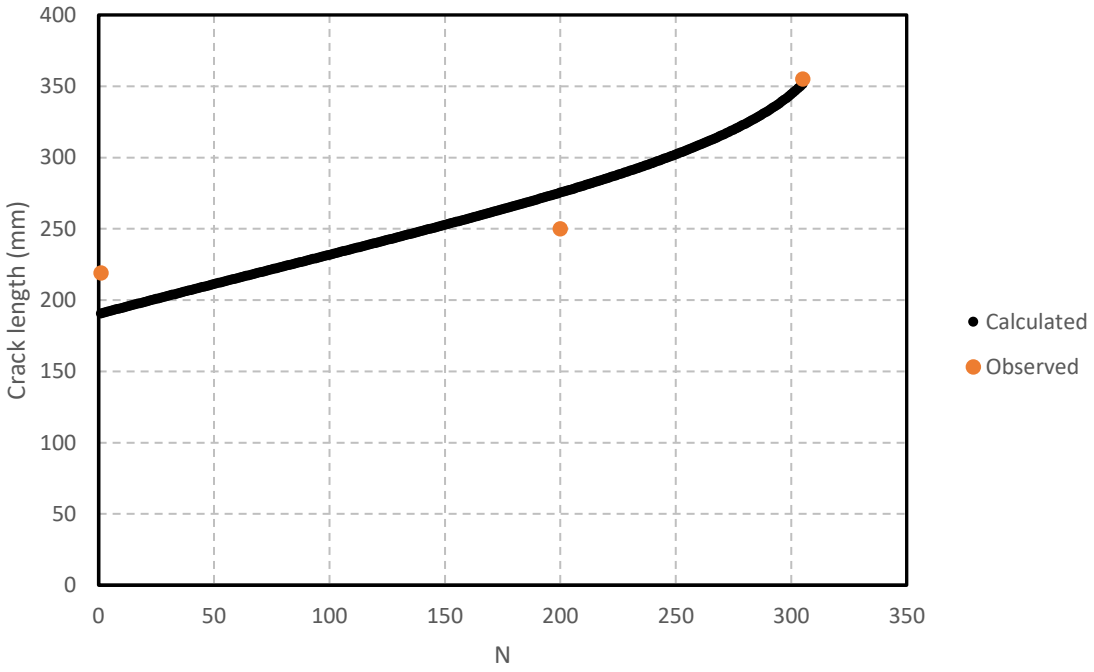

Figure 6.33: Experimental vs. calculated crack length for SC-16-3.0-40%-152

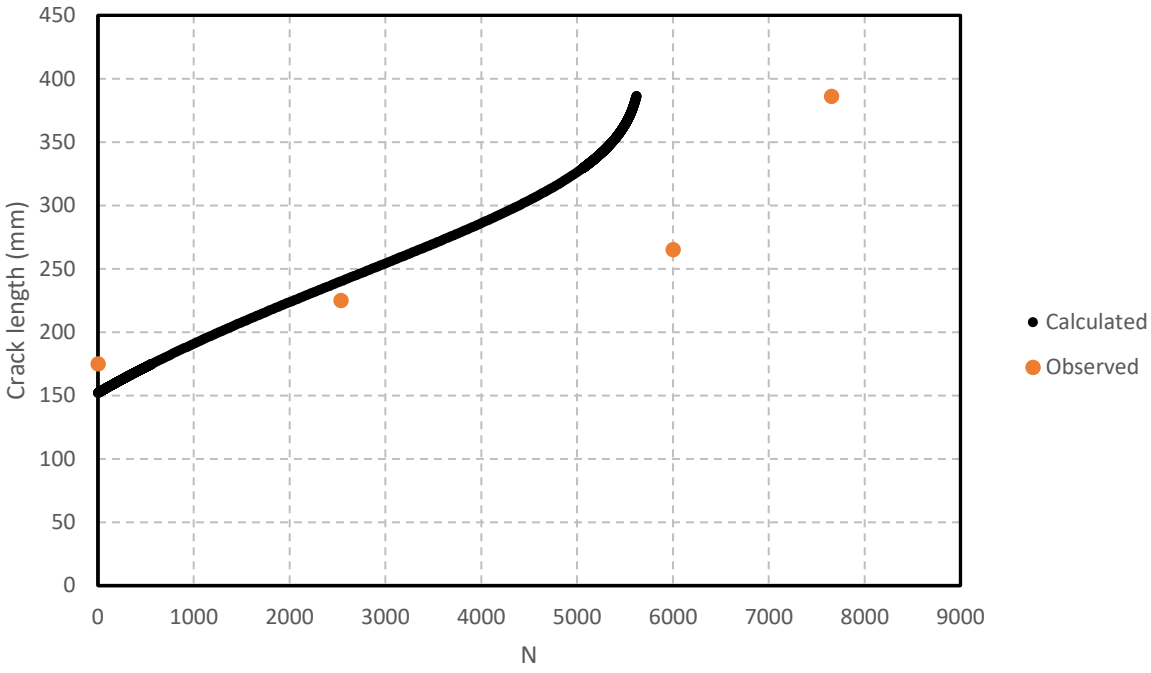

Figure 6.34: Experimental vs. calculated crack length for SC-16-3.0-40%-136

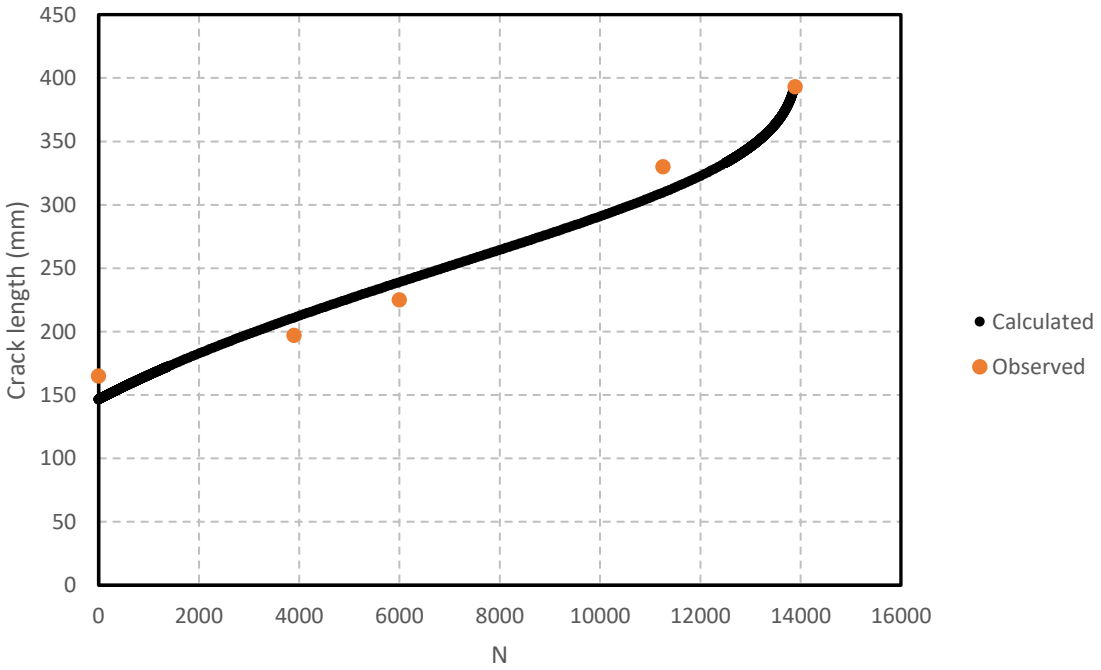

Figure 6.35: Experimental vs. calculated crack length for SC-16-3.0-40%-132

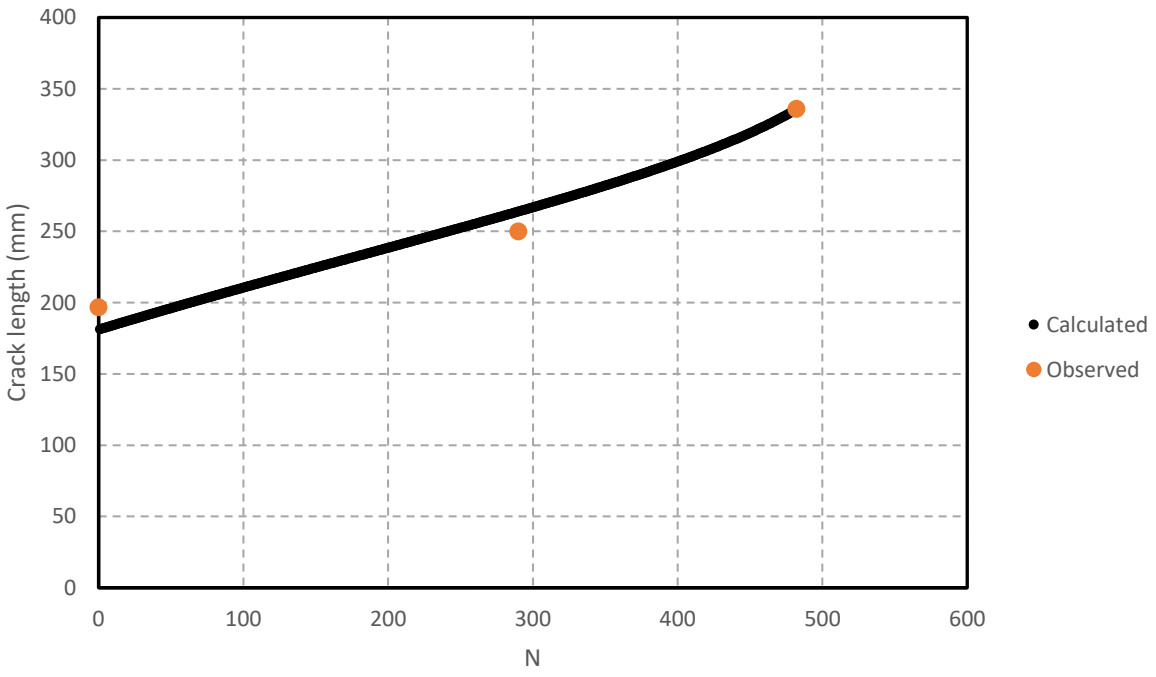

Figure 6.36: Experimental vs. calculated crack length for R-16-1.5-40%-129

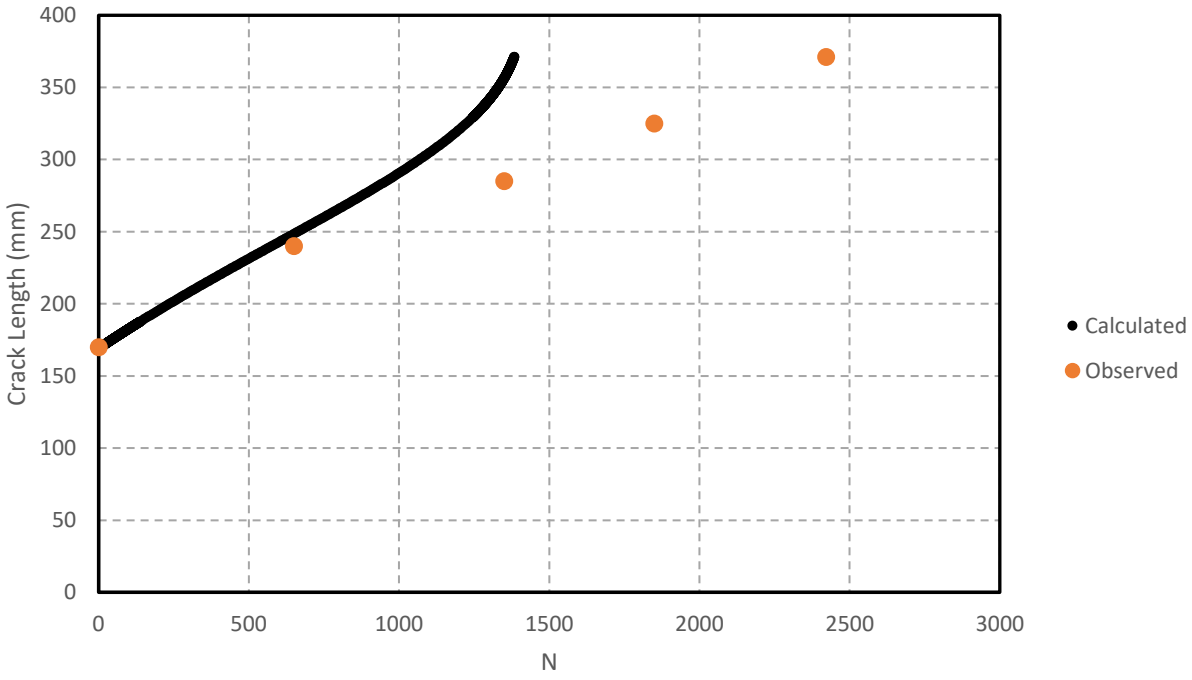

Figure 6.37: Experimental vs. calculated crack length for R-16-1.5-40%-124

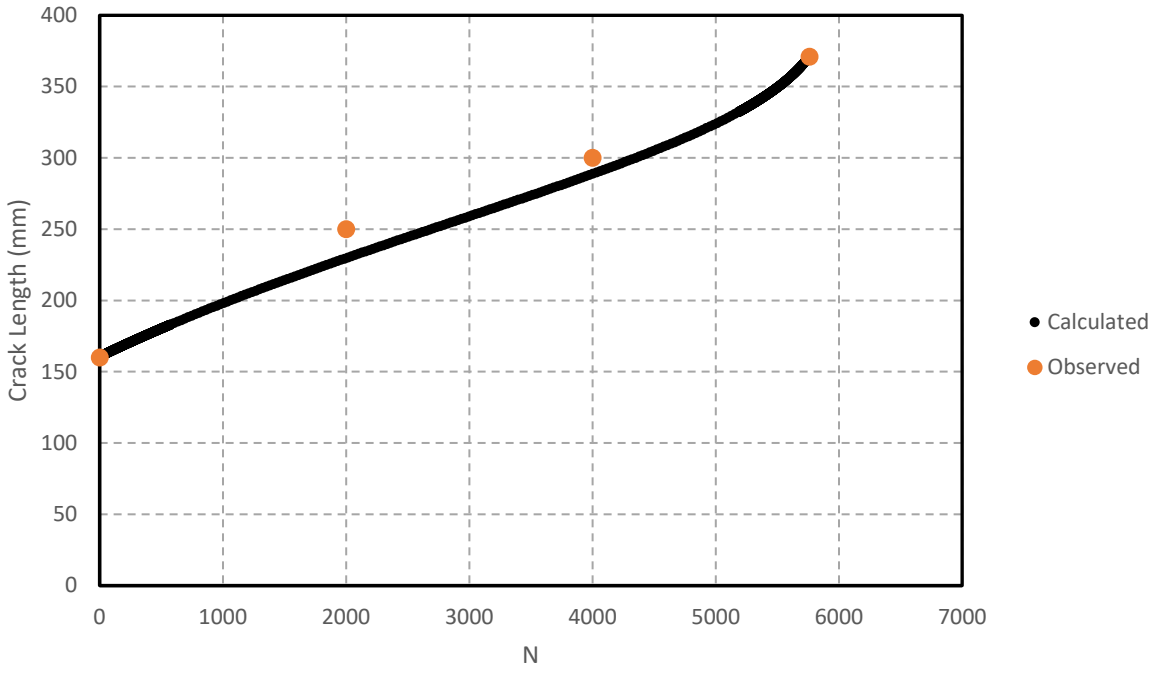

Figure 6.38: Experimental vs. calculated crack length for R-16-1.5-40%-117.5

6.5 Discussion

Figure 6.39 shows a sketch of a predicted crack length (mm) vs. number of fatigue cycles curve. The curve is divided into three stages. The first stage describes the de-bonding cracking that occurs during the first cycle. The second stage shows nearly uniform crack growth during most of the fatigue test. The third stage describes the accelerating crack propagation rate close to failure. During the first cycle, the first crack appeared at the loading point location or within a few millimeters from the loading point. At the same time, a horizontal crack initiated at the bottom of the beam starting close to the loading point.

As the load increased during the first cycle, a de-bonded crack propagated towards the support. The length at which the de-bonded crack stops varies from one beam to another depending on the maximum specified load as shown in Figure 6.40. As the number of cycles increases (second stage) and the crack propagates the shear (bond) stress peak that drives the longitudinal (de-bonded) crack decreases due to the presence of a residual shear stress behind the crack tip. This second stage lasts until near the end of the fatigue test. Close to the end of the fatigue test (third stage), there is not enough uncracked length left to resist the shear force between the GFRP and the surrounding concrete due to loading, and the crack growth rate

accelerates until failure. Figure 6.41 shows typical crack growth rate vs. shear stress results for a test on a log-log scale. The arrows explain where the test starts and how the shear stress first decreases during a test and then increases close to failure. The crack growth rate is affected by many factors including concrete strength, concrete cover, and bar type.

Figure 6.42 shows crack growth rate versus shear stress curves for non-prestressed and prestressed beams reinforced with 16 mm GFRP bar and two different concrete covers (25 mm and 45 mm). The figure shows that the non-prestressed and prestressed results fall onto a single curve.

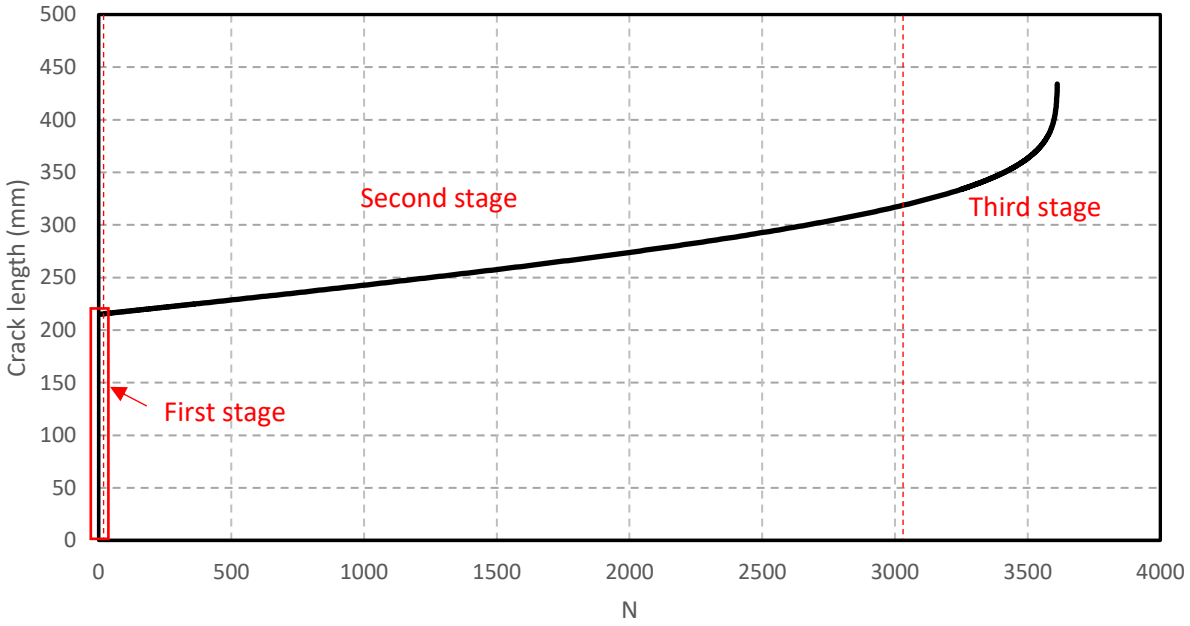

Figure 6.39: Crack length vs. number of cycles

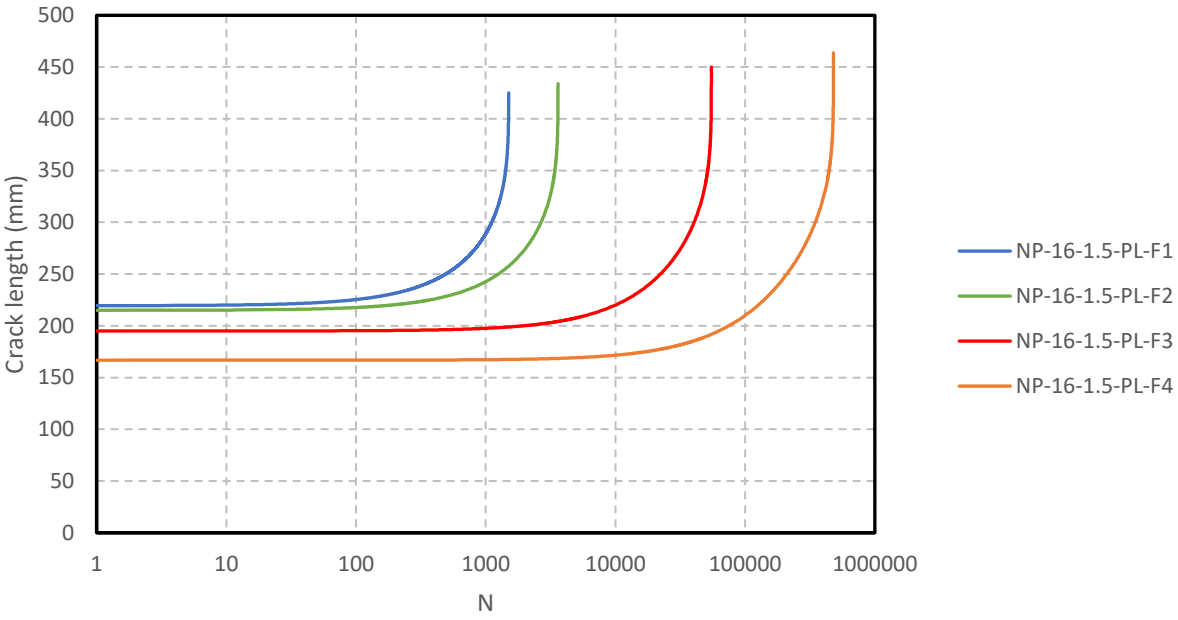

Figure 6.40: Crack length vs. *N* in log-log scale for different fatigue levels

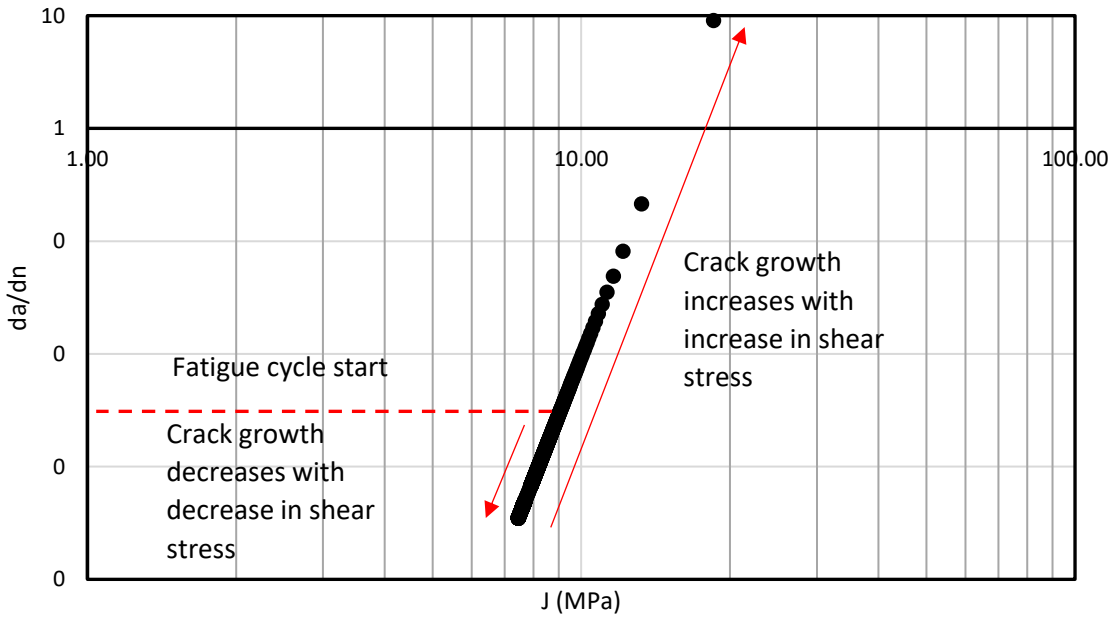

Figure 6.41: Typical crack growth rate vs. shear stress in log-log scale

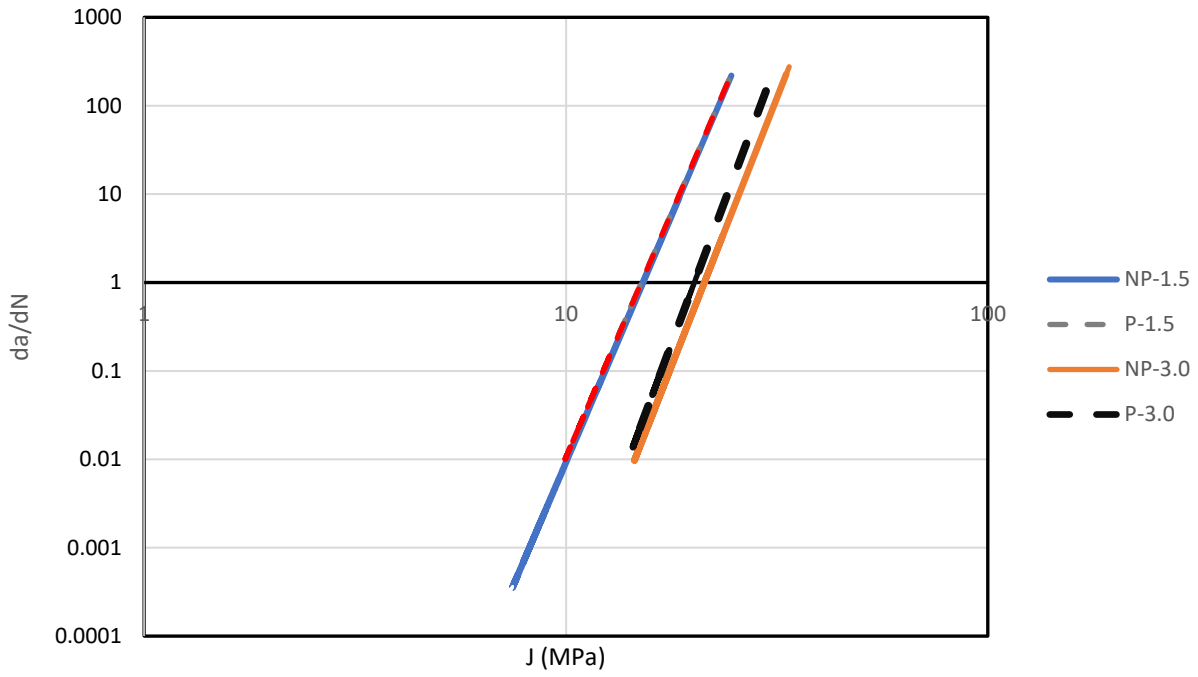

Figure 6.42: Typical crack growth rate vs. shear stress in log-log scale for all beams

Chapter 7: Conclusions and Recommendations for Future Work

7.1 Introduction

This chapter presents the main conclusions drawn from this study and recommendations for future work. This study was designed to investigate the bond mechanisms between GFRP bars and their surrounding concrete under monotonic and fatigue loading. A total of 49 reinforced concrete beams with GFRP bars were cast and tested in four-point loading until failure. The main variables were concrete cover, bar surface type, bar diameter, and prestressing level.

7.2 Conclusions

7.2.1 Test Results for Beams Tested under Monotonic Loading

The main conclusions drawn from the monotonic tests are as follows:

- All of the beams reinforced with prestressed and non-prestressed GFRP bars (sand coated and ribbed) failed by de-bonding between the GFRP bar and concrete when tested under monotonic (static) loading. The de-bonding started at the load point and as the load increased, it spread towards the support until the failure load was reached.

- Increases in the thickness of the concrete cover resulted in increases in the ultimate failure load. The ultimate failure loads for beams reinforced with 16 mm GFRP bar and 45 mm concrete cover were almost 20% than those for beams reinforced with same bar diameter with 25 mm concrete cover. The ultimate failure load for beams reinforced with 12 mm GFRP bar and 45 mm concrete cover was almost 28% greater than those reinforced with same bar diameter with 25 mm concrete cover.

- For all the beams tested under monotonic loading, there was no noticeable difference in ultimate load between the beams reinforced with sand coated GFRP bars and beams reinforced with ribbed GFRP bars.

- The GFRP bars (16 mm and 12 mm) used for reinforcing the beam were prestressed to a force corresponding to 40% of the ultimate strength of the bar.

- Based on the experimental data, the transfer length for the prestressed 16 mm GFRP bar ranged between 280 and 310 mm from the centreline of the support, while the transfer length for the prestressed 12 mm GFRP bar ranged between 260 and 290 mm.

7.2.2 Test Results for Beams Tested under Fatigue Loading

The main conclusions drawn from the fatigue tests are as follows:

- Two modes of failure were observed: 1) bond failure between the GFRP bar and concrete that starting from the loading point and propagated towards the support, and 2) rupture of the GFRP bar.

- As the horizontal crack advanced by fatigue cycling, the shear (bond) stress peak that drives the longitudinal (de-bonded) crack decreased due to the presence of a residual shear stress behind the crack tip. When the crack approached the support with continued cycling, the length of the bonded region ahead of the crack tip (fully bonded) decreased until the value of the shear stress at the crack tip began to increase due to the lack of sufficient uncracked length to accommodate the shear force produced by the change in bar force even though the bar force continues to decrease due to the presence of the residual shear stress.

- For all beams (non-prestressed and prestressed) tested under fatigue loading, the mid-span deflection increased abruptly during the first cycle. The rate of the increase in deflection was then slow from the 5% of the fatigue life to almost 90 % of the fatigue life. Beyond 90% of the fatigue life, the mid-span deflection increased rapidly until failure.

- For all beams tested under fatigue loading, there was no noticeable end slip until the number of cycles reached almost 90% of the total fatigue life.

- The slope of the load and stress vs. fatigue life curves is shallow and consequently a small change in load range will result in a large change in the fatigue life.

- Increasing the concrete cover thickness increased the fatigue strength.

- Comparing the load range (kN) vs. life curve for the non-prestressed and prestressed beams that failed in bond shows that the prestressed beams had longer lives.

- Due to the weakness of the prestressed GFRP bar when subjected to a fatigue loading, beams with a 25 mm concrete cover only failed in bond at lives below 14,000 cycles and those with a 45 mm concrete cover only failed in bond at lives below 15,000 cycles. At longer fatigue lives, they failed by bar rupture. For both beam sets, test stress ranges and load ranges were kept high, so that the beams tested under fatigue loading would avoid bar rupture and fail in bond between the GFRP bar and the concrete.

- The strain range vs. life curves for both non-prestressed and prestressed beam sets fell onto a single curve.

- A crack growth model based on the one developed by Wahab et al., 2015 was used to calculate fatigue lives and predict crack length vs. number of cycles curves. The calculated number of cycles was in good agreement with actual fatigue data for the beams with different concrete thicknesses. Also, the calculated crack length vs. number of cycle curves gave good representations of the initial crack length and the shape of the crack length vs. number of cycles curves.

7.2.3 Recommendations for Future Work

This thesis studied the bond mechanism between non-prestressed and prestressed (sand coated and ribbed) GFRP bar and the concrete under monotonic and fatigue loading for two different concrete cover thicknesses. To increase our knowledge about the bond between GFRP reinforcing bars and surrounding concrete, additional work should include:

- the use of different concrete strengths for the same bonded length and beam geometry,

- the use of a wider range of prestressing levels,

- the use of different shear reinforcement configurations to study the effect of confinement provided by shear reinforcement on the bond strength under fatigue loading,

- changing the spacing between the shear reinforcement to investigate the effect of the shear reinforcement spacing on the bond confinement and bond strength, and

- testing non-prestressed and prestressed GFRP bars under fatigue loading with different concrete covers and spans to investigate flexural capacity effects.

References

Achillides, Z. and Pilakoutas, K. (2004). Bond Behavior of Fiber Reinforced Polymer Bars under Direct Pullout Conditions. *Journal of Composites for Construction*, 8(2), pp.173-181.

ACI Committee 440 (1996). "State of the art report on fibre reinforced plastic (FRP) reinforcement for concrete structures (ACI 440-96, Reapproved 2002)". American Concrete Institute, Farmington Hills, MI, 68 pp.

ACI Committee 408, (2003) "Bond and Development of Straight Reinforcing Bars in Tension" , ACI 408R-03, American Concrete Institute, U.S.A.

ACI Committee 440 2004. ACI 440.4R-04: Prestressing Concrete Structures with FRP Tendons. American Concrete Institute, Detroit, Michigan.

ACI Committee 440 (2007). "Report on fibre-reinforced polymer (FRP) reinforcement for concrete structures." American Concrete Institute, Farmington Hills, MI, 100 pp.

Adimi, M., Rahman, A. and Benmokrane, B. (2000). New Method for Testing Fiber-Reinforced Polymer Rods under Fatigue. *Journal of Composites for Construction*, 4(4), pp.206-213.

Ahmed, S., Fahmy, M. and Wu, Z. (2018). Experimental Study and Numerical Modeling of Cyclic Bond–Slip Behavior of Basalt FRP Bars in Concrete. *Journal of Composites for Construction*, 22(6), p.04018050.

Al-Mayah, A., Soudki, K. and Plumtree, A. (2007). Novel Anchor System for CFRP Rod: Finite-Element and Mathematical Models. *Journal of Composites for Construction*, 11(5), pp.469-476.

ASTM A944-15, Standard Test Method for Comparing Bond Strength of Steel Reinforcing Bars to Concrete Using Beam-End Specimens, ASTM International, West Conshohocken, PA, 2015, www.astm.org.

ASTM C900-15, Standard Test Method for Pullout Strength of Hardened Concrete, ASTM International, West Conshohocken, PA, 2015, www.astm.org.

ASTM D7913 Standard Test Method for Bond Strength of Fiber-Reinforced Polymer Matrix Composite Bars to Concrete by Pullout Testing

Altalmas, A., El Refai, A. and Abed, F. (2018). *Bond degradation of basalt fiber-reinforced polymer (BFRP) bars exposed to accelerated aging conditions*. *Construction and Building Materials*, *81*, 162-171

Alunno Rossetti, V., Galeota, D. and Giammatteo, M. (1995). Local bond stress-slip relationships of glass fibre reinforced plastic bars embedded in concrete. *Materials and Structures*, 25(180), pp.340-344.

Alves, J., El-Ragaby, A. and El-Salakawy, E. (2011). Durability of GFRP Bars' Bond to Concrete under Different Loading and Environmental Conditions. *Journal of Composites for Construction*, 15(3), pp.249-262.

Alyousef, R., Topper, T., & Al-Mayah, A. (2016). Fatigue Bond Stress–Slip Behavior of Lap Splices in the Reinforcement of Unwrapped and FRP-Wrapped Concrete Beams. *Journal of Composites for Construction*, *20*(6), 04016039.

Aly, R. (2007). Stress along tensile lap-spliced fibre reinforced polymer reinforcing bars in concrete. *Canadian Journal of Civil Engineering*, 34(9), pp.1149-1158.

Aly, R., Benmokrane, B. and Ebead, U. (2006). Tensile lap splicing of fibre-reinforced polymer reinforcing bars in concrete. *ACI Structural Journal*, 103(6), pp.857-864.

Aly, R., Benmokrane, B. and Ebead, U. (2006). Tensile Lap Splicing of Bundled CFRP Reinforcing Bars in Concrete. *Journal of Composites for Construction*, 10(4), pp.287-294.

Al-Zahrani, M. (2018). *Bond behaviour of fibre reinforced plastic (FRP) reinforcements with concrete*. PhD. Pennsylvania State Univ.

Ametrano, D. (2011). *Bond Characteristics of Glass Fibre Reinforced Polymer Bars Embedded in High Performance and Ultra-High Performance Concrete*. Master of Applied Science. Ryerson University.

Badawi, M. (2003). *Flexural Response of Uniform and Shear-span Corroded RC beams Repaired with CFRP Laminates*. Master of Applied Science. University of Waterloo.

Badawi, M. (2007). *Monotonic and Fatigue Flexural Behaviour of RC Beams Strengthened with Prestressed NSM CFRP Rods*. Doctor of Philosophy. University of Waterloo.

Badawi, M., Wahab, N. and Soudki, K. (2011). Evaluation of the transfer length of prestressed near surface mounted CFRP rods in concrete. *Construction and Building Materials*, 25(3), pp.1474-1479.

Baena, M., Torres, L., Turon, A. and Barris, C. (2009). Experimental study of bond behaviour between concrete and FRP bars using a pull-out test. *Composites Part B: Engineering*, 40(8), pp.784-797.

Baena, M., Torres, L., Turon, A., Llorens, M. and Barris, C. (2018). *Bond behaviour between recycled aggregate concrete and glass fibre reinforced polymer bars*.

Bajwa, M. (2018). *Bond Behavior of Post-Installed GFRP Bars in Structural Connections*. Master of Science. University of Minnesota.

Bakis, C., Al-Dulaijan, S., Nanni, A., Boothby, T. and Zahrani, M. (1998). Effect of Cyclic Loading on Bond Behavior of GFRP Rods Embedded in Concrete. *Journal of Composites Technology & Research*, 20(1), pp.29-37.

Balazs, G. (1991). Fatigue of Bond. *ACI Materials Journal*, 88(6), pp.620-629.

Bazli, M., Ashrafi, H. and Oskouei, A. (2018). *Experiments and probabilistic models of bond strength between GFRP bar and different types of concrete under aggressive environments*.

Benmokrane, B. and Rahman, H. (1998). First Int. Conf. on Durability of composites for construction, CDCC'98, Sherbrooke, Québec.

Benmokrane, B., Mohamed, H., Manalo, A. and Cousin, P. (2017). Evaluation of Physical and Durability Characteristics of New Headed Glass Fiber–Reinforced Polymer Bars for Concrete Structures. *Journal of Composites for Construction*, 21(2), p.04016081.

Benmokrane, B., Tighiouart, B. and Chaallal, O. (1996). Bond strength and load distribution of composite GFRP reinforcing bars in concrete. *ACI Materials Journal*, 93(3), pp.246-253.

Braimah, A., Green, M. and Campbell, T. (2006). Fatigue behaviour of concrete beams post-tensioned with unbonded carbon fibre reinforced polymer tendons. *Canadian Journal of Civil Engineering*, 33(9), pp.1140-1155.

Brondsted, P., Lilholt, H. and Anderson, S. (1997). Fatigue Damage Prediction by Measurements of the Stiffness Degradation in Polymer Matrix Composites. *Proceedings of the International Conference on Fatigue of Composites Eight International Spring Meeting*.

CAN/CSA S806-02 (2012). "Design and construction of building components with fibre reinforced polymers." Canadian Standards Association, Rexdale, Ontario, Canada, 177 pp.

CAN/CSA S6-06 (2014). "Canadian highway bridge design code." Canadian Standards Association, Rexdale, Ontario, Canada, 788 pp.

Chang, X., Yue, G., Lin, H. and Tang, C. (2010). Modeling the pullout behavior of fiber reinforced polymer bars from concrete. *Construction and Building Materials*, 24(4), pp.431-437.

Cosenza, Z., Manfredi, G. and Realfonzo, R. (1997). Behaviour and modelling of bond of FRP rebars to concrete. *Journal of Composites for Construction*, 1(2), pp.40-51.

DeFreese, J. and Roberts-Wollmann, C. (2002). Glass fibre reinforced polymer bars as top mat reinforcement for bridge decks. *Contract Report for Virginia Transportation Research Council*.

Demers, C. (1998). Fatigue Strength Degradation of E-glass FRP Composites and Carbon FRP Composites. *Construction and Building Materials*, 12, pp.311-318.

Demers, C. (1998). Tension-Tension Axial Fatigue of E-Glass Fiber-Reinforced Polymeric Composites: Tensile Fatigue Modulus. *Construction and Building Materials*, 12(1), pp.51-58.

Ehsani, M., Saadatmanesh, H. and Tao, S. (1993). Bond of GFRP rebars to ordinary-strength concrete. *ACI Int. Symposium. on Non-Metallic Continuous Reinforcement*, pp.333-345.

Ehsani, R., Saadatmanesh, H. and Tao, S. (1996). Design recommendations for bond of GFRP rebars to concrete. *Journal of Structural Engineering-ASCE*, 122(3), pp.247-254.

El Maddaawy, T. (2004). *Performance of corrosion-damaged reinforced concrete beams repaired with CFRP laminates*. PhD. University of Waterloo.

El Refai, A., Ammar, M. and Masmoudi, R. (2015). Bond Performance of Basalt Fiber-Reinforced Polymer Bars to Concrete. *Journal of Composites for Construction*, 19(3), p.04014050.

El-Nemr, A., Ahmed, E., Barris, C. and Benmokrane, B. (2018). *Bond-dependent coefficient of glass- and carbon-FRP bars in normal- and high-strength concretes*.

El-Ragaby, A., El-Salakawy, E. and Benmokrane, B. (2007). Fatigue Life Evaluation of Concrete Bridge Deck Slabs Reinforced with Glass FRP Composite Bars. *Journal of Composites for Construction*, 11(3), pp.258-268.

Elrefai, A., West, J. and Soudki, K. (2007). Performance of CFRP tendon–anchor assembly under fatigue loading. *Composite Structures*, 80(3), pp.352-360.

Erki, M. and Rizkalla, S. (1993). Anchorages for FRP reinforcement. *Concrete International*, 15(6), pp.54-59.

Esfahani, M., Rakhshanimehr, M. and Mousavi, S. (2013). Bond Strength of Lap-Spliced GFRP Bars in Concrete Beams. *Journal of Composites for Construction*, 17(3), pp.314-323.

Faza, S. and GangaRao, S. (1990). Bending and bond behaviour of concrete beams reinforced with plastic rebars. *Transportation Research Record*, 2(1290), pp.185-193.

Fergani, H., Di Benedetti, M., Miàs Oller, C., Lynsdale, C. and Guadagnini, M. (2018). Long-term performance of GFRP bars in concrete elements under sustained load and environmental actions. *Composite Structures*, 190, pp.20-31.

Ferguson, M. and Thompson, N. (1965). Development Length for Large High Strength Reinforcing Bars. *ACI JOURNAL*, 62(1), pp.71-94.

Gu, X., Yu, B., & Wu, M. (2016). Experimental study of the bond performance and mechanical response of GFRP reinforced concrete. *Construction and Building Materials*, *114*, 407-415.

Hailu Tekle, B., Khennane, A. and Kayali, O. (2017). Bond behaviour of GFRP reinforced geopolymer cement concrete. *MATEC Web of Conferences*, 120, p.04002.

Hao, D., Wang, B. and Ou, P. (2006). Fibre reinforced polymer rebar's application to civil engineering. *Concrete*, 9, pp.38-40.

Harajli, M. and Abouniaj, M. (2010). Bond Performance of GFRP Bars in Tension: Experimental Evaluation and Assessment of ACI 440 Guidelines. *Journal of Composites for Construction*, 14(6), pp.659-668.

Heffernan, P. and Erki, M. (2004). Fatigue Behavior of Reinforced Concrete Beams Strengthened with Carbon Fiber Reinforced Plastic Laminates. *Journal of Composites for Construction*, 8(2), pp.132-140.

Henin, E. and Morcous, G. (2018). Bond-Dependent Coefficient of Helically Wrapped Sand-Coated Glass Fiber–Reinforced Polymer (GFRP) Bars. *Advances in Civil Engineering Materials*, 7(1), p.20180009.

Hossain, K., Ametrano, D. and Lachemi, M. (2018). *Bond strength of GFRP bars in ultra-high strength concrete using RILEM beam tests*.

Islam, S., Afefy, H., Sennah, K. and Azimi, H. (2018). *Bond characteristics of straight- and headed-end, ribbed-surface, GFRP bars embedded in high-strength concrete*.

Issa, M., Sen, R. and Amer, A. (1999). Comparative study of transfer length in fiberglass and steel pretensioned concrete members. *Precast/prestressed Concrete Institute. Journal*, 38(6).

Johnson, W., Masters, J., Wilson, D., Bakis, C., Al-Dulaijan, S., Nanni, A., Boothby, T. and Al-Zahrani, M. (1998). Effect of Cyclic Loading on Bond Behavior of GFRP Rods Embedded in Concrete Beams. *Journal of Composites Technology and Research*, 20(1), p.29.

Ju, M. and Oh, H. (2018). *Experimental Assessment on the Flexural Bonding Performance of Concrete Beam with GFRP Reinforcing Bar under Repeated Loading*.

ISIS Canada 2008. Design Manual No. 5 - Prestressing Concrete Structures with Fibre-Reinforced Polymers, Winnipeg, Manitoba, Canada.

Kanakubo, T., Yonemaru, K., Fukuyama, H., Fujisawa, M. and Sonobe, Y. (1993). Bond performance of concrete members reinforced with FRP bars. *ACI Special Publications*, 138, pp.767-788.

Katz, A. (2000). Bond to concrete of FRP rebars after cyclic loading. ASCE. *J. Compos. Construction*, 4(3), pp.137-144.

Katz, A. (2000). Bond to Concrete of FRP Rebars after Cyclic Loading. *Journal of Composites for Construction*, 4(3), pp.137-144.

Katz, A., Berman, N. and Bank, C. (1998). Effect of cyclic loading and elevated temperature on the bond properties of FRP rebars. In International Conference on the Durability of Fiber Reinforced Polymer (FRP) Composites for Construction. pp.403-413.

Kim, B. and Lee, J. (2018). Resistance of interfacial debonding failure of GFRP bars embedded in concrete reinforced with structural fibers under cycling loads. *Composites Part B: Engineering*, 156, pp.201-211.

Konur, O. and Matthews, F. (1989). Effect of the Properties of the Constituents on the Fatigue Performance of Composites: A Review. *Composites*, 20(4), pp.317-328.

Konur, O. and Matthews, L. (1989). Effect of the Properties of the Constituents on the Fatigue Performance of Composites: A Review. *Composites*, 20(4), pp.317-328.

Kotynia, R., Szczech, D. and Kaszubska, M. (2017). Bond Behavior of GRFP Bars to Concrete in Beam Test. *Procedia Engineering*, 193, pp.401-408.

Larralde, J. and Silva-Rodriguez, R. (1993). Bond and slip of FRP reinforcing bars in concrete.". *Journal of Materials in Civil Engineering*, 5(1), pp.30-40.

Lee, J., Lim, A., Kim, J. and Kim, J. (2018). *Bond behaviour of GFRP bars in high-strength concrete: bar diameter effect*.

Lee, Y., Kim, M., Kim, H., Lee, J. and Kim, D. (2013). Experimental study on bond strength of fiber reinforced polymer rebars in normal strength concrete. *Journal of Adhesion Science and Technology*, 27(5-6), pp.508-522.

Li, T., Zhu, H., Wang, Q., Li, J. and Wu, T. (2018). Experimental study on the enhancement of additional ribs to the bond performance of FRP bars in concrete. *Construction and Building Materials*, 185, pp.545-554.

Lin, X. and Zhang, Y. (2018). *Bond–slip behaviour of FRP-reinforced concrete beams*.

Lu, Z., Boothby, T., Bakis, C. and Nanni, A. (2000). Transfer and development lengths of FRP prestressing tendons. *PCI Journal*, 45(2), pp.84-95.

Mahmoud, I., Rizkalla, S. and Zaghoul, R. (1999). Transfer and development lengths of carbon fiber reinforced polymers prestressing reinforcement. *ACI Structural Journal*, 96(4), p.594.

Mahmoud, K., Bassuoni, M., El-Salakawy, E. and El-Gendy, M. (2017). Bond Behaviour of GFRP Bars Embedded in Normal Strength Concrete and Basalt Fibre Reinforced Cementous Composite. In: *APFIS2017 - 6th Asia-Pacific Conference on FRP in Structures*. Singapore, pp.1-4.

Mandell, J. (1982). Fatigue Behavior of Fiber-Resin Composites. *Developments in Reinforced Plasstics*, 2, pp.67-107.

Maranan, G., Manalo, A., Karunasena, W. and Benmokrane, B. (2018). *Pullout behaviour of GFRP bars with anchor head in geopolymer concrete*.

Mazaheripour, H., Barros, J., Sena-Cruz, J., Pepe, M. and Martinelli, E. (2018). *Experimental study on bond performance of GFRP bars in self-compacting steel fiber reinforced concrete*.

Mohamed, N., Farghaly, A. and Benmokrane, B. (2017). Beam-Testing Method for Assessment of Bond Performance of FRP Bars in Concrete under Tension–Compression Reversed Cyclic Loading. *Journal of Composites for Construction*, 21(1), p.06016001.

Mosley, P. (2000). *Bond performance of fibre reinforced plastic (FRP) reinforcement in concrete*. Master of Applied science. Purdue University.

Mutsuddy, R. (2017). *Bond Performance between Lightweight Concrete with Crumb Rubber and Glass Fibre Reinforced Polymer Bar*. Doctor of Philosophy. University of Alberta.

Nanni, A., Al-Zaharani, M., Al-Dulaijan, U. and Boothby, E. (1995). Bond of FRP reinforcement to concrete-experimental results. *In non-metallic (FRP) reinforcement for concrete structures. Proceedings of the Second International RILEM Symposium (FRPRCS-2),*, pp.135-145.

Noël, M. and Soudki, K. (2014). Fatigue Behavior of GFRP Reinforcing Bars in Air and in Concrete. *Journal of Composites for Construction*, 18(5), p.04014006.

Okelo, R. (2007). Realistic Bond Strength of FRP Rebars in NSC from Beam Specimens. *Journal of Aerospace Engineering*, 20(3), pp.133-140.

Okelo, R. and Yuan, R. (2005). Bond Strength of Fiber Reinforced Polymer Rebars in Normal Strength Concrete. *Journal of Composites for Construction*, 9(3), pp.203-213.

Pan, M. and Xu, X. (2017). Research on deformation characteristics and design method of concrete beams reinforced with GFRP bars. *IOP Conference Series: Earth and Environmental Science*, 61, p.012038.

Park, J., Lim, A., Kim, J. and Lee, J. (2015). Bond performance of fiber reinforced polymer rebars in different casting positions. *Polymer Composites*, 37(7), pp.2098-2108.

Pecce, M., Manfredi, G., Realfonzo, R. and Cosenza, E. (2001). Experimental and Analytical Evaluation of Bond Properties of GFRP Bars. *Journal of Materials in Civil Engineering*, 13(4), pp.282-290.

Pleiman, G. (1991). Strength, modulus of elasticity, and bond of deformed FRP rods. *Advanced Composite Materials in Civil Engineering Structures: Proceedings of the Specialty Conference*, pp.99-110.

Pleimann, G. (1991). Strength, modulus of elasticity, and bond of deformed FRP rods. *Advanced Composites Materials in Civil Engineering Structures*, pp.99-110.

Pleimann, L. (1987). Tension and bond pull-out tests of deformed fibre glass rods. *Final report for Marshall-Vega Corporation, Marshall, Arkansas, Civ. Engrg. Dept., Univ. of Arkansas, Fayetteville*, pp.5-11.

Quayyum, S. (2010). *Bond Behaviour of Fibre Reinforced Polymers (FRP) Rebar in Concrete*. Master of Applied Science. the University of Britch Columbia.

Rafi, M., Nadjai, A. and Ali, F. (2007). Experimental Testing of Concrete Beams Reinforced with Carbon FRP Bars. *Journal of Composite Materials*, 41(22), pp.2657-2673.

Rahman, A., Adimi, M. and Benmokrane, B. (1996). Fatigue Behaviour of FRP Reinforcements Encased in Concrete. *Proceedings of the 2nd International Conference on Advanced Composite Materials in Bridges and Structures*, pp.691-698.

Reifsnider, K. (1991). Damage and Damage Mechanics. In Fatigue of Composite Materials, Edited by Reifsnider, K.L. *Elsevier Science Publishing Company*, pp.11-78.

Rezazadeh, M. and Carvelli, V. (2018). A damage model for high-cycle fatigue behavior of bond between FRP bar and concrete. *International Journal of Fatigue*, 111, pp.101-111.

Rolland, A., Quiertant, M., Khadour, A., Chataigner, S., Benzarti, K. and Argoul, P. (2018). Experimental investigations on the bond behavior between concrete and FRP reinforcing bars. *Construction and Building Materials*, 173, pp.136-148.

Ruiz Emparanza, A., De Caso Y Basalo, F., Kampmann, R. and Adarraga Usabiaga, I. (2018). Evaluation of the Bond-to-Concrete Properties of GFRP Rebars in Marine Environments. *Infrastructures*, 3(4), p.44.

Saadatmanesh, H. and Ehsani, M. (1998). Fibre composites in infrastructure. *." Proc., 2nd Int. Conf. on Composites in Infrastructure, ICCI'98, Tucson*.

Saadatmanesh, H. and Tannous, F. (1999). Relaxation, Creep, and Fatigue Behavior of Carbon Fiber Reinforced Plastic Tendons. *ACI Materials Journal*, 96(2), pp.143-155.

Sayed Ahmad, F., Foret, G. and Le Roy, R. (2011). Bond between carbon fibre-reinforced polymer (CFRP) bars and ultra-high performance fibre reinforced concrete (UHPFRC): Experimental study. *Construction and Building Materials*, 25(2), pp.479-485.

Shen, D., Ojha, B., Shi, X., Zhang, H. and Shen, J. (2016). Bond stress–slip relationship between basalt fiber-reinforced polymer bars and concrete using a pull-out test. *Journal of Reinforced Plastics and Composites*, 35(9), pp.747-763.

Shield, C., French, W. and Hanus, J. (1999). Bond of Glass Fiber Reinforced Plastic Reinforcing Bar for Consideration in Bridge Decks. *ACI Special Publication*, 188, pp.393-406.

Shield, K., French, W. and Retika, A. (1997). Thermal and mechanical fatigue effects on GFRP rebar-concrete bond. *Proc., Third Int. Symp. on Non-Metallic Reinforcement for Concrete Structures*, pp.381-388.

Soudki, K. (1998). FRP reinforcement for prestressed concrete structures. *Progress in Structural Engineering and Materials*, 1(2), pp.135-142.

Soudki, K. A., Green, M. F., & Clapp, F. D. (1997). Transfer length of carbon fiber rods in precast pretensioned concrete beams. *PCI Journal*, 42(5), 78-87.

Talreja, R. (1981). Fatigue of Composite Materials: Damage Mechanisms and Fatigue-Life Diagrams. *Proceedings of the Royal Society of London. Series A Mathematical and Physical Sciences*, 378(1775), pp.461-475.

Tekle, B., Khennane, A. and Kayali, O. (2016). Bond Properties of Sand-Coated GFRP Bars with Fly Ash–Based Geopolymer Concrete. *Journal of Composites for Construction*, 20(5), p.04016025.

Tekle, B., Khennane, A. and Kayali, O. (2018). *Bond behaviour of GFRP reinforcement in alkali activated cement concrete*.

Tighiouart, B., Benmokrane, B. and Gao, D. (1998). Investigation of bond in concrete member with fibre reinforced polymer (FRP) bars. *Construction and Building Materials*, 12, pp.453-462.

Tighiouart, B., Benmokrane, B. and Mukhopadhyaya, P. (1999). Bond strength of glass FRP rebar splices in beams under static loading. *Construction and Building Materials*, 13, pp.383-392.

Tran, T., Nguyen, M. and Nguyen, T. (2017). Experimental Investigation of Bond-Dependent Coefficient of Glass Fiber Reinforced Polymer Bars. *Lecture Notes in Civil Engineering*, pp.868-877.

Veljkovic, A., Carvelli, V., Haffke, M. and Pahn, M. (2018). *Concrete cover effect on the bond of GFRP bar and concrete under static loading*.

Vilanova, I., Baena, M., Torres, L. and Barris, C. (2018). *Experimental study of bond-slip of GFRP bars in concrete under sustained loads*.

Wahab, N., Soudki, K. and Topper, T. (2011). Mechanism of Bond Behavior of Concrete Beams Strengthened with Near-Surface-Mounted CFRP Rods. *Journal of Composites for Construction*, 15(1), pp.85-92.

Wahab, N., Soudki, K. and Topper, T. (2012). Experimental Investigation of Bond Fatigue Behavior of Concrete Beams Strengthened with NSM Prestressed CFRP Rods. *Journal of Composites for Construction*, 16(6), pp.684-692.

Wahab, N., Topper, T. and Soudki, K. (2015). Modelling experimental bond fatigue failures of concrete beams strengthened with NSM CFRP rods. *Composites Part B: Engineering*, 70, pp.113-121.

Wambeke, W. and Shield, K. (2006). Development length of glass fibre-reinforced polymer bars in concrete. *ACI Structural Journal*, 103(1), pp.11-17.

Wang, H., Sun, X., Peng, G., Luo, Y. and Ying, Q. (2018). *Experimental study on bond behaviour between BFRP bar and engineered cementitious composite*.

Xue, W., Zheng, Q., Yang, Y. and Fang, Z. (2014). Bond behavior of sand-coated deformed glass fiber reinforced polymer rebars. *Journal of Reinforced Plastics and Composites*, 33(10), pp.895-910.

Yan, F. and Lin, Z. (2016). *Bond behavior of GFRP bar-concrete interface: Damage evolution assessment and FE simulation implementations*.

Yan, F. and Lin, Z. (2018). *Bond behavior of GFRP bar-concrete interface: Damage evolution assessment and FE simulation implementations*.

Yan, F. and Lin, Z. (2018). *Bond behavior of GFRP bar-concrete interface: Damage evolution assessment and FE simulation implementations*.

Yan, F., Lin, Z. and Yang, M. (2018). *Bond mechanism and bond strength of GFRP bars to concrete: A review*.

Yang, S. and Xu, X. (2018). Discussion on Bonding Performance between FRP Bars and Concrete. *IOP Conference Series: Earth and Environmental Science*, 189, p.032031.

Yang, W., He, X. and Dai, L. (2018). *Damage behaviour of concrete beams reinforced with GFRP bars*.

Yoo, D. and Yoon, Y. (2016). Bond behavior of GFRP and steel bars in ultra-high-performance fiber-reinforced concrete. *Advanced Composite Materials*, 26(6), pp.493-510.

Yoo, D., Kwon, K., Park, J. and Yoon, Y. (2018). *Local bond-slip response of GFRP rebar in ultra-high-performance fiber-reinforced concrete*.

Yoo, D., Kwon, K., Park, J. and Yoon, Y. (2018). *Local bond-slip response of GFRP rebar in ultra-high-performance fiber-reinforced concrete*.

Zawam, M. (2015). *Long-Term Behaviour of GFRP Prestressed Concrete Beams*. Doctor of Philosophy. University of Waterloo.

Zemour, N., Asadian, A., Ahmed, E., Khayat, K. and Benmokrane, B. (2018). Experimental study on the bond behavior of GFRP bars in normal and self-consolidating concrete. *Construction and Building Materials*, 189, pp.869-881.